REFERENCE ONLY

UNIVERSITY OF LONDON THESIS

Degree PhD Year 2005 Name of Author MUALLEM M B

COPYRIGHT

This is a thesis accepted for a Higher Degree of the University of London. It is an unpublished typescript and the copyright is held by the author. All persons consulting the thesis must read and abide by the Copyright Declaration below.

COPYRIGHT DECLARATION

I recognise that the copyright of the above-described thesis rests with the author and that no quotation from it or information derived from it may be published without the prior written consent of the author.

LOANS

Theses may not be lent to individuals, but the Senate House Library may lend a copy to approved libraries within the United Kingdom, for consultation solely on the premises of those libraries. Application should be made to: Inter-Library Loans, Senate House Library, Senate House, Malet Street, London WC1E 7HU.

REPRODUCTION

University of London theses may not be reproduced without explicit written permission from the Senate House Library. Enquiries should be addressed to the Theses Section of the Library. Regulations concerning reproduction vary according to the date of acceptance of the thesis and are listed below as guidelines.

A. Before 1962. Permission granted only upon the prior written consent of the author. (The Senate House Library will provide addresses where possible).

B. 1962 - 1974. In many cases the author has agreed to permit copying upon completion of a Copyright Declaration.

C. 1975 - 1988. Most theses may be copied upon completion of a Copyright Declaration.

D. 1989 onwards. Most theses may be copied.

This thesis comes within category D.

☑ This copy has been deposited in the Library of UCL

☐ This copy has been deposited in the Senate House Library, Senate House, Malet Street, London WC1E 7HU.

An Anion Transporter Theory of the Outer Hair Cell Motor Protein

By

Daniella Muallem

University College London

Thesis submitted for the degree of Doctor of Philosophy

ProQuest LLC
789 East Eisenhower Parkway
P.O. Box 1346
Ann Arbor, MI 48106-1346

Acknowledgements

I would like to express my thanks to the following:

To Professor Jonathan Ashmore, for providing me with the opportunity to complete this thesis and encouraging me to be an independent researcher.

To Jean-Marie Chambard for practical help and encouragement.

To Alasdair Gibb and Jonathan Gale for helpful comments on the thesis.

To Nick and Paul at the Biological Services Department for help obtaining bullae.

To Wolfgang for his friendship, continuous encouragement and all the helpful discussions about this work.

To friends, who provided much moral support, made lunch times entertaining, and pub times even more so.

A special thanks to my family for their unconditional support and endless patience.

Abstract

This thesis addresses the mechanism of electromotility in outer hair cells (OHCs) of the mammalian cochlea. Prestin, a protein densely packed in the lateral membrane is assumed to drive electromotility. A current hypothesis is that prestin is an incomplete transporter, shuttling chloride across the membrane without allowing it to dissociate at the extracellular surface. In this thesis kinetic models are formulated to show that this hypothesis cannot reproduce the previously published experimental data from electrical recordings. However an alternative model of prestin as an anion exchanger (modelled here as a chloride/sulphate exchanger) is formulated, which can reproduce many of the experimental observations. In this model the experimentally observed charge movements across the cell membrane are produced by the translocation of a chloride ion combined with some intrinsic charged residues. To further test the predictions of the model, patch clamp recordings were performed on dissociated OHCs, in the excised patch and whole-cell configurations. The OHC non-linear capacitance (NLC) depended on the concentration of intracellular chloride (Cl_i). When Cl_i was removed from internal and external solutions, a residual NLC (~15-30%) was found, which was consistent with the predictions of the model for contaminant levels of $[Cl_i]$ (~10μM). Additionally the effect on the NLC of reducing $[Cl_i]$ depended on the species of anion used to replace Cl_i. The largest effect was produced by replacement with sulphate, whilst the smallest effect was produced by replacement with glutamate. These findings support the model. Finally two potential causes for previous controversy in the literature were identified. 1) The NLC depended on the recording configuration when $[Cl_i]$ was reduced below 1-10mM. 2) The dependence of the NLC on $[Cl_i]$ was affected when $Tris^+$ replaced Na^+ as the major cation in solutions.

Table of Contents

Chapter 1

Introduction

1.1 General Introduction

Hearing depends on the conversion of sound stimuli into electrical signals, which are then sent to the brain for interpretation. This occurs in the inner ear in the cochlea. The cochlea has a complex structure, which enables the vibrations produced by sound waves to be translated into appropriate mechanical stimulation of two types of sensory cells, the inner hair cells (IHCs) and the outer hair cells (OHCs). The two cell types are believed to have different functional roles in hearing. Whilst the IHCs are considered to be primarily responsible for conveying electrical signals to the brain, OHCs are believed to play an important role in enhancing frequency selectivity. One hypothesis suggests that in mammals OHCs enhance frequency selectivity via a process called electromotility in which OHCs are able to change length in response to electrical signals, driven by a 'motor' protein called prestin. At present there is some controversy over the precise way in which prestin functions. Some of the previous experimental observations are contradictory, and no model has yet been presented to account for all these experimental observations. In this thesis a new model for prestin is presented that can account for many of the experimental observations and some predictions of the model are tested. Finally the causes of discrepancies in experimental observations, which have led to the current controversy are investigated.

1.2 The Mammalian Cochlea

1.2.1 Anatomy of the Mammalian Cochlea

The mammalian cochlea is a coiled tube containing three compartments called the scala vestibuli, scala media and scala tympani. Reissner's membrane separates the scala media from the scala vestibuli (Figure 1.1A). The basilar membrane separates the scala media from the scala tympani and supports the organ of Corti. At the apex the scala vestibuli and scala tympani join at an opening called the helicotrema whilst at the base they end at the oval and round windows respectively. When vibrations are transmitted by the stapes from the middle ear to the oval window, fluid is displaced along the length of the cochlea from the oval window to the round window resulting in wave-like displacement of the basilar membrane (BM).

The organ of Corti (Figure 1.1B) is a highly specialised structure, which contains a collection of cells including the sensory cells. It is given rigidity by an arch of pillar cells, which end in the reticular lamina forming its upper surface, and is covered by the tectorial membrane, which is attached at its inner edge to the bony spiral limbus. The two types of sensory cells, IHCs and OHCs, are polarized non-neuronal epithelial cells, which have hair bundles called stereocilia protruding from their apical surface. OHCs are themselves highly specialised, with a cylindrical cell body and a structured lateral wall, consisting of the plasma membrane, the 2-dimensional cortical lattice, composed of cross-linked actin and spectrin filaments (Holley and Ashmore 1990) and the sub-surface cisterna. OHCs typically have a diameter of ~10μm and range in length between 10-20μm in the base and 80-90μm in the apex.

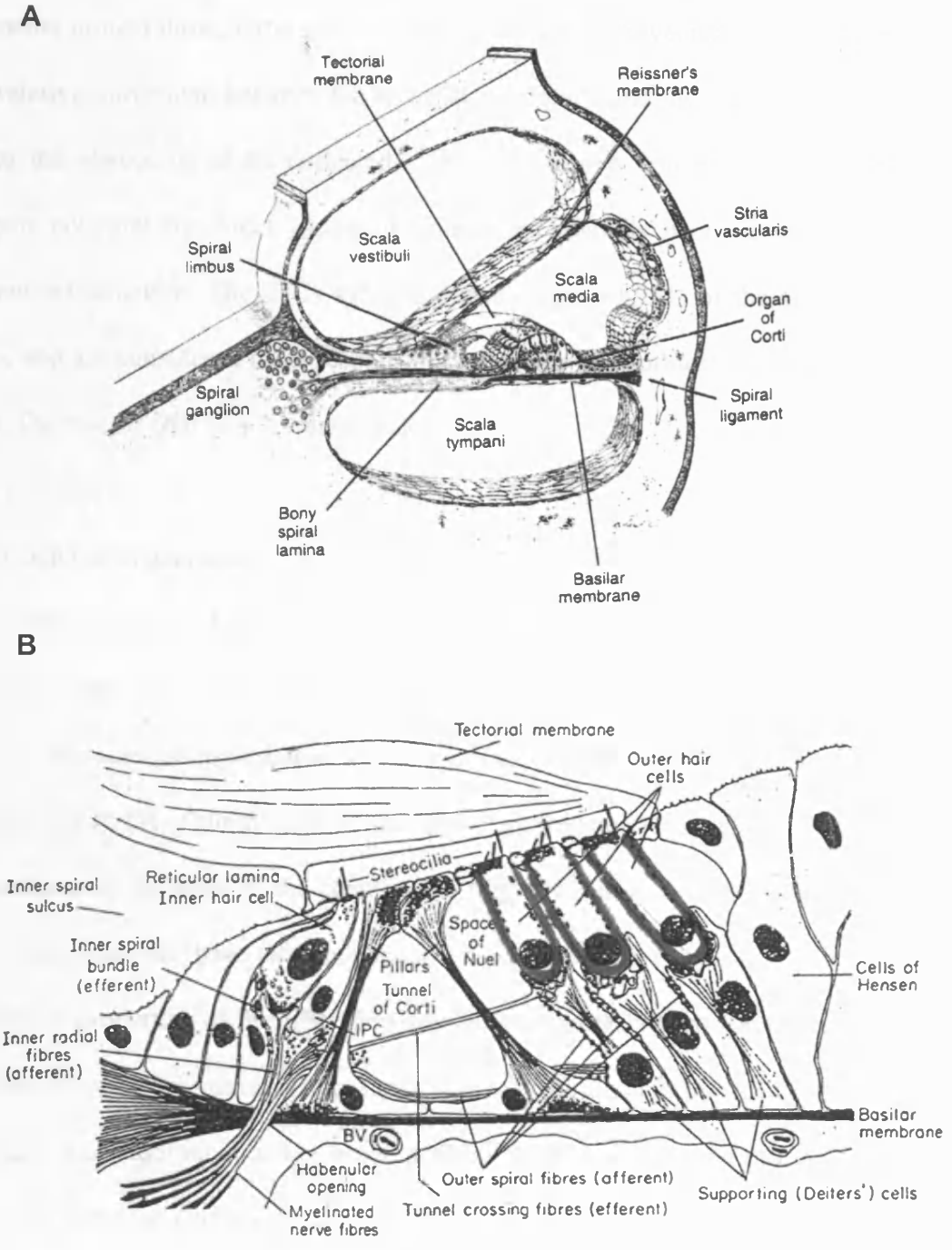

Figure 1.1. Anatomy of the Cochlea. A) A cross-section through one cochlear turn, shows the three scalae and associated structures (Taken from Geisler, 1998). B) A cross-section of the organ of Corti. OHCs are highlighted in red (Taken from Pickles, 1988).

One IHC and three OHCs are aligned radially across the organ of Corti. Their stereocilia project through the reticular lamina, such that movement of the BM results in a relative movement between the tectorial membrane and the reticular lamina that causes the stereocilia to be deflected. This deflection is converted to a change in receptor potential by direct gating of transducer channels in a process known as mechanotransduction. The IHCs synapse directly with 90-95% of the afferent nerve fibres, and are considered to be responsible for conveying auditory information to the brain. The role of OHCs is discussed below.

1.2.2 Cochlear Mechanics

The response of hair cells to sounds of different frequencies depends on the location of the cell on the BM. Thus a cell at a particular location will be most sensitive to sound of a particular frequency. This is not an intrinsic property of the cell, but is a result of the motion of the BM. Low frequency sounds produce a wave that peaks near the apex of the cochlea and high frequency sounds produce a wave that peaks near the base of the cochlea. This is partly a result of the passive mechanical properties of the BM. However measurements which showed that living BM motion was much more sharply tuned than that observed in the dead ear, suggests that there is an additional active process which feeds back energy into the BM and boosts its response (Sellick et al. 1982). Observations that the loss or damage of OHCs results in significant hearing loss (Dallos and Harris, 1978, Liberman, 1987), coupled with their strategic location have led to the acceptance that OHCs are responsible for the amplification process.

1.2.3 Outer Hair Cell Motility

OHCs are accepted to be responsible for the active amplification process in hearing, and are thus referred to as the 'cochlear amplifier'. There are different hypotheses as to how this is achieved, but for mammals the most commonly accepted theory arose from the discovery that OHCs have a unique property known as electromotility (Brownell et al. 1985). When isolated OHCs *in vitro* were electrically stimulated by an electrode, the length of their cylindrical cell body changed. Hyperpolarisation led to an elongation of the cell, whereas depolarisation led to a contraction of the cell. Length changes of up to 4% were observed (Ashmore, 1987). The mechanical response was voltage-dependent and nonlinear (Evans et al. 1989; Santos-Sacchi, 1989), with the length changes displaying a sigmoidal dependence on the applied voltage, V. Thus it was presumed that *in vivo*, the length changes would lead to the generation of force along the longitudinal axis, to be fed back into the BM. There is strong supporting evidence for this view. Indeed electrical stimulation of OHCs *in situ* showed that the electromotile force is sufficient to produce the displacement of neighbouring cells inside the organ of Corti (Mammano et al. 1995), whilst *in vitro* measurements on OHCs showed that the axial force generated by electromotility was ~0.1nN/mV (Iwasa and Adachi, 1997).

Any mechanism, which underlies the amplification process, must be able to function at all frequencies within the hearing range that goes up to 20kHz in humans and higher in many mammals. For example, hearing in guinea pig goes up to around 50kHz. The electromotile response of OHCs, *in vitro*, was shown to be undiminished up to 22.5 kHz (Dallos and Evans, 1995) and a phasic electromotile response

remained up to 100kHz, with a constant electromechanical force up to 50kHz (Frank et al. 1999). Thus, in vitro, motility speeds extend to acoustic frequencies.

In addition, a study of the electromotile properties of gerbil OHCs from birth showed that OHCs only reach adult motility levels around P12 coinciding with the onset of hearing (He et al. 1994).

Finally the electromotile response was reversibly reduced when salicylate (aspirin), which is known to produce hearing loss, was applied to OHCs (Shehata et al. 1991, Lue and Brownell, 1999).

Despite the evidence in favour of the theory that electromotility underlies cochlear amplification, a dilemma over the *in vivo* behaviour of electromotility at high frequencies remains. *In vivo*, fluid mechanics would be expected to damp the response of the BM at higher frequencies. Furthermore, *in vivo*, at high frequencies the receptor potential would be severely attenuated due to the resistance-capacitance (RC) filtering of the lateral cell membrane. Since changes in the receptor potential are assumed to drive electromotility, this attenuation would result in a loss of motility at high frequencies. Several proposals have been made to solve this problem. For example, it has been proposed that rather than the receptor potential driving motility, an extracellular voltage gradient across the OHC might produce a sufficient driving force (Dallos and Evans, 1995). Alternatively, it has been proposed that fast voltage-dependent ionic currents might boost the receptor potential at high frequencies (Ospeck et al. 2003, Rybalchenko et al. 2003). Finally it has been proposed that the mechanics of the cochlea might play an important role in controlling the generation of the receptor potential, and overcoming viscous damping (Nobili et al. 1998).

Although no particular proposal has been generally accepted, it seems likely that, *in vivo*, the attenuation of the receptor potential can be overcome.

Unlike other forms of cellular motility electromotility is voltage-dependent and it is independent of ATP and Ca^{2+}(Holley and Ashmore, 1988).

1.2.4 Outer Hair Cell Non-linear Capacitance

The voltage-dependent process of electromotility requires a charged voltage-sensor, just as voltage-dependent ion channels have voltage sensors. Measurements of gating charge movements under voltage clamp (representing the restricted movement of charge within the membrane) showed that the charge transferred across the membrane, Q had a sigmoidal dependence on V (Santos-Sacchi, 1991), which correlated with the mechanical response of OHCs to changes in V. The dependence of Q on V can be fit with a 2-state Boltzmann function to give a value for the maximum charge moved (Q_{max}) and the V corresponding to half-maximal charge transfer (V_o).

$$Q(V) = \frac{Q_{\max}}{1 + e^{-\beta(V - V_o)}} \qquad (1.1)$$

where $\beta = \frac{ze_o\delta}{k_B T}$, z is number of elementary charges, δ is the fraction of the membrane field crossed, e_o is the elementary charge, k_B is Boltzmann's constant, and T is the absolute temperature. β reflects the slope of the Q vs V curve thus it is often referred to as the 'slope'. Fits of the Boltzmann function to experimental data give values for β, of ~0.033 mV^{-1}(Gale and Ashmore 1997b). This corresponds to one elementary charge crossing ~0.8 of the membrane field.

All membranes have a capacitance, which arises from the dielectric properties of the lipid bilayer. The intrinsic membrane capacitance depends on the area of membrane, its thickness and its intrinsic properties, largely provided by the phospholipids, which are impermeable to ions. The intrinsic membrane capacitance is proportional to the total area of membrane, and is thus described as the linear membrane capacitance (C_{lin}). It is typically $\sim 1 \mu F\ cm^{-2}$.

However a change in the total membrane capacitance (C_m) arises as a result of the redistribution of the charge within the membrane. Since the charge distribution depends on V this gives the cell an additional voltage-dependent non-linear capacitance (NLC) on top of its intrinsic linear membrane capacitance

$$C_m = C_{lin} + NLC(V) \tag{1.2}$$

where,

$$NLC(V) = \frac{dQ}{dV} \tag{1.3}$$

The NLC has a bell-shaped dependence on V (Figure 1.2) and can be described by the derivative of the Boltzmann distribution (B′(V)),

$$NLC(V) = \frac{\beta Q_{max} e^{-\beta(V-V_o)}}{\left(1+e^{-\beta(V-V_o)}\right)^2} \tag{1.4}$$

Therefore the peak NLC (C_{pk}) is dependent on Q_{max}, and β, and occurs at V_o.

$$C_{pk} = \frac{\beta Q_{max}}{4} \tag{1.5}$$

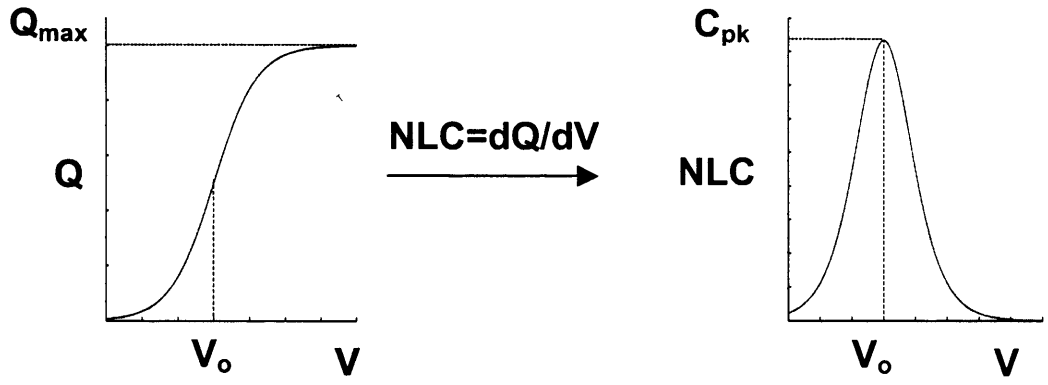

Figure 1.2. Simulated Q(V) curve and its derivative, the NLC.
The charge transferred in response to a perturbation in membrane potential has a sigmoidal dependence on V, which produces a bell-shaped NLC.

In OHCs the NLC that arises due to the redistribution of charge across the membrane has a peak value that is large and often in excess of 10pF, and is thus experimentally convenient to measure. This bell-shaped NLC is often considered to be the signature of OHCs and its properties have been investigated extensively. Typically the V_0 of the NLC associated with adult OHCs, measured *in vitro*, lies at negative membrane potential (V_m) V_0 ~-40mV and for a cell of 60μm length has a C_{pk} of ~ 20pF. Since the magnitude of the NLC is so considerable, it is also possible to detect it in small patches of OHC membrane. Measurements of the NLC in cell-attached patches of OHCs revealed that the NLC was present in the lateral membrane, but was absent from the basal membrane (Gale and Ashmore, 1997a). By considering Q_{max} and the area of membrane generating it, estimates were made for the number of elementary charges that move across the membrane, giving values of ~7500 $e^-/\mu m^2$ (Huang and Santos-Sacchi 1993), and between 4200-8400 $e^-/\mu m^2$ (Gale and Ashmore 1997a).

The Q_{max}, C_{pk} and V_o associated with the NLC are influenced by several factors:

1) An increase in membrane tension, achieved either by perfusing cells with hypo-osmotic solution to increase turgor pressure, or by applying positive pressure inside the cell, led to a significant positive shift in V_o of up to 70mV (Adachi et al. 2000, Kakehata and Santos-Sacchi, 1995).
2) Incubating OHCs in a reagent that promotes Ca^{2+}/calmodulin dependent phosphorylation shifted V_o to more hyperpolarized potentials, whereas incubation in a phosphorylation inhibiting reagent shifted V_o to more depolarised potentials (Frolenkov et al. 2000).
3) A decrease in temperature caused a negative shift in V_o of ~20mV per 10^0C (Santos-Sacchi and Huang 1998).
4) The application of lipophilic ions affected both V_o and C_{pk} (Wu and Santos-Sacchi, 1998), though the exact effect depended on the ion species.
5) The Q_{max}, C_{pk}, and V_o also vary during development from birth until the typical adult characteristics are reached. A study of the NLC measured from rat OHCs from birth, showed that C_{pk} gradually increases and V_o shifts positively from very hyperpolarized potentials during postnatal development. Both V_o and C_{pk} reached adult characteristics around P12, coinciding with the onset of hearing and adult electromotility (Oliver and Fakler 1999).
6) As for electromotility, the NLC is reduced on application of salicylate (Tunstall et al. 1995, Kakehata and Santos-Sacchi 1996).

A change in C_m also arises from a change in membrane area, which causes a change in C_{lin}. Assuming that the cells length changes by up to 4% during

electromotility, but the cells diameter and dielectric properties are constant, the cells lateral membrane area would also change by up to 4%, which would result in a change in C_{lin} of up to 4%. Therefore area changes resulting from electromotility produce a small non-linear component of C_m, which is not normally considered since it is much smaller than the non-linear component due to the redistribution of charge (NLC(V)).

1.2.5 Prestin: The 'Motor' Protein

The correlation between the mechanical response and the non-linear capacitance that arose from the charge movement within the membrane suggested that, electromotility was directly generated by a membrane-bound protein in the basolateral membrane, labelled the 'motor' protein. Further experimental evidence strongly supports this view. Microscopic studies of the cells lateral wall showed an unusually high density of intramembrane particles, which were not observed in IHCs (Gulley and Reese 1977, Forge 1991, Kalinec et al. 1992). Estimates for the diameter of these particles range between 10-15nm, whilst estimates for the density of particles ranges between 2500-6000/μm^2. This is comparable with the estimates for the number of electronic charges per square micron of membrane, suggesting between one and two charges per particle. Moreover when the OHC cytoskeleton was disrupted with intracellular trypsin digestion leaving only the plasma membrane, motility remained (Kalinec et al 1992). Finally the gating charge movements measured from lateral membrane patches were sufficiently rapid to generate electromotility (Gale and Ashmore 1997b). Typically transient currents had a

relaxation time constant between 7 and 50μs. Thus it appears that the particles observed in the lateral membrane generate both electromotility and the NLC.

Adachi and Iwasa (1999) showed that the gating charge movements are coupled to an area change of the membrane. This led to the 'area model', which proposed that prestin can exist in two states, either contracted or expanded, such that when a voltage-dependent conformation change occurs the small change in protein area is translated into a change in cell length due to the high density of proteins in the membrane. A two-state model of the 'motor' as a protein flipping between two conformational states, with different areas, accompanied by the movement of charge, was able to reproduce the NLC (Iwasa 1997).

Recently a candidate for the 'motor' protein was identified (Zheng et al. 2000) and named prestin. Subtractive hybridisation was used to find the cDNA encoding a protein found in OHCs but not in IHCs of gerbils, which produced both charge movement and some electromotility when expressed in a kidney cell line (TSA201). Supporting evidence came from the targeted deletion of the mouse homologue of prestin in mice, which resulted in reduced cochlear sensitivity, and the loss of OHC electromotility (Liberman et al. 2002). Furthermore a variety of cell lines (chinese hamster ovary, CHO and human embryonic kidney, HEK 293) transfected with the rat homologue of prestin produced an electromechanical force and showed a virtually identical NLC to adult OHCs (Ludwig et al. 2001). The NLC in transfected cells had a similar sensitivity to membrane tension as the NLC in OHCs, with the V_0 shifting to more depolarised potentials as membrane tension was increased (Ludwig et al 2001). A positive shift in V_0 was also produced in response to an increase in membrane tension when gerbil prestin was expressed in TSA201 cells (Santos-Sacchi et al

2001). Additionally an immunolocalisation study of prestin, in adult rat OHCs revealed that prestin is highly expressed exclusively in the lateral plasma membrane of OHCs, such that the time-course of immunoreactivity coincides with the onset of electromotility (Belyantseva et al 2000). The NLC generated in cells transfected with prestin, was shown to have a similar dependence on temperature (Meltzer and Santos-Sacchi 2001) and phosphorylation (Matsuda et al 2003) as the NLC of OHCs. Thus it appears likely that electromotility is generated by prestin, a protein in the lateral plasma membrane.

1.2.6 Prestin: Sequence and Structure

Prestin is a 744 amino-acid protein with a relative molecular mass of 81.4kDa. It is predicted to be a hydrophobic membrane protein with ~50% non-polar residues (Zheng et al 2000). Computer modelling failed to predict its membrane topology unambiguously, however FITC-labelled antibodies directed against both N-terminus and C-terminus tagged epitopes of prestin showed immunofluorescence only when the cell membrane was permeabilized (Zheng et al 2001). This indicated that both the N- and C-termini are intracellular, and thus that prestin has an even number of trans-membrane domains. It is currently proposed that prestin has 12 trans-membrane domains (Oliver et al. 2001)(Figure 1.3).

Analysis of prestin's amino acid sequence revealed that it had the greatest homology with members of the SLC26 family of sulphate/anion transport proteins and has been identified as the fifth member, SLC26A5. In particular it has ~40% homology with pendrin (SLC26A4), which is also expressed in the inner ear and is mutated in some forms of hereditary deafness (Everett et al. 1999). Prestin is highly

conserved between species with ~93% of the 744 residues identical for mouse, rat, gerbil and human orthologs of prestin.

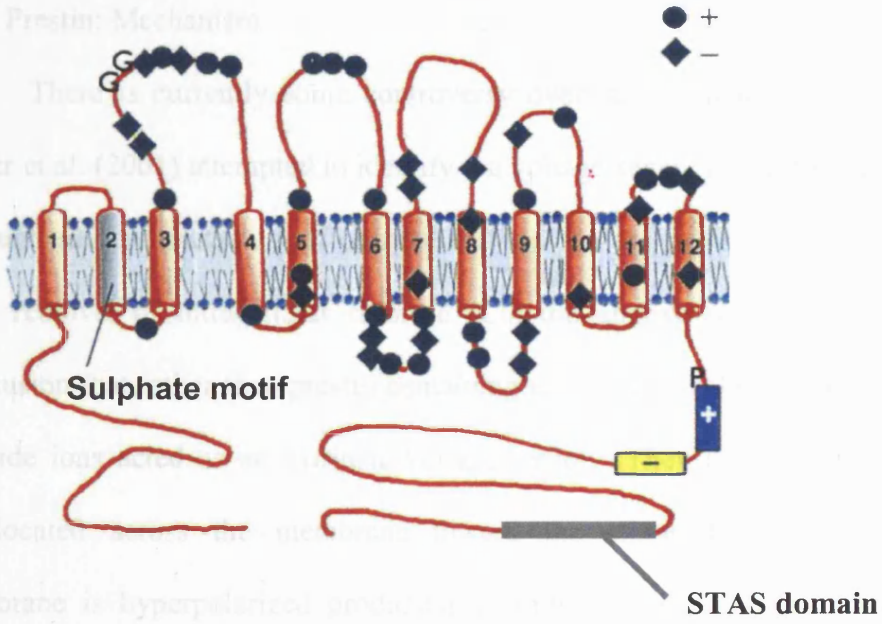

Figure 1.3. Proposed membrane topology for prestin. 12 transmembrane domains are predicted. The extracellular loops are shown above the transmembrane domains, and the cytoplasmic segments are shown below the transmembrane domains. G indicates glycosylation sites, P indicates a phosphorylation site. (Adapted from Zheng et al. 2001)

Prestin (SLC26A5) has a 22 amino-acid sulphate-transport motif within the hydrophobic core (Zheng et al 2000) and a STAS (sulphate transporters and antisigma factor antagonist) domain in the C-terminus, which may bind GTP or ATP to produce specific conformational changes in the STAS domain (Aravind and Koonin 2000). Both are highly conserved within the SLC26 family. Furthermore prestin has two N-linked glycosylation sites in the second extracellular loop, which are also conserved

among members of the SLC26 family (Matsuda et al 2004), and may be involved in determining the V_0 of the NLC.

1.2.7 Prestin: Mechanism

There is currently some controversy over the mechanism of prestin. When Oliver et al. (2001) attempted to identify the voltage-sensor in prestin, they found that although several mutations of charged residues on the protein failed to abolish the NLC removal of intracellular chloride (Cl_i) did abolish it. This led them to the conclusion that rather than prestin containing an intrinsic voltage-sensor intracellular chloride ions acted as an extrinsic voltage-sensor. They proposed that chloride is translocated across the membrane toward the extracellular surface when the membrane is hyperpolarized producing a conformational change of prestin to its expanded state. Since there was no effect on the NLC of removing extracellular chloride (Cl_e), they concluded that this chloride position is inaccessible from the extracellular space. Thus prestin acts as an incomplete transporter, moving ions across the membrane without allowing them to dissociate at the extracellular surface.

In such a model it would be expected that in conditions of lower $[Cl_i]$ a larger driving force would be required to move an equivalent amount of chloride ions across the membrane. Thus it would be predicted that the V_0 of the NLC, which corresponds to the voltage required for half-maximal charge transfer, would shift to more hyperpolarized potentials when $[Cl_i]$ is reduced. However more detailed investigations revealed that V_0 shifted to more depolarised potentials and Q_{max} and C_{pk} decreased as $[Cl_i]$ was reduced (Figure 1.4A) (Fakler and Oliver 2002). These results have led to

some confusion over whether the Oliver model for prestin is adequate (discussed in Gummer, 2003).

Furthermore in contradiction to the observations Oliver et al. (2001), Rybalchenko and Santos-Sacchi (2003) showed that removal of Cl_i led to little or no decrease in C_{pk} and under these conditions removal of Cl_e did affect the NLC. In particular, in complete contrast to Oliver et al. (2001) they showed that sulphate supported a significant NLC with the same slope as the chloride supported NLC (Figure 1.4B). From this they concluded that Cl_i is not the voltage-sensor. On the other hand Rybalchenko and Santos-Sacchi (2003) also found a similar positive shift in V_o when $[Cl_i]$ was reduced, leading them to agree that Cl_i had a critical affect on prestin. They proposed that the effect of chloride is due to an allosteric action of chloride on prestin, whereby the NLC arises from the movement of an intrinsic voltage-sensor and chloride modulates the NLC by binding to a distinct site to produce a conformational change. Thus at present a consensus on the nature of the voltage-sensor has not been reached.

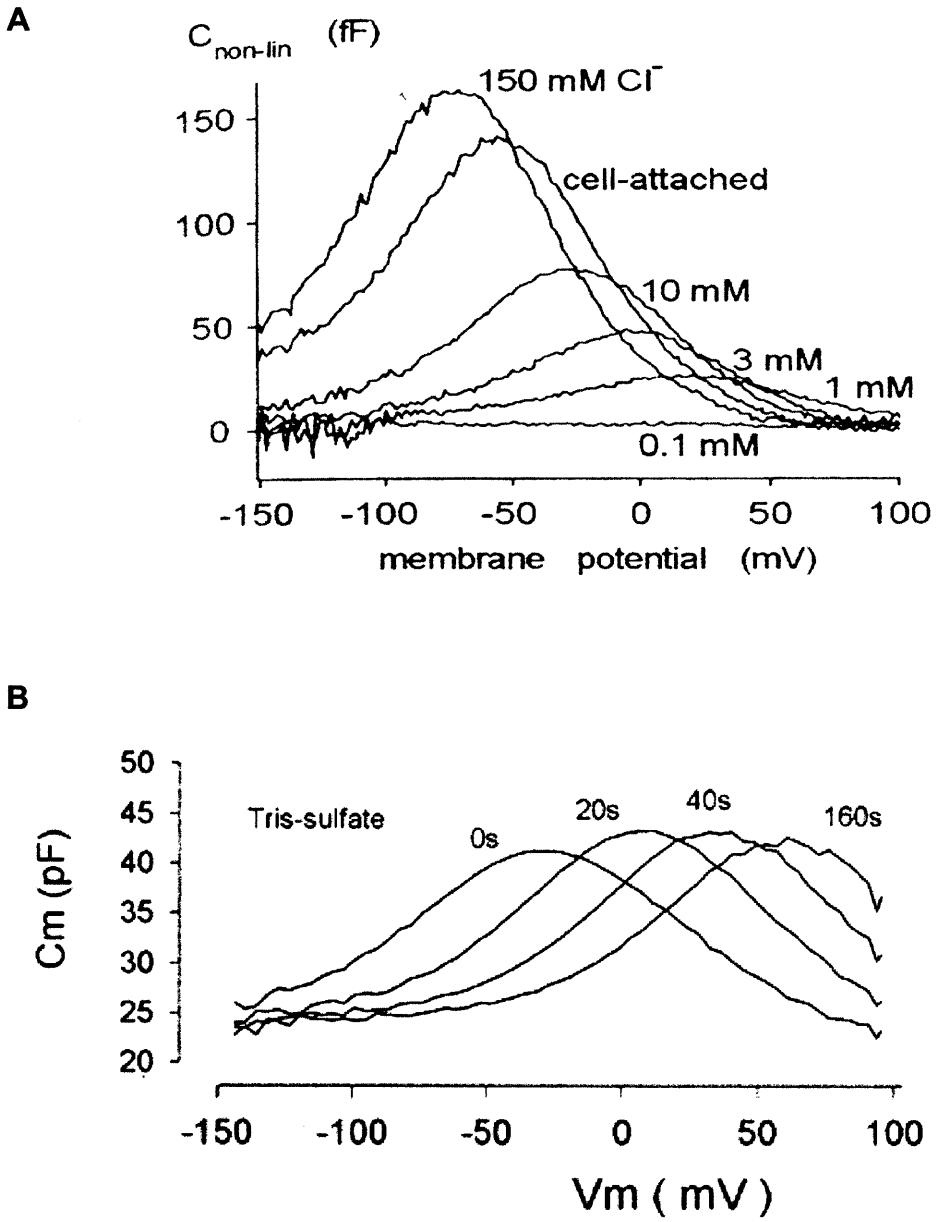

Figure 1.4. Experimental observations of the dependence of the NLC on $[Cl_i]$.
A) NLCs measured for different $[Cl_i]$ in excised inside-out patches from rat OHCs. No NLC is detected when Cl_i is completely replaced with sulphate. Taken from Fakler and Oliver 2002. B) NLCs measured in the whole-cell configuration at different times after break-in with chloride-free and high sulphate solution in the pipette. 160s after break-in V_o has shifted to more positive potentials but no decrease in C_{pk} or Q_{max} is observed. Taken from Rybalchenko and Santos-Sacchi 2003.

1.3 The SLC26 Family

Prestin (SLC26A5) is one member of the mammalian SLC26 family of sulphate/anion transporters. This family was identified when three human genetic diseases were found to share common genetic origins. The three human genes (DTDST, CLD and PDS) associated with the diseases were found to reside within the same gene family and all encoded anion transporters, which were structurally different from the classical SLC4 (or AE) family of anion transporters (Everett and Green 1999). This new family was named the SLC26 family, with the genes DTDST, CLD and PDS renamed SLC26A2, SLC26A3, and SLC26A4 respectively (Lohi et al. 2000). Surprisingly each protein was found to transport a different primary anion; SLC26A2 transports SO_4^{2-}, SLC26A3 transports Cl^- and SLC26A4, which is expressed in the thyroid and kidney in addition to the inner ear, functions as a chloride/iodide transporter and mediates chloride/formate exchange (Mount and Romero 2003, Scott and Karniski 2000).

Since the SLC26 family was identified several new members have been cloned and characterised. SLC26A6, has the greatest homology with prestin (~56%) and is widely expressed with the most abundant expression in the kidney and pancreas (Lohi et al 2000). Though no transport function was detected in human SLC26A6 cRNA injected oocytes (Waldegger et al. 2001), the mouse ortholog is a versatile anion exchanger, capable of transporting SO_4^{2-}, Cl^-, OH^-, HCO_3^-, formate and oxalate (Xie et al. 2002). Furthermore it appears to mediate electrogenic HCO_3^- transport, whereby more than one HCO_3^- ion is exchanged for each Cl^- ion. At present 10 SLC26 family members (SLC26A1-9 and SLC26A11), and one Pseudogene have been identified, with varying expression locations, and transport properties (for review see Mount and

Romero 2003). Thus the SLC26 family encodes a diverse group of non-specific anion transporters, which are expressed throughout the body, mediating both electroneutral and electrogenic anion exchange. To date prestin has not been shown to transport anions, however none of the published studies on prestin have directly investigated potential anion transport function. Both prestin (SLC26A5) and pendrin (SLC26A4) have been shown to act as fructose transporters (Chambard and Ashmore 2003).

1.4 Transporters

Although prestin has not yet been shown to have any anion transport properties, it possesses all the sequence domains conserved throughout the SLC26 family. Furthermore, despite proposals that prestin has a different function from all other members of the SLC26 family, its mechanism has not been clearly established. Thus prestin may share greater similarities with other members of the SLC26 family than is currently assumed. In fact in Chapters 3 and 4, it is proposed that prestin does act as a transporter. In order to elucidate a transport mechanism for prestin, it would be helpful to consider the transport mechanism for other members of the SLC26 family, but as a recently identified family, the underlying mechanism of SLC26 mediated transport, has not been investigated. However, the SLC26 family of anion transporters is only one family of transporters. Transporters form a major class of integral membrane proteins, of which the mechanisms for some other transporters have been more thoroughly investigated.

In this section a general introduction to transporters is presented (Ch.1.4.1) and the current theories concerning the mechanism for transport are considered (Ch.1.4.2-Ch.1.4.3). Finally two of the most studied transporters, for which transport

mechanisms have been predicted and tested are described (Ch.1.4.4-Ch.1.4.5): The anion exchanger AE1, which is functionally similar to members of the SLC26 family, and the Na,K-ATPase, which exhibits some voltage-dependent characteristics comparable with that observed for prestin.

1.4.1 General Introduction to Transporters

Transporters perform a wide range of physiological functions, including responsibility for cell volume control, pH control, maintaining ion gradients, providing nutrients to cells, and sequestering neurotransmitters. There are two classes of transporters: **Active transporters** and **Passive transporters**. Active transporters can move substrates up their concentration gradients, either utilising a primary energy source such as light or ATP-hydrolysis in **primary active transport** or by utilising a gradient of a different substrate in **secondary active transport** (van der Does and Tampe 2004). The Na,K-ATPase is the most commonly described example of a primary active transporter. It is essential for basic cellular functions such as cell excitablilty and generating Na^+ gradients to drive secondary active transporters (Lauger 1991). Secondary active transport, can either be achieved by **co-transport**, or **counter-transport**.

In co-transport the energy from a substrate moving down its gradient is used to transport another substrate in the same direction, up its gradient. Examples of co-transporters are numerous. They include several members of the Na^+/glucose cotransporter family (SGLT1 or SLC5), widely expressed monomers predicted to have 14 transmembrane domains (Wright and Turk 2004), the $Na^+/K^+/Cl^-$ cotransporter family (NKCC or SLC12), widely expressed monomers predicted to

have 12 transmembrane domains (Russel JM 2000) and several neurotransmitter transporters, which may function as multimers (Kilic and Rudnick 2000, Eskandari et al. 2000, Veenhoff et al. 2002). An example of a well-characterised cotransporter is the lactose permease of *E.Coli* (LacY), which co-transports protons and lactose, and for which the crystal structure has been determined (Abramson et al 2003). It is a monomer with 12 transmembrane domains.

In counter-transport the energy from one substrate moving down its gradient is used to drive another substrate against its gradient in the opposite direction. These include the cardiac Na^+/Ca^{2+} exchanger (NKCX1) of mammals, which contributes to the electrical activity of the heart. NKCX1 is currently believed to have 9 transmembrane domains (Philipson and Nicoll 2000).

Passive transporters facilitate the movement of substrates, which would otherwise be membrane impermeable, down their concentration gradient. These include the facilitative glucose transporter (GLUT or SLC2) family, which transport sugars including glucose, and fructose down their concentration gradient, and like many other transporters are monomers with 12 transmembrane domains (Bell et al 1993). The AE (or SLC4) family of Cl^-/HCO_3^- exchangers has also been presumed to mediate passive exchange, but recent evidence suggests they may be active counter-transporters (Knauf et al. 2002).

Coupled transporters have varying stoichiometries, causing some transporters to be electrogenic. In this case they transport net charge across the membrane to produce a measurable current. Others are electroneutral, so no membrane current is produced.

The tight flux coupling between substrates exhibited by many transporters contrasts with ion channels, another major class of membrane proteins, which function as selective pores. Whilst several transporters are able to move substrates against their electrochemical gradients, ion channels only allow movement of ions down their electrochemical gradient. The turnover of transporters is typically much less than for ion channels, $1\text{-}10^4$/s compared with 10^8/s. This is assumed to be because transporters undergo larger, and slower conformational changes in order to move ions across the membrane.

1.4.2 Theory of Transport: Alternating-Access Model

Most contemporary mechanistic descriptions of transporters employ an "alternating-access" model, in which transporters undergo conformational changes, allowing transitions between states with either inward-facing or outward-facing binding sites. An alternating-access model never allows simultaneous access to the binding-site from both internal and external mediums, and thus never affords access to an open channel. The idea of an alternating-access model was first proposed by Patlak (1957) and Vidaver (1966) and was popularised by Jardetzky (1966) and Lauger (1979). These models can be described using simple kinetic diagrams, consisting of the intermediate states of the transporter protein (E_i) and transitions connecting these states. Although these simplified models probably do not accurately describe the actual number of conformational transitions experienced by most proteins, they do produce good approximations to the available experimental data. It has been suggested that the kinetic diagrams represent a reduced model in which only

states that can be recognised within the time-scale of experiments are represented (Hernandez and Valle Lisboa 2004).

Definition of Dielectric Coefficient

With transport considered as a cyclic series of transitions the charge transfer for each individual reaction step can be considered (Lauger 1991). For a reaction step $E_i \rightarrow E_{i+1}$, we assume that an electric charge q_i is translocated across a distance a_i in the membrane dielectric. If the voltage V across the membrane is clamped to a fixed value then the charge movement measured across the entire membrane arising from this transition is Q_i. For a homogenous membrane of thickness d,

$$Q_i = \frac{q_i a_i}{d} = \gamma_i e_o \delta_i \qquad (1.6)$$

e_o is the elementary charge, $\gamma_i = q_i/e_o$ a dimensionless constant and $\delta_i = a_i/d$, the fraction of membrane crossed. Since the membrane is in general an inhomogenous dielectric medium the distance a_i represents an effective dielectric distance rather than a geometric distance, and δ_i represents the effective fraction of the membrane dielectric crossed in the transition.

In general a transition $E_i \rightarrow E_{i+1}$ might involve the movement of ions, and/or the movement of charged residues on the protein. For a transition with $_K$ individual charge movements, Q_i is then given by

$$Q_i = \alpha_i e_o \qquad (1.7)$$

$$\alpha_i = \sum_K \gamma_{iK} \delta_{iK} \qquad (1.8)$$

where $\gamma_{iK} e_o$ is the translocated charge and δ_{iK} is the fraction of the membrane over which the charge moves.

The dimensionless quantity α_i is referred to as the **dielectric coefficient**.

For a full cycle in which n ions, of valency z are moved across the membrane, then the charge movement measured across the entire membrane arising from a full cycle, Q is given by

$$Q = \sum_i Q_i = nze_o \tag{1.9}$$

and the sum of dielectric coefficients of all transitions in the cycle is given by

$$\sum_i \alpha_i = nz \tag{1.10}$$

Voltage Dependence of Reaction Rates

The reaction $E_i \rightleftharpoons E_{i+1}$ may be described by rate constants f_i and b_i for the transitions in the forward and backward direction, with the equilibrium constant K_i given by, $K_i=f_i/b_i$. The application of the Boltzmann distribution, which describes the probability of a particle having a given energy, produces a relationship between K_i and the difference in free energy between the states, ΔG_i (Feynman 1965, Atkins 1986),

$$K_i = \overline{K}_i e^{\frac{\Delta G_i}{k_B T}} \tag{1.11}$$

Where $\overline{K}_i$ is the value of K_i when $\Delta G_i=0$. Since the transition involves the translocation of charge, there is an electrostatic contribution to ΔG_i, equal to the charge q_i times the fraction of the transmembrane voltage V, it moves across. This gives

$$\Delta G_i = q_i \delta_i V = \alpha_i e_o V \tag{1.12}$$

Therefore the rate constants for the transition are voltage-dependent.

$$K_i = \overline{K}_i e^{\frac{\alpha_i e_o V}{k_B T}} \quad (1.13)$$

If the reaction $E_i \rightarrow E_{i+1}$ is treated as a transition over a symmetric energy barrier then

$$f_i = \bar{f}_i e^{\frac{\alpha_i e_o V}{2k_B T}} \quad (1.14)$$

$$b_i = \bar{b}_i e^{-\frac{\alpha_i e_o V}{2k_B T}} \quad (1.15)$$

$\bar{f}_i$ is the forward rate constant when V=0, and $\bar{b}_i$ is the backward rate constant when V=0.

1.4.3 Theory of Transport: Transporters as Pores

In the last 5-10 years an alternative to the alternating-access model of transporters has emerged in which it is suggested that, transporters may sometimes form a pore similar to those of ion-channels (DeFelice 1996, Larsson et al. 1996, Lester et al 1996). This view arose from observations that some neurotransmitter transporters can display channel-like behaviour. For example glutamate transporters have an associated glutamate-gated chloride conductance that is too large to be accounted for by an alternating-access scheme, and noise analysis was consistent with a chloride channel of 0.7fS conductance (Larsson et al.1996, Wadiche and Kavanaugh 1998). Several monoamine transporters including norepinephrine transporters (NETs), the human dopamine transporter (hDAT) and the serotonin transporters also produced large macroscopic currents consistent with channel behaviour (Mager et al. 1994, Galli et al. 1996, Sonders et al. 1997). In particular the serotonin transporter was shown to produce single channel events, measurable by conventional single-channel recordings (Lin et al. 1996). Single channel openings have also been shown in a γ-aminobutyrate (GABA) transporter (GAT1) (Cammack and Schwartz 1996). Thus

alternating-access models were insufficient to explain all the conductances observed (Adams and DeFelice 2003).

A radically different model to the alternating-access type models was proposed to account for channel like behaviour of transporters, which suggested that transporters work as multi-substrate single-file pores (Su et al 1996, Adams and DeFelice 2002). In this pore model the transporter is considered to form a single file of binding sites, which are always accessible from both the internal and external mediums. The coupling between substrates results from interactions between the co-permeating species. This model was able to account for the steady-state conductance data of GAT1, and the serotonin transporter.

Nevertheless despite the success of the pore model the time is not yet up for alternating-access models. In fact an alternating-access model was used to account equally well for the available data on GAT1 (Hilgemann and Lu 1999). Furthermore pore models do not account for single channel events, they have not yet been used to explain counter-transport behaviour and importantly channel like conductances have not been reported for many other types of transporters. One possible explanation is that mulitmeric neurotransmitter transporters may function differently from other monomeric transporters (DeFelice 2004). However although overlap between transport and channel behaviour has predominantly been reported for neurotransmitter transporters, the idea that transporters and ion channels are structurally similar has also been suggested for other types of transporters. In a recent study, CLC-ec1 (a prokaryotic forebear of the large CLC family of chloride channels) was shown to be a secondary active H^+/Cl^-counter-transporter (Accardi and Miller 2004). This was surprising since the crystal structure of CLC-ec1, had been previously resolved

(Dutzler et al. 2002, Dutzler et al. 2003) and successfully used to guide models of gating and anion permeation in ClC-channels. These findings suggested that the structural differences between transporters and channels might be very small but could provide for substantial mechanistic differences.

Therefore it appears that neurotransmitter transporters are not the only type of transporters to share characteristics with ion channels, and neither the alternating-access models nor the multi-substrate single file pore model can account for the behaviour of a range of transporters. When the channel behaviour of neurotransmitter transporters was considered in more detail it was shown that the probability of the occurrence of single-channel events was very low, and that frequently the ion specificity of the 'channel' was not always the same as for the transported substrates (Mager et al. 1994, Cammack and Schwartz 1996, Lin et al. 1996). These findings indicated that the conducting state was not a necessary part of the transport cycle. Thus an intermediate model between the perfect alternating-access model and the open pore model has also been proposed in which transport still primarily works via an alternating-access scheme, but there is a non-zero probability of a conformational change to an open channel (pore) state occurring (Lester et al. 1996, Kavanaugh 1998).

So far the crystal structures of several tranporters, ClC-ec1 (Dutzler et al 2002), LacY (Abramson et al. 2003), a bacterial oxalate transporter, OxlT (Hirai et al. 2002) and a eukaryotic homologue of a glutamate transporter have been determined (Yernool et al. 2004), and all reveal structures that are consistent with an alternating-access scheme. Therefore, despite the mounting evidence that there is a fine

separation between transporters and channels, at present alternating access models are still the favoured way to describe the kinetics of most transporters.

1.4.4 The anion exchanger, AE1

AE1 (previously known as band 3 or capnophorin) mediates electroneutral Cl^- /HCO_3^- exchange, and is expressed at highest levels in the plasma membranes of red blood cells. It belongs to the SLC4 family (Romero et al. 2004), which together with the SLC26 family forms the two major families of bicarbonate exchangers in the genome. In addition to the functional similarities between AE1 and members of the SLC26 family, some inhibitors of AE1 mediated exchange have also been shown to have an effect on SLC26 members. For example the stilbene inhibitor DIDs, inhibits SLC26A6 transport (Lohi et al. 2003), and Niflumic acid has been shown to abolish the prestin associated NLC (Rybalchenko and Santos-Sacchi 2003).

However AE1 appears to have a different topology and structure from SLC26 members. Human AE1 consists of 911 amino acids. As for SLC26 members both the N- and C- termini are cytoplasmic, but the currently predicted topology for AE1 has 13 transmembrane domains (Zhu et al 2003) compared with the 12 predicted transmembrane domains of prestin. Furthermore unlike the monomeric SLC26 proteins AE1 is dimeric (Wang et al. 1994).

AE1 was one of the first transporters to be described with an alternating-access type mechanism (Figure 1.5A) (Gunn and Frohlich 1979, Jennings 1982). Since the rate of net Cl^- flux across the membrane is <0.1% of the rate of Cl^- exchange, it was assumed that a change in conformation from an inward-facing (E_i) to an outward-facing (E_o) state could only occur with an ion bound. However more

recent evidence suggests that including slippage, (the transition $E_i \rightarrow E_o$ is permitted with no ion bound) in the exchange model gives a more accurate description of the time-course of Cl^-/HCO_3^- exchange (Greco and Solomon 1997).

Several studies indicated that the transport system is intrinsically asymmetric, such that more exchanger proteins face the inside than the outside, even when the concentration of substrate is equal on both sides of the membrane (Gunn and Frohlich 1979, Jennings 1982, Knauf and Mann 1984, Gasbjerg and Brahm 1991). The application of the alternating-access model has enabled the asymmetry to be quantified, and added further support to the principle of alternating-access (Knauf and Brahm 1989). Recent evidence showed that exchange of intracellular HCO_3^- for extracellular Cl^- was faster than exchange of extracellular HCO_3^- for intracellular Cl^-, and thus that AE1 exhibits different asymmetric properties with respect to its substrates (Knauf et al. 2002). This indicated that AE1 might be able to mediate active transport. The unidirectional $^{56}Cl^-$ efflux was unaffected by changes in membrane potential, either during Cl^-/Cl^- or Cl^-/HCO_3^- exchange, which supported the hypothesis that the translocation steps in the transport cycle were voltage-independent (Jennings et al. 1990).

1.4.5 The Na,K -ATPase

The Na, K-ATPase is a primary active transporter found in the plasma membrane of most animal cells (for reviews see Apell and Karlish 2001, and Apell 2004). It mediates electrogenic transport of sodium and potassium and consists of two different subunits, α and β. The α-subunit contains about 1000 amino acids, forming

10 transmembrane domains, whilst the β-subunit contains about 300 amino acids and has only one transmembrane segment.

The Na, K-ATPase exchanges 3 Na^+ ions for 2 K^+ ions per ATP hydrolysed, such that the movement of Na^+ is associated with phosphorylation by ATP of the transporter and K^+ movement is associated with dephosphorylation of the transporter. Like AE1, it was also one of the first transporters to be described by an alternating-access type reaction scheme. The reaction cycle that is currently thought to represent a good approximation to the actual mechanism of the pump is more complex than for AE1. It originates from work by Albers (1967) and Post et al. (1972) and is known as the Post-Albers cycle (Lauger 1991) (Figure 1.5B). Unlike the transport model for AE1 a main feature of the Post-Albers cycle is the existence of occluded states, in which the Na^+ or K^+ ions are unable to access either the internal or external media.

Since under physiological conditions transport is electrogenic, steady-state fluxes can be investigated using electrophysiological techniques. The pump current was shown to be voltage-sensitive, with a sigmoid shape, for high concentrations of extracellular Na (Na_e) (Gadsby and Nakao 1989), but became almost voltage-independent when Na_e was removed (Nakao and Gadsby 1989). This indicated that most of the voltage-dependence arose from binding of Na_e. This was consistent with earlier work, which showed that in the absence of K^+ on either side of the membrane, a voltage perturbation caused a transient charge translocation (Nakao and Gadsby 1986). Since in the absence of K^+ the normal transport cycle of the Na,K-ATPase is interrupted and constrained to mediate only electroneutral Na-Na exchange, this indicated that the translocation of Na included a voltage-dependent transition.

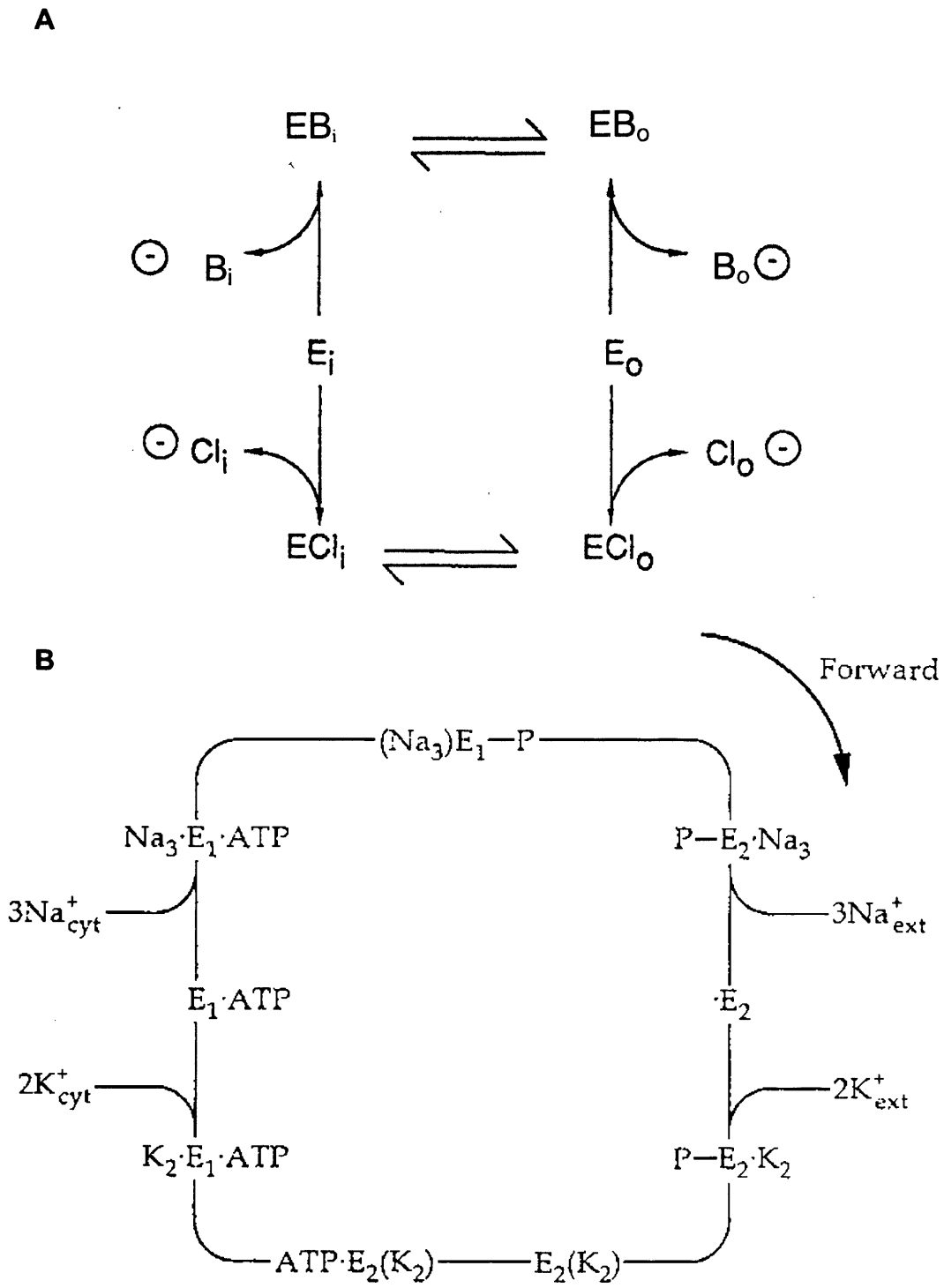

Figure 1.5. Alternating-access transport models. A) Ping-Pong model for AE1 taken from (Knauf and Brahm 1989). The transition $E_i \rightarrow E_o$ is not permitted unless a chloride or bicarbonate ion is bound. B) The Post-Albers cycle for the Na,K-ATPase (taken from Lauger 1991). The states $(Na_3)E_1$-P, ATP-$E_2(K_2)$, $E_2(K_2)$ are occluded states.

The amount of charge moved (Q) during these transients had a sigmoidal dependence on voltage (V). Further experiments performed in the absence of K^+ showed that the Q(V) curve was shifted to more positive potentials as Na_e was increased (Rakowski 1993) and the unidirectional efflux of ^{22}Na mediated by the electroneutral Na-Na exchange had a sigmoidal dependence on voltage, which was also shifted to more positive potentials as Na_e was increased (Gadsby et al. 1993).

These results led to the formulation of the access channel model (Rakowski 1993, Sagar and Rakowski 1994), which proposed that the binding site for Na_e lies within an access channel that crosses the membrane dielectric, such that the concentration of Na at the binding site is voltage-dependent, and therefore the rate of Na_e binding is voltage-dependent.

Thus like prestin the Na,K-ATPase produces transient currents in response to voltage-perturbations. However whereas the decay time of the transient current produced by prestin was only a few μs, the transient current produced by the Na, K-ATPase had both a fast and a slow component. The slow component had a decay time of a few ms, assumed to be a result of the rate-limiting slow occlusion step following Na_e binding and produced the sigmoidal Q(V) curve described above. The fast component decayed within 4μs, preceded the slow component and produced a sigmoidal Q(V) curve that was less steeply dependent on voltage than the slow component (Hilgemann 1994), but also depended on $[Na_e]$. Since three Na^- ions have to bind before being occluded, the fast component was assumed to reflect the binding of the first two Na^+ ions, which are not followed by the occlusion step. This fast component produced an associated NLC that was also shifted to more positive potentials as Na_e was increased (Lu et al. 1995). Thus whilst for prestin the position

of the Q(V) curve depends on $[Cl_i]$, for the Na,K-ATPase the position of the Q(V) curves produced by both the slow and fast components depends on $[Na_e]$.

1.5 Comparison of Prestin with Ion Channels

Although there is no evidence that prestin acts as an ion channel, its dependence on intracellular chloride can be compared with several ion channels whose activation depends on the concentration of certain extrinsic ions. The most well known example is the large conductance calcium-activated K^+ channels referred to as BK (or Slo1) channels. The main feature of these channels is that they are activated in a synergistic manner by both intracellular calcium (Ca_i) and depolarisation. The steady-state open probability P_{open}, has a sigmoidal dependence on voltage, which is shifted to more depolarised potentials as $[Ca_i]$ is decreased. Like the superfamily of voltage-gated K^+ channels these channels also contain the intrinsic S4 voltage sensor, which is assumed to confer all the voltage-dependence of the channel. Binding of Ca_i is believed to be voltage-independent and the Ca-sensing and voltage-sensing processes are believed to function independently of each other (Magelby 2003).

The ClC chloride channels, are activated by both voltage and extracellular chloride (Cl_e). However unlike the BK channels, the chloride-sensing and voltage-sensing functions are not independent, rather Cl_e is required to confer voltage-dependence, such that they use chloride ions as the voltage-sensor instead of an intrinsic voltage-sensing domain (Pusch et al. 1995). Since this is similar to prestin, which has also been proposed to use chloride as a voltage-sensor, the gating mechanism of ClC-channels is described in more detail below.

1.5.1 ClC Channels

ClC channels are members of a family of chloride selective ion channels found in many organisms including bacteria and mammals (for reviews see Maduke et al. 2000, Estevez and Jentsch 2002, Dutzler 2004). They are dimers composed of two homologous subunits, which each form an independently gated pore and are therefore often described as "double-barrelled". The two pores can also be closed together by a slower, common gate. Each subunit has 17 intramembrane (though not necessarily transmembrane) α-helices, and both the N- and C- termini are cytoplasmic. The two most studied ClC channels are ClC-0 from the torpedo electric organ, and ClC-1 from mammalian muscle cells. In particular ClC-0 has been studied extensively since it has a relatively high conductance (~10pS) compared with other family members, which allowed single channel measurements.

The channel activation of ClC-0 was shown to depend on both voltage and the concentration of extracellular chloride (Cl_e) (Pusch et al. 1995). The fast gate on each pore was opened by depolarisation, with the dependence of P_{open} on transmembrane voltage V described by the Boltzmann distribution. As [Cl_e] was reduced and replaced with sucrose the activation curve was shifted to more positive potentials, with its slope unchanged. Changing the concentration of intracellular chloride (Cl_i) had no effect. When Cl_e was replaced with other permeable halides, the shift in the activation curve was abolished, or reduced, whereas when Cl_e was replaced with impermeable ions (including gluconate, methane sulphonate and sulphate) the shift in the activation curve was similar to that produced with sucrose replacement. These results indicated that only permeant anions affect gating and led Pusch et al. (1995) to propose that a single chloride ion binding to a site in the pore, only accessible from

the external medium was required for channel opening. Thus for a constant [Cl_e] the availability of extracellularly derived chloride at the binding site depends on the transmembrane electric field, which confers the observed voltage dependence of gating.

This proposal was tested using single-channel analysis (Chen and Miller 1996). In agreement with Pusch et al. (1995) activation curves were shifted to more positive potentials as [Cl_e] was reduced, (~40mV per 10-fold decrease) however the shift in the hyperpolarising direction saturated as [Cl_e] was increased above 150mM. An increase in [Cl_e] led to an increase in the opening rate, but had very little effect on the closing rate, which suggested that Cl_e acts on the closed channel, and supported the idea that Cl_e is required for channel activation. However whilst the opening rate was shown to be voltage-dependent Cl_e binding was voltage-independent, in contradiction to the Pusch model. This observation combined with the observation that the shift in the activation curve saturated at high [Cl_e], led Chen and Miller (1996) to propose a refined model for gating in which Cl_e binds first at the external end of the conduction pathway, and a subsequent conformational change moves the Cl_e ion across the membrane in the major charge translocation step. In this case the translocation step, rather than Cl_e binding confers the voltage-dependence. The time-constant for the fast gating process in CLC-0 was found to decrease, approaching ~100μs without saturating, as the membrane potential was made more positive up to +200mV(Accardi and Pusch 2000). This was consistent with the model proposed by Chen and Miller (1996) in which binding is voltage-independent, and showed that the translocation event could occur very rapidly.

The channel activation of ClC-1 was also shown to depend on voltage and $[Cl_e]$ in a similar way to that of ClC-0 (Rychkov et al. 1996). Additionally raising intracellular pH cause the activation curve to be shifted to more positive potentials. As for ClC-0, when the effects of different anions on the gating of ClC-1 were investigated, it was found that all permeable anions tested (including bromide, nitrate and iodide) were able to gate the channel, whilst a group of impermeable anions (including gluconate and glutamate) were unable to gate the channel. However in contrast with ClC-0 a third group of anions (including cyclamate and methanesulfonate) were found that although impermeable were able to affect gating (Rychkov et al. 1998). This suggested that the binding site for gating lies external to the selectivity filter, and unlike in ClC-0, the binding site and selectivity filter do not have the same specificities. The fast gating process for ClC-1, was found to be even faster than for ClC-0 with a time constant ~16μs at +200mV (Accardi and Pusch 2000).

1.6 Summary

Prestin has been identified as the motor protein of OHCs. It has a non-linear capacitance that depends strongly on intracellular chloride. Two mechanisms for prestin have been proposed, neither of which include transport. However prestin shares much sequence homology with other members of the SLC26 family in particular SLC26A6, which is a very non-specific transporter. Thus although no transport function has yet been shown for prestin, the possibility remains that prestin may have some transport properties.

Members of the both the SLC26 and SLC4 family mediate counter transport of anions. AE1, which is the most studied member of either family, mediates transport through an alternating-access mechanism. The Na,K-ATPase is another well studied transporter that is thought to employ an alternating-access mechanism. For AE1 the movement of ions across the membrane appears to be voltage-independent, whilst for the Na-K-ATPase the binding of Na_e is voltage-dependent. Similar to prestin the gating of the chloride-gated chloride channels, CLC-0 and ClC-1, depend strongly on extracellular chloride. The gating of these channels is thought to occur by voltage-independent binding of Cl_e followed by a voltage-dependent translocation of the chloride ion through the membrane, which leads to channel opening. Thus the movement of ions through the membrane can either involve no voltage-dependent transitions, or voltage-dependent binding of ions through an access channel, or voltage-dependent translocation of a bound ion.

Chapter 2

Materials and Methods

2.1 Model Simulations

All models used in this thesis could be described by simple kinetic diagrams, consisting of the intermediate states of the protein, E_i, and transitions connecting these states. For each transition, referred to as a reaction step, a forward rate constant, and a backward rate constant were chosen. In cases where the model was cyclic, and involved states that bound internal ions, and states that bound external ions, rate constants were chosen to maintain microscopic reversibility under conditions of no applied voltage, and no concentration gradient.

The Q-matrix method (Colquhoun and Hawkes 1995) was used to simulate; transient currents in response to a voltage-step, Q(V) curves over the range –200mV to +200mV, and I(V) curves over the range –200mV to +200mV. All simulations were performed in Matlab 6.5 (The MathWorks Inc.).

Q(V) curves were differentiated in Igor Pro v.4 (WaveMetrics Inc.) to give NLCs over the range –200mV to +200mV, and fit with the derivative of the Boltzmann function (equation 1.4) to give apparent values for the parameters V_o, Q_{max}, C_{pk} and β.

2.1.1 Q-Matrix method

We consider the simplest two-state model, in which a protein can only exist in either state 1 (E_1) or state 2 (E_2), where E_1 and E_2 are assigned to represent the fraction of proteins in state 1 and state 2 respectively. For a transition $E_1 \Leftrightarrow E_2$ the rate

constant for the transition from state 1 to state 2 can be denoted as q_{12}, and the rate constant for the transition from state 2 to state 1 can be denoted as q_{21}. This gives the following differential equations

$$\frac{dE_1}{dt} = -q_{12}E_1 + q_{21}E_2 \qquad (2.1)$$

$$\frac{dE_2}{dt} = q_{12}E_1 - q_{21}E_2 \qquad (2.2)$$

This can be written in matrix notation as

$$\frac{d}{dt}(E_1 \quad E_2) = (E_1 \quad E_2)\begin{pmatrix} -q_{12} & q_{12} \\ q_{21} & -q_{21} \end{pmatrix} \qquad (2.3)$$

This can be expanded for a model with n states, with the occupancy of state i, given by E_i. In general for a model with n states, and various transitions between these states, the transition rate for a transition from state i to state j can be denoted q_{ij}. All the transition rates for a particular model can then be specified in an n x n square matrix, called the Q-Matrix, $\overline{Q}$. First q_{ij} is entered in the ith row and jth column, which fills the whole matrix apart from the diagonal elements where i=j. The diagonal elements are filled with the value required to make the sum of the entries of each row zero.

It is important to note that the transition rate of a reaction does not always equal the rate constant for that reaction. For example when a reaction involves binding of an ion, the rate constant is the same regardless of the concentration of the ion, whilst the transition rate depends on the concentration of the ion. If only one ion binds then the transition rate is the product of the rate constant and the ion concentration.

If $\bar{p}(t)$ is a row vector with n elements that contain the fraction of proteins in each of the n states at time t,

$$\bar{p}(t) = (E_1(t) \quad E_2(t) \quad . \quad . \quad E_n(t)) \tag{2.4}$$

and the corresponding vector of derivatives is

$$\frac{d\bar{p}(t)}{dt} = \left(\frac{dE_1(t)}{dt} \quad \frac{dE_2(t)}{dt} \quad . \quad . \quad \frac{dE_n(t)}{dt} \right) \tag{2.5}$$

then the differential equations that describe all transitions can be written as

$$\frac{d\bar{p}(t)}{dt} = \bar{p}(t)\bar{Q} \tag{2.6}$$

In the steady-state the fraction of proteins in each state remains constant, and therefore the derivatives are zero.

$$\bar{0} = \bar{p}(\infty)\bar{Q} \tag{2.7}$$

However if a perturbation is made to alter one or more of the transition rates in $\bar{Q}$, then the fraction of proteins in each state will change. For a system, which includes the binding of an ion, and a voltage-dependent step, such a perturbation could be caused by a change in ion concentration or a change in potential. The occupancies of each state will continue to change until a new steady state is reached. The time course of the occupancies following a perturbation is found by solving equation 2.6, which gives

$$\bar{p}(t) = \bar{p}(0)e^{\bar{Q}t} \tag{2.8}$$

where $\bar{p}(0)$ is the steady-state occupancies of each state before the perturbation is made, and the exponential, $e^{\bar{Q}t}$ is also an n x n matrix.

The exponential of a matrix can be directly evaluated in Matlab, using the 'expm' command, thus the time course of occupancies of each state, following a perturbation can be evaluated.

2.1.2 Simulation of Transient Currents Following a Voltage-Step

Following a voltage-step, the occupancies of all states in a kinetic model will change, until a new steady-state is reached. However only the voltage-dependent transitions, which involve the transfer of charge will produce a measurable current. For a transition from state i to state j, where E_i and E_j are the fraction of proteins in those states respectively, and the forward and backward rate constants are given by k_{ij} and k_{ji} respectively

$$E_i \underset{k_{ji}}{\overset{k_{ij}}{\rightleftharpoons}} E_j$$

then the number of proteins changing from state i to state j per second, referred to as the flux, Φ is given by

$$\Phi(t) = N(k_{ij}E_i(t) - k_{ji}E_j(t)) \qquad (2.9)$$

where N is the total number of proteins. If the transition is voltage-dependent then it has a non-zero dielectric coefficient, α (see Ch.1.4.2 for definition) and the current I(t), produced by the transition is then calculated from the flux

$$I(t) = \alpha e_o \Phi(t) \qquad (2.10)$$

If there is more than one voltage-dependent transition then the total current is the sum of the currents produced by each transition.

In order to simulate I(t) for a particular model the Q-Matrix for the initial steady-state was determined. The initial steady-state occupancies were evaluated by solving equation 2.7 directly with the method described in Colquhoun and Hawkes (1995). Subsequently the Q-Matrix was redefined, with all voltage-dependent transition rates assigned new values, corresponding to the new voltage command. The time course of the occupancies of each state $\overline{p}(t)$ was determined numerically at chosen time points. I(t) was evaluated using equation 2.10. In these calculations N is the total number of prestin molecules. N was assumed to be 10,000 for an OHC patch, and 10^7 for a whole OHC.

2.1.3 Simulation of Q(V) curves

Transient currents were simulated for a staircase voltage-ramp consisting of 1mV steps between –200mV and +200mV. The total charge moved across the membrane, Q, for each step was found by taking the area under each transient. This was evaluated in Matlab by numerical integration (trapezium method). Ideally, to give the best approximation of the actual area under the transient, the time interval between each point on the curve is required to be as small as possible. If the time between each point is too large this will lead to an overestimation of the area. It is also necessary to integrate over a sufficiently long time to ensure that steady-state has been reached, or the area under the transient could be underestimated. However increasing the number of time points led to an increase in computational time. The maximum number of time points allowed to keep the computational time for one set of rate constants within 2 minutes was used. Typically with the rate constants used, time points were at 1μs intervals from 0s to 5ms.

Once the area under each transient had been calculated, the cumulative sum of the charge moved in each step from –200mV to +200mV was calculated to give the Q(V) curve from –200mV to +200mV.

2.1.4 Simulation of I(V) Curves

The Q-Matrix corresponding to –200mV was determined. Equation 2.7 was used to evaluate the steady-state occupancies, $\overline{p}(\infty)$ of each state. The steady-state current $I(\infty)$ is then calculated from the steady state flux $\Phi(\infty)$ over voltage-dependent transitions using equations 2.9, and 2.10. The Q-Matrix was then redefined for voltages at 1mV steps up to +200mV, and $I(\infty)$ evaluated for each voltage, to give the I(V) curve.

2.2 Cell Preparation

2.2.1 Removal of Temporal Bone

Young adult male albino guinea pigs (200-400g) were killed by rapid cervical dislocation. Following decapitation, and the removal of the lower jaw both left and right temporal bones (bullae tympanica), which contain both the middle and inner ear compartments were removed using leverage from dissection scissors. One temporal bone was kept on ice, or in Hepes buffered external solution in the fridge for up to 4 hours, for later dissection. The other bulla was used immediately.

2.2.2 Dissection of the Organ of Corti

The bulla was held between the thumb and forefinger, with the smooth rounded surface facing upwards. Bone cutters were used to crack open the bone to reveal the bony outer shell of the cochlea within. With the open bulla bathed in external solution and viewed under the dissection microscope the bony outer shell of the cochlea was cracked and gently peeled away using forceps, to leave the cochlea exposed. A scalpel was used to cut through the mediolus, connecting the base of the cochlea to the temporal bone, and the cochlea was removed with forceps and placed in a new dish of clean external solution. Under the same dissection microscope, the cochlea was held in place with forceps, and a fine hypodermic needle was used to gently pull away the stria vascularis, leaving the organ of Corti exposed. The organ of Corti was easily identified by the translucent lipid globules in the Hensen's cells. The organ of Corti could then be gently pulled away in strips using the same needle. Most of the cells used in experiments were the longer cells from the first two apical turns.

2.2.3 Dissociation of Cells

Isolated outer hair cells were required for patch-clamp experiments. Thus the strips of organ of Corti were broken up by a process of enzymatic digestion followed by gentle mechanical trituration. All the strips of organ of Corti to be used were sucked up within 40μl of external solution using a Gilson pipette, and placed in a droplet on a new petri dish. Subsequently a 40μl droplet of external solution containing 0.5-1mg/ml trypsin (T4665 from Bovine Pancreas, Sigma) was added, to make the final concentration of trypsin 0.25-0.5 mg/ml. After the cell suspension had been left to incubate for 15 minutes, allowing enzymatic digestion, the total volume

was drawn into a Gilson pipette, pushed out and then drawn up again (trituration). At this point it was assumed that cells were fully dissociated. The total volume was then pushed out again to form a droplet on the recording chamber and left for ~5 minutes to allow cells to settle to the bottom of the chamber. Finally ~600µl of external solution was added to the chamber.

2.3 Solutions

Unless stated otherwise all solutions were checked for pH using a pH meter (Corning Medical and Scientific Instruments, Halstead, UK) and adjusted to pH 7.2-7.25 with NaOH. The osmolarity of solutions was checked using a freezing-point depression osmometer (Roebling, Germany), and adjusted to 310-315 mOsm with D-glucose. All chemicals were obtained from Sigma or BDH. All solutions were made up in the week the experiments were performed, and stored in the refrigerator for up to 4 days. Both the pH and osmolarity of the solutions were checked just before use.

2.3.1 External Solutions

The dissections and experiments were performed in a Na^+Cl^- based Hepes buffered solution (Na-HBS) unless otherwise stated. Since the main purpose of experiments was to investigate the mechanism of prestin, rather than physiological behaviour, the solution was kept as simple as possible to limit the number of ions species in contact with prestin. Both Ca^{2+} and Mg^+ were omitted to ensure there was no concentration gradient of any ion apart from chloride and the anion used to replace it. Furthermore Ca^{2+} was omitted to prevent large calcium-activated potassium currents. These conditions were comparable with those used in previous experiments

made from excised patches (Oliver et al. 2001) and to which the experimental results obtained in this thesis are compared. Although the long-term effect of removing Ca^{2+} from the extracellular medium is not known, it has previously been reported that cells incubated in Ca^{2+}-free medium for up to 60 minutes showed no sign of cell deterioration (Dulon et al. 1990). In Ch 6.3.3 the $Tris^{+}$ based Hepes buffered solution (Tris-HBS) used by Rybalchenko and Santos-Sacchi (2003) was used. For details of these solutions see Table 2.1.

2.3.2 Internal Solutions

Experiments were performed to investigate the effect of different concentrations of intracellular chloride (Cl_i) or extracellular chloride (Cl_e) on the function of prestin. Therefore intracellular solutions had the same cationic composition as the extracellular solution (Na-HBS). This also served to reduce all K^{+} currents. When high [Cl_i] or [Cl_e] solutions were required Na-HBS was used. Where lower [Cl_i] or [Cl_e] solutions were required, chloride was replaced with an equimolar amount of monovalent anions (gluconate or glutamate), or with a lower concentration of divalent anions (sulphate or maleate) to maintain ionic strength. Where divalent anions were used sucrose was used to make up the difference in osmolarity. In Ch 6.3.3 the $Tris^{+}$ and sulphate based solution (Tris-sulphate) used by Rybalchenko and Santos-Sacchi (2003) was used. For details of all internal solutions see Table 2.2.

	Na	K	Tris	Cl	HEPES	EGTA	Glucose	$MgSO_4$	$CaSO_4$
Na-HBS	145	5	-	150	10	1	20	-	-
Tris-HBS*	-	-	~155	140	10	-	-	5	0.2

Table 2.1 Composition of extracellular solutions (mM)

*This solution was made with HCl and made up to pH 7.2 with Tris(OH). Therefore [Tris] is approximate. The same solution was used in Rybalechenko and Santos-Sacchi 2003.

	Na	K	Tris	Cl	Gluconate	Glutamate	Sulphate	Maleate	HEPES	EGTA	$MgSO_4$	Glucose	Sucrose
Gluc-10	145	5	-	10	140	-	-	-	10	1	-	20	-
Gluc-1	145	5	-	1	149	-	-	-	10	1	-	20	-
Gluc-0	145	5	-	0	150	-	-	-	10	1	-	20	-
Sulph-10	145	5	-	10	-	-	70	-	10	1	-	20	70
Sulph-1	145	5	-	1	-	-	74.5	-	10	1	-	20	74.5
Sulph-0	145	5	-	0	-	-	75	-	10	1	-	20	75
Glut-10	145	5	-	10	-	140	-	-	10	1	-	20	-
Mal-10 *	145-185	5	-	10	-	-	-	70-90	10	1	-	20	70
Tris-SO_4 **	-	-	~255	0	-	-	110	-	10	10	2	-	-

Table 2.2 Composition of intracellular solutions (mM).

*The solution was made with maleic acid (sodium salt) and made up to pH 7.2 with NaOH. When 70mM Na-maleic acid was used, the solution had a much lower osmolarity than would be expected if maleate was entirely divalent, and behaved as an ideal solute. Since at pH 7.2 maleate is at least 90% divalent (pKa_1=1.97, pKa_2=6.24 at room temperature, 22-25 ^{0}C), the lower osmolarity was attributed to maleate being an imperfect solute with an activity coefficient <1. Thus in order to try and maintain ionic strength, which depends on activity, 90mM Na-maleic acid was used, which produced the correct osmolarity. The effective concentration of divalent maleate lies between 70mM and 90mM.

** This solution was made with H_2SO_4 and made up to pH 7.2 with Tris(OH). Therefore [Tris] is approximate. The same solution was used in Rybalechenko and Santos-Sacchi 2003.

2.3.3 Perfusion

In some experiments the chamber was continuously perfused with external solution using a peristaltic pump (Minipuls 3, Glison, France). However due to the relatively large chamber volume ~700µl, it was found that cells lasted up to 90 minutes without perfusion. In Ch.6.3.3 the peristaltic pump was used to exchange the Na-HBS bath solution, for Tris-HBS bath solution at ~100µL/min.

In experiments where solutions were exchanged, a 4-barrelled gravity fed manifold applicator, mounted on a Huxley micromanipulator (Huxley-Bertram, Cambridge, UK), and positioned close to the cell was used to locally apply different solutions.

2.4 Recording Methods

Experiments were conducted using the voltage-clamp version of the patch-clamp technique developed by Hamill et al. (1981). This technique enables ion flow across cell membranes to be measured as current whilst the membrane voltage is held under experimental control with a feedback amplifier. Experiments were either performed in the excised inside-out patch or whole-cell configurations. All experiments were performed at room temperature (22-25 °C).

2.4.1 Recording Set Up

A schematic of the recording set up is shown in Figure 2.1. An inverted microscope (Zeiss IM, Oberkochen, W.Germany) was mounted on a vibration-free table within a Faraday cage. A 10X objective was used for initial visualisation of cells and a 40X water immersion objective was used for subsequent seal formation. An Axopatch 200A patch amplifier (Axon Instruments, Foster City, California, US) was

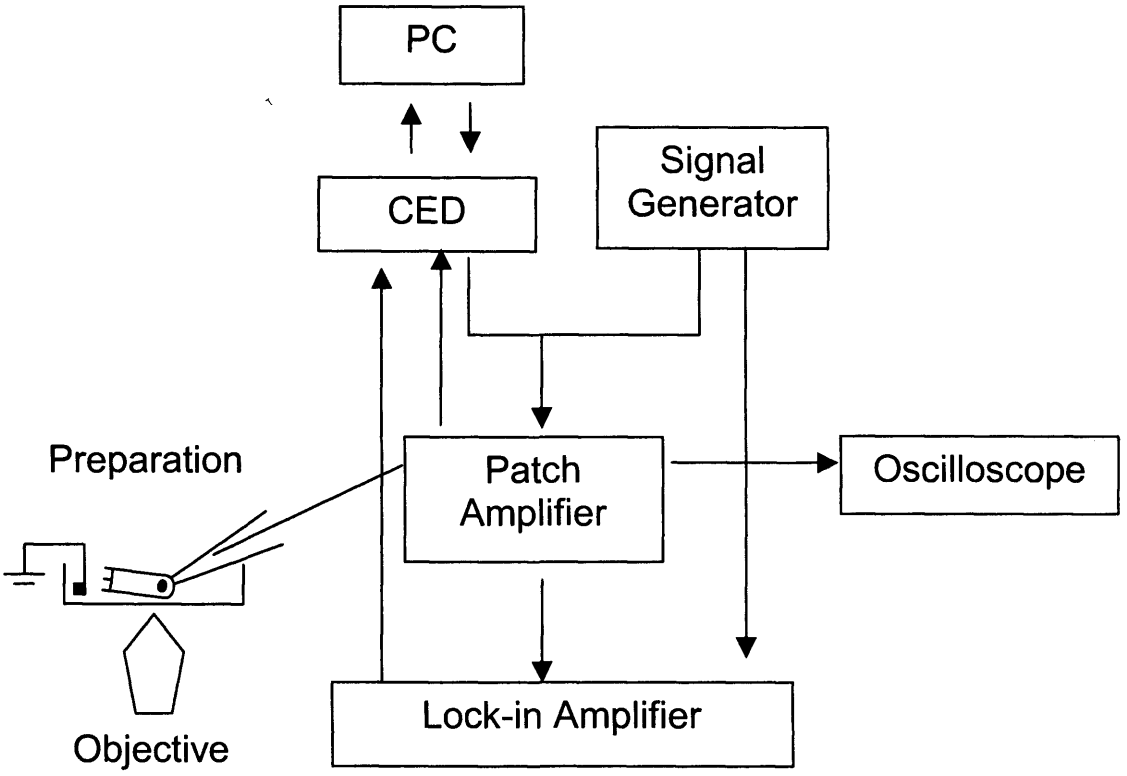

Figure 2.1 Diagrammatic Representation of the Recording Set Up

used in conjunction with a computer based voltage-command generator (see Ch.2.4.6), to clamp the voltage of cells. The patch-amplifier headstage was mounted on a Huxley micromanipulator. In most experiments the chamber was grounded with a AgCl pellet placed directly in the bath. In experiments where chloride-free bath solution was used, a 5% agar salt bridge containing 150mM NaCl was used.

2.4.2 Pipettes

Patch pipettes were fabricated from thin-walled, 1.2mm outer diameter, filamented borosilicate glass (GC120TF, Clark Electromedical, UK) on a two-stage vertical puller (Narishige, Japan). Typically pipettes had a resistance of 3.5-4.5 MΩ measured with Na-HBS. In excised patch experiments pipette tips were coated with ski wax to minimise stray pipette capacitance.

2.4.3 Seal Formation

Positive pressure was applied to the tip of the pipette by mouth before the pipette was lowered into the bath. This ensured the pipette tip stayed clean until it was manoeuvred towards the cell surface using a Huxley micromanipulator. Any pipette offsets were then removed using the pipette offset control on the patch amplifier to zero the current with the command voltage at 0mV. With the positive pressure still on the pipette was pushed against the cell membrane until it was possible to observe the cells' membrane dimpling. At this point the pressure was removed, and gentle suction was applied. This initiated the formation of a seal, which usually also required the application of a negative pipette potential (~-50mV) to reach a seal in excess of 1GΩ (giga-seal). The seal resistance was monitored by continuous administration of a

10mV 'sealing voltage-pulse'. On formation of a giga-seal, the current trace becomes essentially flat apart from fast capacitative transients at the beginning and end of the voltage-pulse. These were minimised, by compensation, using the "fast pipette capacitance compensation" control on the patch amplifier.

For excised patch experiments, seals were formed on the basolateral membrane of OHCs, where there is a high density of prestin. However since it is most difficult to form seals on this part of the cell, and the location of the seal is unimportant in whole-cell experiments, seals were formed on the base of the cell in whole-cell experiments.

2.4.4 Excised Patch Recordings

Once a giga-seal was achieved on the basolateral membrane of the OHC, the patch of membrane enclosed by the pipette tip was excised from the cell so that the inside of the membrane faced the bath solution, forming an excised inside-out patch. In this configuration positive pipette potentials correspond to a hyperpolarisation of the membrane potential (V_m).

$$V_m=-V_{pip} \qquad (2.11)$$

Patches were excised either by sharply pulling the pipette away from the cell or by slowly raising the pipette out of the bath, to pull the cell off the pipette and replacing the pipette in the bath with the pipette-patch assembly intact. In order to maintain the seal, V_{pip} was held at negative potentials, typically –20mV,which corresponds to a V_m of 20mV. Stable excised patches were very difficult to obtain, but in the best cases recordings could be made for up to 20 minutes.

2.4.5 Whole-Cell Recordings

Once a giga-seal on the base of the cell had been formed, the whole-cell configuration was achieved by additional gentle suction to form a hole in the membrane, giving access to the cell interior. Occasionally this happened spontaneously. In this configuration positive pipette potentials correspond to a depolarisation of the membrane potential.

$$V_m=V_{pip} \qquad (2.12)$$

On reaching the whole-cell configuration two additional capacitative transients, attributed to the cell capacitance, appeared at the beginning and end of the voltage-pulse. These were compensated using the whole-cell capacitance and series resistance (R_s) compensation controls on the patch amplifier, which gave estimates for the cell capacitance and R_s.

2.4.6 Voltage-Clamp Protocols

Voltage-clamp protocols were generated by patch-clamp software (WCP 3.5, J.Dempster, Strathclyde University). This program was operated by a personal computer, via an analogue to digital/ digital to analogue interface, CED 1401 (Cambridge Electronic Design, UK). In all experiments the pipette was held at negative potentials between –20mV and –50mV, and the commands involved voltage-ramps, which ranged from -130mV to 100mV, and were 5-5.5s in duration. In whole-cell experiments the first ramp was applied 10s after break-in, to allow time to compensate the capacitative transients, and were repeated every 18s. Data was sampled at 256 Hz. These protocols enabled the non-linear capacitance and the instantaneous I(V) to be determined simultaneously.

2.4.7 Capacitance Measurements

Voltage-ramps were summed with a 2kHz, ~10mV peak-to-peak sinusoidal command voltage, generated by a signal generator. The summed command was fed directly to the headstage, and the current output from the patch amplifier was fed to a lock-in amplifier (Stanford Research SR350). The 2kHz sinusoidal command was also fed directly from the signal generator to the lock-in amplifier to act as a reference signal.

The lock-in amplifier is essentially a phase sensitive detector. It converts the AC current output into a DC signal by multiplying the current output with the reference signal shifted by a chosen phase angle, and passing the output through a low-pass filter to remove the AC component. The remaining DC component is the component of the current output at the reference frequency and the selected phase (Gillis 1995).

The lock-in used had two phase-sensitive detectors, which gave the components of the current output at two phases, which were orthogonal to each other. Therefore the output of the lock-in was recorded in two channels. The piece-wise linear technique (Neher and Marty 1982, Gillis 1995) showed that for small changes in membrane capacitance C_m, or membrane conductance G_m, the phase of the change in current produced by a change in C_m is orthogonal to the phase of the change in current produced by a change in G_m. Thus the phase was set so that one channel was sensitive to changes in C_m and one channel was sensitive to changes in conductance (G_m). Using an electrical model cell, the phase of the lock-in was varied manually until changes in C_m (generated by turning the whole-cell capacitance compensation control) only produced a change in one channel. It was found that only minor adjustments to

the phase were required for real cells, though the phase required for excised patches was completely different from that required for whole-cells.

The capacitance trace was calibrated using a capacitance dither. In the excised patch configuration, a 100fF capacitance dither generated by the WCP 3.5 software, to occur shortly before the beginning of the voltage-ramp, was used to calibrate the capacitance trace. In the whole-cell configuration the current produced was much larger than in excised patches and caused the lock-in to saturate. Therefore a voltage-divider was used to reduced the input to the lock-in by a factor of 100. A 2pF dither generated by manually turning the whole-cell capacitance compensation control was used to calibrate the capacitance trace.

2.4.8 Data Acquisition

Data was acquired with the WCP 3.5 software used to generate the voltage-protocol. Four channels were required to record; the summed command voltage, the current response, and the output from the two channels of the lock-in amplifier. Data could then be converted into '.ABF' files for analysis in Matlab.

2.5 Data Analysis

Data files were read in Matlab, and all primary analysis of individual cells was performed in Matlab. Further analysis was done in Excel and Igor Pro.

2.5.1 Correction for Series Resistance

In the whole-cell configuration the control of V_m by V_{pip} is not actually complete as described by equation 2.12, but depends on the size of the access

resistance between the pipette and the cell interior, which produces a voltage-drop across it. The access resistance is equivalent to R_s since it is in series with the membrane. Thus from Ohm's Law, the actual V_m is given by

$$V_m=V_{pip} - I_mR_s \quad (2.13)$$

where I_m is the membrane current flowing across R_s.

The correction for R_s was conducted offline, in Matlab using the value of R_s estimated from the whole-cell capacitance compensation.

2.5.2 Analysis of I(V) curves

The current response to the voltage-ramp gave the I(V) directly. However since the voltage-ramp was summed with a sinusoid the current response was also sinusoidal. Various methods were tried to remove the sinusoidal component. It was found to be simplest to smooth both the current and voltage traces. The smoothed I(V) curve was found to be identical to the I(V) curve generated with the sinusoidal command voltage switched off.

2.5.3 Analysis of NLCs

The non-linear capacitance was measured directly, using a voltage-ramp. NLCs were fitted with the derivative of a Boltzmann function (B′(V)) to give values for V_o, Q_{max}, β and C_{pk}.

2.5.4 Correction for Liquid Junction Potentials

The potential difference formed at the interface between two solutions of different ionic composition due to the different mobility of various anions and cations

in solution is called the liquid junction potential (LJP). LJPs can cause apparent shifts in the voltage dependence of ionic currents and the NLC when the pipette solution differs from the bath solution or solutions are exchanged during an experiment. Since many of the solutions used contained very low chloride, the LJPs ranged from 5.1mV to 11mV, therefore corrections for these potentials were made using the methods described below.

Excised Patch Configuration

In the excised patch configuration the pipette solution was identical to the bath solution. Therefore when the pipette was lowered into the bath there was no LJP. At this point all other pipette offsets were removed. Subsequently different solutions were applied locally to the patch causing LJPs to develop (Figure 2.2).

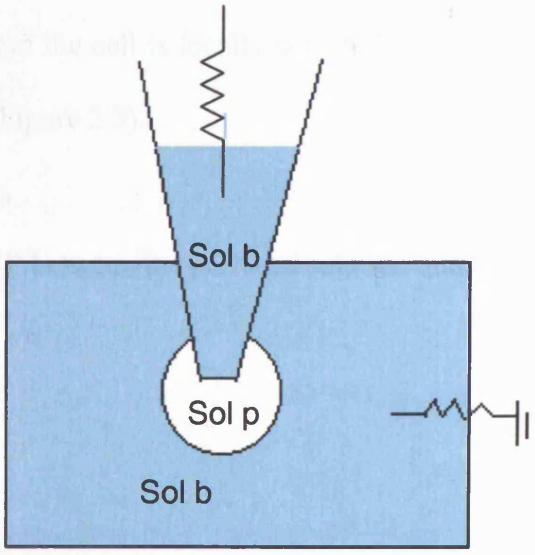

Figure 2.2. Schematic for excised patch configuration. The solution in the pipette is the same as in the bath, solution b. The patch is locally perfused with a different solution, solution p.

If the solution in the pipette is the same as the bath solution, solution b, and the solution applied by local perfusion to the patch is solution p, then the true membrane potential is given by

$$V_m = -V_{pip} - V_{bp} \quad (2.14)$$

Where V_{bp} is the LJP between the bath solution to the perfused solution.

Whole-Cell Configuration

In the whole-cell configuration the pipette contained intracellular solution, which was often different from the bath solution. Therefore when the pipette was lowered into the bath there was an LJP present. This was compensated for by adjusting the pipette offset but must be corrected for. If the intracellular solution is solution i, and the bath solution is solution b, then the true membrane potential is given by

$$V_m = V_{pip} - V_{bi} \quad (2.15)$$

Where V_{bi} is the LJP between the bath solution and the intracellular solution.

If the solution around the cell is locally perfused with solution p this causes a further change in the LJP (Figure 2.3).

$$V_m = V_{pip} - V_{bi} - V_{pb} \quad (2.16)$$

Where V_{pb} is the LJP between the perfused solution and the bath solution.

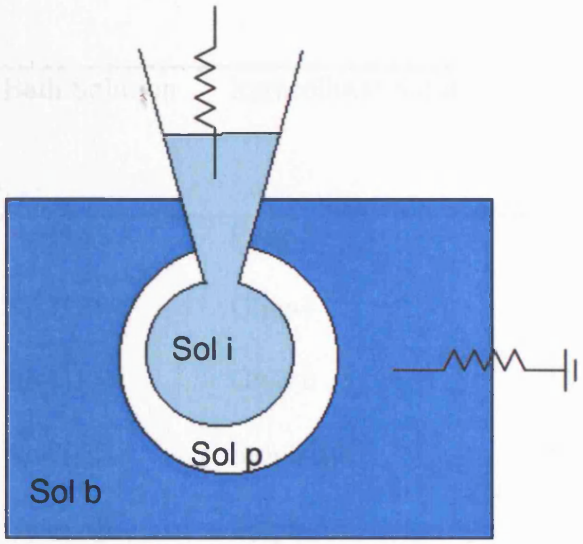

Figure 2.3. Schematic for whole-cell configuration. The intracellular solution, solution i, is different from the bath solution, solution b. The whole cell is locally perfused with a different solution, solution p.

LJPs were calculated off-line using a windows version of JPCalc (Barry 1993) in Clampex 7.0 (Axon Instruments, Inc, USA), which uses a generalised form of the Henderson Equation to calculate LJPs. This equation requires knowledge of both the valency and mobility of each ion in the solution. Values for LJPs between the bath solutions listed in table 2.1 and the intracellular solutions listed in table 2.2 are given in table 2.3.

Bath Solution	Intracellular Solution	LJP(V_{bi}) (mV)
Na-HBS	Gluc-10	9.8
Na-HBS	Gluc-1	10.6
Na-HBS	Gluc-0	10.7
Na-HBS	Sulph-10	5.6
Na-HBS	Sulph-1	6.0
Na-HBS	Sulph-0	6.0
Na-HBS	Glut-10	11
Na-HBS	Mal-10	7.4 *
Tris-HBS	Tris-SO_4	5.1

*LJP for 145mM Na/ 70mM Maleate

Table 2.3 Liquid junction potentials formed between bath solutions and intracellular solutions.

Chapter 3

Modelling Prestin: Chloride as the Voltage-Sensor

3.1 Introduction

The dependence of prestin associated non-linear capacitance (NLC) on intracellular chloride (Cl_i) has been established in previous studies (Oliver et al. 2001, Fakler and Oliver 2002, Rybalchenko and Santos-Sacchi 2003). Unfortunately the details of the experimental observations of these studies, which investigated the role of Cl_i, were contradictory. Oliver et al. (2001) found that when Cl_i was totally removed and replaced with sulphate, the NLC was completely abolished whereas Rybalchenko and Santos-Sacchi (2003) showed that the magnitude of the NLC was almost unaffected when Cl_i was completely replaced with sulphate.

There are several possible reasons for this, which are investigated in Ch.5 and Ch.6. At this stage it is assumed that since the results presented by Oliver et al. (2001) were obtained using the excised patch configuration of the patch clamp technique where $[Cl_i]$ can be accurately controlled, they best reflect the dependence of prestin on $[Cl_i]$.

The key experimental observations made in the excised patch configuration were (Oliver et al. 2001, Fakler and Oliver 2002):

1) The V_o of the NLC shifted to a more positive membrane potential (V_m) as $[Cl_i]$ was decreased (Figure 1.4A).
2) The magnitude of the shift in V_o was 40mV per ten-fold decrease in $[Cl_i]$.
3) Q_{max} and C_{pk} decreased as $[Cl_i]$ was decreased.
4) When Cl_i was completely removed, the NLC was abolished.

5) The NLC was unaffected by changes in extracellular chloride (Cl_e).

6) No change in β was observed as [Cl_i] was decreased.

These observations suggested that intracellular chloride ions act as the voltage-sensor, such that a chloride ion is pushed across the membrane when V_m is hyperpolarized, thereby underlying the voltage-dependent charge movement, which can be detected as a transient current in response to a voltage-step or as a NLC. The apparent absence of any dependence on [Cl_e] has led to the simplest proposal that prestin acts as an incomplete transporter, shuttling chloride across the membrane without allowing it to dissociate at the extracellular surface (Oliver et al. 2001).

The aim of this chapter is to find a model that can reproduce the key experimental observations described above. Whilst the previously proposed, incomplete transporter model for prestin is shown to be inadequate, a complete transporter model of prestin is shown to give a closer reproduction of the experimental observations.

3.2 Methods

Simulations were performed in Matlab. For more details see Ch 2.1. All NLCs were simulated for a patch containing 10,000 prestin molecules.

3.2.1 Definitions

The following definitions are used in Ch.3 and Ch.4:

Ei: This notation is used to label each of the different states in kinetic models. It is also assigned to represent the fraction of molecules in that state.

Ei.A: The point indicates that an anion A, is bound to the state Ei. For example if a chloride ion is bound to the state E1, this bound state would be labelled 'E1.Cl'.

Boltzmann Parameters: The parameters, Q_{max}, V_o, and β, which appear in the derivative of the Boltzmann distribution (B'(V)) used to fit the NLCs (equation (1.4)) are referred to as the Boltzmann parameters. C_{pk}, which is calculated from Q_{max} and β (equation (1.5)) is also referred to as a Boltzmann parameter.

Apparent β: In all models a value for β was chosen to generate the NLCs. However in several cases the β used to generate the NLCs was different from the β of the NLCs produced. In these cases the value for β found by fitting the B'(V) to the NLCs produced was termed the apparent β.

3.3 Results

3.3.1 Model 1: An Access Channel Model

It has been suggested that prestin works as an incomplete transporter using intracellular chloride (Cl_i) $ions_i$ as a voltage sensor without releasing chloride on the extracellular side (Oliver et al. 2001). The simplest way to describe this model is with a 2 state 'access channel' model (Figure 3.1), reminiscent of that described for the Na^+/K^+-ATPase (Rakowski 1993, Sagar and Rakowski 1994). The protein is considered to have a half-pore facing the intracellular medium, so that an ion moving into the pore will experience part of the voltage drop across the membrane (V_m). This leads the effective affinity of chloride at the Cl^- binding site to depend on V_m, and would cause a change in V_m to have kinetically the same effect as a change in $[Cl_i]$.

This model can be expressed as a reaction scheme (Figure 3.1B), where E0 and E1.Cl are the proportion of prestin in the unbound or bound state respectively.

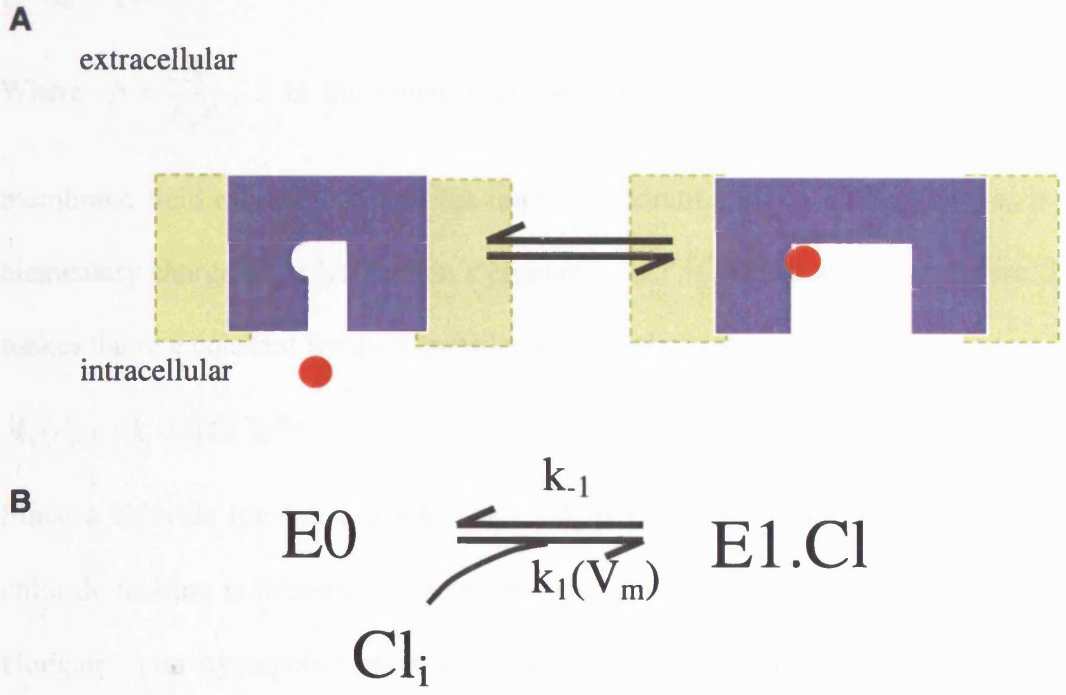

Figure 3.1. Illustration of an access-channel model. A) Prestin changes from a contracted to an expanded state when a chloride ion moves to a binding site inside the pore. B) The reaction scheme used to describe this model. Prestin changes from its initial unbound state E0 to its bound state E1.Cl. The forward rate ($k_1(V_m)$) of this reaction depends on V_m and $[Cl_i]$. The backward rate (k_{-1}) is independent of V_m, and $[Cl_i]$, and simply reflects the rate of dissociation of Cl_i from the chloride binding site.

If chloride ions can reach the binding site by diffusion through the pore then the effective concentration of chloride at the binding site ($[Cl_i]_{bs}$) depends on both the concentration of chloride in the intracellular medium ($[Cl_i]$) and the electric potential difference between the intracellular medium and the binding site. The equilibrium

distribution of chloride between the internal medium ($[Cl_i]$) and the binding site ($[Cl_i]_{bs}$) can be described by a Boltzmann expression:

$$[Cl_i]_{bs} = [Cl_i]e^{\beta V_m} \quad (3.1)$$

Where $\beta = \frac{z\delta e_o}{k_B T}$, z is the valence of the chloride ion, δ is the fraction of the membrane field crossed between the internal medium and the binding site, e_o is the elementary charge, k_B is Boltzmann's constant and T is the absolute temperature. This makes the rate constant for the forward reaction voltage-dependent.

$$k_1(V_m) = k_1(0)[Cl_i]e^{\beta V_m} \quad (3.2)$$

Since a chloride ion has a valence, z = –1, **β is negative** and the forward rate of chloride binding is increased by hyperpolarising the membrane. OHCs are known to elongate upon hyperpolarisation, corresponding with an increase in area (Ashmore 1987, Adachi and Iwasa 1999), therefore we assume that chloride binding results in a conformation change of prestin into an expanded state.

In simulations β was chosen to be $-0.033mV^{-1}$, which corresponds to a chloride ion moving across ~0.8 of the membrane and is comparable with previous measurements (Gale and Ashmore 1997b). The dissociation rate k_{-1} was assumed to be fast and chosen to be $10^5 s^{-1}$, which is comparable to known dissociation rates for fast binding and release, where binding from the aqueous phase is diffusion-controlled (Lauger and Apell 1988, Hille 1992). $k_1(0)$ was varied over a range of values between 10^4 and $10^8 M^{-1}s^{-1}$.

This access channel model produces a NLC, which depends on $[Cl_i]$, in that the V_0 of the NLC depends on $[Cl_i]$ (Figure 3.2). However unlike the experimental observations there is no change in C_{pk} or Q_{max} when $[Cl_i]$ is reduced. Furthermore the

shift in V_0 at reduced $[Cl_i]$ is in the hyperpolarising direction (~-70mV per ten-fold reduction in $[Cl_i]$), which is opposite to that observed. Although the absolute position of V_0 is affected by the value of $k_1(0)$, the magnitude and direction of the shift in V_0 for a 10-fold reduction in $[Cl_i]$ is unaffected. It can be shown that the same magnitude and direction of shift in V_0 is produced for all possible combinations of $k_1(0)$ and k_{-1}.

In this model the charge transferred across the membrane ($Q(V_m)$) in response to a perturbation in either V_m or $[Cl_i]$ is proportional to the increase in the amount of prestin in the state E1.Cl. Therefore $Q(V_m)$ is proportional to the steady-state proportion of E1.Cl at a given V_m, given by

$$E1.Cl = \frac{k_1(V_m)}{k_1(V_m) + k_{-1}} \tag{3.3}$$

As $k_1(V_m)$ increases such that $k_1(V_m) >> k_{-1}$, E1.Cl → 1. Therefore Q_{max} loosely corresponds to the condition that all the prestin molecules are in the state E1.Cl. Assuming that more chloride ions than prestin molecules are present even at very low $[Cl_i]$, then for any $[Cl_i]$, $k_1(V_m)$ can be made large enough to force all the prestin molecules into the state E1.Cl. Therefore no decrease in C_{pk} or Q_{max} can be observed.

V_0 occurs when half the maximal charge has been transferred. This corresponds to the case where half the prestin molecules are in the state E1.Cl, and half are in the state E0. Equation (3.3) leads to the following expression for V_0:

$$V_o = \frac{1}{\beta}\ln\left(\frac{k_{-1}}{k_1(0)[Cl_i]}\right) \tag{3.4}$$

Thus the shift in V_0 due to a change in $[Cl_i]$ from a first concentration, $[Cl_i]_1$ to a second concentration, $[Cl_i]_2$ is given by

$$\Delta V_o = \frac{1}{\beta}\ln\left(\frac{[Cl_i]_1}{[Cl_i]_2}\right) \tag{3.5}$$

The derivations for equations (3.3)–(3.5) are shown in Appendix 1. A similar derivation for the access channel of the Na^+/K^+-ATPase was shown by Rakowski (1993).

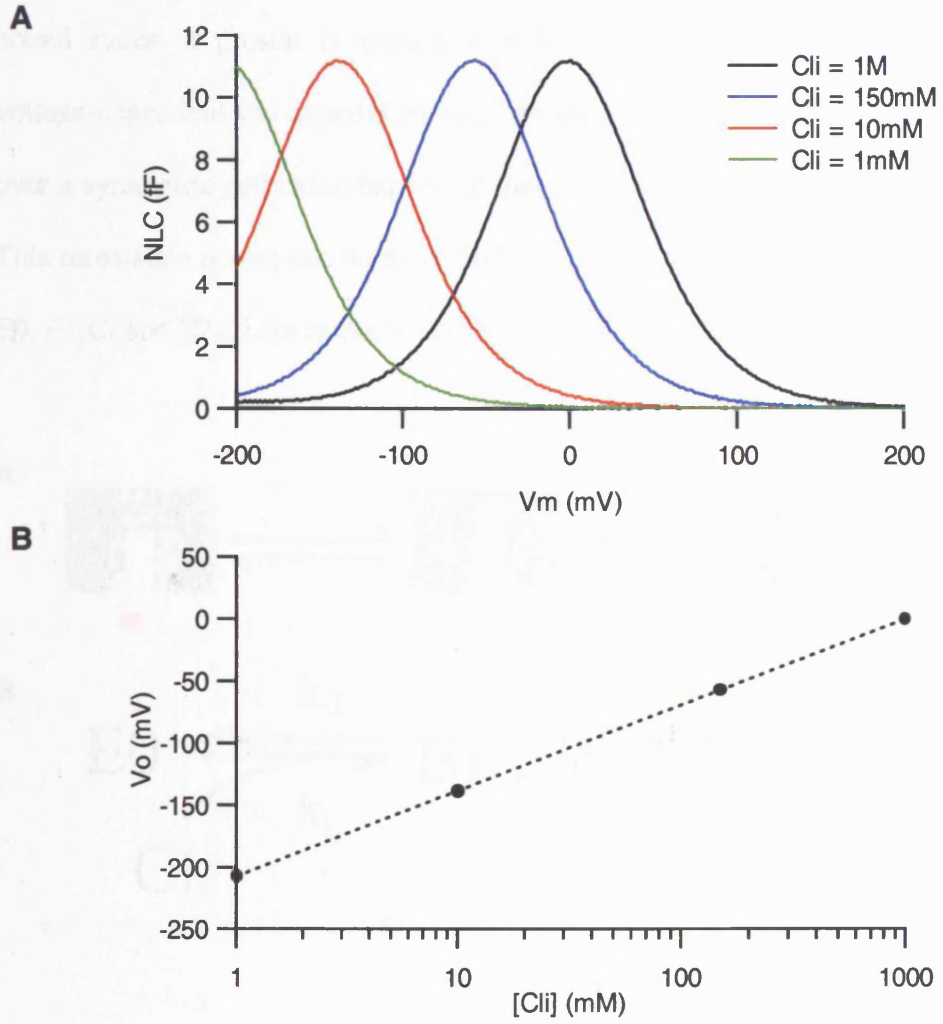

Figure 3.2. Effect of $[Cl_i]$ on the NLC produced by an access channel model. In this example $k_1(0)=10^5M^{-1}s^{-1}$, $k_{-1}=10^5s^{-1}$. A) NLC depends on the $[Cl_i]$. There is no change in C_{pk}, Q_{max} or β as $[Cl_i]$ is decreased but the V_o of the NLC is shifted to more hyperpolarized potentials. B) V_o shifts by ~-70mV per ten-fold reduction in $[Cl_i]$.

3.3.2 Model 2: A Three-State Model

An extension of the access channel model is a three-state model. The chloride ion binds first at the mouth of the pore and is then translocated across the membrane to a second site at the top of the pore (Figure 3.3). Since the transition between the bound states of prestin is associated with charge translocation this step must be voltage-dependent and depends on V_m. Consequently this step is treated as a transition over a symmetric activation barrier, so that it is voltage-dependent in both directions. This three-state model can be described with a reaction scheme (Figure 3.3B), where E0, E1.Cl and E2.Cl are respectively the proportion of prestin in that state.

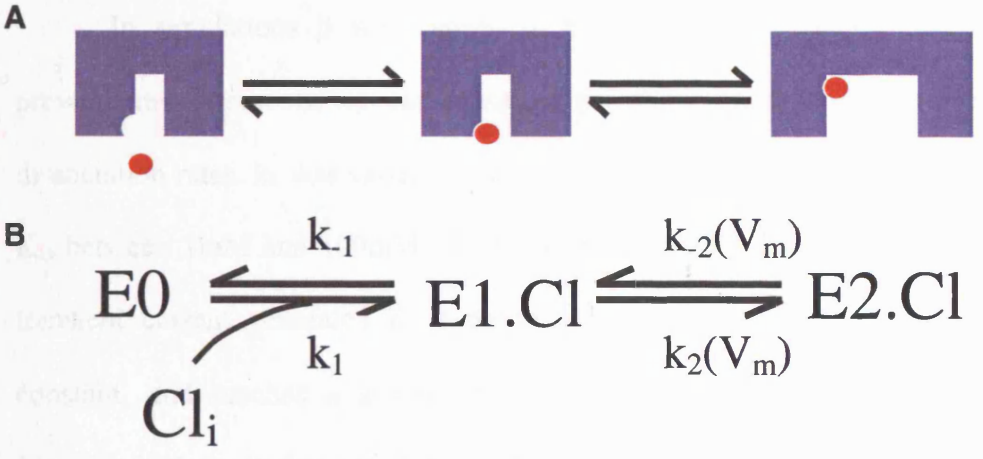

Figure 3.3. Illustration of a three-state model. A) Prestin changes from a contracted to an expanded state when a chloride ion moves from the first binding site at the mouth of the pore to a second site at the top of the pore. B) The reaction scheme used to describe this model. In the first step prestin changes from its initial unbound state E0 to an intermediate bound state E1.Cl. The forward rate depends on $[Cl_i]$, whilst the backward rate (k_{-1}) is a constant, and simply reflects the rate of dissociation of Cl_i from the chloride binding site. In the second step the chloride ion moves through the membrane to the second binding site. Both the forward (k_2) and backward (k_{-2}) rate constants depend on V_m.

The dissociation constant for the first step is given by

$$K_D(Cl_i) = \frac{k_{-1}}{k_1} \qquad (3.6)$$

Both the forward and backward rate constants of the second step are voltage-dependent, and depend on V_m.

$$k_2(V_m) = k_2(0)e^{\frac{\beta V_m}{2}} \text{ and } k_{-2}(V_m) = k_{-2}(0)e^{-\frac{\beta V_m}{2}} \qquad (3.7)$$

Since hyperpolarisation increases the forward rate of the transition E1.Cl→E2.Cl, and OHCs elongate on hyperpolarisation, we assume that this transition results in a conformational change of prestin into an expanded state.

In simulations β was chosen to be $-0.033mV^{-1}$, which is comparable to previous measurements. k_{-1} was chosen to be $10^5 s^{-1}$, which is comparable to known dissociation rates. k_1 was varied between 10^6 $M^{-1}s^{-1}$ and 10^8 $M^{-1}s^{-1}$ to give values for K_D between 1mM and 100mM. Previous experimental results have shown that the transient current generated in response to a voltage-step has a fast decay time-constant, and reaches a steady-state within 300μs (Gale and Ashmore 1997b). Therefore relatively fast values for $k_2(0)$ and $k_{-2}(0)$ were tested to reflect this. $k_2(0)$ and $k_{-2}(0)$ were varied between 10^3 s^{-1} and 10^5 s^{-1}.

The three-state model produces similar results to the access channel model. There is no decrease in C_{pk} or Q_{max} when $[Cl_i]$ is reduced and the shift in V_o in response to reduced $[Cl_i]$ is in the hyperpolarising direction (Figure 3.4). The main difference between the two models is that in the three-state model V_o saturates at high $[Cl_i]$. This can be shown to be true for all possible combinations of rate constants.

In the three-state model the charge transferred across the membrane ($Q(V_m)$) is proportional to the increase in the amount of prestin in the state E2.Cl given by,

$$E2.Cl = \frac{1}{1+\left(\frac{k_{-2}}{k_2}\left(1+\frac{k_{-1}}{k_1[Cl_i]}\right)\right)} \tag{3.8}$$

As $k_2(V_m)$ increases such that $k_2(V_m) >> k_{-2}(V_m)$, E2.Cl→1. Therefore Q_{max} loosely corresponds to the condition that all the prestin molecules are in the state E2.Cl. Assuming that $k_2(V_m)$ is not limited and that more chloride ions than prestin molecules are present even at very low $[Cl_i]$, $k_2(V_m)$ can be made large enough to force all the prestin molecules into the state E2.Cl at any concentration. Therefore no decrease in C_{pk} or Q_{max} can be observed.

V_0 occurs when half the maximal charge has been transferred. This corresponds to the case where half the prestin molecules are in the state E2.Cl. Equation (3.8) leads to the following expression for V_0;

$$V_o = \frac{1}{\beta}\ln\left(\frac{k_{-2}(0)}{k_2(0)}\left(1+\frac{k_{-1}}{k_1[Cl_i]}\right)\right) \tag{3.9}$$

Thus as $[Cl_i]\rightarrow\infty$, $V_o \rightarrow \frac{1}{\beta}\ln\left(\frac{k_{-2}(0)}{k_2(0)}\right)$, which is a constant, thus V_0 saturates. As $[Cl_i]\rightarrow 0$, $V_0 \rightarrow -\infty$ since β is negative.

The shift in V_0 due to a change in $[Cl_i]$ from a first concentration, $[Cl_i]_1$ to a second concentration, $[Cl_i]_2$ is found directly from equation (3.9)

$$\Delta V_o = \frac{1}{\beta}\ln\left(\frac{1+\frac{k_{-1}}{k_1[Cl_i]_2}}{1+\frac{k_{-1}}{k_1[Cl_i]_1}}\right) \tag{3.10}$$

The derivations for equations (3.8-3.10) are shown in Appendix 2.

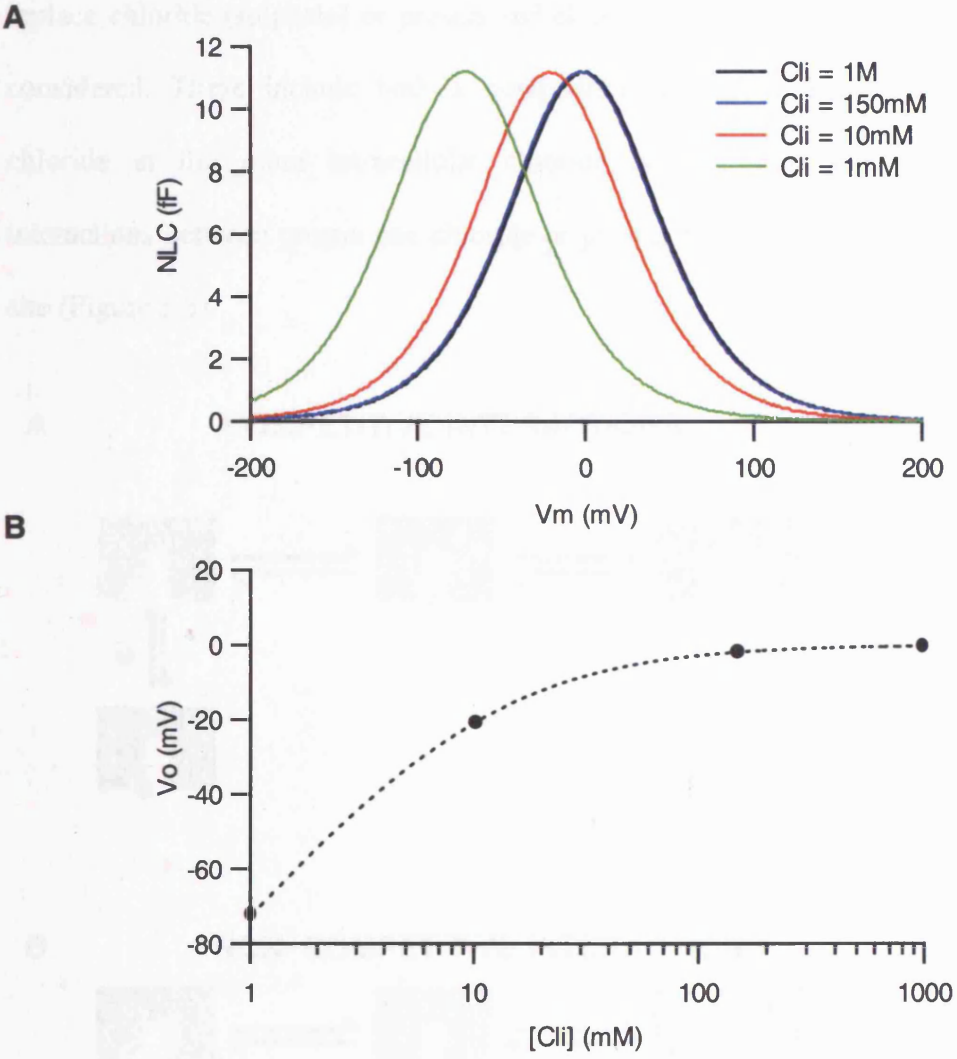

Figure 3.4. Effect of $[Cl_i]$ on the NLC produced by a three-state model. In this example $K_D(Cl_i)$=10mM, $k_2(0)=k_{-2}(0)=10^4\ s^{-1}$. A) NLC depends on $[Cl_i]$. There is no change in C_{pk}, Q_{max} or β as $[Cl_i]$ is decreased but V_o of the NLC is shifted to more hyperpolarized potentials. B) The V_o of NLC saturates at high $[Cl_i]$. The dotted line shows the fit of equation (3.9).

3.3.3 Effect of Interactions with the Three-State Model

It is clear that the simplest models cannot reproduce the experimental data. Thus the effects of several possible interactions between prestin and the anion used to replace chloride (sulphate) or prestin and chloride on the three-state model are now considered. These include both a competitive interaction between sulphate and chloride at the more intracellular chloride binding site, and non-competitive interactions between prestin and chloride or prestin and sulphate at a second binding site (Figure 3.5).

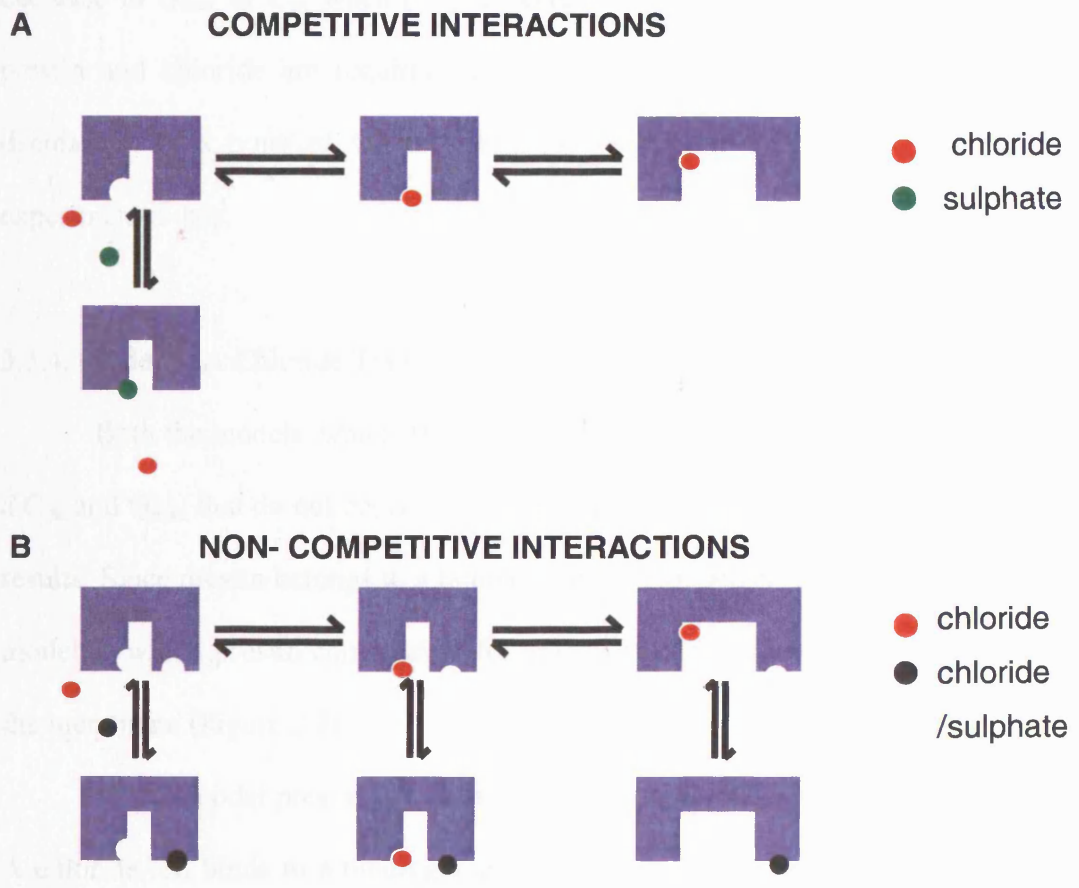

Figure 3.5. Illustration of potential interactions between intracellular anions and prestin for the three-state model. A) Competitive interactions include the voltage-independent binding of sulphate at the more intracellular chloride binding site. B) Non-competitive interactions include the binding of chloride or sulphate at a second binding site.

A decrease in Q_{max} or C_{pk} with decreasing $[Cl_i]$ cannot be produced with any of these interactions. Furthermore in most cases V_o shifts in the hyperpolarising direction when $[Cl_i]$ is reduced (Figure 3.6A). However in certain cases it is possible to produce a shift in V_o in the depolarising direction when $[Cl_i]$ is reduced (Figure 3.6B). This shows that including more complex interactions can affect the direction of the shift in V_o.

In summary with both the access channel model and the three-state model there are only inward-facing binding sites. Neither of these models predicts any decrease in Q_{max} or C_{pk} when $[Cl_i]$ is decreased, and complex interactions between prestin and chloride are required to produce a positive shift in V_o when $[Cl_i]$ is decreased. Thus none of the models presented so far are able to reproduce the experimental data.

3.3.4. Model 3: A Chloride Transporter Model

Both the models, which only allowed intracellular chloride binding, resulted in a C_{pk} and Q_{max} that do not depend on voltage thus being in contrast with experimental results. Since prestin belongs to a family of anion exchangers (Ch.1.3), I considered a model in which prestin completes a full transport cycle, transporting chloride across the membrane (Figure 3.7).

In this model prestin can be either inward facing (E0) or outward facing (E4). A chloride ion binds to a binding site facing the intracellular medium. The chloride ion then moves through the membrane to a second site, accompanied by a conformational change from where it moves to a third site facing the extracellular

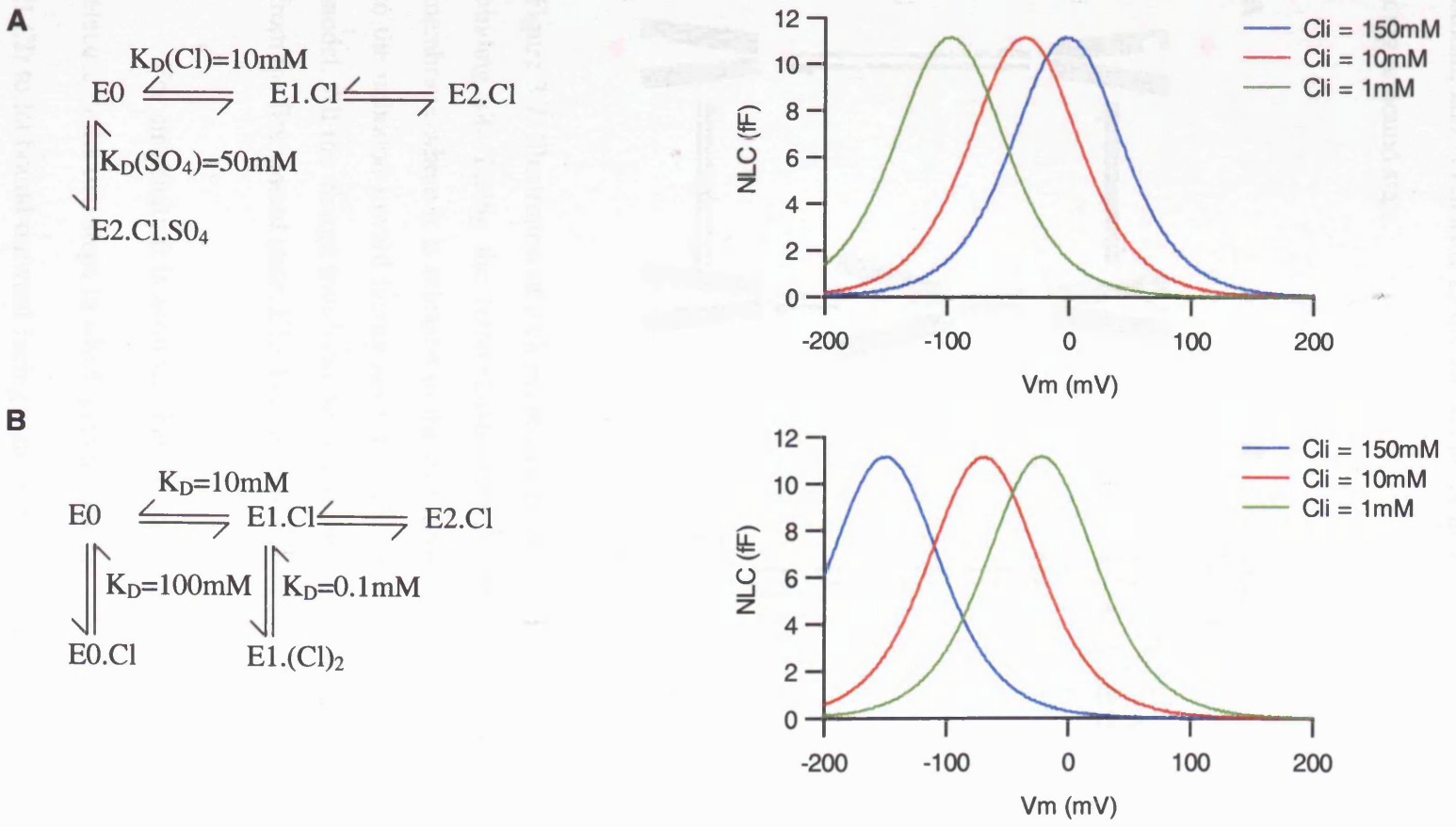

Figure 3.6. Effect of [Cl_i] on the NLC when interactions between intracellular anions and the three-state model of prestin are considered. A) If sulphate competes with chloride at the more intracellular binding site then the shift in the hyperpolarising direction is increased. B) If Cl_i is predicted to self-inhibit, by binding to a second binding site with greater affinity once one chloride ion is already bound, a positive shift in V_o is produced as [Cl_i] is reduced.

medium, and is released to the extracellular medium, forcing prestin into its outward facing unbound state.

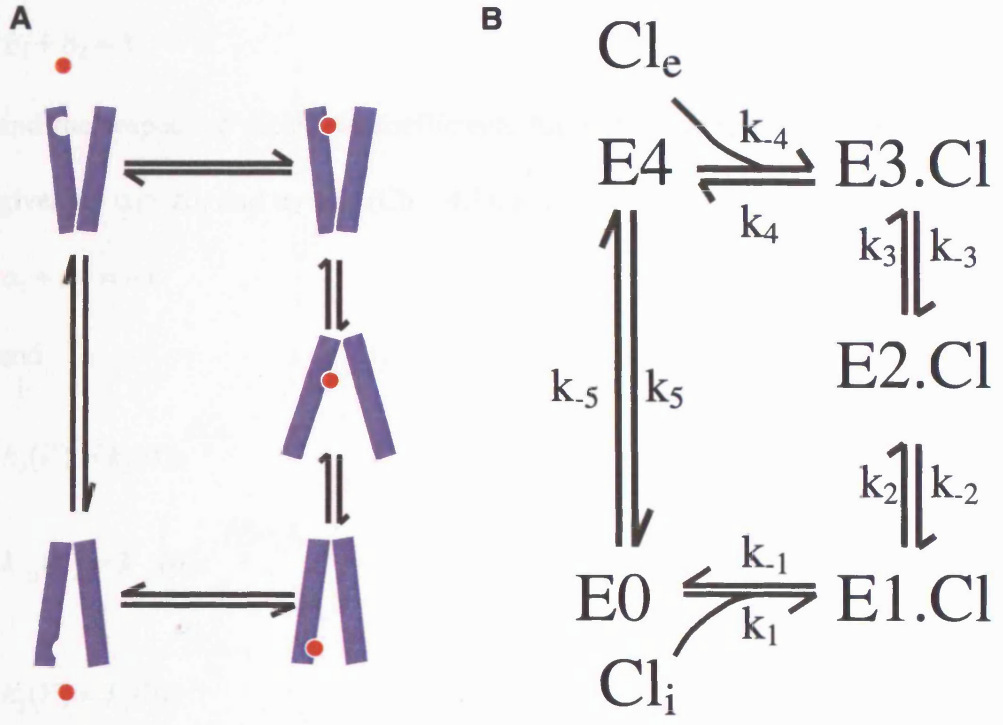

Figure 3.7. Illustration of a chloride transporter model. A) Chloride binds first to a binding site facing the intracellular medium. It is then transported across the membrane where it is released to the extracellular medium, before prestin returns to the unbound inward facing state. B) The reaction scheme used to describe this model. All the charge translocation is assumed to occur across the two transitions from the first bound state, E1.Cl to the third bound state E3.Cl.

For simplicity it is assumed that the chloride ion crosses the whole membrane dielectric in the two steps in which prestin changes from its bound inward facing state (E1.Cl) to its bound outward facing state (E3.Cl). The binding and unbinding of both intracellular and extracellular chloride are assumed to be voltage-independent.

If the fraction of the membrane dielectric crossed in the transition E1.Cl → E2.Cl is δ_1 and the fraction of the dielectric crossed in the second transition E2.Cl → E3.Cl is δ_2, then

$$\delta_1 + \delta_2 = 1 \tag{3.11}$$

and the respective dielectric coefficients for a chloride ion with valence, z = –1 are given by $\alpha_1 = z\delta_1$ and $\alpha_2 = z\delta_2$ (Ch.1.4.1), so

$$\alpha_1 + \alpha_2 = -1 \tag{3.12}$$

and

$$k_2(V) = k_2(0)e^{\frac{\beta_1 V_m}{2}} \tag{3.13}$$

$$k_{-2}(V) = k_{-2}(0)e^{-\frac{\beta_1 V_m}{2}} \tag{3.14}$$

$$k_3(V) = k_3(0)e^{\frac{\beta_2 V_m}{2}} \tag{3.15}$$

$$k_{-3}(V) = k_{-3}(0)e^{-\frac{\beta_2 V_m}{2}} \tag{3.16}$$

where $\beta_1 = \frac{\alpha_1 e_o}{k_B T}$ and $\beta_2 = \frac{\alpha_2 e_o}{k_B T}$.

Two cases were considered. In Case 1, all the charge translocation occurred across the first transition ($\alpha_1 = -1$, $\alpha_2 = 0$), resulting in one voltage-dependent step. In Case 2, both transitions were voltage-dependent ($\alpha_1 = -0.8$, $\alpha_2 = -0.2$). Since the forward rate of the transition E1.Cl→E2.Cl is increased on hyperpolarisation this transition is assumed to coincide with a conformational change of prestin to an expanded state.

For a cyclic process microscopic reversibility must be obeyed. (The product of the clockwise rate constants must equal the product of the anti-clockwise rate

constants for the case where there is no membrane potential and no concentration gradient of chloride across the membrane). Thus there are nine independent rate constants for this model. Since none of the rate constants are known, various combinations were tested using rate constants that were comparable to those known for other transporters. Table 3.1 shows the range of rate constants tested.

Rate constant	Range of values tested
k_1	10^6 to 2 x 10^7 $M^{-1}s^{-1}$
k_{-1}	10^5 s^{-1}
$k_2(0)$	10^3 to 10^4 s^{-1}
$k_{-2}(0)$	10^4 to $10^5 s^{-1}$
$k_3(0)$	10 to 10^4 s^{-1}
$k_{-3}(0)$	10 to 10^4 s^{-1}
k_4	10^5 s^{-1}
k_{-4}	10^6 to 2 x 10^7 $M^{-1}s^{-1}$
k_5	0 to 4 x 10^4 s^{-1}
k_{-5}	0 to 4 x $10^4 s^{-1}$

Table 3.1. Rate constants tested in simulations for the chloride transporter model.

In agreement with experimental observations, whenever the inward facing state (E0) of prestin is permitted to change to the outward facing state (E4) without chloride bound (k_5 and k_{-5} >0) a decrease in C_{pk} and Q_{max} is produced as $[Cl_i]$ is reduced. Furthermore for particular combinations of rate constants a shift in V_o in the depolarising direction is produced as $[Cl_i]$ is reduced.

Although this applies to both Case 1 and Case 2, in Case 2 NLCs become very asymmetric as $[Cl_i]$ is reduced (data not shown). The closest reproduction of experimental results is produced for Case 1(Figure 3.8). The NLC produced when $[Cl_i]$ is 150mM, has a V_0 of –44mV, and an apparent β of 0.031, in good agreement with experimental observations (Gale and Ashmore 1997b). A positive shift in V_0 (by 55mV) and a decrease in C_{pk} and Q_{max} (to 29%, and 42%, respectively) are produced when $[Cl_i]$ is reduced from 150mM to 1mM. Thus the transporter model for prestin is able to reproduce both the correct direction for the shift in V_0, and a decrease in C_{pk} and Q_{max} as $[Cl_i]$ is reduced.

In addition although the transporter model predicts a significant effect on the NLC of removing Cl_e (V_0 shifted by –7mV and C_{pk} and Q_{max} decreased to 88% and 92% respectively), it remains a much smaller effect than that due to Cl_i removal. The importance of Cl_e is better revealed when $[Cl_i]$ is low. The transporter model predicts that if $[Cl_e]$ is reduced with $[Cl_i]$ at 1mM, then a large negative shift and increase in Q_{max} and C_{pk} is produced (Figure 3.9).

In contrast with the experimental observations, the shifts in V_0 produced by the model are much smaller than those observed experimentally, for all combination of rate constants tested. Additionally, in contrast with experimental observations this model predicts a significant NLC when Cl_i is completely removed and a decrease in the apparent β (to 70%) is also produced when Cl_i is reduced to 1mM. No decrease in the apparent β was measured in experiments.

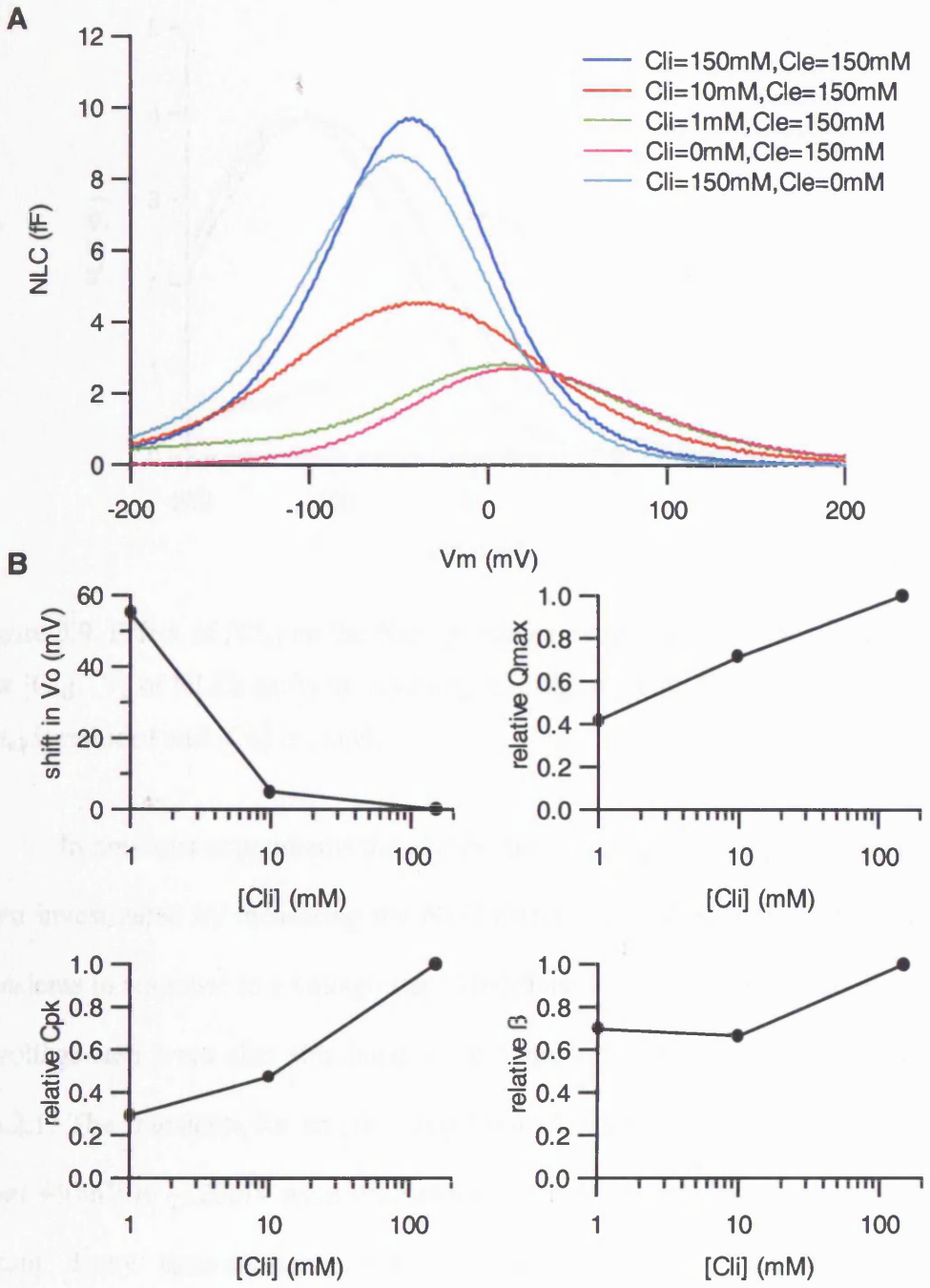

Figure 3.8.Effect of $[Cl_i]$ on the NLC produced by a chloride transporter model. A) The transporter model reproduces aspects of experimental data when $\alpha_1=1,\alpha_2=0$. In this example NLCs were produced by a model with the following rate constants; $k_1=33350s^{-1}mM^{-1}$,$k_{-1}=100000s^{-1}$, $k_2(0)=2000s^{-1}$, $k_{-2}(0)=10000s^{-1}$, $k_3=3000s^{-1}$, $k_{-3}=10000s^{-1}$, $k_4=100000s^{-1}$, $k_{-4}=1500s^{-1}mM^{-1}$, $k_5=30000s^{-1}$, $k_{-5}=40000s^{-1}$. B) The Boltzmann parameters depend on $[Cl_i]$.

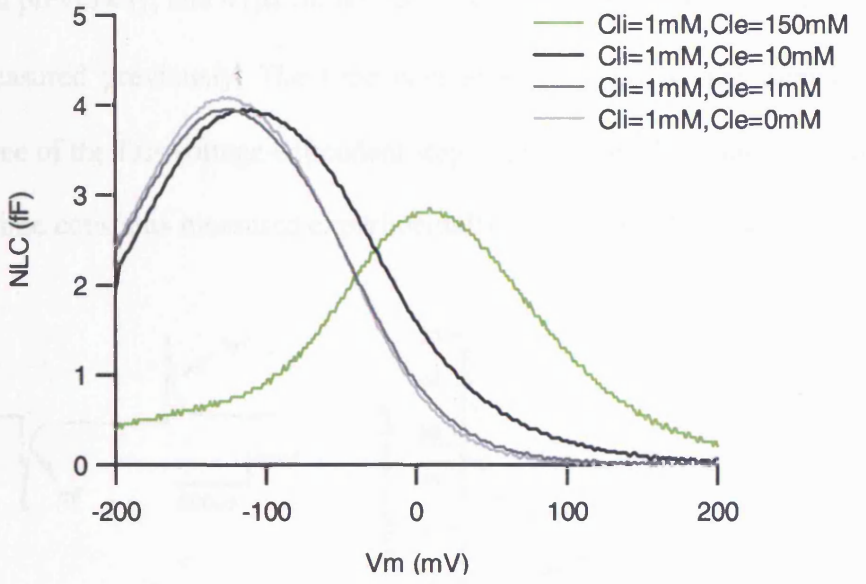

Figure 3.9. Effect of $[Cl_e]$ on the NLC produced by the chloride transporter model with low $[Cl_i]$. V_o of NLCs shifts to more negative V_m and both C_{pk} and Q_{max} increase when $[Cl_e]$ is reduced and $[Cl_i]$ is 1mM.

In previous experiments the charge-moving properties of prestin have not only been investigated by measuring the NLC directly, but also by recording the current transients in response to a voltage step. Therefore the current transients resulting from a voltage-step were also simulated for this model, using the methods described in Ch.2.1. The transients for an 'on' step from –120mV to +40mV, and an 'off' step from +40mV to –120mV were simulated (Figure 3.10) and fitted with exponentials to obtain decay time-constants, for comparison with the previous experimental measurements of Gale and Ashmore (1997b). Since the experimental measurements were made from OHC patches, with high Cl_i and high Cl_e, transients were simulated for a patch estimated to contain 10,000 prestin molecules, under the condition that $[Cl_i]=[Cl_e]=150$mM. The transients were best fitted with a single exponential, giving time constants of 42μs for the 'on' step compared with a fast time constant of 10μs

measured previously, and 41μs for the 'off' step compared with a fast time constant of 13μs measured previously. The time constants predicted by the model reflect the dominance of the fast voltage-dependent step in the model. They are the same order as the fast time constants measured experimentally, differing only by a factor of ~4.

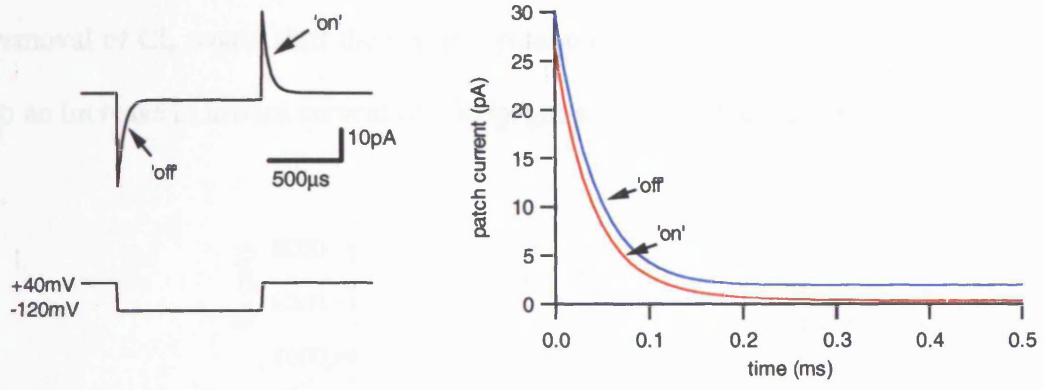

Figure 3.10 Simulated transient currents in response to a voltage-step. A) Fast current transients are generated in response to an 'off' voltage-step from +40mV to –120mV and an 'on' step back to +40mV. B) The same transients plotted over an expanded time scale. Currents are estimated for a patch containing 10,000 prestin molecules.

In the example shown in Figure 3.10 it is clear that the transient current for the 'off' step from +40mV to –120mV does not decay to zero, thus when V_m is at -120mV a detectable stead-state current is present. The existence of steady-state current when there is either a concentration gradient of chloride or a potential difference across the membrane is an important consequence of a full transport model and could potentially be measured experimentally. Therefore the effect of removing either intracellular or extracellular chloride on the voltage-dependent steady-state current, I(V) was predicted. Since I(V) curves are typically measured for a whole cell, I(V) curves were predicted for a cell estimated to contain 10 million copies of prestin

(Figure 3.11). For the condition of high chloride inside and outside the cell, a reversal potential of 0mV is predicted and both an outwardly rectifying current at positive V_m, and an inwardly rectifying current at negative V_m are predicted. Complete removal of Cl_i would shift the reversal potential to an infinitely negative V_m, and lead to an increase in outward current of ~4nA at a holding potential of 0mV. Complete removal of Cl_e would shift the reversal potential to an infinitely positive V_m, and lead to an increase in inward current of ~500pA at a holding potential of 0mV.

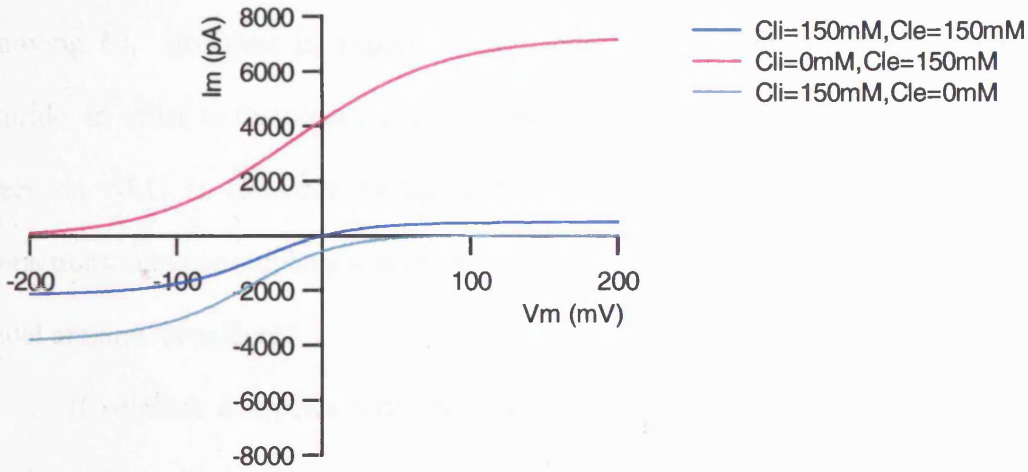

Figure 3.11. Simulated I(V)s for an OHC with the chloride transporter model. Removing Cl_i leads to a negative shift in the reversal potential and an increase in outward current. Removing Cl_e leads to a positive shift in reversal potential and an increase in inward current.

In summary the chloride transporter model is able to reproduce many aspects of the dependence of the NLC on $[Cl_i]$ and $[Cl_e]$ observed experimentally. It also produces similar transient currents in response to a voltage-step to those measured previously. Additionally it predicts large effects on the I(V) of removing either Cl_i or Cl_e.

3.3.5 Effect of Interactions with the ChlorideTransporter Model

The transporter model of prestin described in Ch.3.3.4 is able to produce both a decrease in Q_{max} and C_{pk} and a shift in V_0 in the depolarising direction when $[Cl_i]$ is reduced. Furthermore the current transients produced in response to a voltage-step are similar to those measured experimentally. However discrepancies between the model and the experimental data remain. In particular the magnitude of the shifts in V_0 for reduction of $[Cl_i]$ to 10mM and 1mM are smaller than the measured values. Up to now it has been assumed that the effect on NLC is entirely due to the effect of removing Cl_i. However in experimental conditions sulphate was used to replace chloride, in order to maintain ionic strength, therefore it is possible that some of the effect on NLC is also due to the addition of sulphate. The effect of possible interactions between sulphate and prestin on the predictions of the chloride transporter model are now considered.

If sulphate competes with chloride at the intracellular binding site, then the positive shift in V_0 is decreased, or a negative shift in V_0 is produced (Figure 3.12). However if a sulphate binding-site becomes available following the conformational change in the transition E1.Cl→ E2.Cl, such that a sulphate ion binds to the state E2.Cl, then the positive shift in V_0 is increased (Figure 3.13). If the binding of sulphate to the state E2.Cl has a $K_D(SO_4)$ = 50mM, the shift in V_0 at reduced $[Cl_i]$ when replaced with sulphate is comparable to that observed by Fakler and Oliver (2002).

The binding of sulphate to the state E2.Cl only has a very slight effect on the other Boltzmann parameters, when compared to the predictions without sulphate binding. On reduction of $[Cl_i]$ from 150mM to 1mM, the decrease in apparent β was

slightly reduced (to 73% compared with 70%), the decrease in Q_{max} was slightly reduced (to 48% compared with 42%) and the decrease in C_{pk} was slighlty reduced (to 35% compared with 29%).The effect on the I(V) of removing either Cl_i or Cl_e when this interaction was included was very similar to that produced in the absence of any interaction (Data not shown).

In summary this model proposes that the magnitude of the shift observed when $[Cl_i]$ is reduced and replaced with sulphate is due partly to the reduction of $[Cl_i]$ and partly due to the addition of sulphate. Therefore if Cl_i was replaced with a different, non-interacting anion, smaller shifts in V_o comparable with those shown in Figure 3.8 would be predicted.

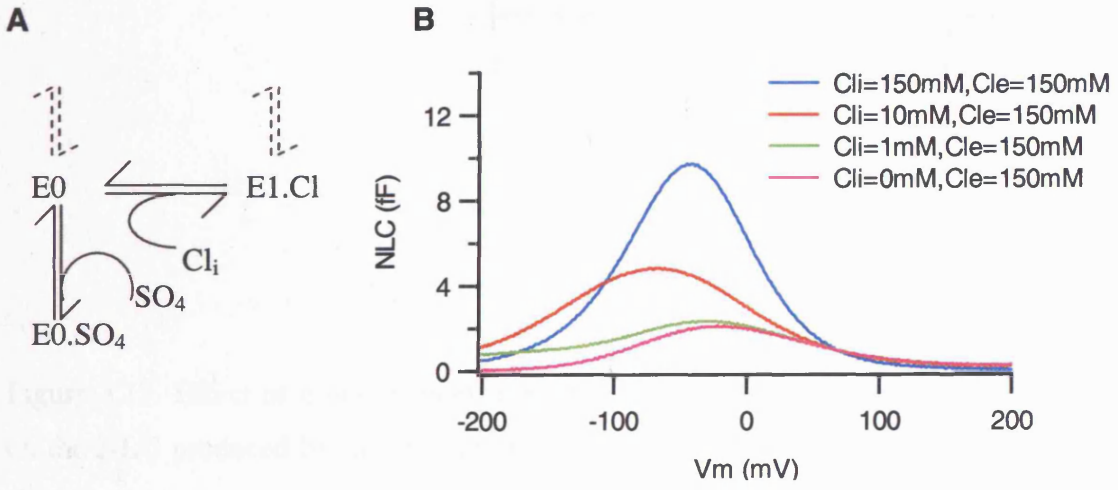

Figure 3.12. Effect of competition between sulphate and chloride on the NLC produced by the chloride transporter model. A) The reaction scheme shows the states involved in competitive binding to the state E0. The dotted arrows indicate the rest of the transport cycle, which is not shown here. B) NLCs produced by this interaction with a $K_D(SO_4)$=10mM show that the shift in V_o is in the hyperpolarising direction as $[Cl_i]$ is reduced to 10mM, and the positive shift in V_o on reduction of $[Cl_i]$ to 1mM is much smaller.

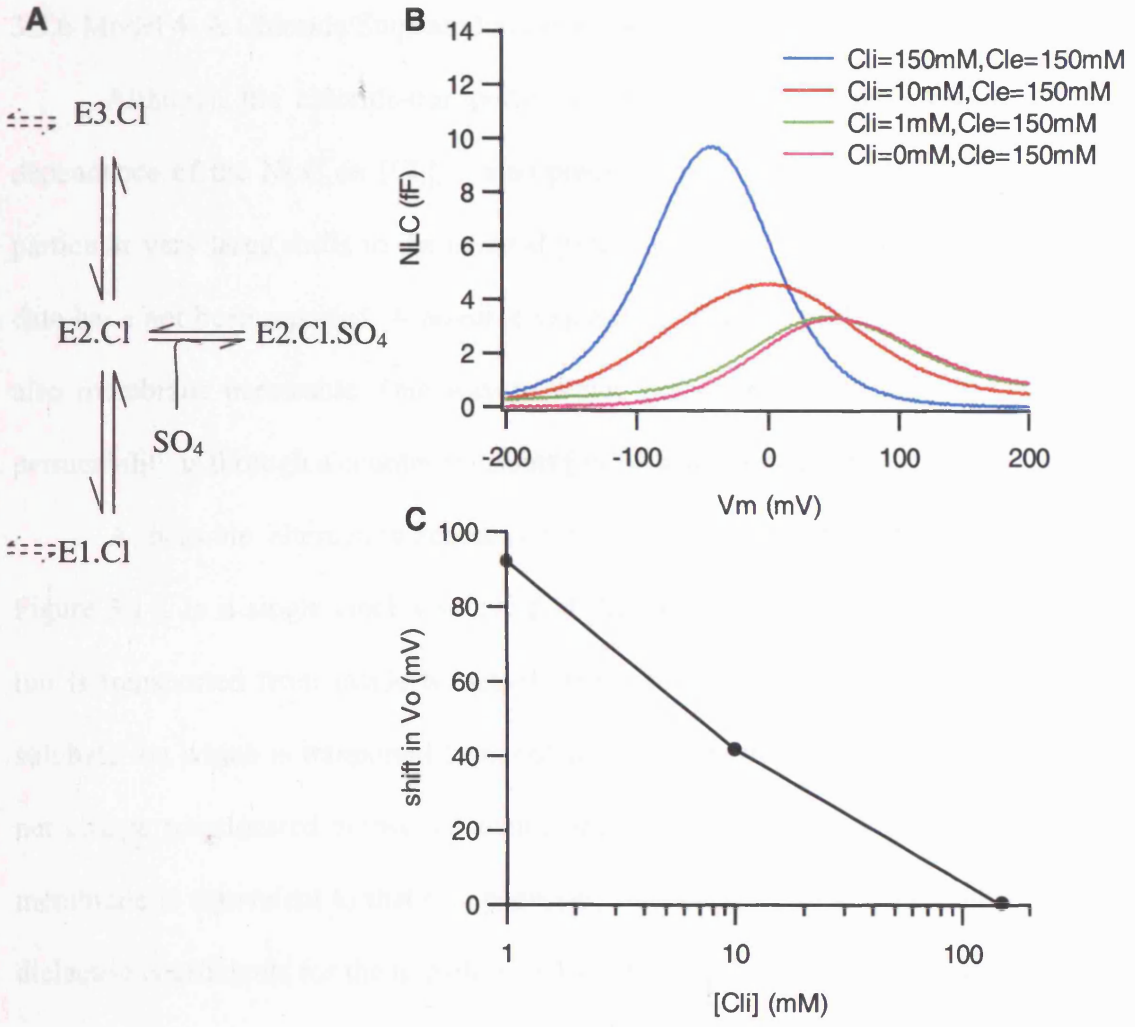

Figure 3.13. Effect of a non-competitive interaction between sulphate and prestin on the NLC produced by the chloride transporter model. A) The reaction scheme shows a sulphate ion binding to the state E2.Cl. For simplicity only some states of the transport cycle are shown, the dotted arrows indicate the rest of the transport cycle, which are not shown. B) NLCs generated when the binding of sulphate to the state E2.Cl has a $K_D(SO_4)$ = 50mM. C) The shift in V_o is increased to ~90mV when $[Cl_i]$ is reduced to 1mM.

3.3.6 Model 4: A Chloride/Sulphate Exchanger Model

Although the chloride-transporter model gives a close reproduction of the dependence of the NLC on $[Cl_i]$, it also predicted very large effects on the I(V), in particular very large shifts in the reversal potential, of removing Cl_i or Cl_e, which to date have not been reported. A possible explanation for this could be that sulphate is also membrane permeable. One way in which prestin might mediate this sulphate permeability is through a counter-transport (or exchange) mechanism.

A possible alternating-access scheme for Cl^-/SO_4^{2-} exchange is shown in Figure 3.14. In a single clockwise cycle of the exchanger, one monovalent chloride ion is transported from inside to outside the membrane in exchange for a divalent sulphate ion which is tranported from outside to inside the membrane. Therefore the net charge translocated across the membrane from the inside to the outside of the membrane is equivalent to that of a positively charge ion with a valence of +1. If the dielectric coefficients for the transitions E1.Cl→E2.Cl and E2.Cl→E3.Cl are given by α_1 and α_2 respectively, and the dielectric coefficient for the transition $E3.SO_4$→$E2.SO_4$ and $E2.SO_4$→$E1.SO_4$ are given by α_3 and α_4 then

$$\alpha_1 + \alpha_2 + \alpha_3 + \alpha_4 = 1 \qquad (3.17)$$

If we assume that the translocation of chloride is voltage-dependent and that $\alpha_1 + \alpha_2 = -1$, this gives

$$\alpha_3 + \alpha_4 = 2 \qquad (3.18)$$

Therefore the translocation of sulphate across the membrane must also be voltage dependent. The case where $\alpha_1 = -1$, $\alpha_2 = 0$ and $\alpha_3 = 0$, $\alpha_4 = 2$ and therefore k_2, k_{-2}, k_7 and k_{-7} are voltage-dependent, was considered.

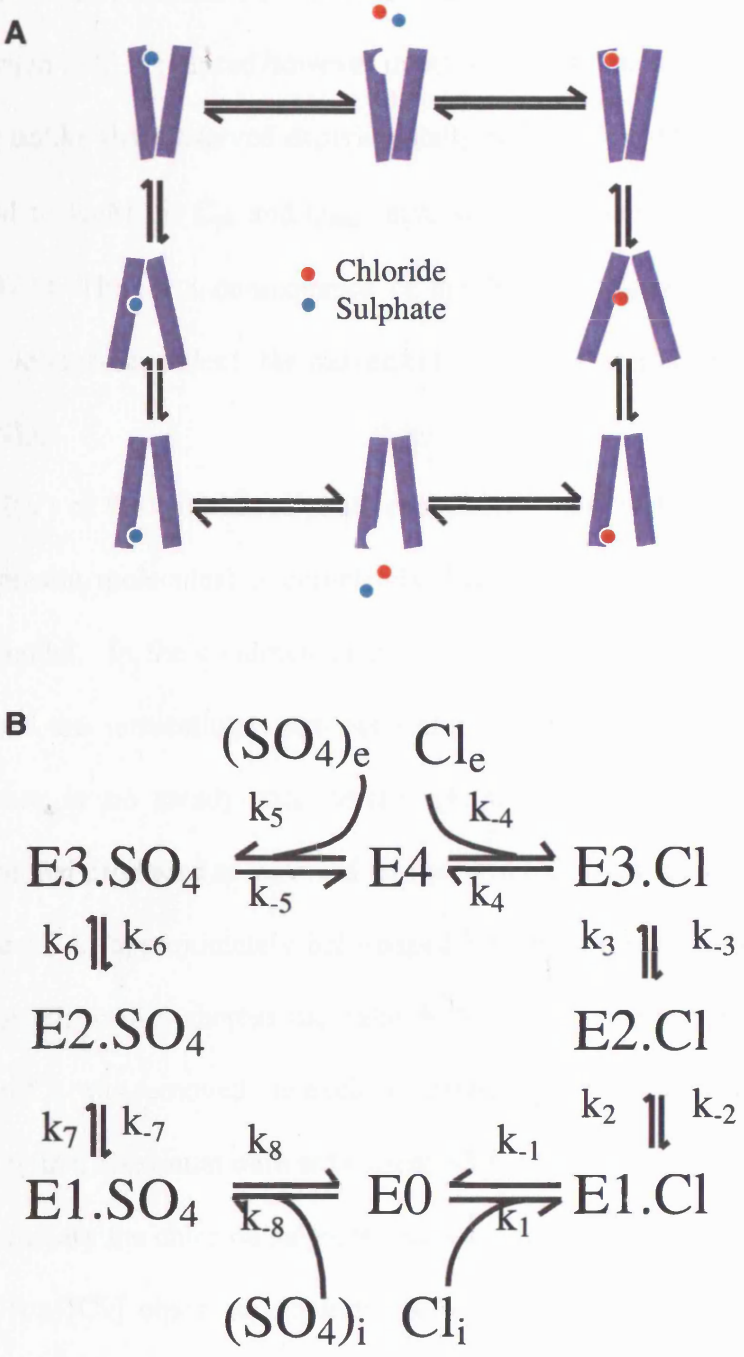

Figure 3.14. Illustration of a chloride/sulphate exchanger model. A) Prestin can only change from the inward facing to the outward facing state if either a chloride or a sulphate ion is bound. B) The reaction scheme for this model.

With certain combinations of rate constants this model can produce a positive shift in V_o when $[Cl_i]$ is reduced however in other respects the dependence of NLC on $[Cl_i]$ is very unlike that observed experimentally (Figure 3.15A). As $[Cl_i]$ is reduced from 150mM to 1mM the C_{pk} and Q_{max} increase and the apparent β increases (from ~0.04 to ~0.06). This is a consequence of the fact that since the translocation of sulphate is voltage-dependent, the movement of sulphate across the membrane also produces a NLC.

The I(V) of the chloride/sulphate exchanger model (estimated for a cell with 10 million prestin molecules) is completely different from the I(V) of the chloride transporter model. In the condition of high $[Cl_i]$ and high $[Cl_e]$ and the absence of sulphate from the intracellular and extracellular media, no full cycle can occur, therefore there is no steady-state current (Figure 3.15). Whereas the chloride transporter model produced an outward current when Cl_i was removed the exchanger model produced an approximately bell-shaped I(V) with a maximum inward current of ~1.7nA. Additionally whereas the chloride transporter model produced an inward current when Cl_e was removed the exchanger model produced an approximately bell-shaped I(V) with a maximum outward current ~300pA.

In summary the chloride/sulphate exchanger cannot reproduce the dependence of the NLC on $[Cl_i]$ observed experimentally. Furthermore although I(V)s for the exchanger model are very different from the I(V)s for the transporter model, a significant effect on the I(V) of removing either Cl_i or Cl_e, is still predicted.

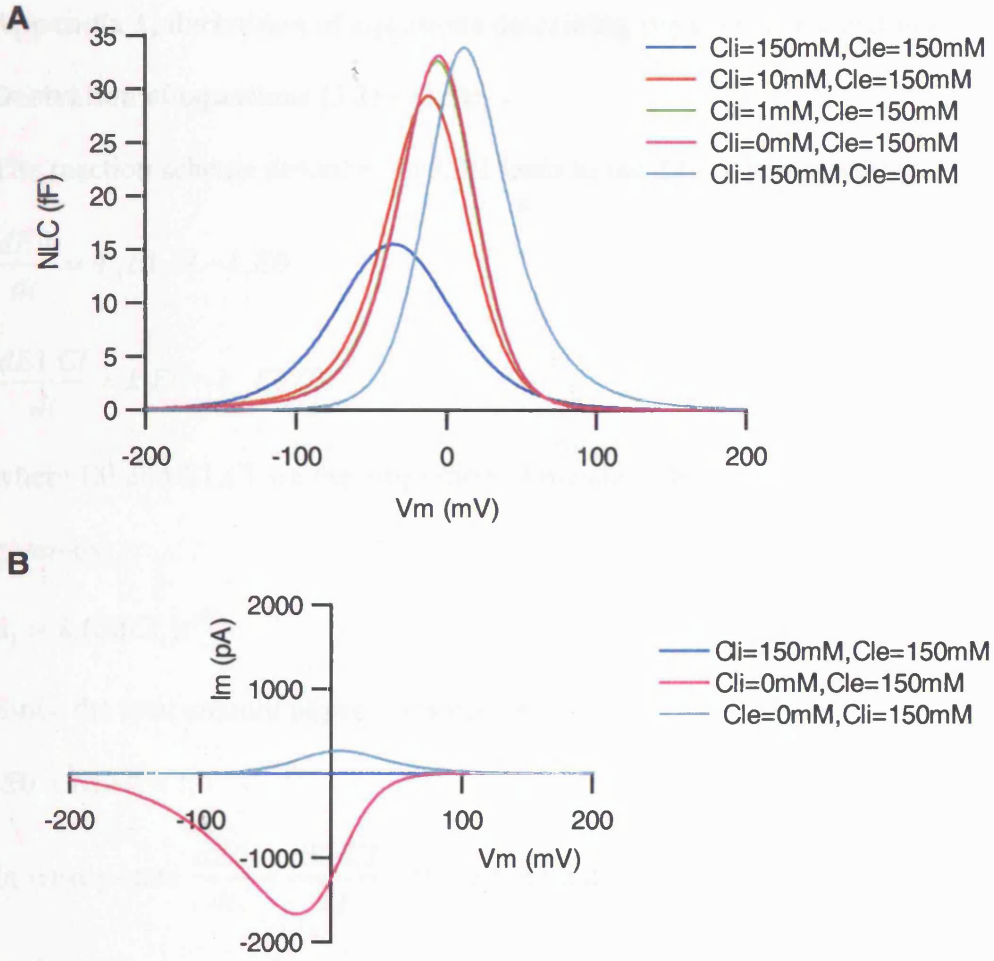

Figure 3.15. Effect of $[Cl_i]$ and $[Cl_e]$ on the NLCs and I(V)s produced by the chloride/sulphate exchanger. A) NLC depends on $[Cl_i]$, and $[Cl_e]$. V_o shifts to more positive V_m and C_{pk} and Q_{max} increase as either $[Cl_i]$ or $[Cl_e]$ is reduced and replaced with sulphate. B) No steady-state current is present when there is high chloride in both the intracellular and extracellular solutions. The I(V)s produced when either Cl_i or Cl_e are completely removed and replaced with sulphate are approximately bell-shaped.

Appendix 1; derivation of equations describing the access channel model

Derivation of equations (3.3) - (3.5):

The reaction scheme described in 3.3.1 leads to the differential equations;

$$\frac{dE0}{dt} = k_{-1}E1.Cl - k_1E0 \tag{3.19}$$

$$\frac{dE1.Cl}{dt} = k_1E0 - k_{-1}E1.Cl \tag{3.20}$$

where E0 and E1.Cl are the proportion of prestin in those states respectively and k_1 is given by

$$k_1 = k_1(0)[Cl_i]e^{\beta V_m} \tag{3.21}$$

Since the total amount of prestin is conserved;

$$E0 + E1.Cl = 1 \tag{3.22}$$

In steady-state $\frac{dE0}{dt} = \frac{dE1.Cl}{dt} = 0$, so combining equations (3.19-3.22) gives

$$E1.Cl = \frac{1}{\left(1 + \frac{k_{-1}}{k_1(0)[Cl_i]e^{\beta V_m}}\right)} \tag{3.23}$$

This is equivalent to equation (3.3). V_0 corresponds to the potential at which half the prestin molecules are in the state E0 and half are in the state E1.Cl, therefore

$$\frac{k_1(0)[Cl_i]e^{\beta V_0}}{k_{-1}} = 1 \tag{3.24}$$

which leads to equation (3.4):

$$V_o = \frac{1}{\beta}\ln\left(\frac{k_{-1}}{k_1(0)[Cl_i]}\right)$$

If $(V_o)_1$ is the V_o corresponding to a first concentration $[Cl_i]_1$, and $(V_o)_2$ is the V_o to a second concentration $[Cl_i]_2$,, then changing the concentration of Cl_i from $[Cl_i]_1$ to $[Cl_i]_2$ causes a shift in V_o of $\Delta V_o = (V_o)_2 - (V_o)_1$, which gives equation (3.5)

$$\Delta V_o = \frac{1}{\beta}\ln\left(\frac{[Cl_i]_1}{[Cl_i]_2}\right)$$

Appendix 2; derivation of equations describing the three-state model

Derivation of equations (3.8) - (3.10);

The reaction scheme described in 3.3.2 leads to the following differential equations;

$$\frac{dE0}{dt} = k_{-1}E1.Cl - k_1[Cl_i]E0 \qquad (3.25)$$

$$\frac{dE1.Cl}{dt} = k_1[Cl_i]E0 + k_{-2}E2.Cl - (k_{-1} + k_2)E1.Cl \qquad (3.26)$$

$$\frac{dE2.Cl}{dt} = k_2\ E1.Cl - k_{-2}E2.Cl \qquad (3.27)$$

where E0, E1.Cl and E2.Cl are the proportion of prestin in those states respectively. Since the total amount of prestin is conserved;

$$E0 + E1.Cl + E2.Cl = 1 \qquad (3.28)$$

In steady state $\frac{dE0}{dt} = \frac{dE1.Cl}{dt} = \frac{dE2.Cl}{dt} = 0$, so combining equations (3.25-3.28) gives equation (3.8)

$$E2.Cl = \frac{1}{1 + \left(\frac{k_{-2}}{k_2}\left(1 + \frac{k_{-1}}{k_1[Cl_i]}\right)\right)}$$

V_o corresponds to the potential at which half the prestin molecules are in the state E2.Cl, therefore

$$\frac{k_{-2}}{k_2}\left(1+\frac{k_{-1}}{k_1[Cl_i]}\right)=1 \tag{3.29}$$

and

$$e^{\beta V_o}=\frac{k_{-2}(0)}{k_2(0)}\left(1+\frac{k_{-1}}{k_1[Cl_i]}\right) \tag{3.30}$$

which gives equation (3.9)

$$V_o=\frac{1}{\beta}\ln\left(\frac{k_{-2}(0)}{k_2(0)}\left(1+\frac{k_{-1}}{k_1[Cl_i]}\right)\right)$$

If $(V_o)_1$ is the V_o corresponding to a first concentration $[Cl_i]_1$, and $(V_o)_2$ is the V_o to a second concentration $[Cl_i]_2$,, then changing the concentration of Cl_i from $[Cl_i]_1$ to $[Cl_i]_2$ causes a shift in V_o of $\Delta V_o = (V_o)_2 - (V_o)_1$, which gives equation (3.10)

$$\Delta V_o=\frac{1}{\beta}\ln\left(\frac{1+\frac{k_{-1}}{k_1[Cl_i]_2}}{1+\frac{k_{-1}}{k_1[Cl_i]_1}}\right)$$

3.4 Discussion

3.4.1 Incomplete Transport Models

In Ch.3.3.1 and Ch.3.3.2 two alternative 'incomplete transport' models for prestin, based on the model proposed by Oliver et al. (2001) were formulated, in which chloride was the voltage-sensor. Neither model is able to reproduce the key experimental observations made in the excised patch configuration (Oliver et al. 2001, Fakler and Oliver 2002). The predictions of the models differ from key experimental observations in two ways:

1) When $[Cl_i]$ is reduced the shift in V_0 is in the hyperpolarising direction, rather than the depolarising direction.
2) No decrease in C_{pk} or Q_{max} is produced when $[Cl_i]$ is reduced.

These models are therefore inconsistent with the existing evidence, from excised OHC patches.

In fact Fakler and Oliver (2002) have already acknowledged that the observed shift in V_0 is difficult to reconcile with their own model. This problem has been discussed previously (Gummer, 2003). One suggestion to overcome this contradiction was that the movement of intrinsic positive charges might accompany the movement of chloride. This possibility is addressed in Ch.4.

However even if it is possible to account for the shift in V_0 it is more difficult to explain the origin of the observed decrease in C_{pk} or Q_{max} with an 'incomplete transport' model. Even after additional interactions between intracellular anions and prestin were considered (Ch.3.3.3), no decrease in C_{pk} or Q_{max} could be produced.

3.4.2 Complete Transport Models

The 'complete transporter' model described in Ch.3.3.4 gave a much closer reproduction of the key experimental observations. The predictions of the chloride transporter model are similar to the experimental observations in several ways:

1) For certain combinations of rate constants, the V_0 of the NLC shifts in the depolarising direction when $[Cl_i]$ is reduced.
2) A decrease in C_{pk} and Q_{max} is produced as $[Cl_i]$ is reduced.
3) Removal of Cl_e had very little effect on the NLC, when $[Cl_i]$ was high.

Additionally, the fast decay time constants of the transient currents produced in response to a voltage-step were the same order as those measured experimentally. However some discrepancies between the predictions of the model and the key experimental observations remained.

1) The shift in V_0 predicted by the model is smaller than the shift observed.
2) The NLC is not abolished when Cl_i is removed.
3) The apparent β decreases when Cl_i is reduced.

Furthermore whilst most combinations of rate constants tested produced a decrease in C_{pk} and Q_{max}, only particular combinations of rate constants produced a depolarising shift. In fact, small changes in any of the rate constants, by as little as a factor of 2, caused the direction of the shift in V_0 to be changed. Thus this model is only able to reproduce the key experimental observations for very specific combinations of rate constants.

Therefore although the chloride transporter model appears to account for key experimental observations much better than the 'incomplete transport' models, its lack of robustness, and inability to predict some of the key observations, suggests it needs refinement.

3.4.3 A Role for Sulphate

Two different modifications of the chloride transporter model, in which potential interactions between sulphate (the anion used to substitute chloride) and prestin were considered in Ch.3.3.5 and Ch.3.3.6.

In Ch.3.3.5 it was shown that if sulphate binds to the state of prestin in which chloride is bound at the top of the pore, E2.Cl (Figure 3.13), then the positive shift in

V_0 when $[Cl_i]$ is reduced, is greater than if no interaction with sulphate occurs. In fact the dependence of the shift in V_0 on $[Cl_i]$ becomes the same as that observed experimentally, which suggests that sulphate might be more than a 'spectator' anion.

In Ch.3.3.6 a chloride/sulphate exchanger model was considered. However the predictions of this model are very different from the experimental observations. A chloride/sulphate exchanger in which the anions are the only voltage-sensors is clearly not an appropriate model.

3.4.4 Predictions of the Chloride Transporter Model

There are several predictions of the chloride transporter model, which cannot be compared with any available experimental data from excised patches. In particular complete transport models are distinguishable from incomplete transport models because they mediate ion fluxes, and extracellular chloride plays an important role. Thus the complete transporter model predicts that:

1) Significant steady-state currents will arise from the removal of either Cl_i or Cl_e. When Cl_i is removed there would be an increase in outward current, and a negative shift in the reversal potential of the I(V). When Cl_e is removed there would be an increase in inward current and a positive shift in the reversal potential of the I(V).
2) Significant changes to the NLC will arise from removing Cl_e when $[Cl_i]$ is 1mM. The V_0 of the NLC would shift to more hyperpolarized potentials and the C_{pk} and Q_{max} would increase.

Furthermore if sulphate does interact with prestin to increase the shift in V_0 it is predicted that:

3) If an alternative anion is used to replace chloride the shift in V_o would be smaller.

These predictions are discussed in the context of evidence from whole-cell experiments in Ch.5.

Chapter 4

Modelling Prestin: Chloride Combined with Intrinsic Charge as the Voltage-Sensor

4.1 Introduction

In the previous chapter, it was shown that a model of prestin as a chloride transporter can reproduce many of the key experimental observations of the dependence of the NLC on $[Cl_i]$ made in excised patches (Oliver et al. 2001, Fakler and Oliver 2002). However although with certain rate constants this model produces a depolarising shift in V_o when $[Cl_i]$ is reduced, a specific interaction between prestin and sulphate is required to produce the correct magnitude of shift. Furthermore other discrepancies with the experimental observations remain. A significant NLC is predicted when Cl_i is removed, and the apparent β is predicted to decrease as $[Cl_i]$ is reduced. Thus it is concluded that the transporter model described in Ch.3 must be refined.

It has been proposed that the movement of some intrinsic charge might accompany the movement of chloride (Gummer 2003). In this chapter models which incorporate the movement of intrinsic charge are tested for their ability to reproduce the key experimental observations outlined in Ch.3.1. Whilst an incomplete transporter model, with intrinsic charge movement is shown to be inadequate, a chloride/sulphate exchanger model, with intrinsic charge movement is able to qualitatively reproduce all the key experimental observations.

4.2 Methods

Simulations were performed in Matlab. For details see Ch. 2.1. All NLCs are predicted for a patch containing 10,000 prestin molecules. Definitions are the same as those described in Ch.3.2.

4.3 Results

4.3.1 Model 5: A Three-State Model with Intrinsic Charge Movement

In the three-state model with intrinsic charge movement, the chloride ion binds to a first binding site facing the intracellular medium and is then transported across the membrane to a second site (Figure 4.1). This is the same as the three-state model described in Ch.3.3.2 (Figure 3.3) except the transition between the two bound states is assumed to include the movement of some intrinsic charged residues, such that there is a net movement of positive charge across the membrane. Thus in contrast to the three-state model in Ch.3.3.2 where the only charge translocation is due to the movement of a chloride ion, depolarisation increases the rate at which chloride is moved across the membrane to the second site. Since depolarisation increases the forward rate of the transition from E1.Cl→E2.Cl, and OHCs are known to contract upon depolarisation this transition is assumed to coincide with a conformation change to a contracted state.

This three-state model can be described with a reaction scheme (Figure 4.1B) where E0, E1.Cl, and E2.Cl are respectively the proportion of prestin in that sate. The reaction scheme is the same as for the three-state model with chloride as the only voltage sensor (Figure 3.3B), so the dissociation constant for the first step is given by

equation (3.6) and the forward and backward rate constants of the second step are given by equation (3.7).

$$k_2(V) = k_2(0)e^{\frac{\beta V_m}{2}} \text{ and } k_{-2}(V) = k_{-2}(0)e^{\frac{\beta V_m}{2}} \qquad (3.7)$$

However for this model, since there is a net movement of positive charge, **β is positive**.

The dependence of V_o on $[Cl_i]$ is given by equations (3.9) and (3.10), but with a positive β. In consequence, as was observed experimentally, the shift in V_o is in the depolarising direction when $[Cl_i]$ is reduced. However there is no decrease in C_{pk} or Q_{max} as $[Cl_i]$ is reduced. V_o saturates at high $[Cl_i]$.

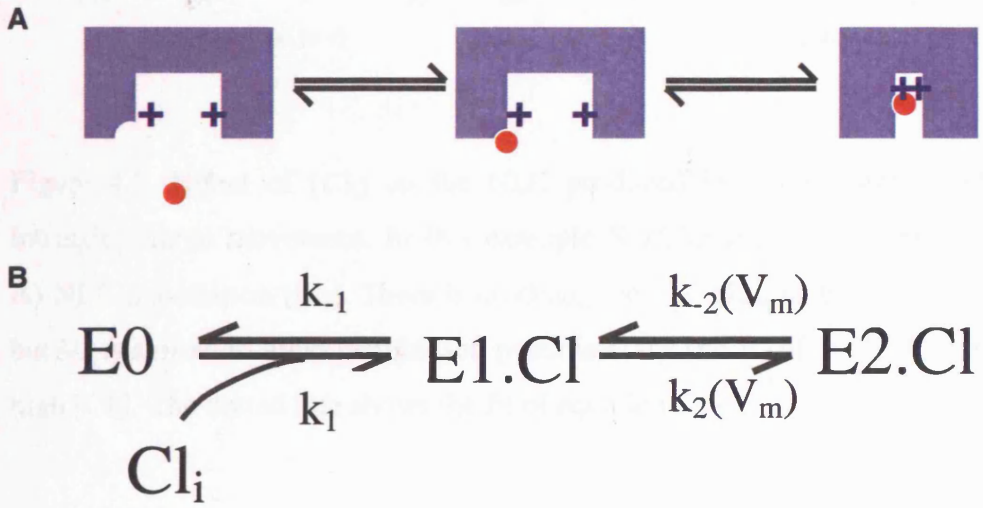

Figure 4.1. Illustration of a three-state model with intrinsic charge movement. A) Prestin changes from an expanded to a contracted state when a chloride ion moves from the first binding site at the mouth of the pore to a second binding site at the top of the pore, accompanied by the movement of positive residues. B) The reaction scheme used to describe this model is the same as that for the three-state model with chloride as the voltage sensor (Figure 3.3B). k_1 reflects the rate of chloride binding and depends on $[Cl_i]$, k_{-1} is a constant and depends simply on the rate of dissociation of chloride from the binding site. Both k_2 and k_{-2} are voltage-dependent.

In simulations β was chosen to be $0.033mV^{-1}$, k_{-1} was chosen to be $10^5 s^{-1}$, and k_1 was varied between $10^6 M^{-1}s^{-1}$ and $10^8 M^{-1}s^{-1}$ to give values for K_D between 1mM and 100mM. $k_2(0)$ and $k_{-2}(0)$ were varied between 10^3 s^{-1} and 10^5 s^{-1}. An example is shown in Figure 4.2. In this particular example V_o saturates at 0mV, however the saturating value of V_o depends on the combination of rate constants chosen.

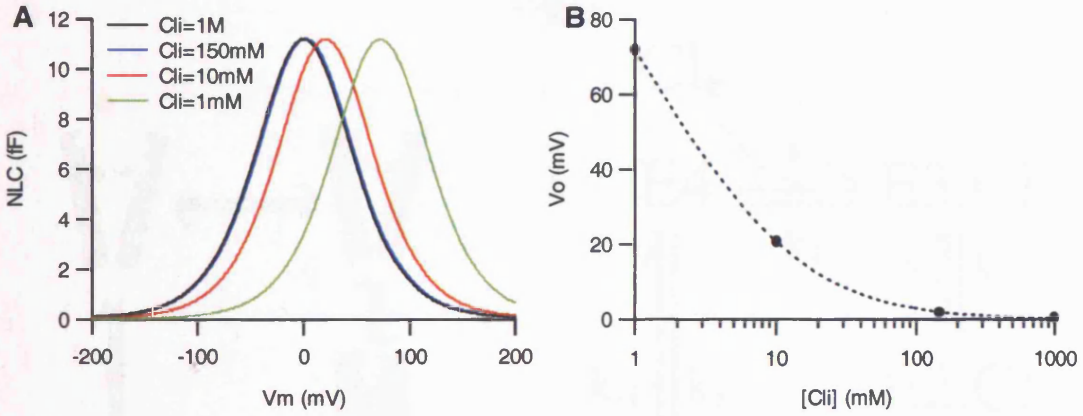

Figure 4.2. Effect of $[Cl_i]$ on the NLC produced by a three-state model with intrinsic charge movement. In this example $K_D(Cl_i)$=10mM, $k_2(0)=k_{-2}(0)=10^4 s^{-1}$. A) NLC depends on $[Cl_i]$. There is no change in C_{pk}, Q_{max} or β as $[Cl_i]$ is reduced but V_o is shifted to more depolarised potentials. B) The V_o of the NLC saturates at high $[Cl_i]$. The dotted line shows the fit of equation (3.9).

4.3.2 Model 6: Prestin as a Chloride Transporter with Intrinsic Charge Movement

It was shown in Ch.4.3.1 that if the movement of intrinsic positively charged residues accompanies the movement of chloride across the membrane, then the shift in V_o is in the depolarising direction when $[Cl_i]$ is reduced. It was also shown in Ch.3.3.4 that when chloride is fully transported across the membrane, with the transition between the unbound inward and outward facing states permitted, then a

decrease in C_{pk} and Q_{max} is predicted as $[Cl_i]$ is reduced. From these two findings it follows that a model, which includes both the movement of intrinsic charge and the full transport of chloride should predict a NLC that decreases and shifts to more depolarised V_m when $[Cl_i]$ is reduced. A chloride transporter model, which is the same as that described in Ch.3.3.4 (Figure 3.7), but with intrinsic charge movement is represented in Figure 4.3.

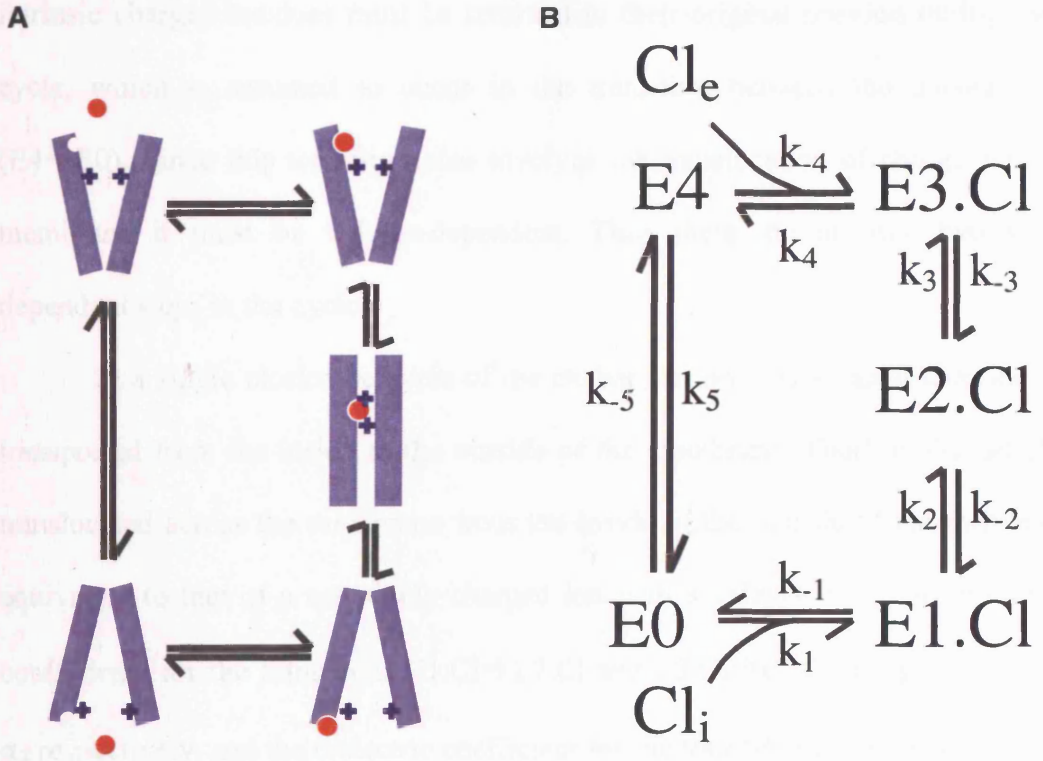

Figure 4.3. Illustration of a chloride transporter model with intrinsic charge movement. A) Chloride binds first to a binding site facing the intracellular medium. It is then translocated across the membrane and released to the extracellular medium, before prestin returns to the unbound inward facing state. Positively charged residues accompany the movement of chloride across the membrane. B) The reaction scheme used to describe this model is the same as that described for the chloride transporter model with chloride as the voltage sensor (Figure 3.7B).

In this model prestin can be either inward facing (E0) or outward facing (E4). A chloride ion binds to a binding site facing the intracellular medium. The chloride ion, then moves through the membrane to a second site, accompanied by the movement of intrinsic positively charged residues, and a conformational change. From there it moves to a third site facing the extracellular medium, and is released to the extracellular medium, forcing prestin into its outward facing unbound state. The intrinsic charged residues must be returned to their original position during the full cycle, which is assumed to occur in the transition between the unbound states (E4→E0). Since this transition also involves the translocation of charge across the membrane it must be voltage-dependent. Thus there are at least two voltage-dependent steps in the cycle.

In a single clockwise cycle of the exchanger, one monovalent chloride ion is transported from the inside to the outside of the membrane. Therfore the net charge translocated across the membrane from the inside to the outside of the membrane is equivalent to that of a negatively charged ion with a valence of –1. If the dielectric coefficients for the transitions E1.Cl→E2.Cl and E2.Cl→E3.Cl are given by α_1 and α_2 respectively, and the dielectric coefficient for the transition E4→E0 is given by α_3, then

$$\alpha_1 + \alpha_2 + \alpha_3 = -1 \tag{4.1}$$

with

$$\alpha_1 = z\delta_1 + \mu_1 \tag{4.2}$$

$$\alpha_2 = z\delta_2 + \mu_2 \tag{4.3}$$

$$\alpha_3 = -\mu_1 - \mu_2 \tag{4.4}$$

where z is the valence of the chloride ion, δ_1 and δ_2 are the fraction of the dielectric crossed in the transition and μ_1 and μ_2 are the contributions due to the intrinsic charge movement.

The case where both the chloride ion and the positively charged residues are moved across the whole membrane dielectric in the transition E1.Cl→E2.Cl, and the positively charged residues are re-oriented in the transition E4→E0 (α_1=1, α_2=0 and α_3=-2) was investigated. In this model for certain combinations of rate constants, V_o shifts in the depolarising direction when [Cl_i] is reduced. However the magnitude and apparent β of the NLC increases when either [Cl_i] or [Cl_e] are very low (Figure 4.4).

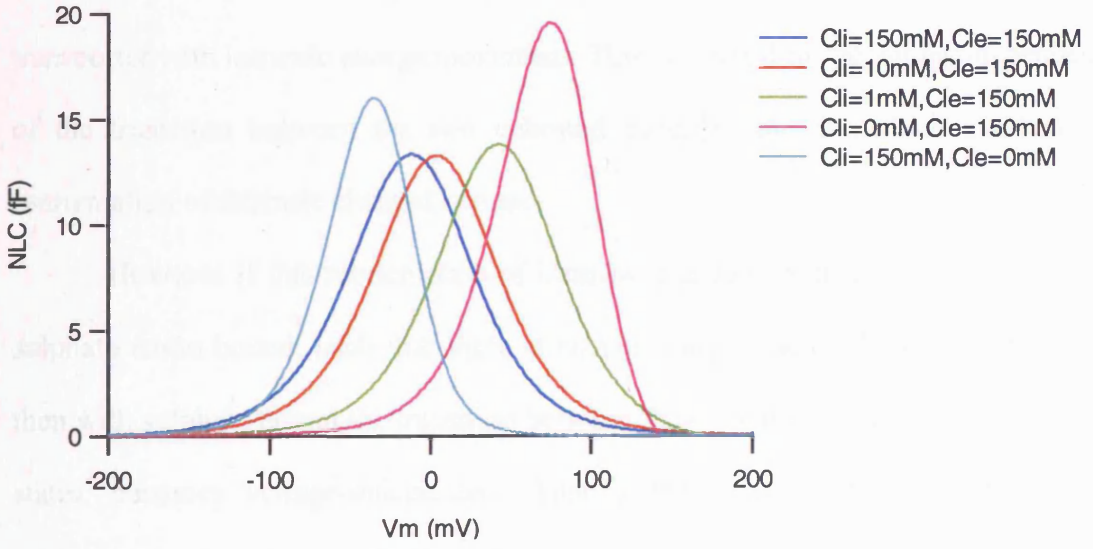

Figure 4.4. Effect of [Cl_i] on the NLC produced by a chloride transporter model with intrinsic charge movement. In this example $k_1=10^7M^{-1}s^{-1}$,$k_{-1}=10^5s^{-1}$, $k_2(0)=k_{-2}(0)=10^4s^{-1}$,$k_3=k_{-3}=100s^{-1}$,$k_4=10^5s^{-1}$,$k_{-4}=10^7M^{-1}s^{-1}$,$k_5=k_{-5}=10s^{-1}$. NLCs shift to more positive V_m when [Cl_i] is reduced. However NLC is increased when either Cl_i, or Cl_e is removed.

The increase in C_{pk}, Q_{max} and apparent β of the NLC when either $[Cl_i]$ or $[Cl_e]$ are very low is produced because under these conditions the contribution to the NLC that arises from the voltage-dependent transition E4→E0 increases. This contribution to the NLC has a larger C_{pk} , Q_{max} and β, as a consequence of the fact that more net charge is transferred across the transition E4→E0 than across the transition E1.Cl→E2.Cl (i.e the magnitude of the dielectric coefficient is larger).

The same behaviour is produced for the case where α_1=0.8, α_2=0.2, α_3=-2.

4.3.3 Model 7: Prestin as a Chloride/Sulphate Exchanger with Intrinsic Charge Movement

In Ch. 4.3.2 it was shown that the key experimental observations made from excised patches are not reproducible if prestin is considered to be a chloride transporter with intrinsic charge movement. This is a result of the voltage-dependence of the transition between the two unbound states of prestin, which involves the reorientation of intrinsic charged residues.

However if this reorientation of intrinsic charged residues only occurs with a sulphate anion bound, such that there is no net charge moved during the transition, then with sulphate bound the transition between the outward facing and inward facing states, becomes voltage-independent. This is the basis of the alternating-access exchanger model shown in Figure 4.5.

In a single clockwise cycle of the exchanger, one monovalent chloride ion is transported from the inside to the outside of the membrane in exchange for a divalent sulphate ion which is tranported from the outside to the inside of the membrane. The net charge translocated across the membrane from the inside to the outside of the

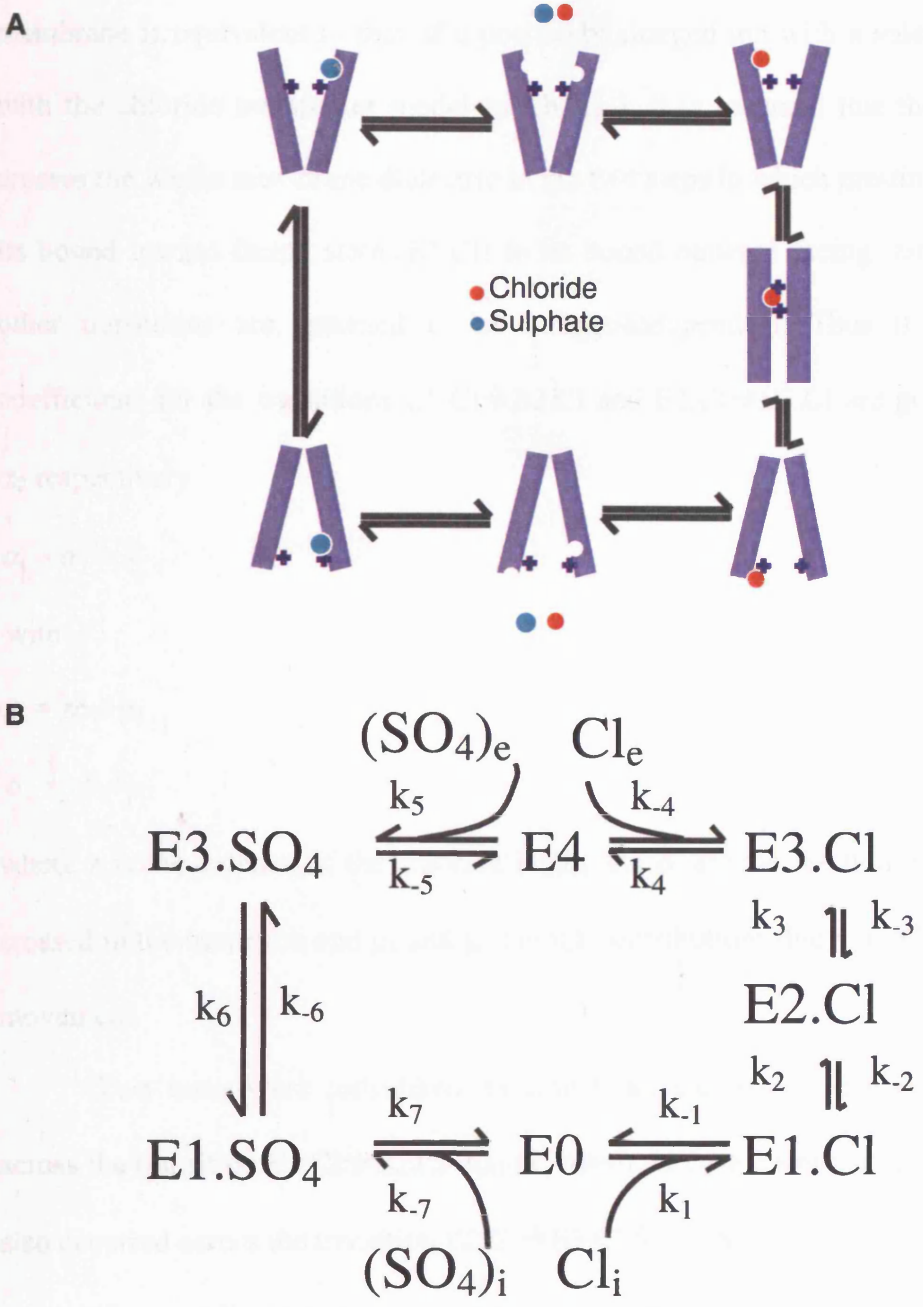

Figure 4.5 Illustration of a chloride/sulphate exchanger model with intrinsic charge movement. A) An alternating-access exchanger model for prestin, in which prestin can only change between the inward and outward facing states by binding either chloride or sulphate. B) The reaction scheme for this model.

membrane is equivalent to that of a positively charged ion with a valence of +1. As with the chloride transporter model in Ch.3.3.4. it is assumed that the chloride ion crosses the whole membrane dielectric in the two steps in which prestin changes from its bound inward facing state (E1.Cl) to its bound outward facing state (E2.Cl). All other transitions are assumed to be voltage-independent. Thus if the dielectric coefficients for the transitions E1.Cl→E2.Cl and E2.Cl→E3.Cl are given by α_1 and α_2 respectively

$$\alpha_1 + \alpha_2 = 1 \tag{4.5}$$

with

$$\alpha_1 = z\delta_1 + \mu_1 \tag{4.6}$$

$$\alpha_2 = z\delta_2 + \mu_2 \tag{4.7}$$

where z is the valence of the chloride ion,δ_1 and δ_2 are the fraction of the dielectric crossed in the transition and μ_1 and μ_2 are the contributions due to the intrinsic charge movement.

Two cases were considered. In case 1, all the charge translocation occurred across the transition E1.Cl→E2.Cl (α_1=1, α_2=0), in case 2 some charge translocation also occurred across the transition E2.Cl→E3.Cl (α_1=0.8, α_2=0.2).

For a cyclic process microscopic reversibility must be obeyed. Thus there are 13 independent rate constants for this model. Since none of the rate constants are known, various combinations were tested using rate constants that were comparable to those known for other transporters. Table 4.1 shows the range of rate constants tested.

Rate constant	Range of values tested
k_1	10^6 to $2x10^7$ $M^{-1}s^{-1}$
k_{-1}	10^5 s^{-1}
$k_2(0)$	10^4 to 3×10^4 s^{-1}
$k_{-2}(0)$	10^4 s^{-1}
$k_3(0)$	8 to 500 s^{-1}
$k_{-3}(0)$	50 to 10^3 s^{-1}
k_4	10^5 s^{-1}
k_{-4}	10^6 to 10^7 $M^{-1}s^{-1}$
k_5	10^6 to 2×10^7 $M^{-1}s^{-1}$
k_{-5}	$10^5 s^{-1}$
k_6	10 to $10^3 s^{-1}$
k_{-6}	100 to $2 \times 10^3 s^{-1}$
k_7	$10^5 s^{-1}$
k_{-7}	10^6 to $10^7 M^{-1}s^{-1}$

Table 4.1. Rate constants tested in simulations for chloride/sulphate exchanger model with intrinsic charge movement.

In agreement with experimental observations all combinations of rate constants tested produce a positive shift in V_o and a decrease in C_{pk} and Q_{max} when $[Cl_i]$ is reduced. The closest reproduction of the experimental observations is produced for case 2 (Figure 4.6). In this case when $[Cl_i]$ is reduced from 150mM to 1mM there is both a large positive shift in V_o (by 102mV) and a decrease in C_{pk} and Q_{max} (to 26% and 28% respectively). A comparison of the $[Cl_i]$ dependence of the Boltzmann parameters predicted by the model with the values determined by Fakler and Oliver (2002) show that the predictions of the model are qualitatively consistent with the experimental observations (Figure 4.6B).

In addition there is no effect on the NLC of removing Cl_e and although a significant NLC remains when Cl_i is removed its V_o is shifted to very positive V_m (~120mV), and its Q_{max} and C_{pk} are reduced to ~20% of the NLC for high $[Cl_i]$. Hence it is possible that such a NLC would not be detected over the range of V_m used experimentally (typically −100mV to 100mV). Therefore the chloride/sulphate exchanger model with intrinsic charge movement can qualitatively reproduce all of the key experimental observations relating to the dependence of NLC on $[Cl_i]$.

The experimental observation that removing Cl_e did not lead to a change in the NLC led to the proposal that prestin did not fully transport chloride across the membrane, but rather shuttled chloride from the intracellular medium back and forth across the membrane without allowing it to dissociate at the extracellular surface. In this section it has been shown that even if a full transport cycle is included no effect on the NLC is produced when Cl_e is removed in the presence of high $[Cl_i]$. However this model does predict a significant effect on the NLC if Cl_e is removed in the presence of low $[Cl_i]$ (Figure 4.7). When $[Cl_i]$ is 1mM, reducing $[Cl_e]$ leads to a further positive shift in the V_o of the NLC and an increase in C_{pk} and Q_{max}, if both Cl_i and Cl_e are replaced with sulphate.

As a further test of the model the current transients resulting from an 'on' voltage-step from -120mV to +40mV, and an 'off' voltage-step from +40mV to -120mV were also simulated for a patch containing 10,000 prestin molecules under the condition that $[Cl_i]=[Cl_e]=150$mM. Exponential fits of these transients give decay time constants for both transients that are in good agreement with the fast decay time constants measured by Gale and Ashmore (1997b) with a similar protocol (Figure 4.8).

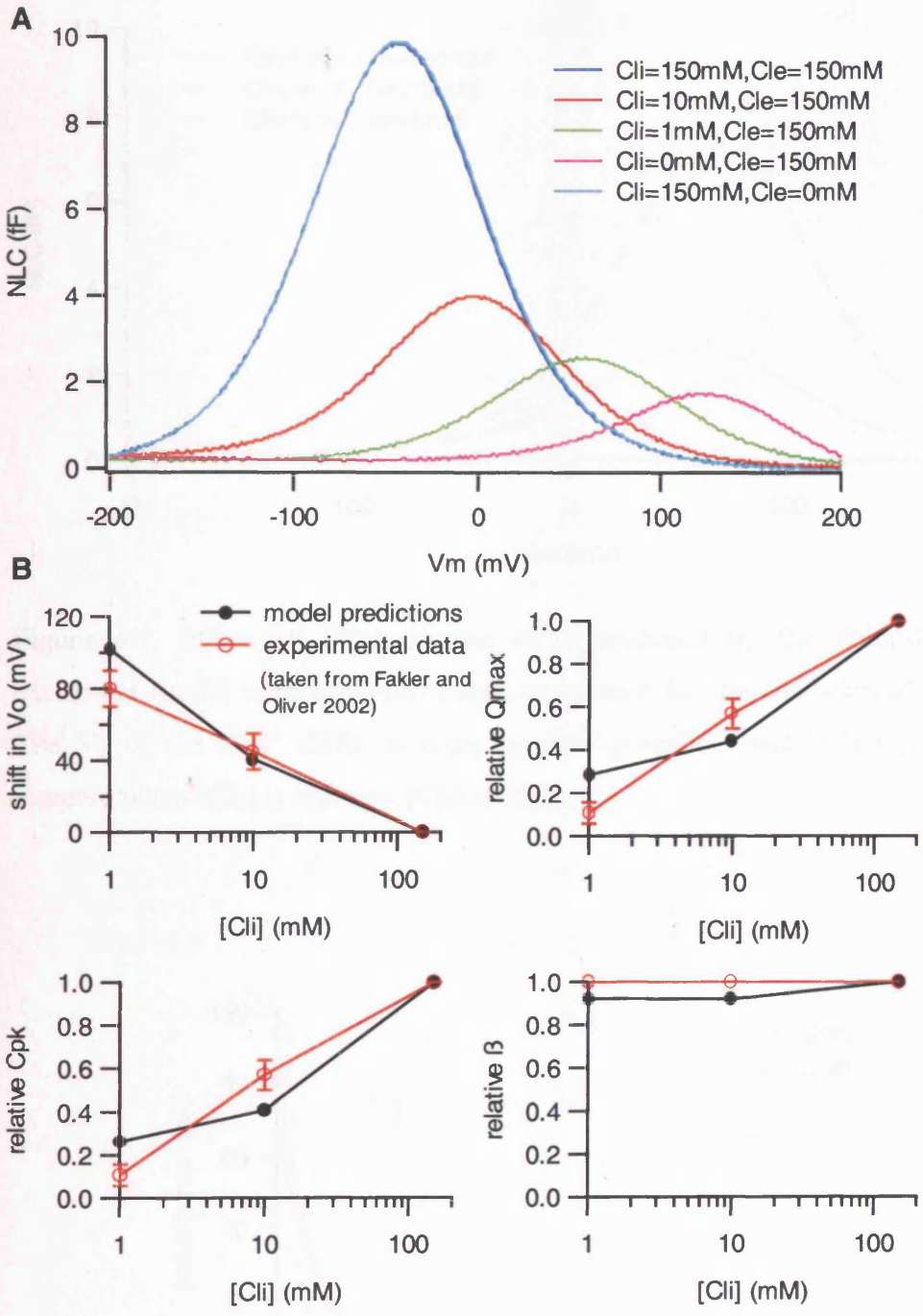

Figure 4.6. Effect of $[Cl_i]$ on the NLC produced by a chloride/sulphate exchanger model with intrinsic charge movement (α_1=0.8,α_2=0.2). The exchanger model reproduces most aspects of experimental observations. A) NLCs produced by model with rate constants; $k_1=2x10^4 mM^{-1}s^{-1}$, $k_{-1}=10^5 s^{-1}$, $k_2(0)=4x10^4 s^{-1}$, $k_{-2}(0)=10^4 s^{-1}$, $k_3(0)=8s^{-1}$, $k_{-3}(0)=100s^{-1}$, $k_4=10^5 s^{-1}$, $k_{-4}=8x10^3 mM^{-1}s^{-1}$, $k_5=10^4 s^{-1}$, $k_{-5}=10^5 s^{-1}$, $k_6=250s^{-1}$, $k_{-6}=10^3 s^{-1}$, $k_7=10^5 s^{-1}$, $k_{-7}=2x10^3 mM^{-1}s^{-1}$. B) Comparison of the predicted $[Cl_i]$ dependence of the Boltzmann parameters with experimental observations.

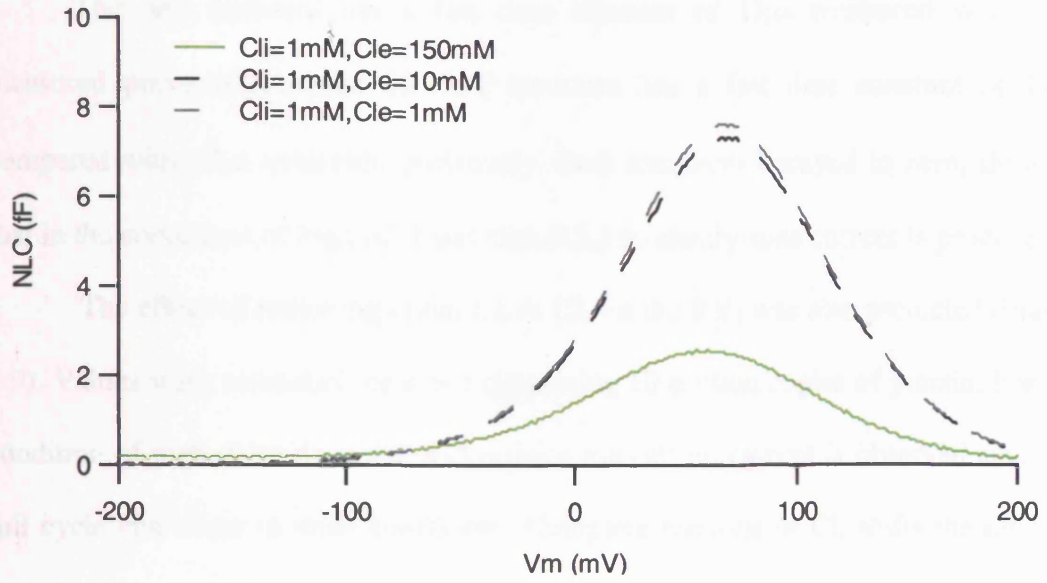

Figure 4.7. Effect of $[Cl_e]$ on the NLC produced by the chloride/sulphate exchanger model with intrinsic charge movement for the condition of low $[Cl_i]$. The V_o of the NLC shifts to more positive potentials and both C_{pk} and Q_{max} increase when $[Cl_e]$ is reduced. $[Cl_i]$ is 1mM.

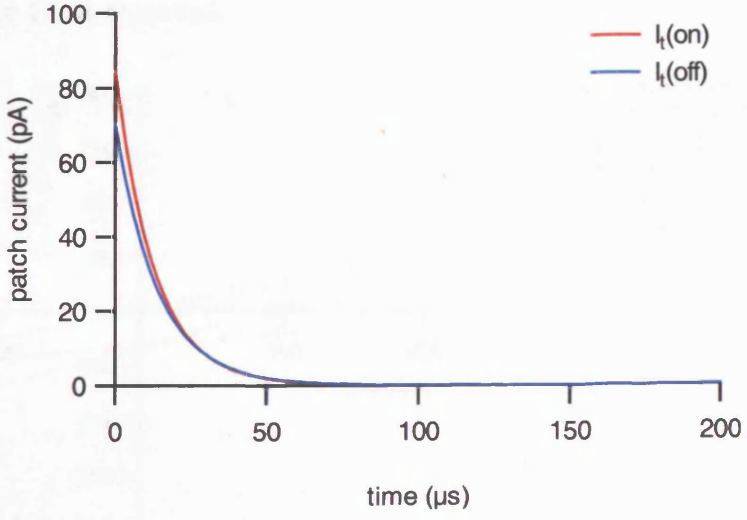

Figure 4.8. Simulated transient currents in response to a voltage-step. I_t(on) is the transient current following an 'on' step from -120mV to +40mV, I_t(off) is the transient current following an 'off' step from +40mV to –120mV. Both transients decay to zero. Currents are estimated for a patch with 10,000 prestin molecules.

The 'on' transient has a fast time constant of 13μs compared with 10μs measured previously, whilst the 'off' transient has a fast time constant of 14μs compared with 13μs measured previously. Both transients decayed to zero, showing that in the conditions of high [Cl_i] and high [Cl_e] no steady-state current is produced.

The effect of removing either Cl_i or Cl_e on the I(V) was also predicted (Figure 4.9). Values were estimated for a cell containing 10 million copies of prestin. For the condition of high chloride inside and outside the cell no current is observed since no full cycle can occur in these conditions. Complete removal of Cl_i shifts the reversal potential to an infinitely positive V_m, and leads to an inward current of ~120pA at a holding potential of 0mV. Complete removal of Cl_e shifts the reversal potential to an infinitely negative V_m, and leads to a very small outward current of ~10pA at a holding potential of 0mV. If a 1nS pipette leak (I_{pip}) is added to the currents through prestin, then in experimental conditions a shift in reversal potential of +87mV would be observed when Cl_i is removed and a shift in reversal potential of -10mV would be observed when Cl_e is removed.

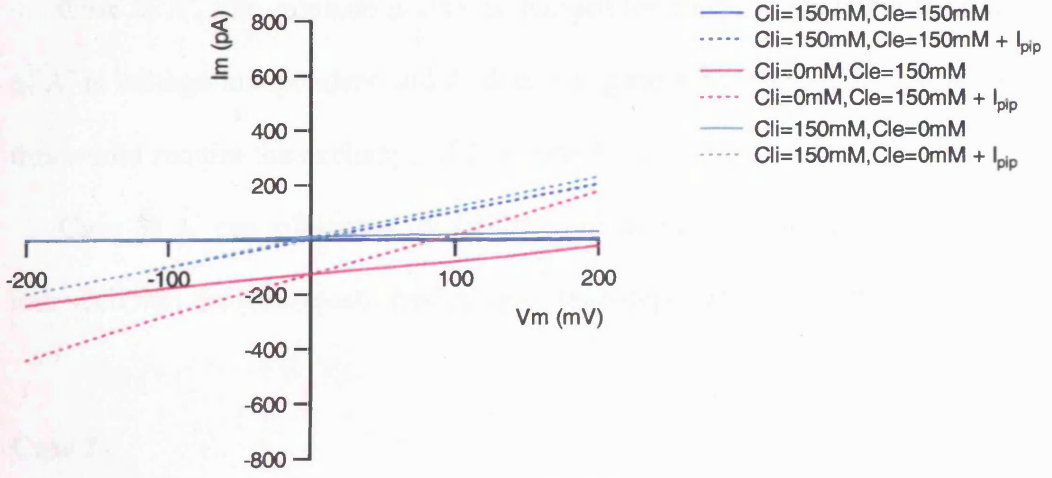

Figure 4.9. Simulated I(V)s for an OHC, produced by the chloride/sulphate exchanger model with intrinsic charge movement. Removal of Cl_i, leads to a positive shift in the reversal potential and an increase in inward current at 0mV. Removal of Cl_e leads to a negative shift in the reversal potential and an increase in outward current at 0mV.

4.3.4 Model 7: Predictions for Replacing Cl_i with a Different Anion

In Ch.4.3.3 it was shown that a model of prestin as a chloride/sulphate exchanger with intrinsic charge movement reproduces many aspects of the key experimental observations. If prestin does behave as a chloride/sulphate exchanger, then the dependence of the NLC on $[Cl_i]$ when Cl_i is replaced with an alternative anion to sulphate could be very different. In this section predictions are made about the dependence of the NLC on $[Cl_i]$ when Cl_i is replaced with a different anion. In Ch.5 the dependence of the NLC on $[Cl_i]$ with different substituting anions is investigated.

If a monovalent anion, A^- is used to replace Cl_i there are several possible ways for A^- to affect the dependence of the NLC on $[Cl_i]$:

Case 1) If A^- does not interact with prestin, only part of the exchange cycle involving chloride (E0→E1.Cl→E2.Cl→E3.Cl→E4) can occur. A complete cycle cannot occur since without sulphate present, prestin is unable to return from the unbound outward facing state (E4) to the unbound inward facing state (E0).

Case 2) A^-, like sulphate is also exchanged for chloride, such that the translocation of A^- is voltage-independent and A^- does not generate a NLC. Since A^- is monovalent this would require the exchange of 2 A^- ions for 1 Cl^- ion.

Case 3) A^- can substitute for Cl^- or equivalently 1 A^- ion is exchanged for 1 Cl^- ion, such that the translocation of A^- is voltage-dependent and generates a NLC.

Case 1)

In this case only the chloride part of the exchange cycle is involved. The V_o of the NLC shifts to more positive V_m as $[Cl_i]$ is reduced and replaced with A^-, but no decrease in C_{pk} or Q_{max} is produced (Figure 4.10). When either Cl_i or Cl_e are

completely removed the NLC is abolished. Furthermore since a full cycle cannot occur there is no steady-state current through prestin regardless of the concentration gradient across it.

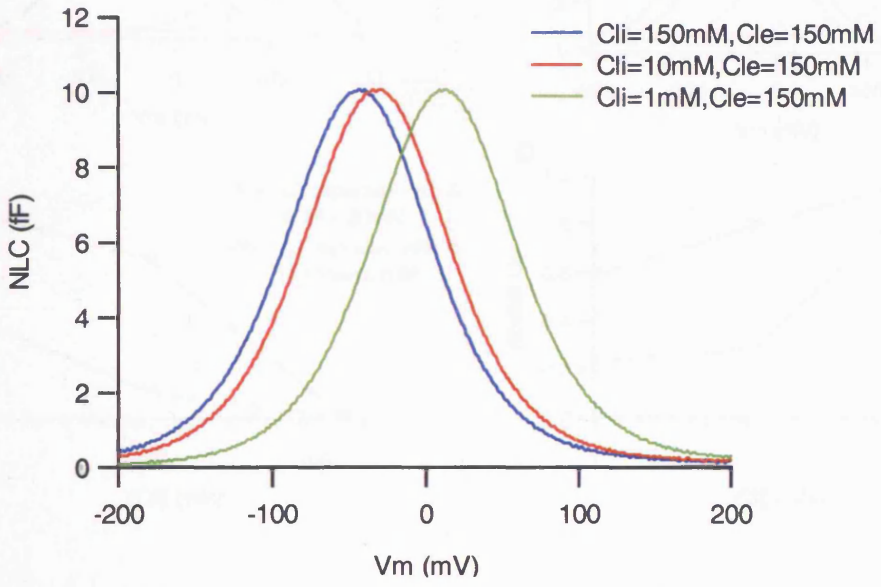

Figure 4.10. Effect of $[Cl_i]$ on the NLC produced by the chloride/sulphate exchanger model with intrinsic charge movement, when Cl_i is replaced with a non-interacting anion. V_o of NLC shifts to more positive V_m, when Cl_i is reduced and replaced with A^-.

Case 2)

V_o shifts to more positive V_m as $[Cl_i]$ is reduced, and C_{pk} and Q_{max} decrease. The exact shift in V_o and decrease in C_{pk} and Q_{max} depend on the affinity of A^- for its binding sites. If we assume that the binding of the two A^- ions are equivalent such that the affinity of the second A^- ion is equal to the affinity of the first A^- ion, then it is predicted that the shift in V_o and decrease in C_{pk} and Q_{max} increase as the affinity of A^- increases (Figure 4.11). If chloride is removed from both intracellular and extracellular media then there is no NLC since A^- does not generate NLC.

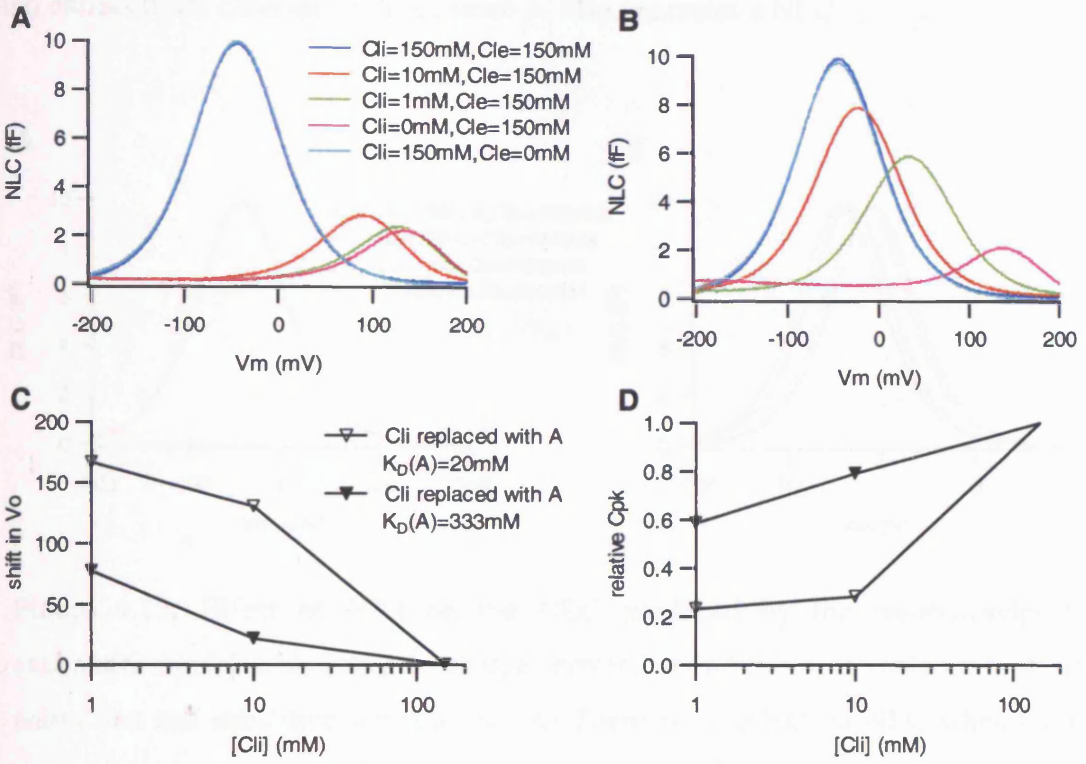

Figure 4.11. Effect of $[Cl_i]$ on the NLC produced by the chloride/sulphate exchanger model with intrinsic charge movement, when Cl_i is progressively replaced with an alternative exchangeable anion, to sulphate. V_o shifts to more positive V_m and C_{pk} and Q_{max} decrease as $[Cl_i]$ is reduced and replaced with A^-, if 2 A^- ions are exchanged for 1 Cl^- ion. A) Example with $K_D(A)$=20mM. B) Example with $K_D(A)$=333mM. C) The shift in V_o is greater if the affinity of A^- is greater. D) The decrease in C_{pk} is greater if the affinity of A^- is greater.

Case 3

Assuming the rate at which A^- is translocated across the membrane is equal to that for Cl^- then if the affinity of $A^- \geq$ the affinity of Cl_i, there is no effect on the NLC of replacing Cl_i with A^-. If the affinity of A^- is much less than for Cl_i then a positive shift in V_o is produced as Cl_i is replaced with A^-, but no change in C_{pk} or Q_{max} is

produced (Figure 4.12). C_{pk} and Q_{max} are not affected by replacing both intracellular and extracellular chloride with A^-, since A^- also generates a NLC.

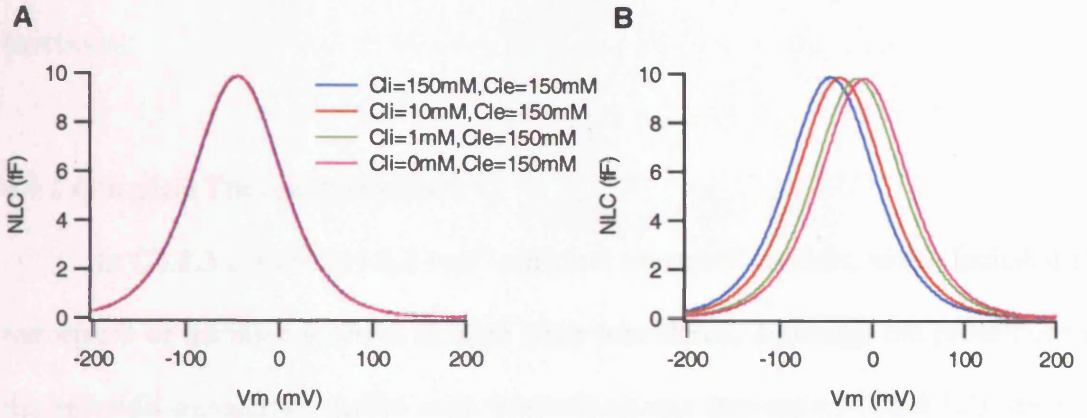

Figure 4.12. Effect of $[Cl_i]$ on the NLC produced by the chloride/sulphate exchanger model with intrinsic charge movement, when Cl_i is replaced with an anion that can substitute for chloride. A) There is no effect on NLC when Cl_i is replaced with A^- if the affinity of $A^- \geq$ the affinity of Cl_i. In the example shown, $K_D(Cl_i)$=5mM, $K_D(A)$=0.33mM. B) V_o shifts to more positive V_m when Cl_i is replaced with A^-, if the affinity of $A^- <<$ the affinity of Cl_i. In the example shown $K_D(A)$=333mM.

4.4 Discussion

4.4.1 Incomplete Transport Model

In Ch.4.3.1 an 'incomplete transport' model for prestin, based on the model proposed by Oliver et al. (2001) was formulated to include the modification that the movement of chloride was accompanied by the movement of intrinsic positively charged residues. In comparison with the incomplete transport models with chloride as the only voltage-sensor, this model gives a better reproduction of the key

experimental observations in that it produces the correct direction for the shift in V_o when $[Cl_i]$ is reduced. Nevertheless it does not predict any change in C_{pk} and Q_{max} as $[Cl_i]$ is reduced, and is therefore an inadequate model to describe how prestin functions.

4.4.2 Complete Transport Models

In Ch.4.3.2 and Ch.4.3.3 two 'complete transport' models, which included the movement of intrinsic positive charges were considered. Although the predictions of the chloride transporter model with intrinsic charge movement (Ch.4.3.2) are very different to the experimental observations, the chloride/sulphate exchanger with intrinsic charge movement (Ch4.3.3) produces a close reproduction of the key experimental observations. The predictions of the chloride/sulphate exchanger model with intrinsic charge movement are similar to the experimental observations in several ways:

1) The V_o of the NLC shifts in the depolarising direction when $[Cl_i]$ is reduced, by a similar magnitude to the shift in V_o measured experimentally (Figure 4.6B).
2) A decrease in C_{pk} and Q_{max} is produced as $[Cl_i]$ is reduced.
3) Removal of Cl_e has no effect on the NLC, when $[Cl_i]$ is high.
4) The NLC is not abolished when Cl_i is removed, but is shifted to such positive V_m that it would likely be undetectable within the range of V_m used in experiments.
5) The apparent β decreases only slightly (by <10%) when $[Cl_i]$ is reduced, and might not be detected.

Additionally, the fast decay time constants of the transient currents produced in response to a voltage-step are similar to those measured experimentally.

Most combinations of rate constants tested produce these general trends. Thus the qualitative dependence of the NLC on $[Cl_i]$ produced by the model is not sensitive to small changes in any of the rate constants. Therefore the chloride/sulphate exchanger model with intrinsic charge movement is qualitatively consistent with all the key experimental observations.

4.4.3 Predictions of the Chloride/Sulphate Exchanger Model with Intrinsic Charge Movement

There are several additional predictions of the chloride/sulphate exchanger model with intrinsic charge movement, which cannot be compared with the key experimental observations outlined in Ch.3.1. The chloride/sulphate exchanger model with intrinsic charge movement predicts that:

1) Significant steady-state currents will arise from the removal of either Cl_i or Cl_e. When Cl_i is removed there would be an increase in inward current, and a positive shift in the reversal potential of the I(V). When Cl_e is removed there would be an increase in outward current and a negative shift in the reversal potential of the I(V).
2) Significant changes to the NLC will arise from removing Cl_e when $[Cl_i]$ is 1mM. The V_o of the NLC would shift to more derpolarized potentials and the C_{pk} and Q_{max} would increase.

Furthermore since sulphate is an important component in this chloride/sulphate exchanger model, it is predicted that

3) If an alternative anion to sulphate is used to replace Cl_i then the dependence of the NLC on $[Cl_i]$ would be altered.

4.4.4 Comparison of the Chloride Transporter Model (Model 3) with the Chloride/Sulphate Exchanger Model with Intrinsic Charge Movement (Model 7)

Both the chloride transporter model with chloride as the voltage-sensor (Ch.3.3.4) and the chloride/sulphate exchanger with intrinsic charge movement (Ch.4.3.3) can predict a positive shift in V_o and a decrease in C_{pk} and Q_{max} as $[Cl_i]$ is reduced. However whilst clear discrepancies remain between the experimental observations and the predictions of the chloride transporter model, the predictions of the choride/sulphate exchanger are qualitatively consistent with all the key experimental observations. Furthermore whilst the chloride transporter model requires very specific combinations of rate constants to reproduce the experimental observations the chloride/sulphate exchanger produces the same general trends for most combinations of rate constants. Therefore, at present the chloride/sulphate exchanger model is the best model to describe how prestin functions.

The chloride transporter model, and the chloride/sulphate exchanger model with intrinsic charge movement, give very different predictions for the dependence of the I(V) on $[Cl_i]$ and $[Cl_e]$, and the NLC on $[Cl_e]$, but importantly both require that sulphate also interacts with prestin. In fact none of the models considered in Ch.3 and Ch.4, in which sulphate did not play a part, were able to reproduce the experimental observations. The involvement of sulphate has been suggested previously (Rybalchenko and Samtos-Sacchi 2003) but has not gained widespread acceptance, thus the potential involvement of sulphate is addressed in Ch.5.

Chapter 5

Testing the 'Complete Transport' Model: Effect of Replacing Chloride with Different Anions

5.1 Introduction

In previous studies it was shown that the non-linear capacitance (NLC) of outer hair cells (OHCs) depended on the concentration of intracellular chloride (Cl_i), when Cl_i was replaced with sulphate (Oliver et al. 2001, Fakler and Oliver 2002, Rybalchenko and Santos-Sacchi 2003). Many of the key observations from the experiments performed on excised OHC patches (Oliver et al. 2001, Fakler and Oliver 2002), were reproduced by two different models in which chloride was completely transported across the membrane: the chloride transporter model (Ch.3.3.4 and Ch.3.3.5) and the chloride/sulphate exchanger model with intrinsic charge movement (Ch.4.3.3). Of these two models the chloride/sulphate exchanger model with intrinsic charge movement was found to give the closest reproduction of the experimental observations. The chloride/sulphate exchanger model requires that sulphate interacts with prestin, and accordingly predicts that the dependence of the NLC on $[Cl_i]$ would be changed by replacing Cl_i with an alternative anion. The model also predicts that the I(V) would be considerably altered by the removal of Cl_i or extracellular chloride (Cl_e), and that there would be a significant effect on the NLC if $[Cl_e]$ was reduced when $[Cl_i]$ was low.

The aim of this chapter is to test some of these predictions. In particular the role of sulphate was examined. Thus experiments are described which investigate the

effect on the NLC of replacing Cl_i with sulphate, gluconate, glutamate or maleate. Since it is easier to control the intracellular ionic concentrations in the excised patch configuration, replacement with gluconate was first carried out in excised patches. However due to the difficulty of obtaining patches the approach was subsequently changed to using the whole-cell configuration. Additionally for comparison with the predictions of the model, the I(V)s that were recorded simultaneously with the NLC, were analysed. Finally an experiment to investigate the effect on the NLC when $[Cl_e]$ was reduced with only 1mM $[Cl_i]$ is described.

5.2 Methods

The experiments described in this chapter were performed using the patch clamp technique in either the excised inside-out patch configuration or the whole-cell configuration. Cells were visually monitored for changes in morphology such as cell swelling. No cell swelling was noted, but since changes were not quantified it is possible small changes in cell volume did occur. All values for V_o and V_{rev} were corrected for liquid junction potentials, unless otherwise stated. For more details see Ch.2.

5.2.1 Data Analysis

In the whole-cell experiments of Ch.5.3.2 to Ch.5.3.5, the NLC was recorded 10s after break-in, and then every 18s for up to 5 minutes. Each trace was fitted with the B′(V) (equation 1.4) to give values for the Boltzmann parameters (V_o, C_{pk}, Q_{max} and β), and subsequently, each of the Boltzmann parameters was plotted as a function of time. In the whole-cell configuration the time-course of equilibration for the ionic concentration in the cell to reach the same concentration as in the pipette is

approximately exponential, when the pipette-cell assembly is treated as a two-compartment model (Marty and Neher 1995), thus the changes in the Boltzmann parameters were assumed to follow approximately exponential time-courses.

In each cell the time-course of the parameters V_o and C_{pk} were well fitted with an exponentially decaying curve, which was used to extrapolate the value of V_o and C_{pk} corresponding to the instant of break-in (t=0s). This allowed the time-courses of V_o and C_{pk} for each cell to be normalised to the value at t=0s, thus the time-courses of the mean values ± SD of the shift in V_o (V_o-V_o(t=0s)), and the relative decrease in C_{pk} (C_{pk}/C_{pk}(t=0s)) from the instant of break-in were determined.

In each cell the time-course of the parameters Q_{max} and β were found to deviate more from an exponentially decaying curve, as such it was not possible to fit exponentially decaying curves to the data from individual cells. Thus Q_{max} and β were normalised to the first record at t=10s, and the time-courses of the mean values ± SD of the relative changes in Q_{max} (Q_{max}/Q_{max}(t=10s)) and β (β/β(t=10s)) from 10s after break-in were determined.

The time-courses of the mean values of the shift in V_o, relative C_{pk} and relative Q_{max} were weighted by the reciprocal of their variance and fitted with exponentially decaying curves to give values for the asymptotes, which corresponded to the value of the parameter after equilibration. The fitting procedure (performed in Igor Pro v.4) also gave an estimate for the standard deviation (SD) of the final value. However the average time-course for β could not be fit with an exponentially decaying curve. Thus paired t-tests were used to test whether there was any significant change in β over time, by comparing the first 3 time-points for each cell with the last 3 time-points for each cell. An unpaired t-test was used in all other cases where two mean values from different sample populations were compared.

Criteria for Excluding Cells

In certain cases the data set corresponding to the time-course of a Boltzmann parameter for one cell was excluded from the average time-course of that parameter. There were two reasons for excluding data sets:

1) The data set was considered to be an outlier if the mean of the final 3 time-points were more than two standard deviations away from the mean.
2) If the parameter was too variable over the time-course to be analysed using the methods described above.

5.3 Results

5.3.1 Replacing Cl_i with Gluconate in Excised Inside-Out Patches

The NLC was measured in excised inside-out patches in the presence of varying [Cl_i]. The NLC was first measured shortly after excision in the bath, containing 150mM [Cl_i]. The values measured for the Boltzmann parameters were; V_o = -45.5 ± 20.2 mV, Q_{max} = 5.38 ± 1.13 fC, C_{pk} = 41.5 ± 2.19 fF, $\beta = 0.0290 \pm 0.004$ /mV (n=6). Subsequently [Cl_i] was reduced from 150mM to 10mM, 1mM and 0mM and replaced with gluconate (Figure 5.1). Solutions were exchanged by local application with a manifold applicator (Ch.2.3.4).

Reduction of [Cl_i] from 150mM to 10mM (n=5) and 1mM (n=3), led to an increasing positive shift in the V_o of the NLC (by 5.2 ± 5.2 mV and 22.0 ± 1.7 mV respectively), a decrease in the Q_{max} (to 71 ± 24% and 41 ± 29% respectively) and a decrease in the C_{pk} (to 63 ± 9% and 30 ± 15% respectively) (Figure 5.1 and Figure 5.2). Where it was possible to return to control and wash-in 150mM [Cl_i] the shift in V_o was reversible (n=4). The decrease in Q_{max} and C_{pk} were only partially

reversible (data not shown), suggesting there may have been some decrease in the size of the NLC that was not due to the reduction of $[Cl_i]$. This would explain the large variability in the measured values of Q_{max} and C_{pk}. There also appeared to be a decrease in the mean β at lower $[Cl_i]$, however this decrease was not significant ($p>0.05$).

Complete removal of $[Cl_i]$ led to the apparent removal of any measurable NLC (n=3). An example of the recording from one of these patches is shown in Figure 5.3. On appearance it looks like the trace for 0mM $[Cl_i]$ might be part of a NLC shifted to very positive V_m, however it was not possible to fit the B'(V) to the trace, thus it was concluded that no NLC was detectable. The abolishment of the NLC was found to be almost completely reversible by subsequent wash-in of 150 mM $[Cl_i]$.

The I(V) measured simultaneously with a voltage-ramp, was also affected by the reduction of $[Cl_i]$. An increase in outward current at positive membrane potential (V_m) was observed when $[Cl_i]$ was reduced in all patches (n=6). However this increase was only reversible in 2 patches (Figure 5.4A). No significant change in reversal potential (V_{rev}) was observed when $[Cl_i]$ was reduced in any of the patches. V_{rev} remained close to 0mV, once corrections for liquid junction potentials had been made. In comparison no consistent changes in the I(V) of Deiters cell patches was observed (n=3). An example of an I(V) from a Deiters cell patch recorded in both high and low $[Cl_i]$ is shown. In this case no increase in outward current was observed as $[Cl_i]$ was removed, but rather there was an irreversible decrease in the outward current.

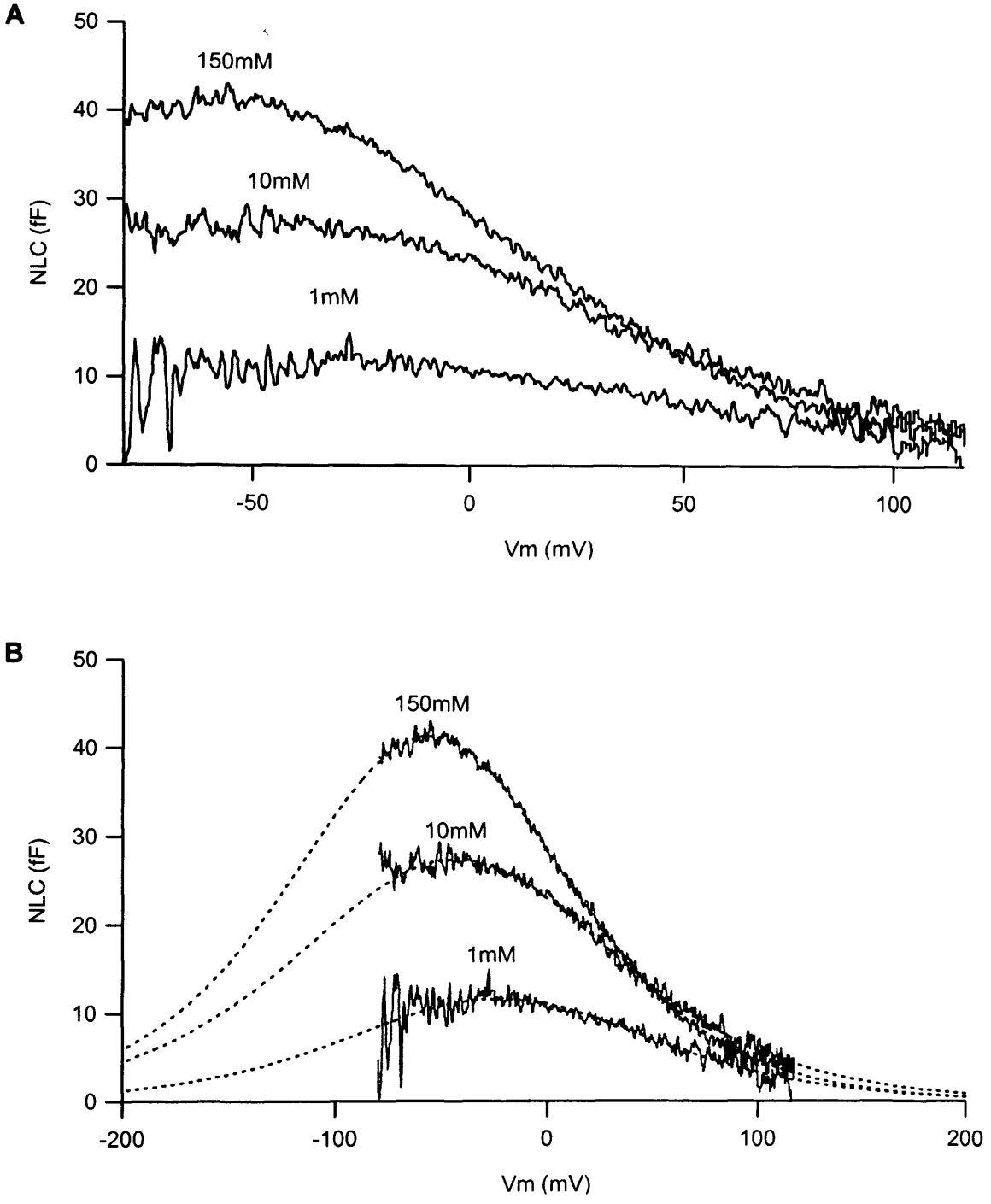

Figure 5.1 The NLC depends on $[Cl_i]$, when Cl_i is replaced with gluconate, measured in excised inside-out patches. NLCs were fitted with the B′(V) and the traces were baseline corrected so the fit was constrained to go to zero. The traces show raw data and were not corrected for liquid junction potentials. A) V_o of the NLC shifted to more depolarised potentials and C_{pk} decreased as $[Cl_i]$ was reduced. B) The same traces are shown with the B′(V) fits used to obtain values for the Boltzmann Parameters.

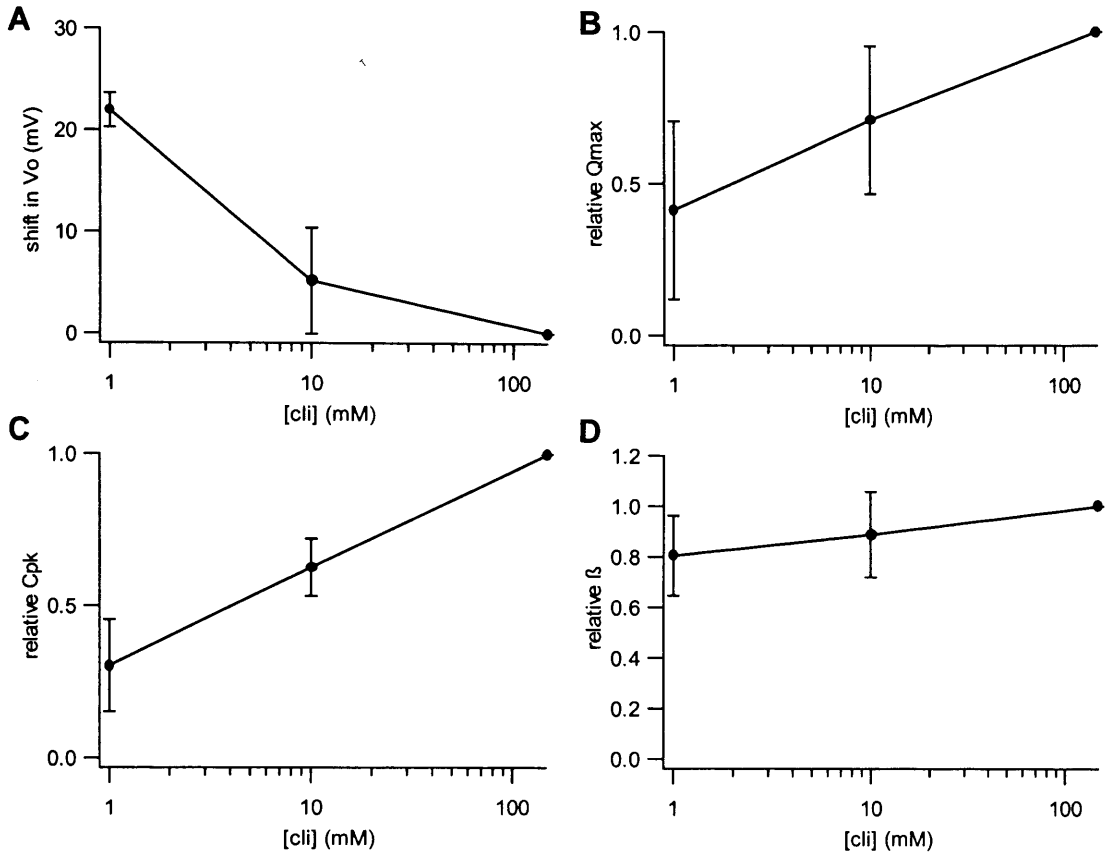

Figure 5.2 The Boltzmann parameters of the NLC depend on $[Cl_i]$ when Cl_i is replaced with gluconate. Summary shows the effect on the Boltzmann parameters of reducing $[Cl_i]$ to 10mM (n=5) and 1mM (n=3). All values were determined relative to the values at 150mM $[Cl_i]$. Data is shown as mean ± SD A) There was a significant shift in V_o to more positive potentials as $[Cl_i]$ was reduced to 10mM (n=5, $p<0.05$) and 1mM (n=3, $p<0.01$). B) There was a significant decrease in Q_{max} when $[Cl_i]$ was reduced to 10mM (n=5, $p<0.05$) and 1mM (n=3, $p<0.05$). C) There was a significant decrease in C_{pk} when $[Cl_i]$ was reduced to 10mM (n=5, $p<0.01$) and 1mM (n=3, $p<0.01$). D)β did not significantly decrease when $[Cl_i]$ was reduced ($p>0.05$).

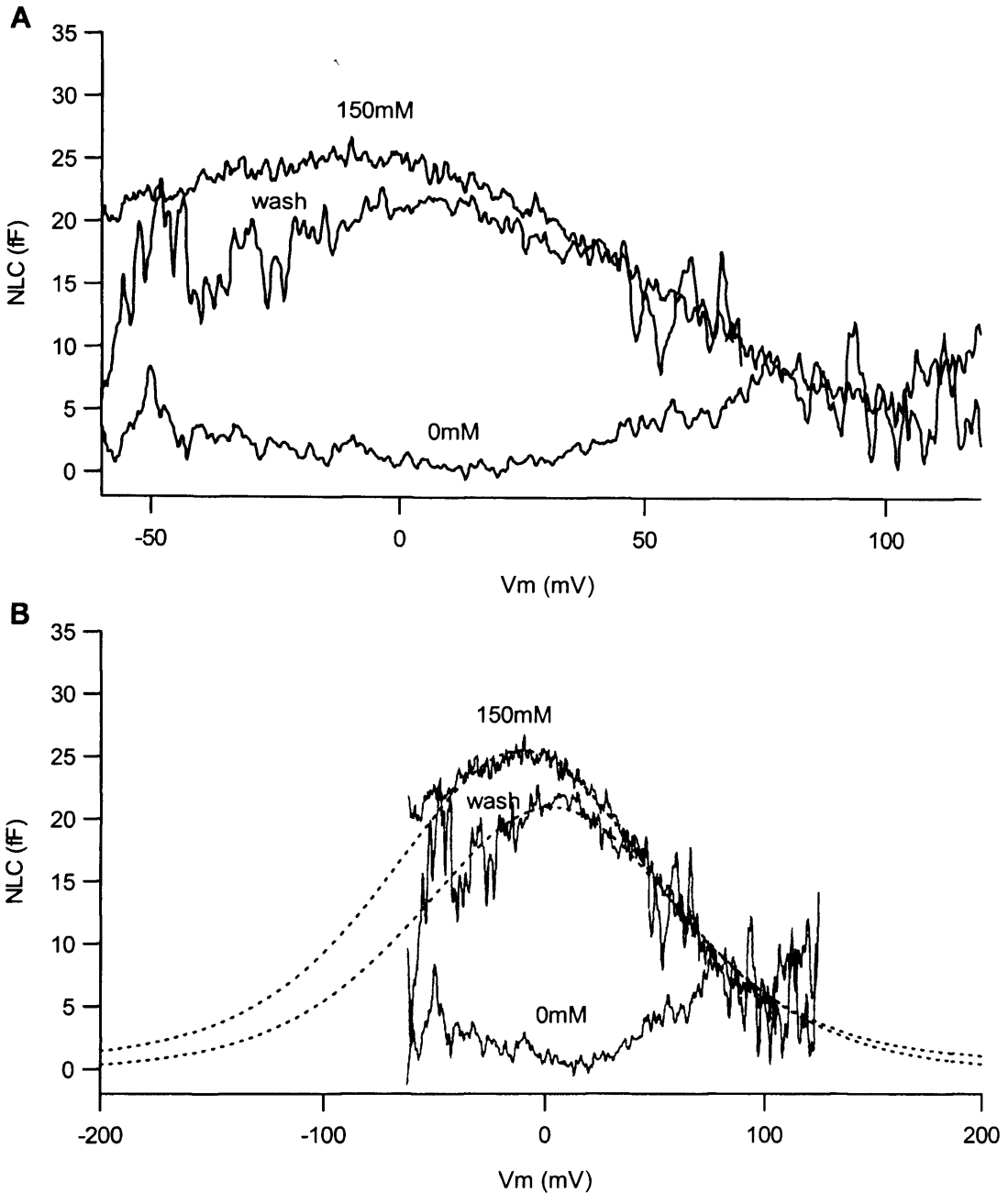

Figure 5.3 The NLC was abolished when Cl_i was completely replaced with gluconate, measured in excised inside-out patches. NLCs were fitted with the B'(V) and the traces were baseline corrected so the fit was constrained to go to zero. For the 0mM trace this was not possible so the minimum value of the trace was set to zero. The traces show raw data and were not corrected for liquid junction potentials. A) An example patch showing no detectable NLC after application of 0mM [Cl_i] and almost complete recovery following wash-in of 150mM [Cl_i]. B) The same patch shown with the B'(V) fits used to obtain the Boltzmann parameters.

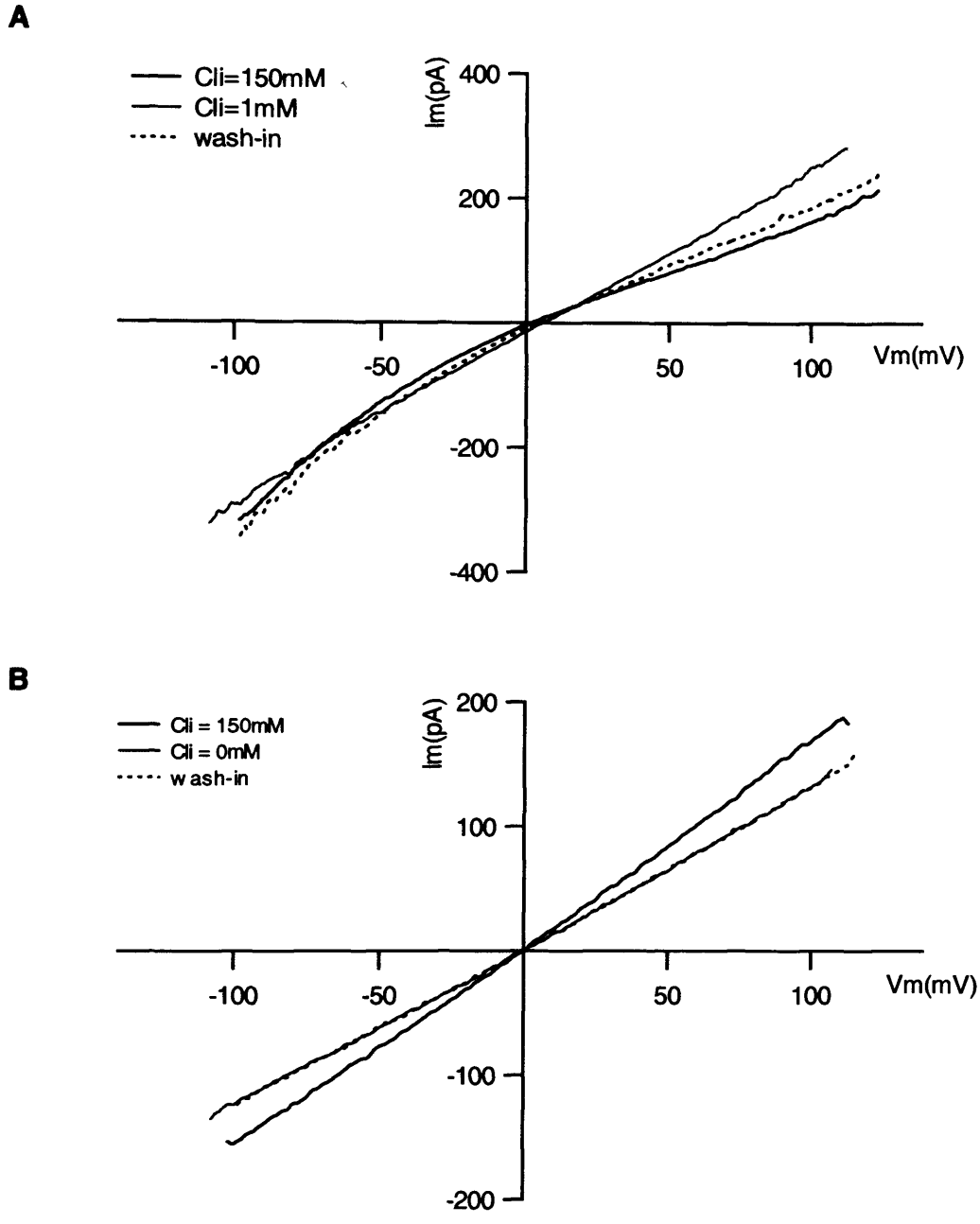

Figure 5.4 The effect on the I(V) of reduction of $[Cl_i]$. I(V)s for excised inside-out patches were recorded with a voltage ramp, at a holding potential of +20mV. A) The I(V) for an OHC patch. Reduction of $[Cl_i]$ to 1mM led to an increase in the outward current at positve V_m. In this example this was partially reversed upon subsequent wash-in of 150mM $[Cl_i]$ B) The I(V) for a Deiters cell patch. No increase in outward current was observed. The change in I(V) was not reversible on subsequent wash-in of 150mM $[Cl_i]$.

5.3.2 Replacing Cl_i with Gluconate in the Whole-Cell Configuration

Cells were patched with Na-based solutions containing either 150mM (control), 10mM, 1mM or 0mM concentration of chloride in the pipette, Cl_{pip}, (solutions Na-HBS, Gluc-10, Gluc-1 and Gluc-0, Tables 2.1 and 2.2), where the chloride was replaced with gluconate. It was expected that, following break-in, the cell's internal medium was replaced with the pipette solution via diffusion, until a steady-state was reached when the $[Cl_i]$ surrounding the plasma membrane reflected $[Cl_{pip}]$. NLCs were measured from 10s after break-in until steady-state was approached (~5mins). Example cells are shown in Figure 5.5.

With low $[Cl_{pip}]$, V_o shifted towards more positive potentials with time (Figure 5.6), Q_{max} decreased with time (Figure 5.7) and C_{pk} decreased with time (Figure 5.8). Unlike recordings in excised patches, a considerable NLC remained after 5mins when cells were patched with 0mM $[Cl_{pip}]$ in the whole-cell configuration (Figure 5.5). When cells were patched with 150mM $[Cl_{pip}]$, no shift in V_o or decrease in Q_{max} and C_{pk} was observed. This suggested that the $[Cl_i]$ in the cell prior to break-in was at saturating levels, where any further increase in $[Cl_i]$ up to 150mM, does not alter the NLC. Although the $[Cl_i]$ prior to break-in must have been greater than 10mM, it is unlikely that it was as great as 150mM, however the exact $[Cl_i]$ prior to break-in cannot be determined without further investigation. Previous experimental observations suggest that $[Cl_i]$ reaches saturation levels around 100mM (Oliver et al. 2001) whereas more recently it has been suggested that $[Cl_i]$ approaches saturating levels at 20mM (Song et al. 2004).

Regardless of the exact $[Cl_i]$ in the cell prior to break-in the initial NLC is the same as the NLC that would be measured with a $[Cl_i]$ of 150mM. Therefore in all further calculations, the initial V_o, Q_{max} and C_{pk} were considered to correspond to the

NLC that would be produced with 150mM $[Cl_i]$. Accordingly patching cells with various $[Cl_{pip}]$ was equivalent to reducing $[Cl_i]$ from 150mM to the $[Cl_{pip}]$. Thus reduction of $[Cl_i]$ to 10mM, 1mM or 0mM led to an increasing positive shift in V_o (of 13.3 ± 5.1 mV, 21.1 ± 2.9 mV, 47.7 ± 22 mV respectively), a decrease in C_{pk} (to 59.9 ± 7.5%, 49.6 ± 7.5%, 39.8 ± 6.1% respectively), and a decrease in Q_{max} (to 70.6 ± 11.5%, 61.4 ± 9.3%, 59.5 ± 6.9% respectively) (Figure 5.10).

In addition β appeared to decrease with time when cells were patched with low $[Cl_{pip}]$ (Figure 5.9), compared to the control cells in which no change was observed in β after 5minutes. The decrease in β (of up to 20%) for cells patched with 10mM, 1mM, and 0mM $[Cl_i]$, was significant ($p<0.01$).

The exponential fits to the time-courses of the mean shift in V_o, and relative decreases in C_{pk} and Q_{max}, also gave the time-constants for the approach of these parameters to steady-state, which is an indication of the time required for complete exchange of solution between the pipette and cell. Time constants were between 53s and 123s, as expected for intracellular diffusion through patch pipettes (Pusch and Neher 1988).

Figure 5.5 Examples of NLCs recorded in the whole-cell configuration; $[Cl_i]$ was reduced and replaced with gluconate. In each cell traces were recorded at 18s intervals from 10s after break-in. They are shown here at 54s intervals, from the first record. Arrows show the direction of time. The dotted lines show the fits of the B′(V) to the NLC traces. For control cells the maximum C_{pk} corresponded to the maximum C_{pk} found during the time of recording. For cells patched with 10mM, 1mM and 0mM $[Cl_{pip}]$, the maximum C_{pk} was estimated for the instant of break-in (t=0s). The maximum C_{pk} of the NLC was not significantly different for any of the solutions used to patch cells ($p>0.05$). Maximum C_{pk} was 8.1 ± 4.9pF (n=21).

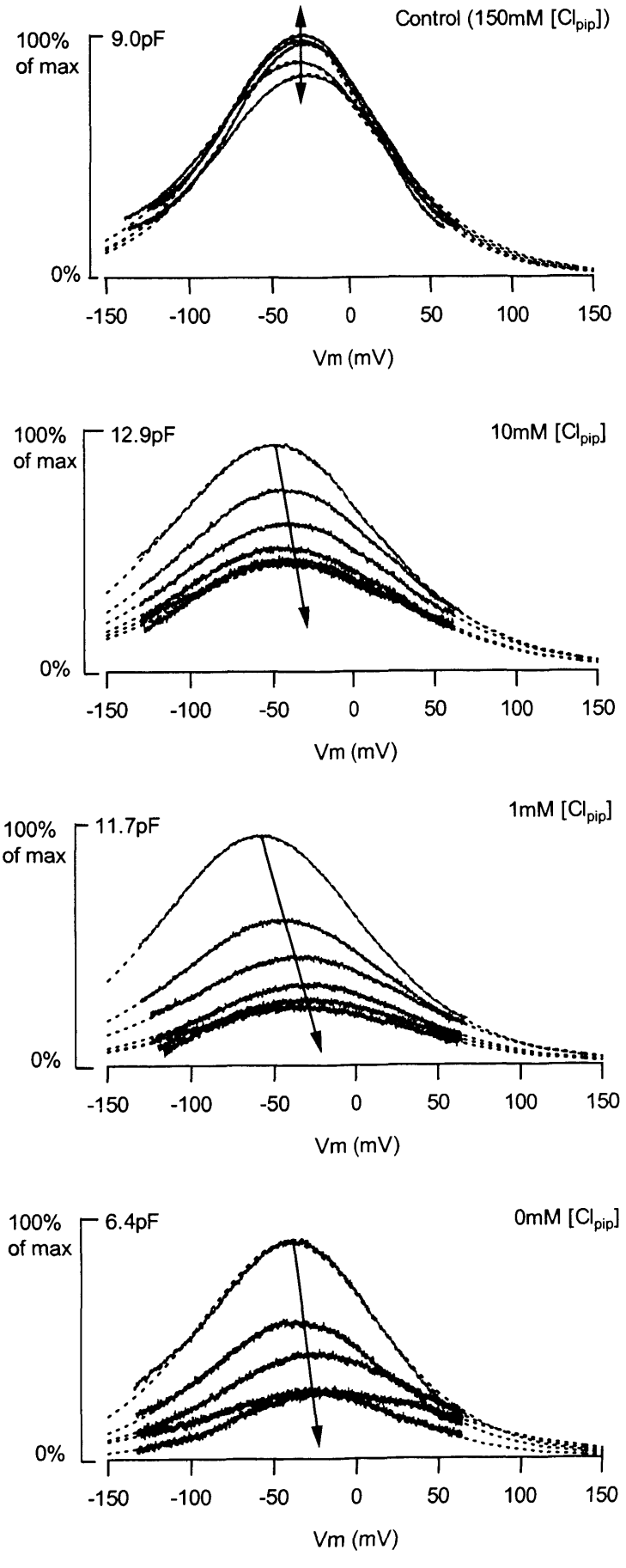

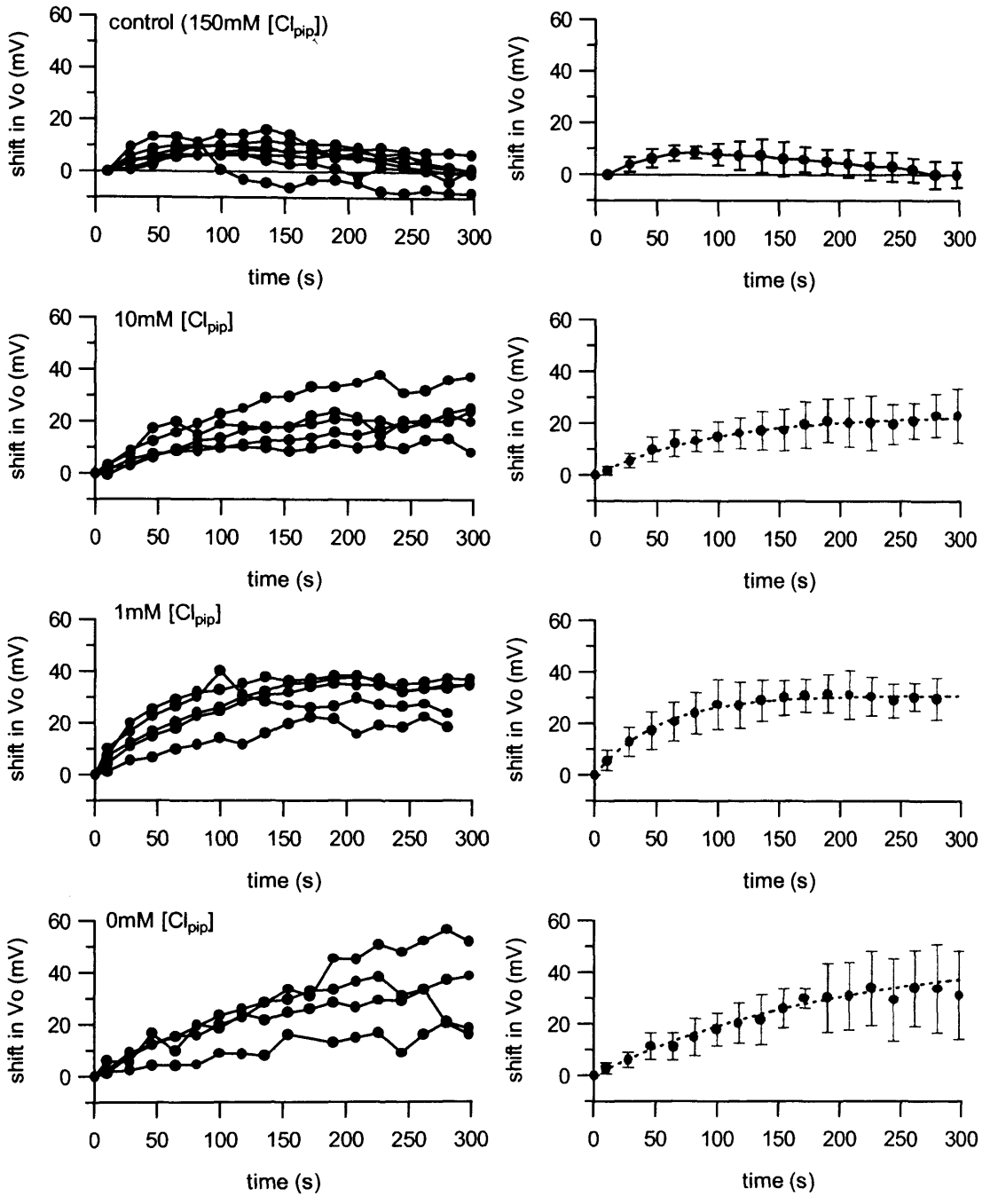

Figure 5.6. The time-course of V_o after break-in; Cl_i was replaced with gluconate. The shift in V_o was determined relative to the V_o at instant of break-in (V_o-V_o(t=0s)). The left panel shows the time-course for individual cells, and the right panel shows the time-course of the mean values ± SD. The values for V_o shown here were not corrected for liquid junction potentials. There was no shift in V_o after 5 minutes in control cells (150mM [Cl_{pip}], n=7). A shift in V_o was observed for cells patched with; 10mM [Cl_{pip}] (n=5), 1mM [Cl_{pip}] (n=5), or 0mM [Cl_{pip}] (n=4).

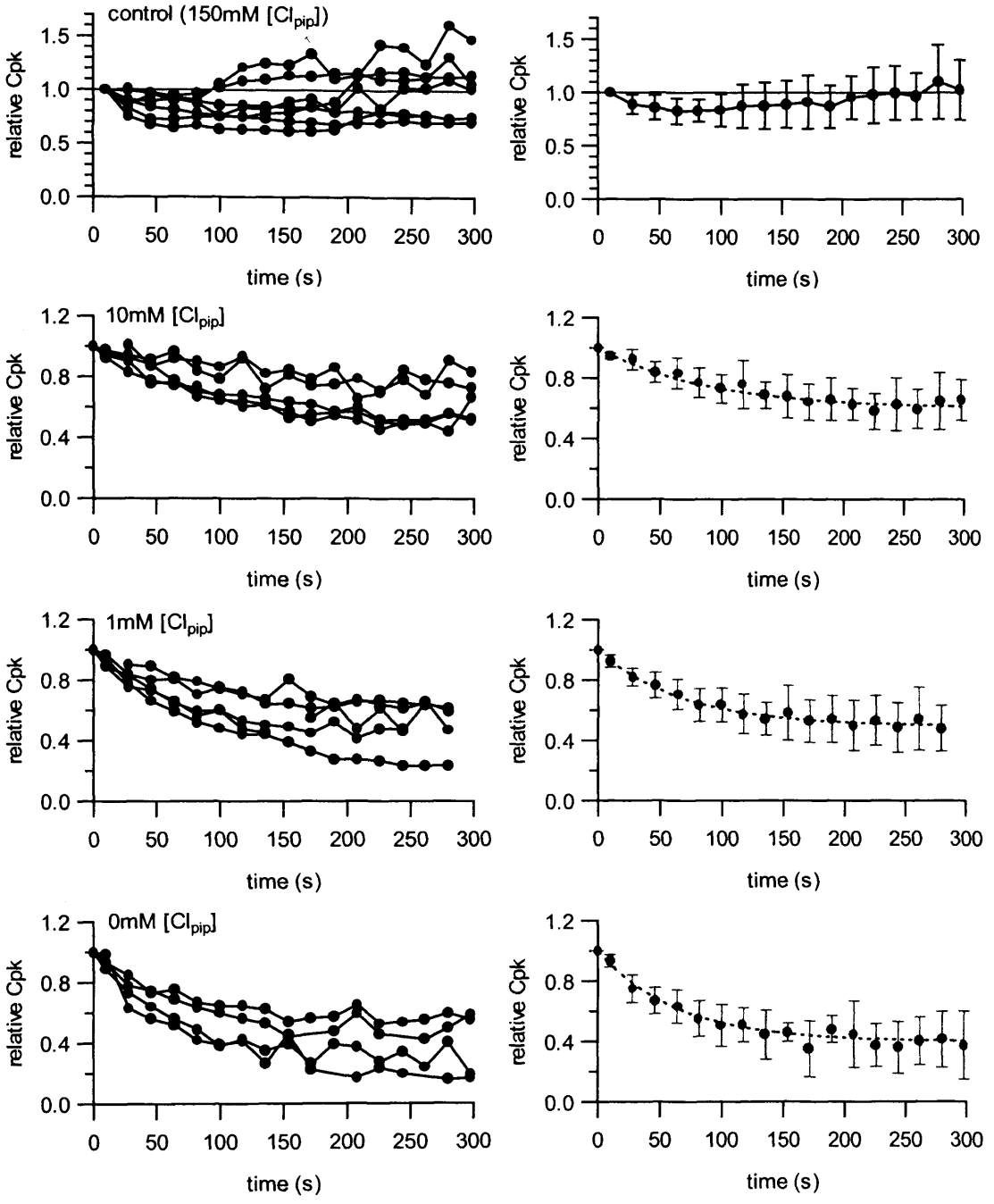

Figure 5.7 The time-course of C_{pk} after break-in; Cl_i was replaced with gluconate. The decrease in C_{pk} was determined relative to the C_{pk} at instant of break-in ($C_{pk}/C_{pk}(t=0s)$). The left panel shows the time-course for individual cells, and the right panel shows the time-course of the mean values ± SD. There was no decrease in C_{pk} after 5 minutes in control cells (150mM [Cl_{pip}], n=7). A decrease in C_{pk} was observed when cells were patched with; 10mM [Cl_{pip}] (n=5), 1mM [Cl_{pip}] (n=5) or 0mM [Cl_{pip}] (n=4)

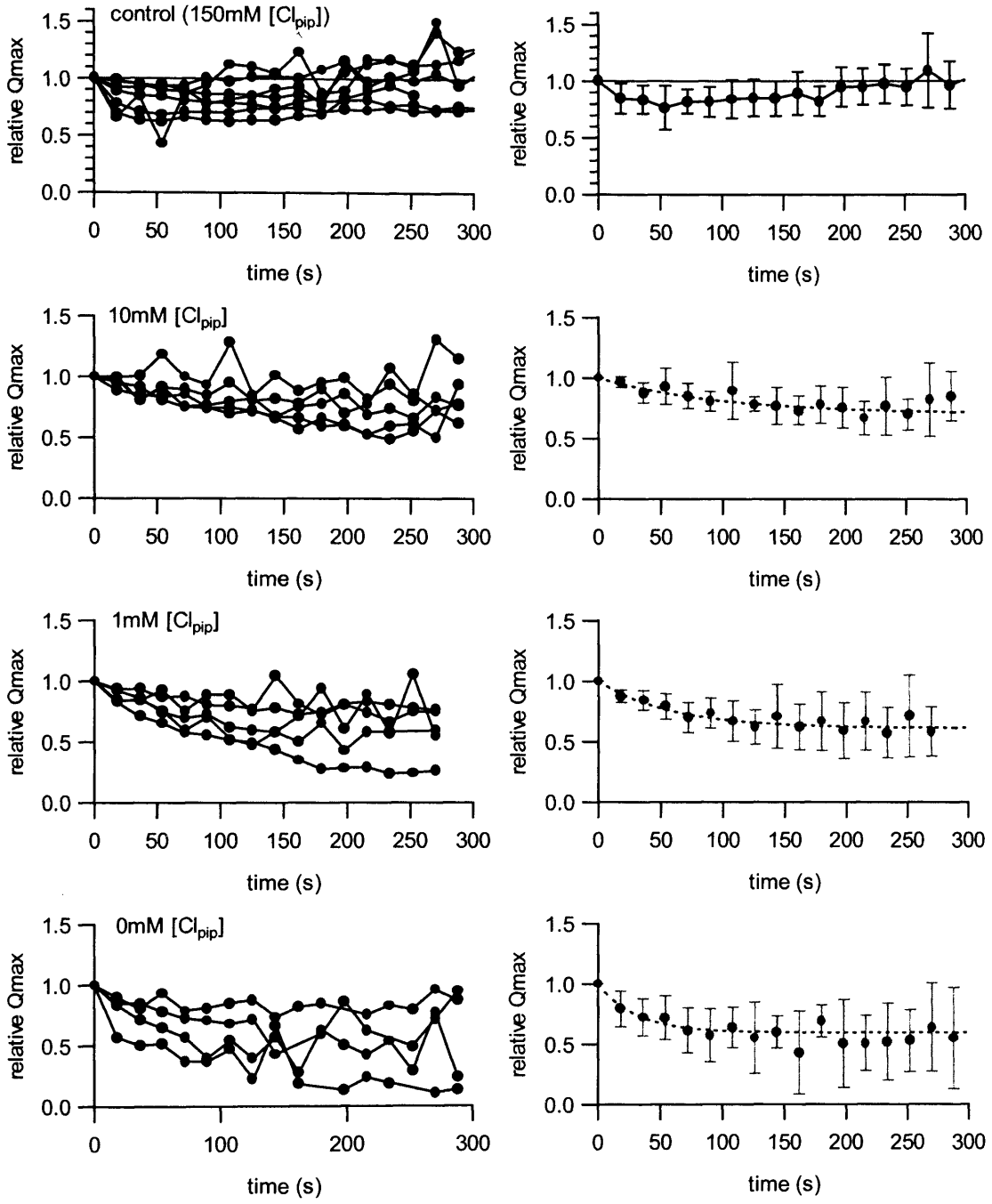

Figure 5.8 The time-course of Q_{max} after break-in; Cl_i was replaced with gluconate. The decrease in Q_{max} was determined relative to the Q_{max} 10s after break-in ($Q_{max}/Q_{max}(t=10s)$). The left panel shows the time-course for individual cells, and the right panel shows the time-course of the mean values ± SD. There was no decrease in Q_{max} after 5 minutes in control cells (150mM [Cl_{pip}] n=7). A decrease in Q_{max} was observed when cells were patched with; 10mM [Cl_{pip}] (n=5), 1mM [Cl_{pip}] (n=5) or 0mM [Cl_{pip}] (n=4)

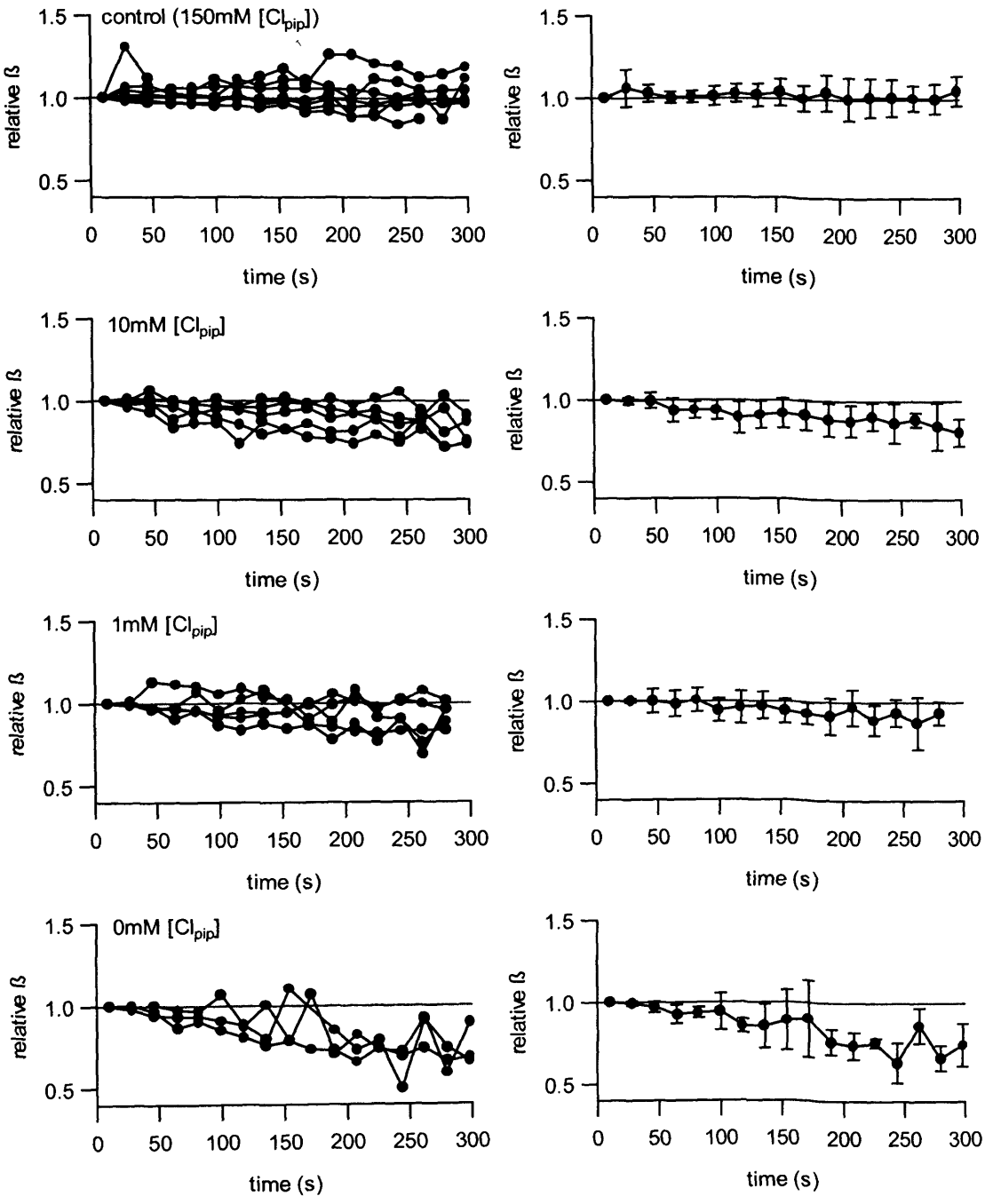

Figure 5.9 The time-course of β after break-in; Cl_i was replaced with gluconate. The decrease in β was determined relative to the β 10s after break-in (β/β(t=10s)). The left panel shows the time-course for individual cells, and the right panel shows the time-course of the mean values ± SD. There was no decrease in β after 5 minutes in control cells (150mM $[Cl_{pip}]$ n=7). A decrease in β was observed when cells were patched with; 10mM $[Cl_{pip}]$ (n=5), 1mM $[Cl_{pip}]$ (n=5) or 0mM $[Cl_{pip}]$ (n=3).

A comparison of the measurements recorded in the whole-cell configuration with those recorded in excised inside-out patches shows that for reductions of $[Cl_i]$ to 10mM, where Cl_i was replaced with gluconate the values measured for the Boltzmann parameters were generally in close agreement (Figure 5.10). Measurements for C_{pk}, Q_{max}, and β were not significantly different, although the mean shift in V_o was significantly smaller in excised patches ($p<0.01$). For reductions of $[Cl_i]$ to 1mM measurements for V_o and β were not significantly different, and although the mean relative C_{pk} and Q_{max} were smaller in excised patches, only the relative C_{pk} was significantly smaller ($p<0.05$). Thus in general for reductions of $[Cl_i]$ to 10mM and 1mM measurements from the different recording configurations were in good agreement. However for reduction of $[Cl_i]$ to 0mM the measurements from the whole-cell configuration were in complete contradiction to measurements from excised patches. Whilst the NLC became undetectable in patches (Figure 5.3), a considerable NLC remained in the whole-cell configuration (Figure5.5).

The I(V)s recorded simultaneously with the NLCs were also analysed. The I(V)s acquired ~ 5 minutes after break-in, when the $[Cl_i]$ of the cell was assumed to be equivalent to the $[Cl_{pip}]$, had reversal potentials close to 0mV, for all $[Cl_i]$ used. This is as expected for a Na-based internal. The mean V_{rev} for 10mM, 1mM and 0mM $[Cl_i]$ (-2.8 ± 3.1mV, -7.2 ± 2.0mV, -7.1 ± 4.8mV) were not significantly different from the mean V_{rev} of control cells (-5.8 ± 4.6mV). In each cell the I(V) acquired 5 minutes after break-in was also compared with the I(V) acquired 10s after break-in, to investigate whether any changes occurred due to the $[Cl_i]$ of the cell changing over time. In some cells changes in the I(V) occurred due to the reduction of $[Cl_i]$ that could not be interpreted as an increase in a leak conductance, or a worsening of the seal, however no consistent change in the I(V) was observed upon reduction of $[Cl_i]$.

Thus further investigations are required, to form any conclusions about the dependence of the I(V) on $[Cl_i]$.

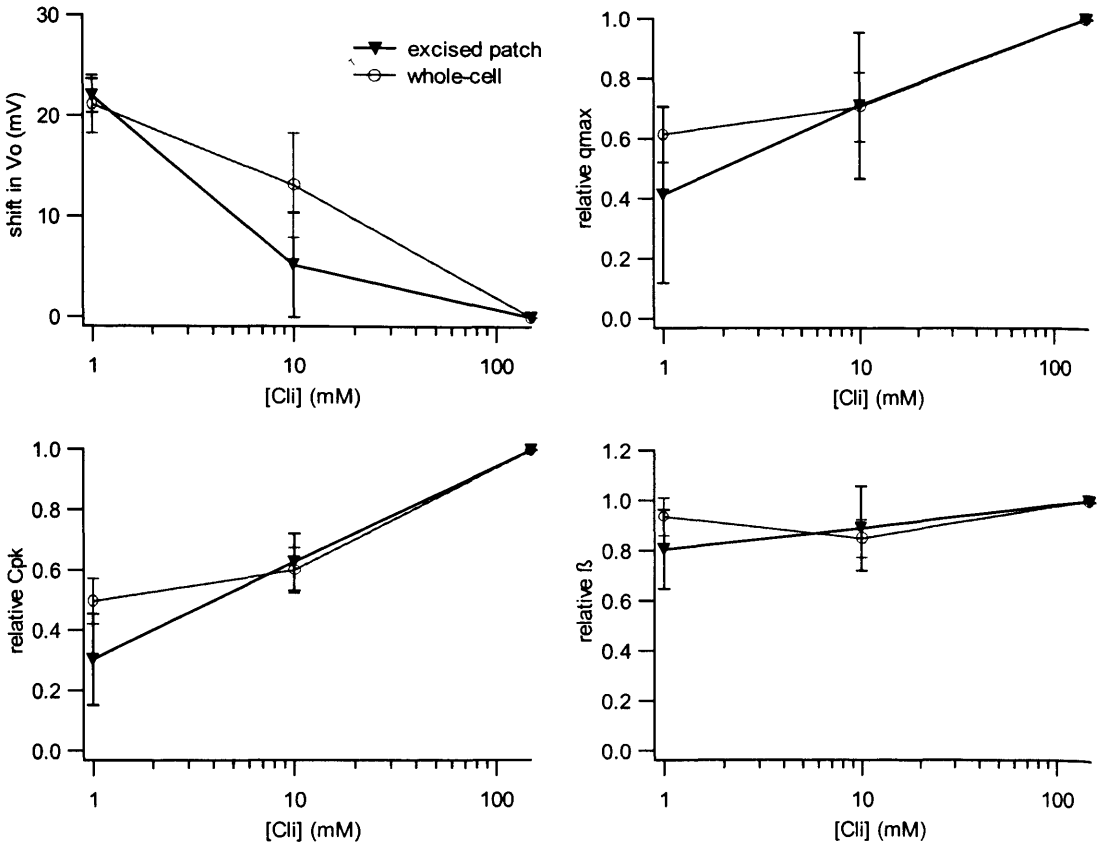

Figure 5.10 A comparison of the Boltzmann parameters measured from whole-cell recordings with those measured from excised patches; $[Cl_i]$ was reduced and replaced with gluconate. All values were determined relative to the values at 150mM $[Cl_i]$. Data is shown as mean ± SD.

5.3.3 Replacing Cl_i with Sulphate in the Whole-Cell Configuration

Cells were patched with Na-based solution containing 10mM, 1mM or 0mM [Cl_{pip}] (Solutions Sulph-10, Sulph-1 or Sulph-0, Table 2.2) where the chloride was replaced with sulphate. The concentration of sulphate used was chosen to replace chloride and maintain ionic strength, and the osmolarity was made up with sucrose. NLCs were recorded from 10s after break-in until steady state. Example cells are shown in Figure 5.11.

Assuming that [Cl_i] reflected [Cl_{pip}] once steady-state was reached and that the initial [Cl_i] was at saturating levels, the V_o of the NLCs shifted to more positive potentials as [Cl_i] was reduced from a level which produced the same NLC as a [Cl_i] of 150mM, to 10mM, 1mM and 0mM (by 55.5 ± 4.1 mV, 87.2 ± 6.86 mV, 90.0 ± 3.28 mV, respectively), (Figure 5.12). These shifts in V_o were much greater than those measured when Cl_i was replaced with gluconate. A decrease in C_{pk} (to 45.5 ± 3.3%, 43.6 ± 2.8%, 28.7 ± 1.4%, respectively), (Figure 5.13) and Q_{max} (to 44.5 ± 3.8%, 46.8 ± 4.1%, 35.8 ± 2.3%, respectively), (Figure 5.14) was also observed. No significant change in β was observed for any concentration of [Cl_i] ($p>0.05$) (Figure 5.15). A considerable NLC remained when Cl_i was completely removed (Figure 5.11). This contrasts with previous data from excised patches (Oliver et al. 2001), which showed that the NLC was abolished on complete replacement of Cl_i with sulphate.

A comparison of the measurements recorded in the whole-cell configuration with those recorded in excised inside-out patches (Fakler and Oliver 2002) shows that for reductions of [Cl_i] to 10mM, where Cl_i was replaced with sulphate, although the values for the Boltzmann parameters appeared to be similar, there were significant differences between the measurements from the two recording configurations (Figure 5.16). The shift in V_o was significantly greater in whole-cell recordings ($p<0.05$) and

the decreases in the relative C_{pk} and Q_{max} were greater in whole-cell recordings ($p<0.01$). However these differences were small compared to the differences observed when $[Cl_i]$ was reduced to 1mM, where the decrease in relative C_{pk} and Q_{max} were considerably greater in excised patches. Furthermore when Cl_i was completely removed the measurements from the whole-cell configuration were in complete contradiction to measurements from excised patches. Whilst the NLC became undetectable in patches, a considerable NLC remained in the whole-cell configuration (Figure5.11).

The I(V)s recorded simultaneously with the NLCs were also analysed. The I(V)s acquired ~ 5 minutes after break-in had reversal potentials close to 0mV, for all $[Cl_i]$ used. The V_{rev} for 10mM, 1mM and 0mM $[Cl_i]$ (-5.5 ± 2.2mV, -5.2 ± 2.2mV, -4.3 ± 4.9mV respectively) were not significantly different from the control V_{rev} . As for the experiments in which $[Cl_i]$ was replaced with gluconate, further investigations are required to form any conclusions about the dependence of the I(V) on $[Cl_i]$.

The exponential fits to the time-courses of the mean shift in V_o, and relative decreases in C_{pk} and Q_{max}, gave time-constants between 42s and 84s.

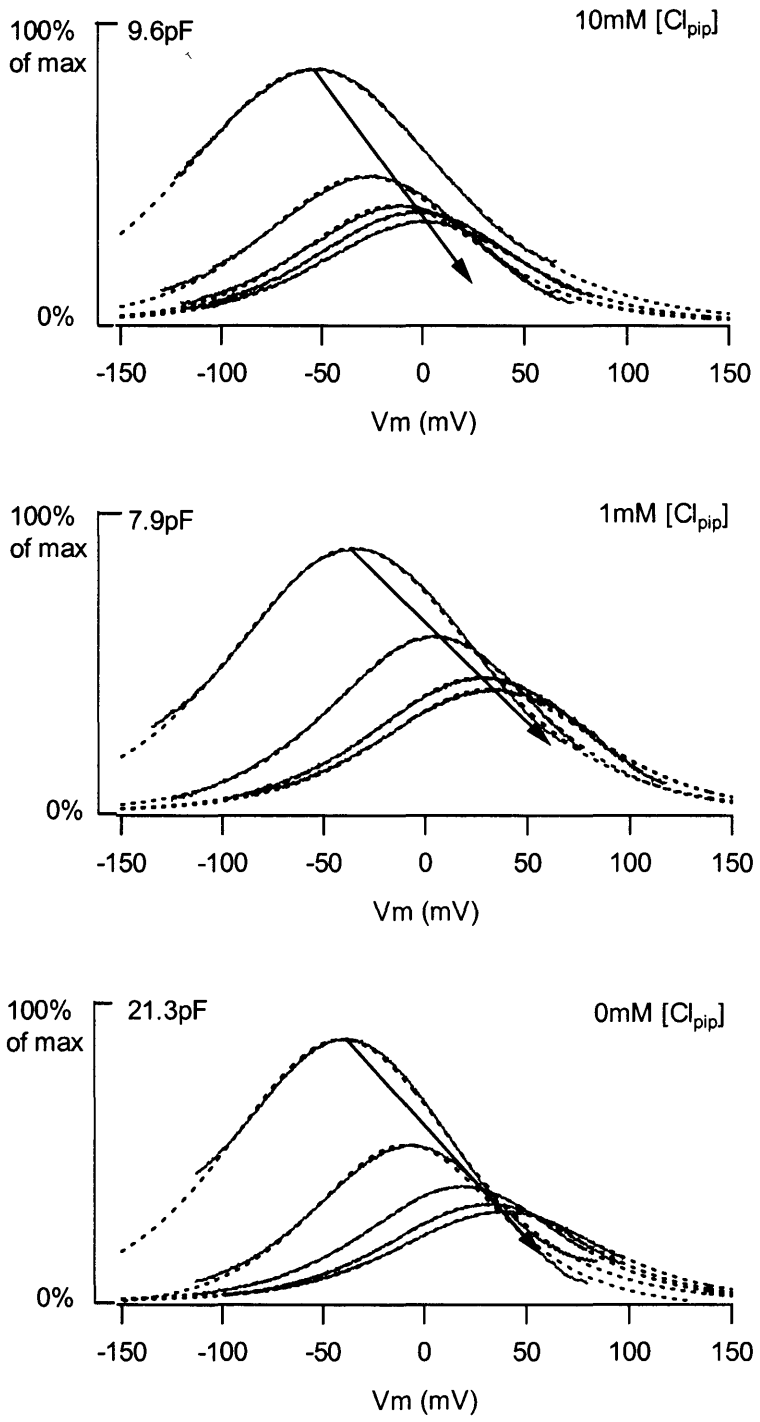

Figure 5.11 Examples of non-linear capacitances recorded in the whole-cell configuration; Cl_i was replaced with sulphate. In each cell traces were recorded at 18s intervals from 10s after break-in. They are shown here at 54s intervals, from the first record. Arrows show the direction of time. The dotted lines show the fits of the B′(V) to the NLC traces. Maximum C_{pk} was estimated for the instant of break-in. The maximum C_{pk} of the NLC was not significantly different for any of the solutions used to patch cells ($p>0.05$). Maximum C_{pk} was 9.4 ± 4.1pF ($n=17$).

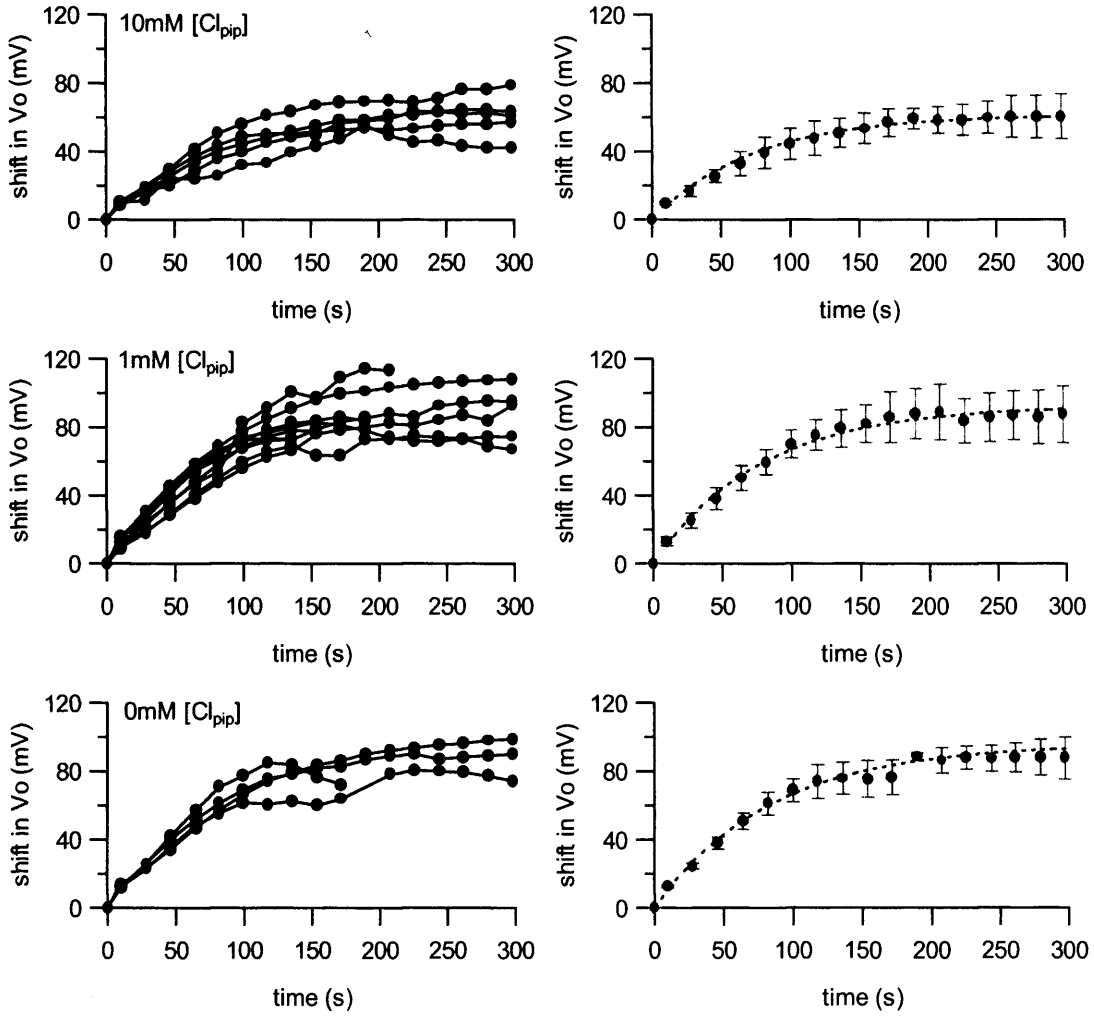

Figure 5.12 The time-course of V_o after break-in; Cl_i was replaced with sulphate. The shift in V_o was determined relative to the V_o at instant of break-in (V_o-V_o(t=0s)). The left panel shows the time-course for individual cells, and the right panel shows the time-course of the mean values ± SD. The values for V_o shown here were not corrected for liquid junction potentials. A shift in V_o was observed for cells patched with; 10mM [Cl_{pip}] (n=5), 1mM [Cl_{pip}] (n=9 at 0s,n=5 at 298s) or 0mM [Cl_{pip}] (n=4 at 0s, n=3 at 298s).

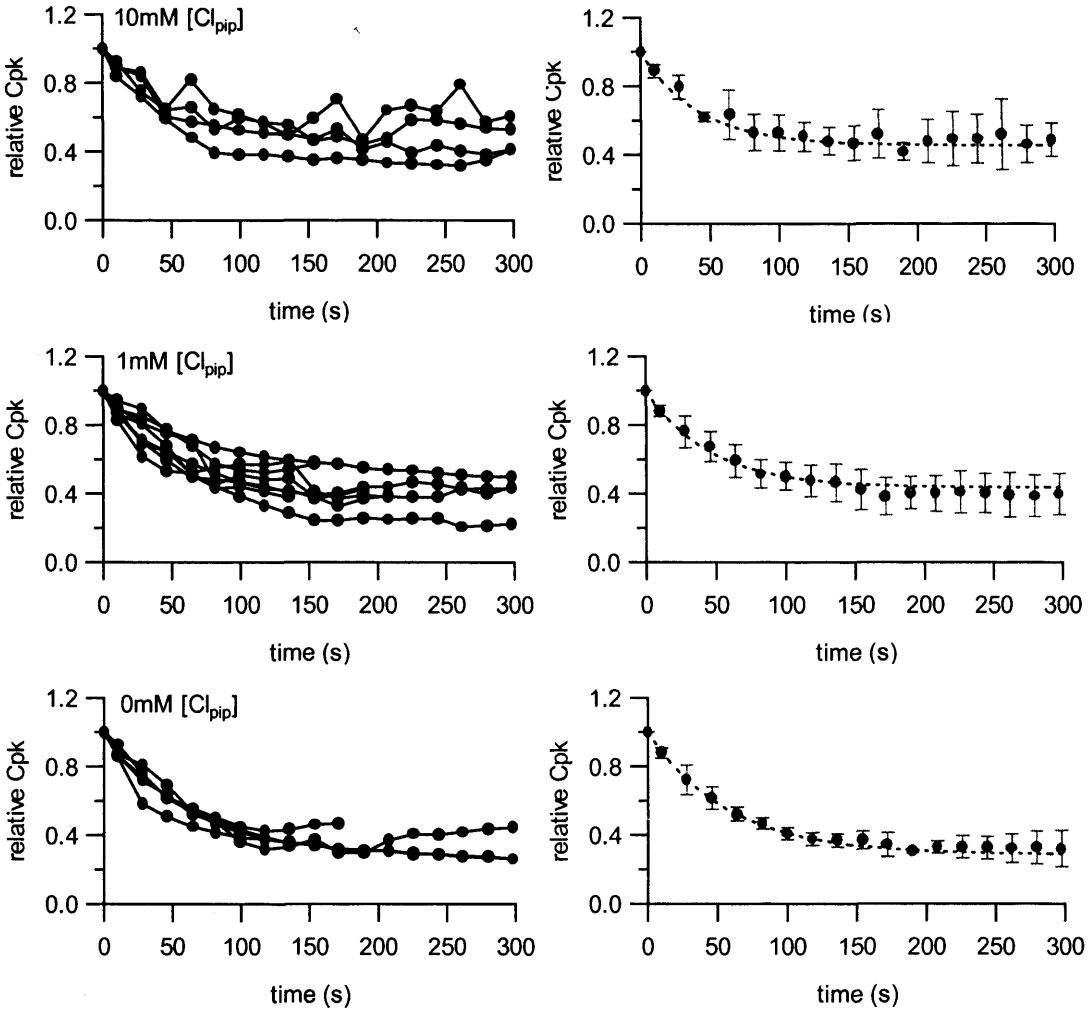

Figure 5.13 The time-course of C_{pk} after break-in; Cl_i was replaced with sulphate. The decrease in C_{pk} was determined relative to the C_{pk} at instant of break-in ($C_{pk}/C_{pk}(t=0s)$). The left panel shows the time-course for individual cells, and the right panel shows the time-course of the mean values ± SD. A decrease in C_{pk} was observed for cells patched with; 10mM [Cl_{pip}] (n=4), 1mM [Cl_{pip}] (n=8 at 0s,n=4 at 298s) or 0mM [Cl_{pip}] (n=5 at 0s, n=3 at 298s).

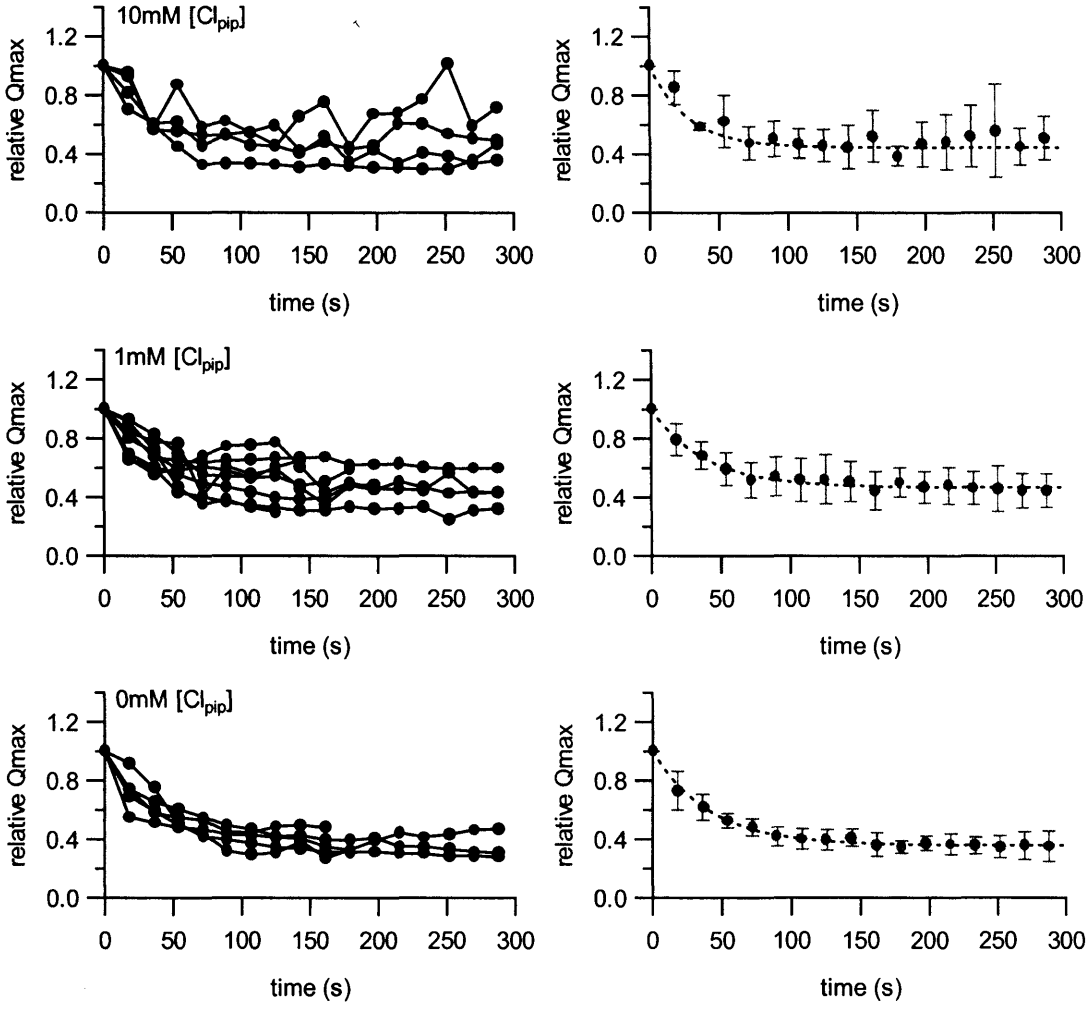

Figure 5.14 The time-course of Q_{max} after break-in; Cl_i was replaced with sulphate. The decrease in Q_{max} was determined relative to the Q_{max} 10s after break-in ($Q_{max}/Q_{max}(t=10s)$). The left panel shows the time-course for individual cells, and the right panel shows the time-course of the mean values ± SD. A decrease in Q_{max} was observed for cells patched with; 10mM [Cl_{pip}] (n=4), 1mM [Cl_{pip}] (n=8 at 10s,n=4 at 298s) or 0mM [Cl_{pip}] (n=5 at10s, n=3 at 298s).

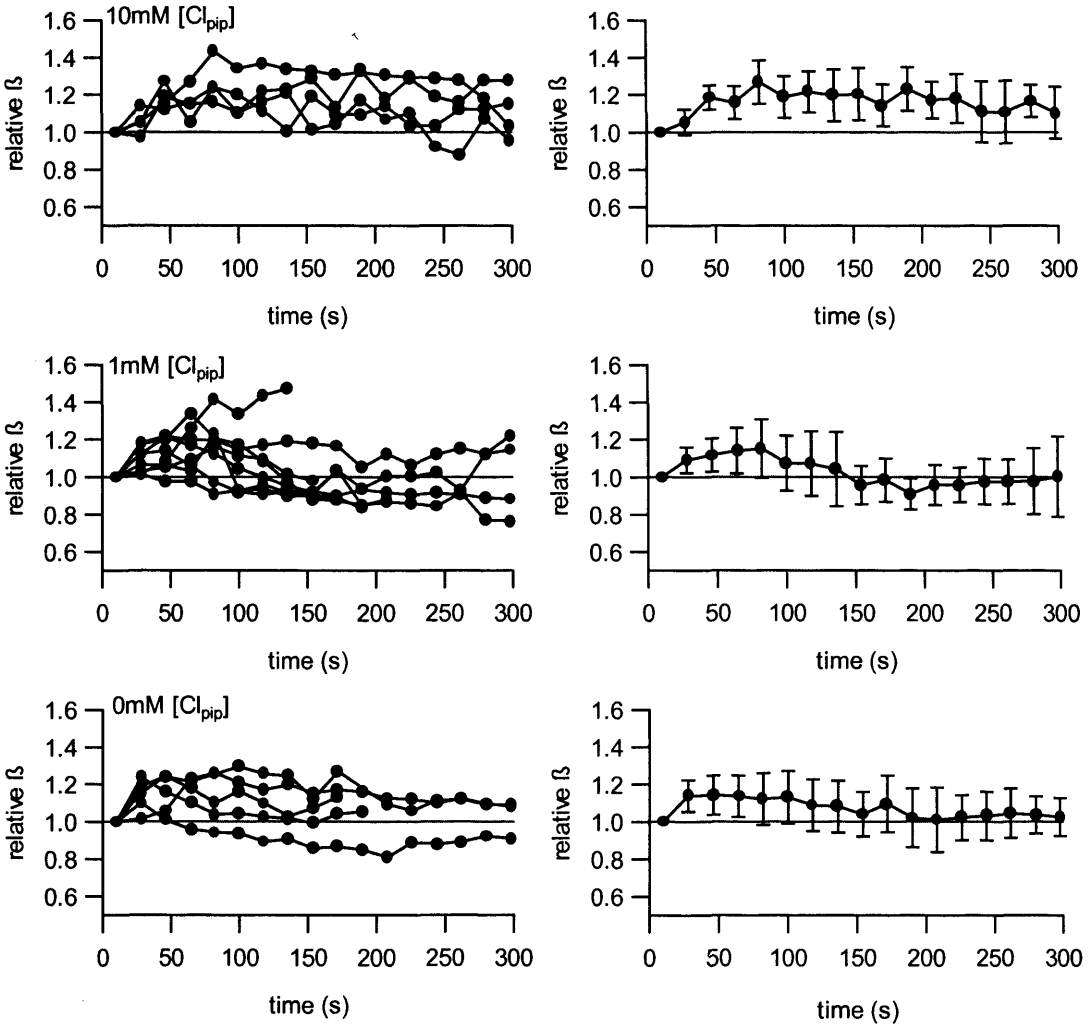

Figure 5.15 The time-course of β after break-in; Cl_i was replaced with sulphate. The decrease in β was determined relative to the β 10s after break-in (β/β(t=10s)). The left panel shows the time-course for individual cells, and the right panel shows the time-course of the mean ± SD. No significant change in β was observed when cells were patched with; 10mM [Cl_{pip}] (n=4), 1mM [Cl_{pip}] (n=8 at 10s, n=4 at 298s) or 0mM [Cl_{pip}] (n=5 at 10s n=3 at 298s)

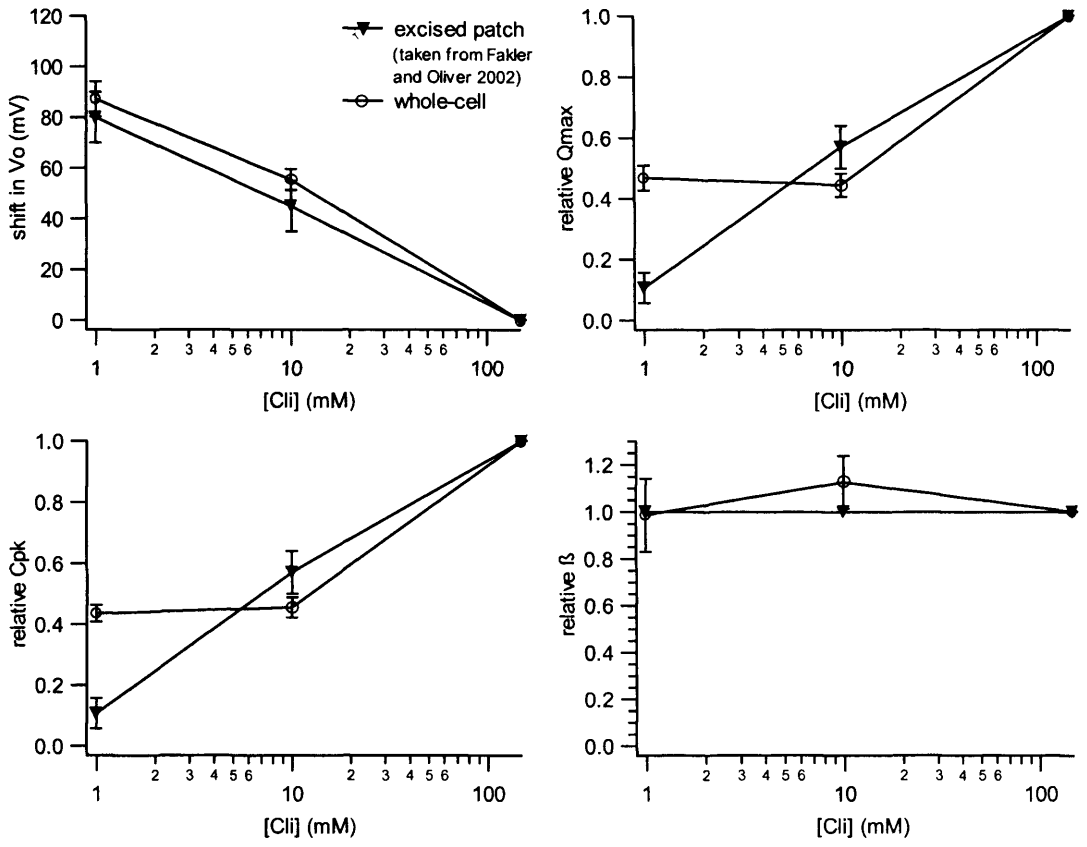

Figure 5.16 A comparison of the Boltzmann parameters measured from whole-cell recordings with those measured from excised patches; Cl_i was replaced with sulphate. All values were determined relative to the values at 150mM [Cl_i]. Data is shown as mean ± SD.

5.3.4 Replacing Cl_i with Glutamate in the Whole-Cell Configuration

Cells were patched with Na-based solutions containing 10mM [Cl_{pip}], where chloride was replaced with glutamate (Solution Glut-10 Table 2.2). NLCs were measured from 10s after break-in until stead-state (Figure 5.17). Following break-in there was a positive shift in the V_o of the NLC (by 3.7 ± 1.5 mV) and a decrease in C_{pk} (to 65.7 ± 5.0%) and Q_{max} (to 72.4 ± 9.0%). There was also a small but significant decrease in β to 96 ± 3% ($p<0.05$). The shift in V_o was much smaller than that observed when [Cl_i] was reduced to 10mM by replacement with sulphate.

The I(V)s recorded 5 minutes after break-in, when [Cl_i] is equivalent to [Cl_{pip}], had V_{rev} close to 0mV (-6.3 ± 5.0mV). The mean V_{rev}, when [Cl_i] was reduced to 10mM, was not significantly different to the mean V_{rev} from control cells.

The exponential fits to the time-courses of the mean shift in V_o, and relative decreases in C_{pk} and Q_{max}, gave time-constants between 52s and 84s.

5.3.4 Replacing Cl_i with Maleate in the Whole-Cell Configuration

It could be argued that since sulphate is divalent, gluconate and glutamate are more likely to interact with prestin, thus reducing the shift in V_o, as opposed to sulphate interacting with prestin to increase the shift. Therefore if it were the case that divalent anions do not interact, an alternative divalent anion such as maleate would be expected to produce as large a shift as sulphate.

Cells were patched with Na-based solution containing [Cl_{pip}] of 10mM, where chloride was replaced with maleate (Solution Mal-10, Table 2.2). The concentration of maleate was chosen to maintain ionic strength and sucrose was used to make up the osmolarity. NLCs were measured from 10s after break-in until stead-state (Figure 5.18). Following break-in was a positive shift in the V_o of the NLC (by 28.3 ± 2.4

mV) and a decrease in C_{pk} (to 53.0 ± 3.7%) and Q_{max} (to 60.0 ± 7.1%). There was no significant change in β. The shift in V_o observed was smaller than that observed when $[Cl_i]$ was reduced to 10mM by replacement with sulphate.

The I(V)s recorded 5 minutes after break-in, when $[Cl_i]$ is equivalent to $[Cl_{pip}]$ had a V_{rev} close to 0mV (-4.2 ± 4.5mV). The mean V_{rev}, when $[Cl_i]$ was reduced to 10mM, was not significantly different to the mean V_{rev} from control cells.

The exponential fits to the time-courses of the mean shift in V_o, and relative decreases in C_{pk} and Q_{max}, gave time-constants between 45s and 70s.

5.3.6 Comparison of the Effects of Different Anions on the NLC

The shift in V_o, and decrease in C_{pk} observed when cells were patched with 10mM $[Cl_{pip}]$ depended on the anion used to replace chloride. In all cases the shift in V_o was in the depolarising direction. The shift in V_o was greatest for replacement with sulphate and lessened when alternative replacement anions were used in the following order; sulphate>maleate>gluconate>glutamate (Figure 5.19A). In all cases the C_{pk} of the NLC decreased. The mean decrease in C_{pk} was greatest for replacement with sulphate and lessened when alternative anions were used following the same general order as the shift in V_o, although the decrease in C_{pk} when chloride was replaced with gluconate was not significantly greater than when chloride was replaced with glutamate (Figure 5.19B).

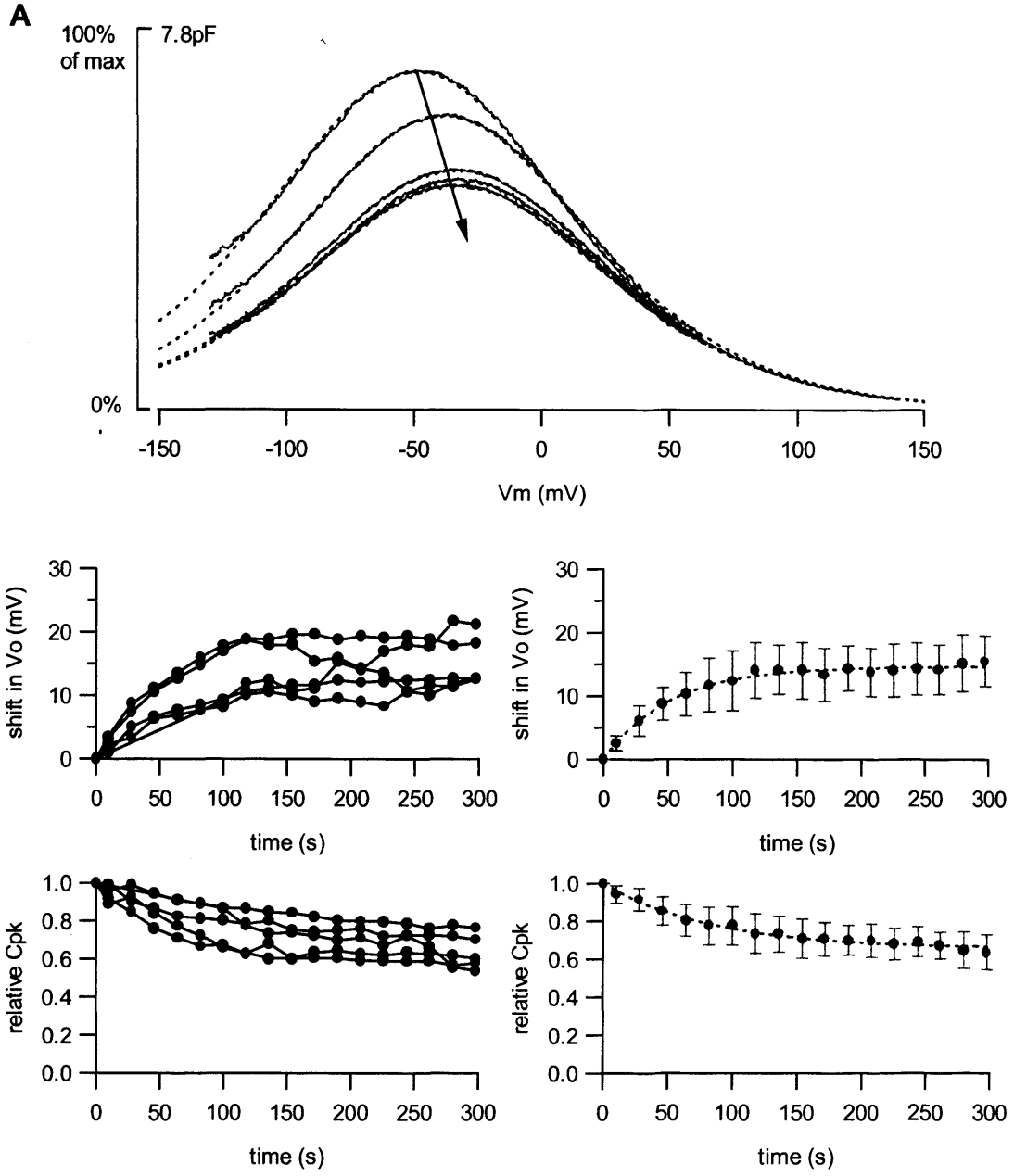

Figure 5.17 The effect of reducing [Cl_i] to 10mM, where Cl_i was replaced with glutamate. A) An example cell showing NLCs recorded in the whole-cell configuration. Traces were recorded at 18s intervals from 10s after break-in. They are shown here at 54s intervals, from the first record. The arrow shows the direction of time. The dotted lines show the fits of the B′(V) to the NLC traces. On average maximum C_{pk} estimated at the instant of break-in was 7.3 ± 2.1pF (n=5). B) The time-course of V_o and C_{pk} after break-in. The shift in V_o (V_o-V_o(t=0s)) and decrease in C_{pk} (C_{pk}/C_{pk}(t=0s)) were determined relative to the instant of break-in. The left panel shows the time-course for individual cells, and the right panel shows the time-courses of the mean values ± SD (n=5).

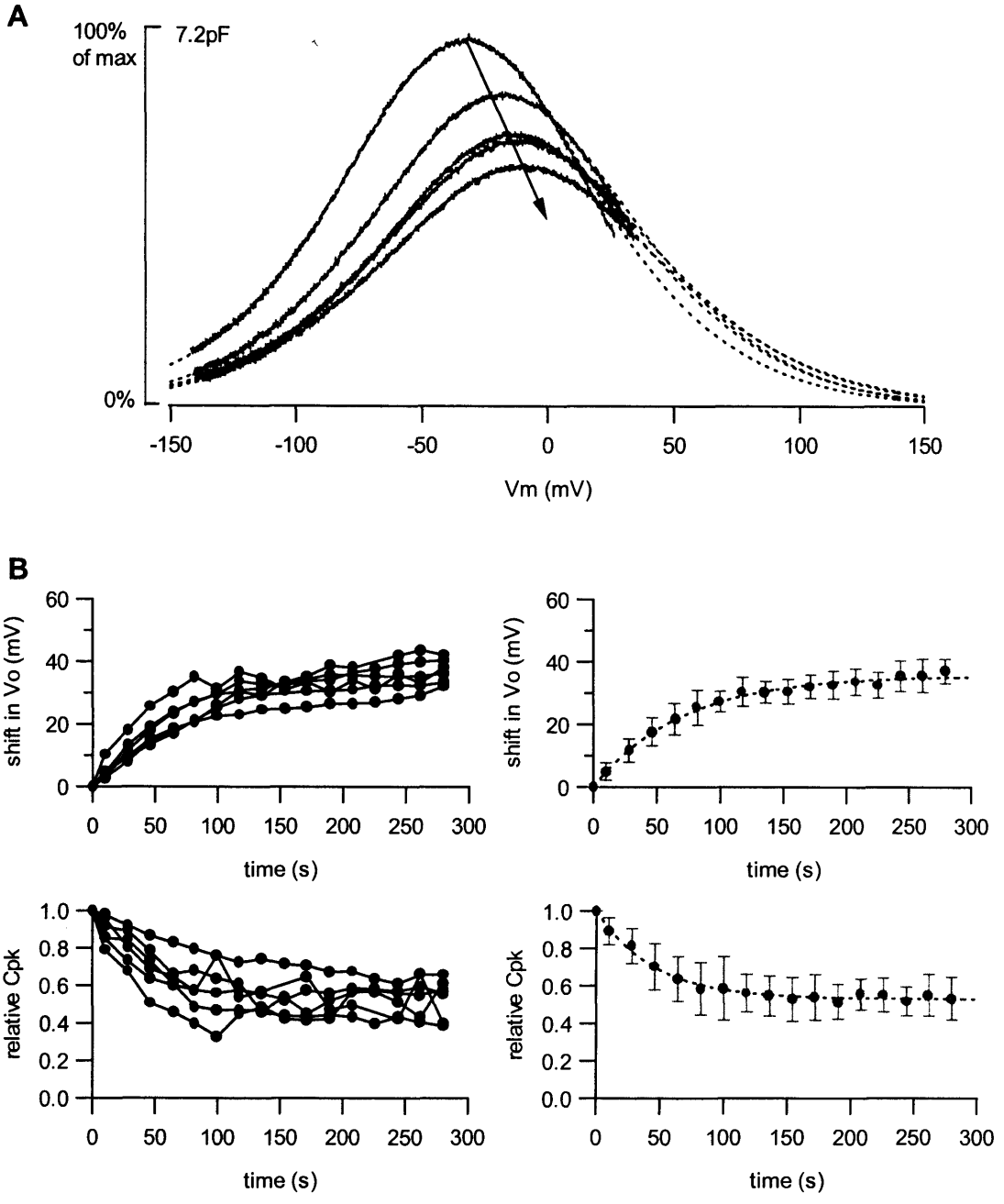

Figure 5.18 The effect of reducing $[Cl_i]$ to 10mM, where Cl_i was replaced with maleate. A) An example cell showing NLCs recorded in the whole-cell configuration. Traces were recorded at 18s intervals from 10s after break-in. They are shown here at 54s intervals, from the first record. The arrow shows the direction of time. On average maximum C_{pk} estimated at the instant of break-in was 9.8 ± 2.1pF (n=6). The dotted lines show the fits of the B′(V) to the NLC traces. B) The time-course of V_o and C_{pk} after break-in. The shift in V_o (V_o-V_o(t=0s)) and decrease in C_{pk} (C_{pk}/C_{pk}(t=0s)) were determined relative to the instant of break-in. The left panel shows the time-course for individual cells, and the right panel shows the time-courses of the mean values ± SD (n=6).

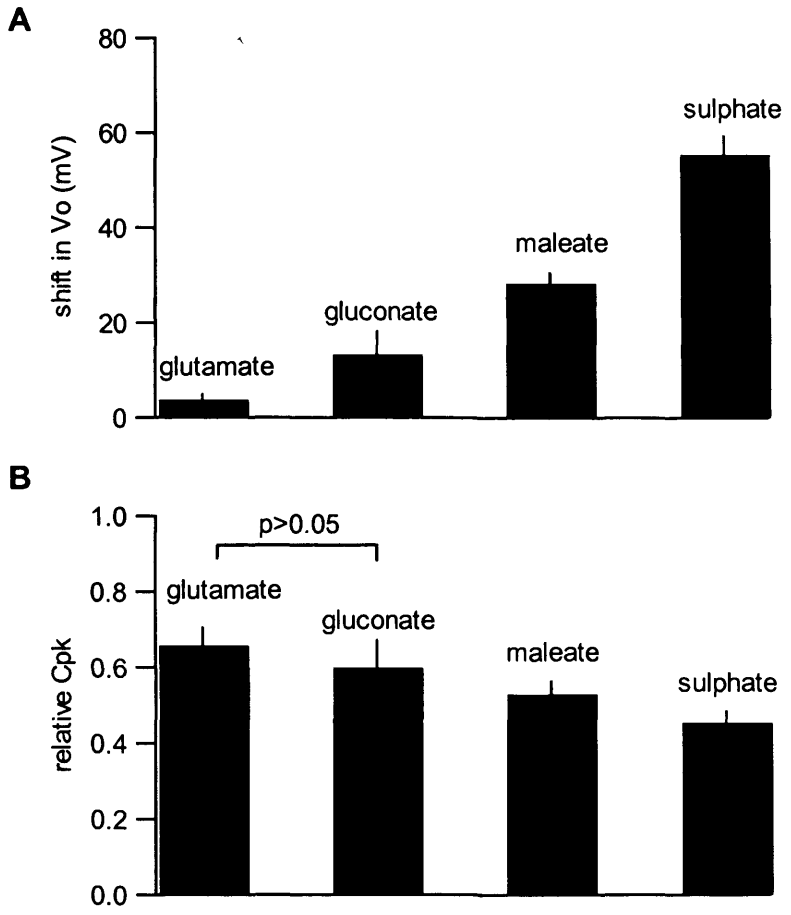

Figure 5.19 The effect of different replacement anions on the shift in V_o and the decrease in C_{pk}, when $[Cl_i]$ is reduced to 10mM. Both the shift in V_o and the decrease in C_{pk} were measured relative to the values at the instant of break-in. This corresponded to saturating levels of $[Cl_i]$, which produce the same NLC as 150mM $[Cl_i]$. A) The shift in V_o depended on the anion used to replace chloride. The largest shift was observed for sulphate. All values were significantly different from all other values ($p<0.01$). B) The decrease in C_{pk} also depended on the replacing anion. All values were significantly different from all the other values ($p<0.05$), except there was no significant difference between glutamate and gluconate ($p>0.05$).

5.3.6 Replacing Cl_e with Gluconate

Cells were patched with Na-based, 1mM [Cl_{pip}], where chloride was replaced with gluconate (solution Gluc-1, Table 2.2). Approximately 5 minutes after break-in once [Cl_i] had equilibrated, [Cl_e] was reduced first to 10mM and subsequently to 1mM. Cl_e was replaced with gluconate. External solutions were exchanged by local application with a manifold applicator. An example cell is shown in Figure 5.20.

As [Cl_e] was reduced to 10mM (n=9) and 1mM (n=7), there was a positive shift in the V_o of the NLC (by 13.5 ± 2.16 mV, and 25.8 ± 2.81 mV), C_{pk} decreased (to 87.8 ± 5.1% and 77.4 ± 8.5% respectively) and Q_{max} decreased (to 90.4 ± 7.8% and 81.3 ± 9.1% respectively) (Figure 5.21). In cases where the reduction of [Cl_e] was followed by the wash-in of 150mM [Cl_e], these effects were partially reversible. (n=7). There was no significant change in β ($p>0.05$).

The I(V)s recorded simultaneously with a voltage-ramp were also analysed. Unlike in the experiments described in Ch.5.3.2-5.3.4, continuous voltage-ramps were not performed between 10s after break-in and 5 minutes after break-in. Thus in this experiment changes in the I(V) between 10s and 5minutes, due to the seal worsening were less likely, and enabled consistent changes in the I(V) from 10s after break-in to 5minutes after break-in to be observed. A typical example is shown in Figure 5.22.

When cells were patched with 1mM [Cl_{pip}] there was a change in the I(V) from 10s after break-in to 5 minutes after break-in, as the [Cl_i] approached the [Cl_{pip}] from its initial concentration assumed to be at saturating levels, greater than 10mM. An increase in outward current at positive V_m and a decrease in inward current at negative V_m was observed. The shift in V_o could not be accurately determined since the exact ionic composition of the cell shortly after break-in was unknown, and thus the liquid junction potential 10s after break-in could not be determined.

A comparison of I(V)s for different concentrations of $[Cl_e]$ with $[Cl_i]$ at 1mM, shows that the outward current at positive V_m decreased as $[Cl_e]$ was decreased, but there was very little effect on the inward current. No significant changes in V_{rev} were observed as $[Cl_e]$ was reduced ($p>0.05$).

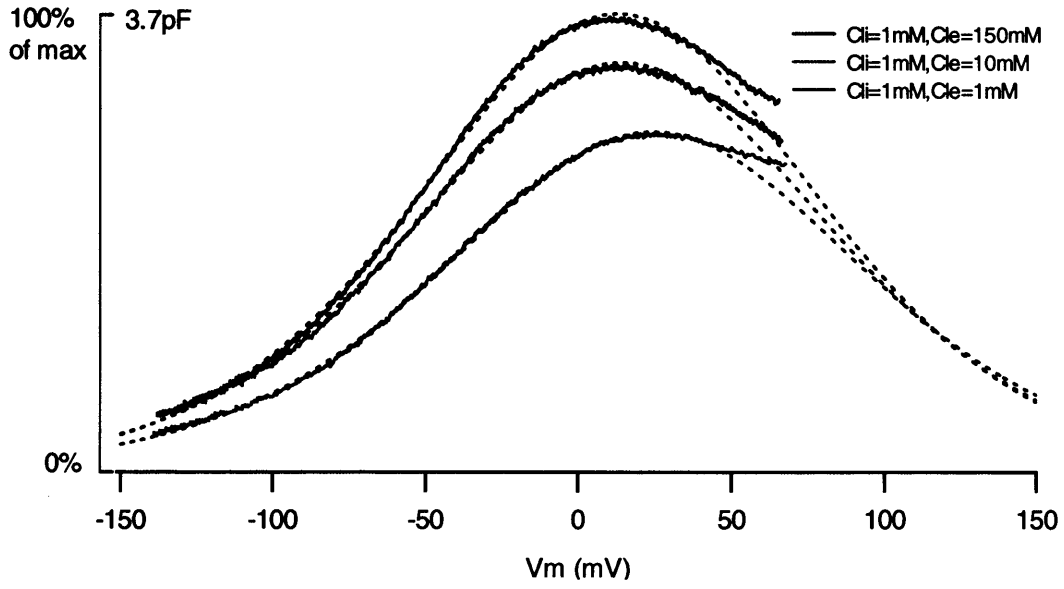

Figure 5.20 The effect on the NLC of reducing $[Cl_e]$, when $[Cl_i]$ is low. Cells were patched with 1mM $[Cl_{pip}]$, where chloride was replaced with gluconate. At least 5 minutes after break-in $[Cl_e]$ was reduced to 10mM and 1mM, by replacement with gluconate. Maximum C_{pk} corresponds to the NLC recorded 5 minutes after break-in with 150mM $[Cl_e]$. Maximum C_{pk} was 3.0 ± 0.7 (n=9). Reduction of $[Cl_e]$ produced a positive shift in V_o and a decrease in C_{pk}. The traces show raw data and were not corrected for liquid junction potentials.

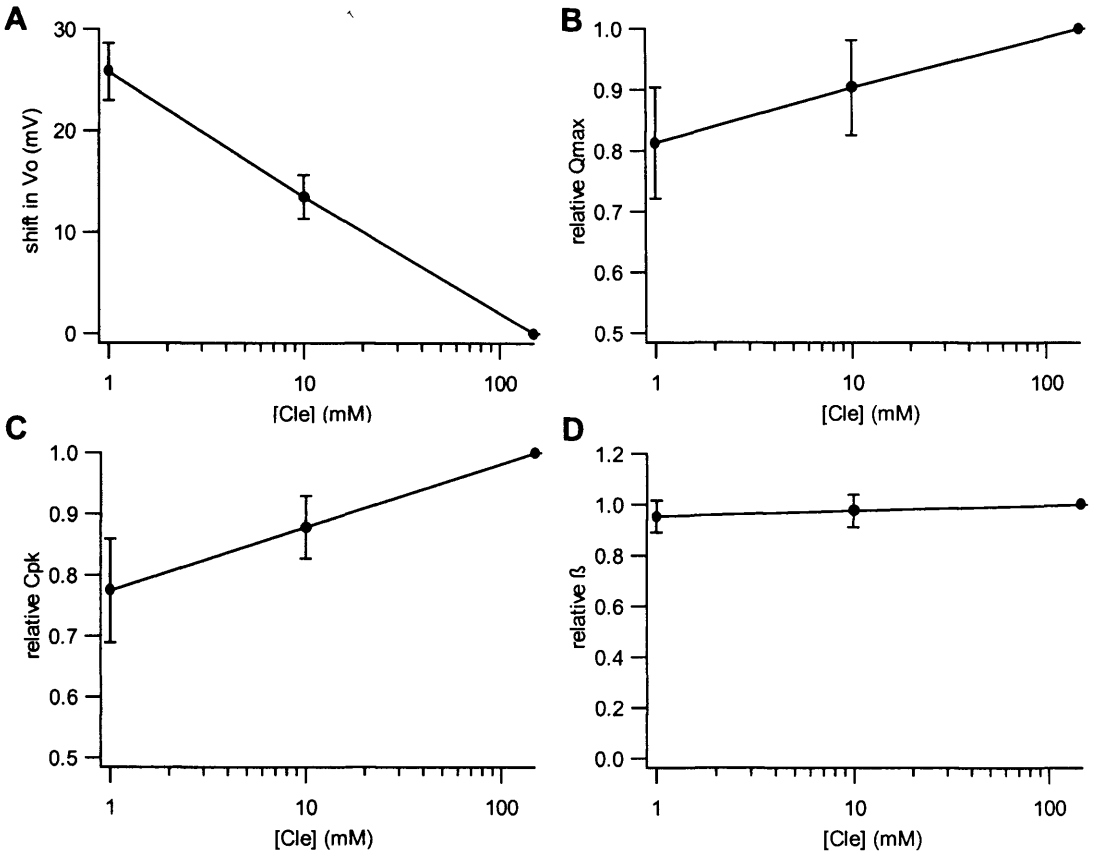

Figure 5.21 The Boltzmann parameters of the NLC depend on $[Cl_e]$ when $[Cl_i]$ is 1mM and both Cl_i and Cl_e are replaced with gluconate. Summary shows the effect on the Boltzmann parameters of reducing $[Cl_e]$ to 10mM (n=5) and 1mM (n=3). All values were determined relative to the values determined in 150mM $[Cl_e]$. Data is shown as mean ± SD A) V_o shifted to more positive potentials as $[Cl_e]$ was reduced. B) Q_{max} decreased when $[Cl_e]$ was reduced. C) C_{pk} decreased when $[Cl_e]$ was reduced. D) There was no significant change in β when $[Cl_e]$ was reduced ($p>0.05$).

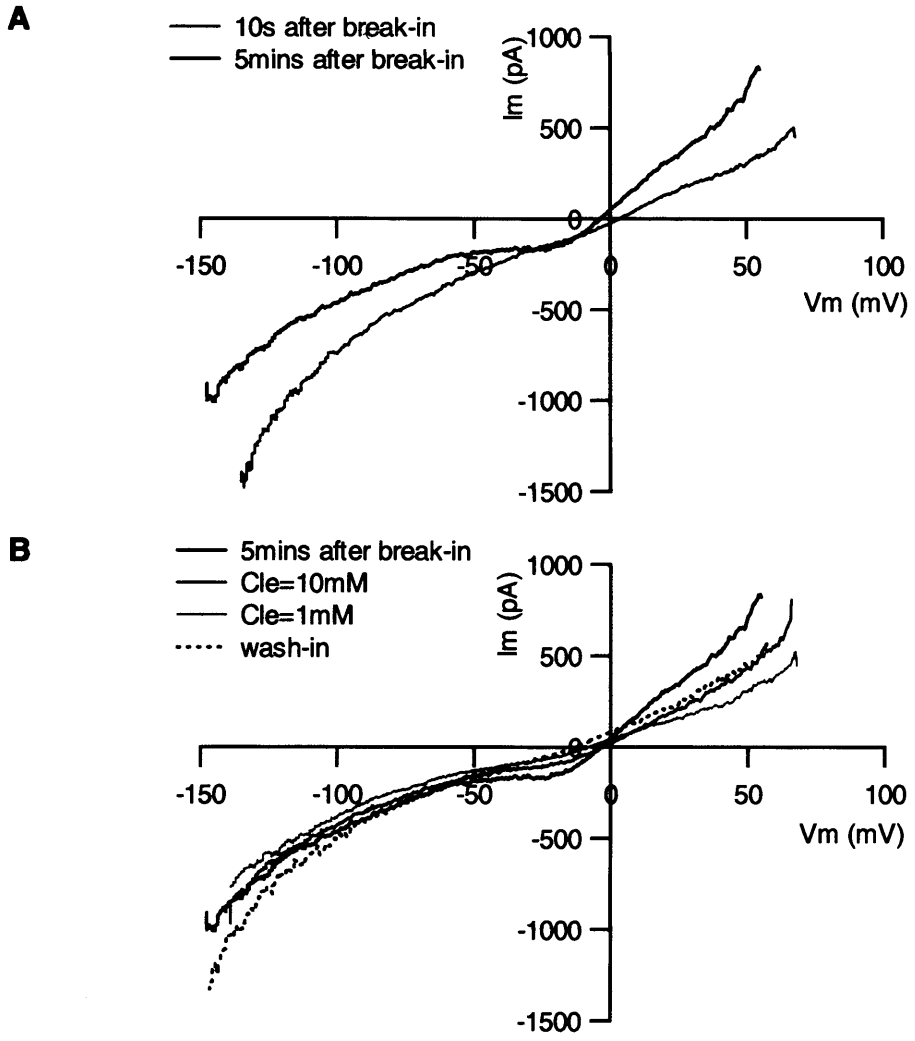

Figure 5.22 The effect on the I(V) of reducing $[Cl_i]$ or $[Cl_e]$. A) The I(V) changed over time when cells were patched with 1mM $[Cl_{pip}]$, which corresponded with $[Cl_i]$ decreasing from >10mM to 1mM. Chloride was replaced with gluconate. B) Subsequent reduction of $[Cl_e]$ to 10mM and 1mM led to a continual decrease in the outward current, that was partially reversible by subsequent wash-in of 150mM $[Cl_e]$ solution.

5.4 Discussion

5.4.1 The Observed Effect on the NLC of Reducing [Cl_i] Depends on the Recording Configuration

Although [Cl_i] can be more accurately controlled in the excised patch recording configuration, due to the difficulty of obtaining excised OHC patches from the lateral membrane, the majority of experiments described in this chapter were performed in the whole-cell configuration. However previous studies raised concerns over the influence of the recording configuration on the measurement of the NLC. Whilst measurements obtained from excised OHC patches (Oliver et al. 2001) showed that the NLC was abolished when Cl_i was completely replaced with sulphate, measurements made in the whole-cell configuration (Rybalchenko and Santos-Sacchi 2003) found that the magnitude of the NLC was almost unaffected by completely replacing Cl_i with sulphate. This contradiction has alternatively been attributed to the inability to control [Cl_i] in the whole-cell configuration (Gummer 2003) or to the effects of disrupting the membrane structure (Rybalchenko and Santos-Sacchi 2003). Thus it was necessary to establish the extent to which the recording configuration influences the observations made, and whether it was appropriate to use measurements from the whole-cell configuration to describe the exact dependence of the NLC on [Cl_i].

In Ch.5.3.1 and Ch.5.3.2 the effect of reducing [Cl_i] and replacing it with gluconate was determined in both excised inside-out patches and the whole-cell configuration. It was found that for reductions of [Cl_i] to 10mM or 1mM, the measurements obtained in the different recording configurations were generally consistent. However when Cl_i was completely removed the results were inconsistent.

Complete replacement of Cl_i with gluconate led to the abolishment of NLC in excised patches, but not in whole-cell recordings where a considerable NLC remained. In Ch.5.3.3 the effect of reducing $[Cl_i]$ and replacing it with sulphate was determined in the whole-cell configuration and compared with the previous measurements made from excised patches (Fakler and Oliver 2002). Although the measurements appeared to be consistent, significant differences between the measurements from the two recording configurations were present on reduction of $[Cl_i]$ to 10mM. However since the measurements made from excised patches were performed in a different laboratory, with different solutions, and on a different species (rat rather than guinea pig), these differences in the experimental conditions might be sufficient to account for the small differences observed. On the other hand on reduction of $[Cl_i]$ to 1mM the decrease relative C_{pk} and Q_{max} was considerably larger in excised patches, which is unlikely to be only a result of different experimental conditions. Additionally when Cl_i was completely removed the NLC in excised patches was abolished, but a considerable NLC remained in whole-cell recordings. Thus the measurements from the two experimental configurations could be considered consistent for reductions of $[Cl_i]$ to 10mM, but were inconsistent when $[Cl_i]$ was reduced to lower concentrations.

The fact that excised patch recordings and whole-cell recordings were predominantly inconsistent when $[Cl_i]$ was reduced below 1-10mM, suggests that this may be due to the inability to accurately control $[Cl_i]$ in the whole-cell configuration when $[Cl_i]$ is low. This could be due to the influx of chloride from the external solution combined with the presence of the sub-surface cisternae. The sub-surface cisternae form a continuous membraneous layer parallel to the plasma membrane and thereby form a restricted compartment between them and the plasma membrane of ~30nm width (Pollice and Brownell 1993, Holley 1996). Since the sub-surface

cisternae terminate at the apical and basal extremes of the OHC, this compartment has limited diffusional access from the cytosol, and might therefore be able to maintain a higher concentration of chloride than the bulk cytosol. The possible influence of extracellular chloride on the concentration of chloride at the intracellular side of the plasma membrane is addressed in Ch.6. For the remaining experiments it was assumed that [Cl_i] could be accurately controlled when reduced to 10mM, and therefore whole-cell recordings could be used to accurately determine the effect on the NLC of reducing [Cl_i] to 10mM.

The measurements obtained in Ch.5.3.3 were also found to contradict those made previously in the whole-cell configuration by Rybalchenko and Santos-Sacchi (2003) (Figure 1.4B). The results presented in this section showed a considerable reduction in the C_{pk} and Q_{max} when cells were patched with chloride-free solution, compared to almost no reduction found previously. The origin of this discrepancy is also addressed in Ch.6.

5.4.2 Comparison of the Predictions of the Model with the Experimental Observations

5.4.2.1 Evidence of a Role for Sulphate

The chloride/sulphate exchanger model with intrinsic charge movement requires that sulphate interacts with prestin (Ch.4.3.3). The evidence presented in this chapter suggests it is likely that sulphate does interact with prestin.

In Ch.5.3.2-Ch.5.3.5 the effect on the NLC of reducing [Cl_i] to 10mM, where Cl_i was replaced with either gluconate, sulphate, glutamate or maleate was described. The shift in the NLC, and the decrease in the C_{pk} produced by reducing [Cl_i] was shown to depend on the anion species used to replace chloride. This is consistent with

observations made by Ryblachenko and Santos-Sacchi (2003), which showed that the shift in V_o and decrease in C_{pk} produced by replacing Cl_i with sulphate was different to that produced by replacement with Hepes. In this chapter sulphate was found to produce the largest shift in V_o, and also the largest decrease in C_{pk}, whilst glutamate produced the smallest shift in V_o and the smallest decrease in C_{pk}. In general, a larger shift in V_o appeared to correspond to a larger decrease in C_{pk} (Figure 5.19).

The fact that all the anions tested produced different effects on the NLC suggests that at least three of the anions used probably interact with prestin to affect the NLC. It is unlikely that these different effects arose from different interactions between the replacement anions and a possible intracellular chloride buffer as significant differences were also observed when $[Cl_i]$ was reduced to 10mM, where chloride buffering is unlikely to produce large changes in free $[Cl_i]$. Since two monovalent anions were used (gluconate and glutamate) and two divalent anions were used (sulphate and maleate), it appears that both monovalent and divalent anions are able to interact with prestin. Thus it is likely that sulphate interacts with prestin.

The experimental observations of the dependence of the NLC on $[Cl_i]$ when Cl_i was replaced with alternative anions were consistent with the predictions of the chloride/sulphate exchanger model with intrinsic charge movement, where the alternative anion used to replace chloride was also transported across the membrane. In this case as was observed experimentally the model predicts that a larger positive shift in V_o would be correlated with a larger decrease in C_{pk}.

Therefore at this stage the experimental observations are generally consistent with the predictions of the model. However currently there it is no direct evidence that any of the anions used to replace chloride are actually transported across the

membrane, or that clarifies what type of interaction occurs between the replacement anions and prestin.

5.4.2.2 The Effect on the I(V) of Reducing $[Cl_i]$ or $[Cl_e]$

The chloride/sulphate exchanger model with intrinsic charge movement predicts that steady-state currents will arise in the presence of a chloride or sulphate gradient. Therefore the V_{rev} of the I(V), and the magnitude of the currents would change as a result of reducing either $[Cl_i]$ or $[Cl_e]$. For example a large positive shift in the V_{rev}, and an increase in inward current is predicted when Cl_i is removed. The evidence presented in this chapter indicates the presence of a chloride conductance, but the exact dependence of the I(V) on $[Cl_i]$ does not appear to be consistent with the predictions of the model.

The I(V) curves measured simultaneously with the NLC, via a voltage-ramp were analysed in all experiments. V_{rev} was found to be independent of $[Cl_i]$, and was close to 0mV, in all experiments. However the magnitude of the current was found to be dependent on both $[Cl_i]$ and $[Cl_e]$, when Cl_i and Cl_e were replaced with gluconate.

In Ch.5.3.1, an increase in outward current at positive V_m was observed as $[Cl_i]$ was reduced in excised OHC patches. In Ch.5.3.7 consistent changes in the I(V) were also observed when $[Cl_i]$ was reduced and replaced with gluconate, in the whole-cell configuration. An increase in outward current was produced at positive V_m, and a decrease in the inward current was produced at negative V_m. Furthermore when $[Cl_e]$ was reduced from 150mM to 10mM and 1mM, with $[Cl_i]$ at 1mM, the outward current at positive V_m decreased as $[Cl_e]$ was reduced.

These results indicated the presence of a chloride conductance and were partially consistent with recent observations made by Rybalchenko and Santos-Sacchi (2003),

who also identified a chloride conductance, which they attributed to a stretch-activated channel. Consistent with the data presented in Ch.5 they found that, increasing $[Cl_e]$, with low $[Cl_i]$ also led to an increase in outward current when Cl_i and Cl_e were replaced with Hepes. However unlike the data presented here, they found that increasing $[Cl_e]$ with low $[Cl_i]$ produced an increase in inward current, and a negative V_{rev} (~-12mV).

In summary, although the experimental observations of Ch.5 did indicate the presence of a chloride conductance they were inconsistent with the predictions of the model in two ways:

1) No dependence of V_{rev} on $[Cl_i]$ or $[Cl_e]$ was found in any experiment.
2) An increase in outward current, rather than an increase in inward current was produced when $[Cl_i]$ was reduced.

Possible reasons for these discrepancies are discussed below:

1) It is likely that it is not possible to accurately control $[Cl_i]$ in the whole-cell configuration, and that the actual $[Cl_i]$ was higher than 1mM, thus reducing the effect on the I(V) predicted.
2) The presence of other conductances, might mask the effect of reducing $[Cl_i]$. OHCs are known to have a characteristically low membrane resistance, which has been attributed to the presence of several ionic conductances in the OHC membrane. These include a calcium-activated K^+ current, I_K, a voltage-gated K^+ current (I_{KN}), and a non-specific 'cation leak' current (Housley and Ashmore 1992). Additionally stretch-activated channels, which are either selective for K^+ (Iwasa et al. 1991), non-specific cation selective (Ding et al 1991) or completely non-specific (Rybalchenko and Santos-Sacchi 2003) have been proposed to be present in the basolateral membrane. In the experiments

presented in this chapter, K^+ was kept at 5mM on either side of the membrane, thus the contribution to the I(V) from K^+ currents should be minimised. However the contribution to the I(V) from any non-specific cation leak current would still be present due to the high concentration of Na^+ on either side of the membrane, and has been shown to increase with time in dissociated OHCs (Ashmore 1987). Since this cation conductance is expected to be much larger than the chloride conductance predicted due to prestin, the V_{rev} would be expected to remain close to the V_{rev} for Na^+, which was 0mV in all experiments. For example for the cell shown in Figure 5.22, the conductance at –50mV was ~6.7nS compared with 0.6nS predicted by the model when $[Cl_i]$ is 1mM and $[Cl_e]$ is 150mM. Therefore in this example the cells' conductance is ~10 times larger than the predicted conductance due to prestin.

3) In excised patches, the number of prestin molecules is reduced by a factor of ~1000, thus the magnitude of the predicted currents through prestin would be ~1000 times smaller than measured in the whole-cell configuration. Thus the current due to an imperfect seal is a considerable contribution to the total current measured.
4) The predictions for the effect on the I(V) of removing Cl_i were made for the condition that sulphate is used to replace chloride, however it was only possible to detect consistent changes in the I(V) in Ch.5.3.7 where gluconate rather than sulphate was used to replace chloride. The effect on the I(V) of replacing chloride with gluconate has not been modelled.

Thus further investigations are required to separate the effect of reducing $[Cl_i]$ or $[Cl_e]$ on the I(V) by minimising the contribution from cationic conductances, and the effect on the I(V) of reducing $[Cl_i]$ or $[Cl_e]$ where chloride is replaced with sulphate.

5.4.2.3 The Effect on the NLC of Reducing [Cl_e]

The chloride/sulphate exchanger model with intrinsic charge movement also predicts that there should be a significant effect on the NLC of reducing [Cl_e] with [Cl_i] low. The evidence presented in this chapter shows that this is indeed the case, however the exact dependence found in Ch.5.3.7 was unlike the predictions of the model.

The model predicts that when [Cl_i] is low, a reduction of [Cl_e] should lead to a positive shift in the V_o of the NLC and an increase in the C_{pk} of the NLC. In Ch.5.3.7 it was shown that reducing [Cl_e] with 1mM [Cl_i], where both Cl_i and Cl_e were replaced with gluconate did lead to a positive shift in the V_o, but C_{pk} decreased further. These results were consistent with observations made by Rybalchenko and Santos-Sacchi (2003) who found that reducing [Cl_e] with [Cl_i] low, led to a positive shift in V_o and a further decrease in C_{pk} when Cl_i was replaced with sulphate and Cl_e was replaced with Hepes.

There are several possible reasons for the discrepancy between the experimental observations and the predictions of the model. In particular there may be considerable limitations to the experimental approach used. It is likely that in whole-cell recordings [Cl_i] cannot accurately be controlled for reductions to 1mM, and therefore the actual [Cl_i] facing prestin, is higher than assumed. This would affect the predictions. Furthermore if chloride fluxes can occur between the intracellular and extracellular medium then it would be impossible to determine whether the observations made are a result of the direct action of Cl_e on prestin, or due to the indirect effect of an efflux of chloride causing [Cl_i] to be reduced further as [Cl_e] is reduced. To accurately determine the effect of reducing [Cl_e] when [Cl_i] is low, it would be ideal to carry out the experiment in excised outside-out patches, where both

$[Cl_i]$ and $[Cl_e]$ could be accurately controlled. However this would be technically very difficult. Finally the predictions of the model were made for the condition that chloride was replaced with sulphate, whereas in the experiment described chloride was replaced with gluconate. The effect of replacing Cl_i with gluconate has not been modelled.

Chapter 6

Addressing Discrepancies in the Experimental Observations

6.1 Introduction

As a consequence of contradictions in the previously published data, there is currently a debate about whether chloride is really necessary to generate a NLC. Recordings made from excised inside-out patches (Oliver et al. 2001) showed that the NLC was abolished upon complete replacement of Cl_i with sulphate, which led to the conclusion that chloride was the voltage-sensor and was required to generate a NLC. However recordings made in the whole-cell configuration showed no change in the C_{pk} of the NLC when Cl_i was completely replaced with sulphate (Rybalchenko and Santos-Sacchi 2003), which led to an alternative conclusion that chloride was not required to generate a NLC but had an allosteric effect on prestin, whereby chloride modulates the NLC by binding to a distinct site to produce a conformational change of prestin.

In order to understand the role of chloride, it is first necessary to understand to the origin of the contradictions in the experimental observations. One obvious proposal is that the different recording configurations are responsible. This proposal was supported by data from chapter 5, which showed that measurements made in the whole-cell configuration were consistent with measurements from excised patches when $[Cl_i]$ was reduced to 1-10mM, but were inconsistent when $[Cl_i]$ was reduced to lower concentrations. One interpretation of this finding was that it is impossible to

accurately reduce [Cl_i] to very low levels in the whole-cell configuration, possibly due to an influx of chloride from the extracellular solution into the compartment between the plasma membrane and the sub-surface cisternae.

The aim of Ch.6 is to investigate whether the residual NLC found in whole-cell recordings is due to the limitations of the experimental approach or indicates that there is a component of NLC that does not require the presence of chloride. Thus experiments are described, in which cells were patched with chloride-free solution in chloride-free bath solution to eliminate the possibility of chloride entering the cell from the bath solution, and ensure that chloride was completely removed from the cell.

In addition a further contradiction was found between the previously published measurements made in the whole-cell configuration (Rybalchenko and Santos-Sacchi 2003) and those presented in the previous chapter, which described the effect of patching with chloride-free solution where chloride was replaced with sulphate. Whilst the previously published data showed no change in the C_{pk} of the NLC when Cl_i was removed (Figure 1.4B), in the previous chapter a significant decrease in the C_{pk} of the NLC was observed (Figure 5.11). The main difference between the experiment described previously and the experiment described in Ch.5, was the cationic composition of both the internal and external solutions. In the previously described experiment $Tris^+$ was used as the major cation, whereas in the experiment of Ch.5, Na^+ was used as the major cation. To identify if this was the source of the discrepancy between the two experiments, the experiment was repeated using the same internal and external solutions that were used previously.

6.2 Methods

The experiments described in this chapter were performed using the patch clamp technique in the whole-cell configuration. For more details see Ch.2. Data was analysed using the same methods described in Ch.5.2.1.

6.3 Results

6.3.1 Replacing both Cl_i and Cl_e with Sulphate

Cells were dissected and bathed in chloride-free solution (Sulph-0, Table 2.2), and subsequently patched with the same chloride-free solution in the pipette, so that they were never presented with any exogenous source of chloride. Both Cl_i and Cl_e were replaced with sulphate. All 13 of the cells recorded from showed a clear presence of a NLC 10s after break-in with 0mM [Cl_{pip}]. However the mean C_{pk} of the NLC 10s after break-in (3.07 ± 1.31 pF) was smaller than that observed when cells were patched with the same solution in a high chloride bath solution (11.85 ± 4.47 pF, n=5). In addition the mean V_o of the NLC 10s after break-in (38.4 ± 16.8 mV) was significantly more positive ($p<0.01$) than that observed when cells were patched with the same solution in a high chloride bath solution (-38.3 ± 6.6 mV, n=5). Furthermore when the V_o of the NLC 10s after break-in, for each cell, was compared with the total time the cell had been in chloride-free bath solution, it was found that the initial V_o tended to be more positive for cells that had spent more time in the chloride-free bath solution before being patched (Figure 6.1).

Following break-in, the C_{pk} of the NLC decreased and the V_o of the NLC appeared to shift to more positive potentials, such that in later recordings the peak of

the NLC was not observable within the range of V_m recorded. Unfortunately it was not possible to extend the range of V_m recorded without compromising the stability of the recording. An example is shown in Figure 6.2. In 4 cells it became impossible to measure a NLC within the range of V_m recorded (Figure 6.3). In all other cells (n=9) it remained possible to fit the B'(V) to the visible part of the trace. However the value for β found from the fits was very variable and in some cases varied by more than ± 40%, during the time of recording (between 82 and 334 s) for each cell. This differs from recordings made with the same solution in the pipette but high chloride bath solution, where no significant change in β was observed during the time of recording. This could indicate that the traces observed were not part of a NLC.

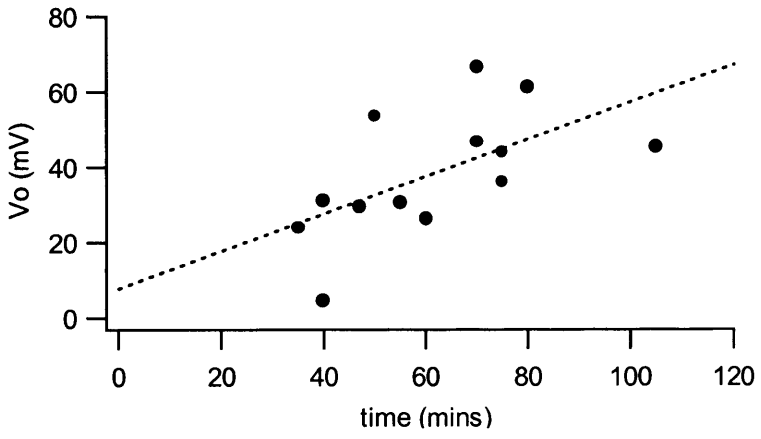

Figure 6.1 The initial V_o of the NLC depends on the time spent by cells in chloride-free bath solution, Cl_i and Cl_e were replaced with sulphate. The V_o of the NLC 10s after break-in, for each cell is plotted against the total time the cell was in chloride-free bath solution. This included 30 minutes for dissection and enzyme digestion, in addition to the time spent in the bath before being patched. The initial V_o was more positive for cells that spent more time in chloride-free solution. The dotted line indicates the best-fit line, however since it is not known what function best describes the time dependence of the initial V_o, the intercept has no significance.

Nevertheless if we assume that these traces were part of a residual NLC, the data shows that on average C_{pk} decreased with time after break-in to 1.35 ± 1.41pF (Figure 6.4A). In comparison the maximum C_{pk} estimated for the instant of break-in when cells were patched with the same solution in high chloride bath solution was 13.6 ± 5.25pF. Thus only ~10% of the NLC remained when no exogenous source of chloride was presented to the cells. Moreover the V_o of the NLC shifted to very positive V_m (Figure 6.4B). Once steady-state was achieved the V_o of the NLC when cells were bathed in chloride-free solution (134 ± 29.2 mV) was ~90mV more positive than when cells were patched with the same solution in high-chloride bath solution (44.0 ± 5.1mV).

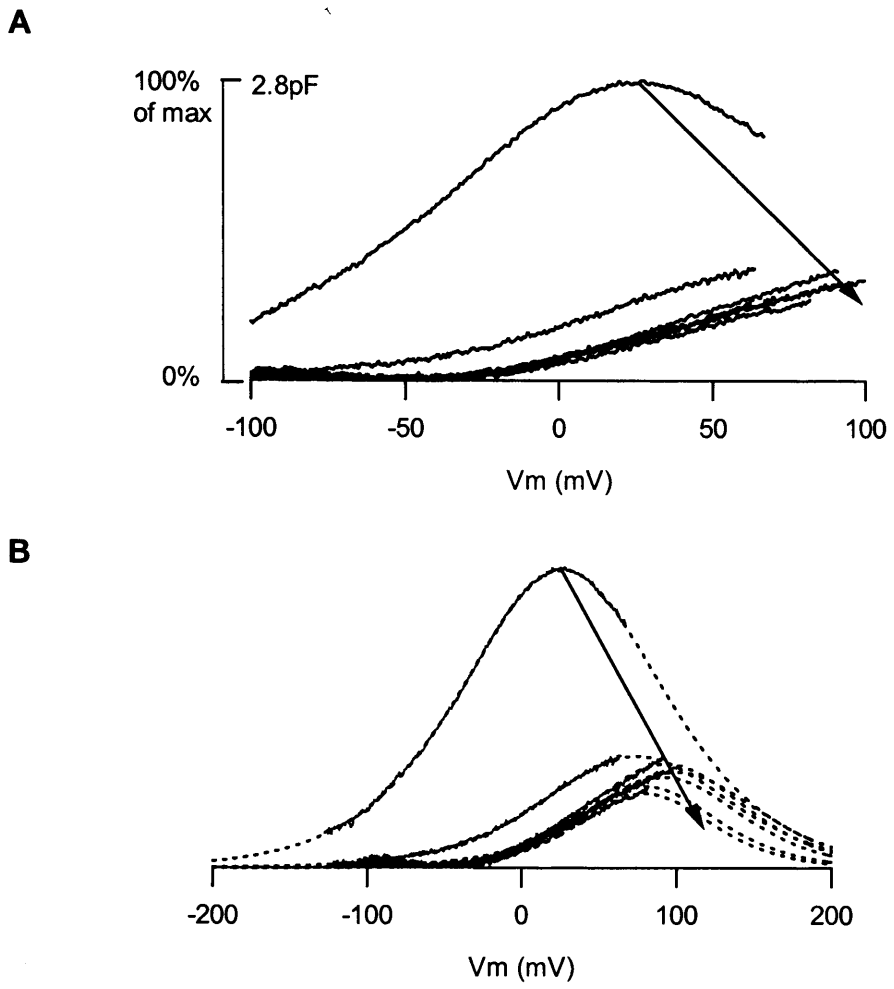

Figure 6.2 The peak of the NLC shifted beyond the range of applied V_m, when both Cl_i and Cl_e were replaced with sulphate. Traces were recorded at 18s intervals from 10s after break-in. They are shown here at 54s intervals, from the first record. Arrows show the direction of time. The maximum C_{pk} corresponded to the NLC recorded 10s after break-in. On average the maximum C_{pk} was 3.07 ± 1.37pF (n=13). A) Following break-in the V_o of the NLC shifted to more positive potentials and C_{pk} decreased. B) The same traces are shown with the B′(V) fits used to obtain values for the Boltzmann parameters.

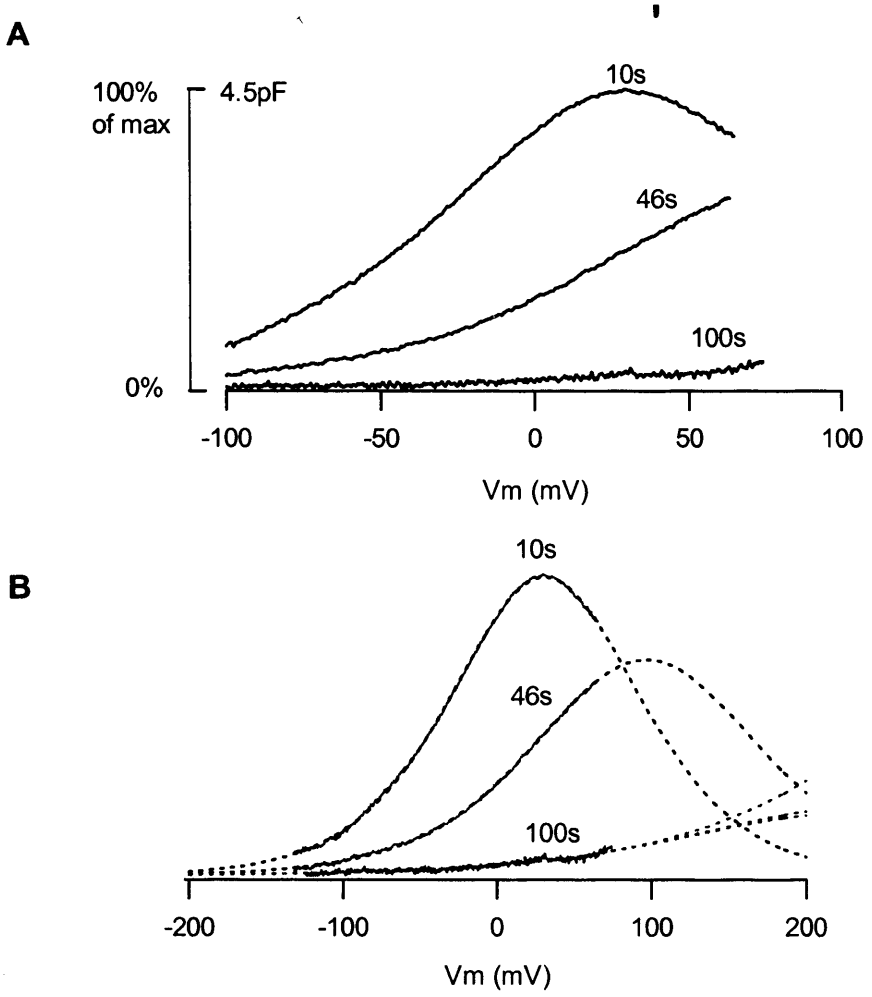

Figure 6.3 The NLC became immeasurable in some cells when both Cl_i and Cl_e were replaced with sulphate. A) An example cell in which no clear NLC could be measured by 100s after break-in. B) The same traces are shown with the B′(V) fits used to obtain values for the Boltzmann parameters. Attempting to fit a B′(V) to the trace at 100s gave several possible fits with a wide range of possible values for all parameters. Some of these are shown in red. All of them gave a value for β at least 50% smaller than the NLC at 10s. Therefore it was concluded that no measurable NLC was present 100s after break-in.

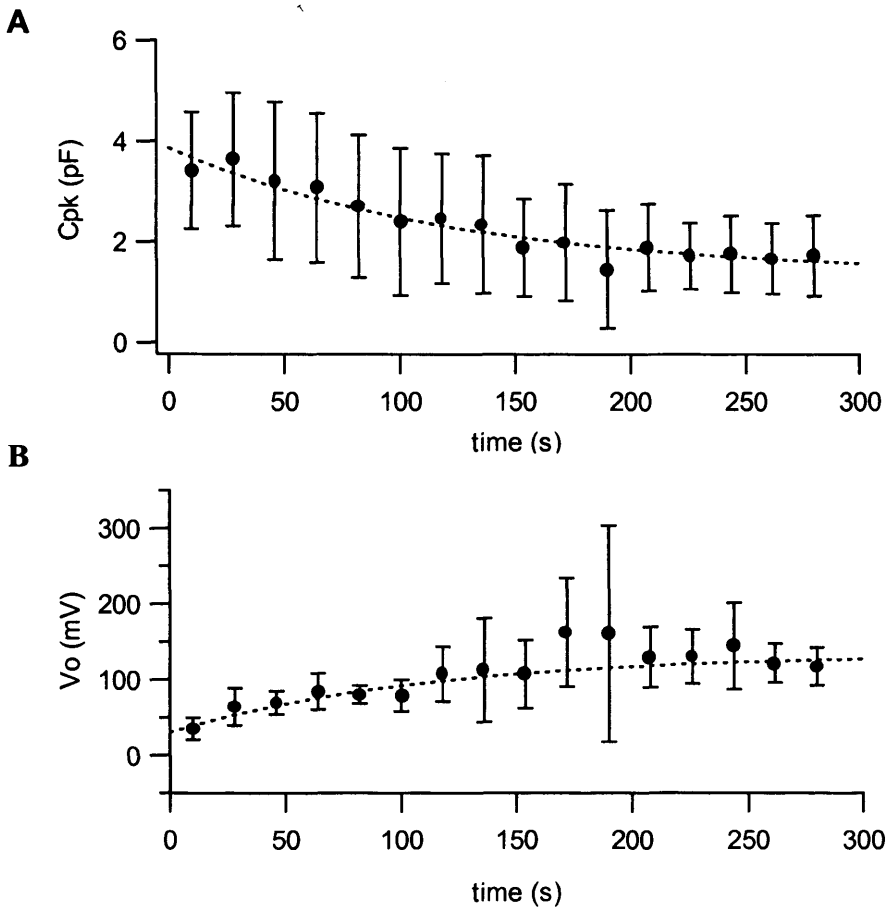

Figure 6.4 The time-course of C_{pk} and V_o after break-in, when both Cl_i and Cl_e were completely replaced with sulphate. The time-courses of the mean V_o and C_{pk} ± SD are shown. A) Following break-in there was a decrease in C_{pk} (n=9) B) Following break-in the V_o of the NLC shifted to very depolarised potentials.

6.3.2 Replacing both Cl_i and Cl_e with Gluconate

Cells were dissected and bathed in chloride-free solution (Gluc-0, Table 2.2), and subsequently patched with the same chloride-free solution in the pipette, so that they were never presented with any exogenous source of chloride. Both Cl_i and Cl_e were replaced with gluconate. All 10 of the cells recorded from showed a clear presence of a NLC 10s after break-in with 0mM [Cl_{pip}]. However the mean C_{pk} of the NLC 10s after break-in (3.03 ± 1.57 pF) was smaller than that observed when cells were patched with the same solution in a high chloride bath solution (5.91 ± 0.44 pF, n=4). In addition the mean V_o of the NLC 10s after break-in (1.5 ± 10.1 mV) was more positive than that observed when cells were patched with the same solution in a high chloride bath solution (-45.8 ± 16.8 mV, n=5). Furthermore the initial V_o tended to be more positive for cells that had spent longer in the chloride-free bath solution before being patched. (Figure 6.5).

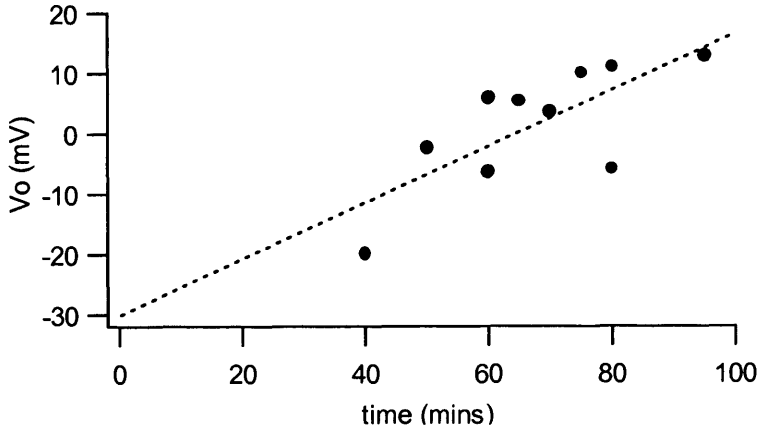

Figure 6.5 The initial V_o of the NLC depends on the time spent by cells in chloride-free bath solution, Cl_i and Cl_e were replaced with gluconate. The V_o of the NLC 10s after break-in, for each cell is plotted against the total time the cell was in chloride-free bath solution. This included 30minutes for dissection and enzyme digestion, in addition to the time spent in the bath before being patched. The initial V_o was more positive for cells that spent more time in chloride-free solution. As in Figure 6.1, the intercept has no significance.

Following break-in, the C_{pk} of the NLC decreased and the V_o of the NLC shifted to more positive potentials. An example cell is shown in Figure 6.6. On average C_{pk} decreased with time after break-in, to 1.89 ± 0.31 pF (Figure 6.7A). In comparison the maximum C_{pk} estimated for the instant of break-in when cells were patched with the same solution in high chloride bath solution was 6.34 ± 0.58 pF. Thus ~30% of the NLC remained when no exogenous source of chloride was presented to the cells. Once steady-state was achieved the V_o of the NLC shifted to more positive V_m (to 42.0 ± 9.6 mV) when cells were bathed in chloride-free solution (Figure 6.7B), which was ~50mV more positive than when cells were patched with the same solution in high-chloride bath solution (-7.5 ± 25.4 mV).

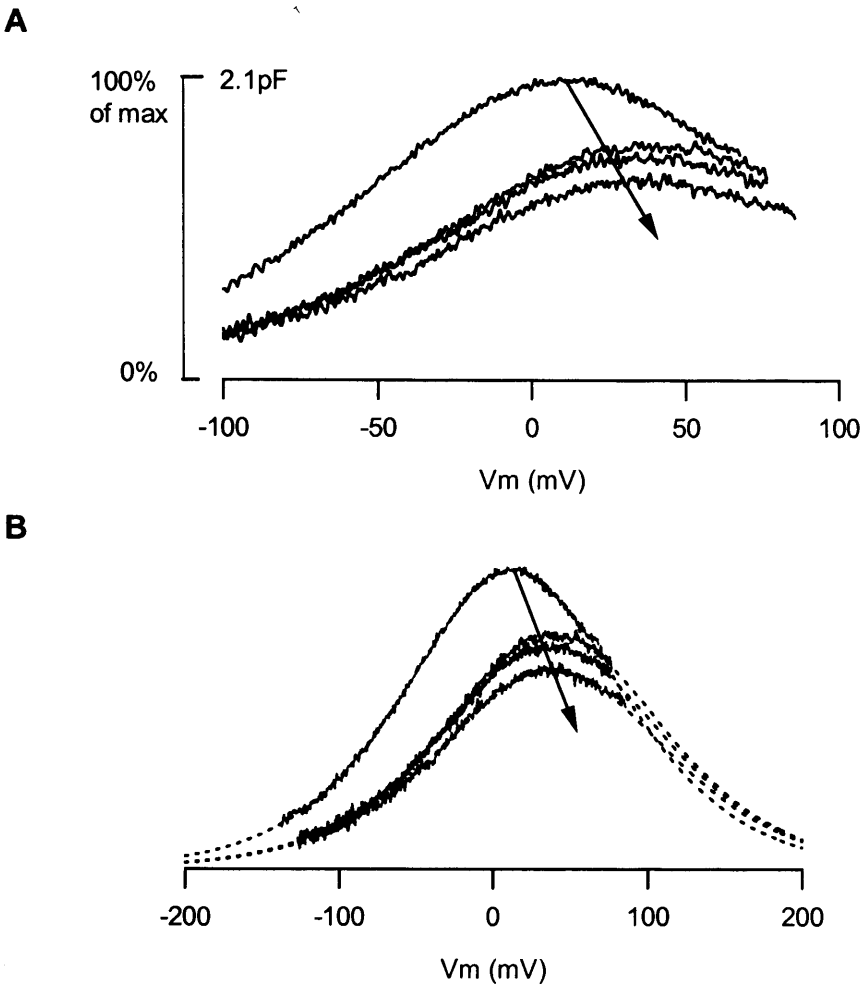

Figure 6.6 A residual NLC remained in cells when both Cl_i and Cl_e were replaced with gluconate. Traces were recorded at 18s intervals from 10s after break-in. They are shown here at 54s intervals, from the first record. Arrows show the direction of time. The maximum C_{pk} corresponded to the NLC recorded 10s after break-in. On average the maximum C_{pk} was 3.03 ± 1.57pF (n=10). A) An example cell showing that following break-in the C_{pk} of the NLC decreased and V_o shifted to more positive potentials. B) The same traces are shown with the B′(V) fits used to obtain values for the Boltzmann parameters.

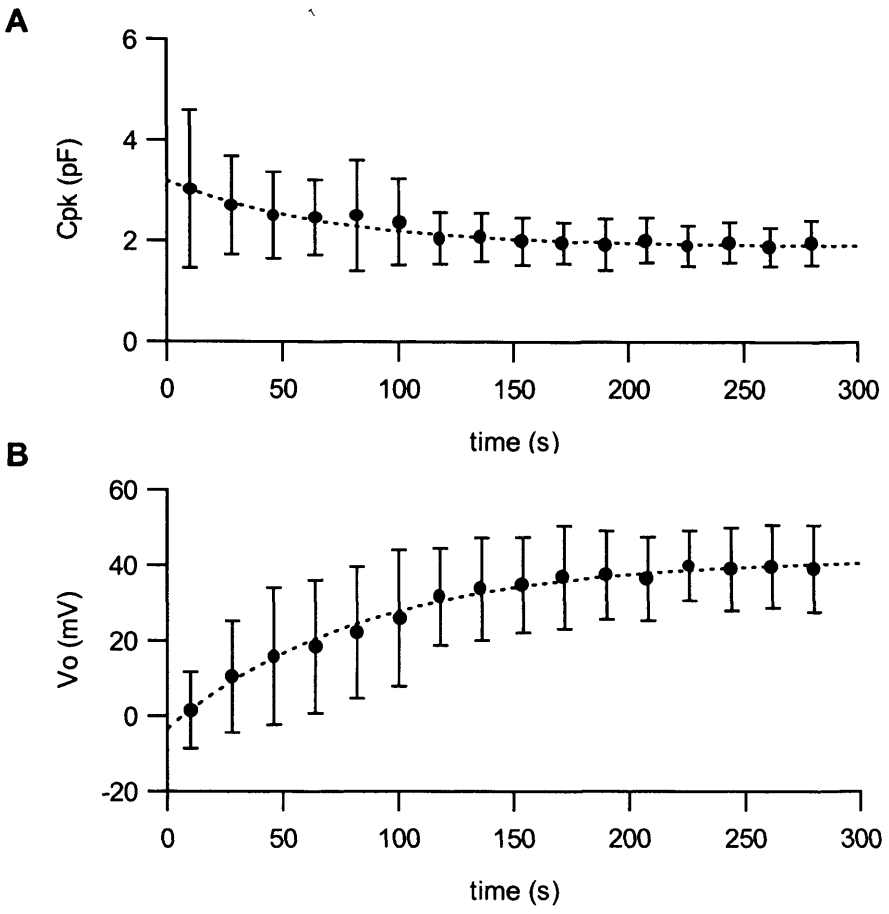

Figure 6.7 The time-course of C_{pk} and V_o after break-in, when both Cl_i and Cl_e were completely replaced with gluconate. The time-courses of the mean V_o and C_{pk} ± SD are shown. A) Following break-in there was a decrease in C_{pk} (n=10) B) Following break-in the V_o of the NLC shifted to very depolarised potentials (n=10).

6.3.3 Replacing Cl_i with Sulphate, $Tris^+$ as the Major Cation

In all the experiments described in Ch.5 solutions contained 145mM Na^+, and 5mM K^+ as the major cations. In the experiment described here, solutions in which $Tris^+$ was the major cation were used. Cells were either dissected in Tris-based bath solution (Tris-HBS, Table 2.1), or dissected in Na-based bath solution (Na-HBS, Table 2.1) and then perfused with Tris-based bath solution for at least 10 minutes. Subsequently cells were patched with Tris-based internal solution (Tris-sulphate, Table 2.2), in which sulphate was the major anion. NLCs were measured from 10s after break-in. There was no difference between the results obtained using either method. An example cell is shown in Figure 6.8A.

Following break-in 8 out of 11 cells showed a maintained positive shift in the V_o of the NLC (by 82.8 ± 4.9 mV) (Figure 6.8B). The other 3 cells showed an initial positive shift that recovered back to more negative V_m. Although all cells displayed some variation in the C_{pk} of the NLC, only 2 cells showed a maintained decrease in the C_{pk} of the NLC. The mean behaviour of the other 9 cells showed no significant decrease in C_{pk} by 118s after break-in (Figure 6.8B). For each cell, Q_{max} and β varied by up to ± 20% during the time of recording, however no time-dependent change was observed.

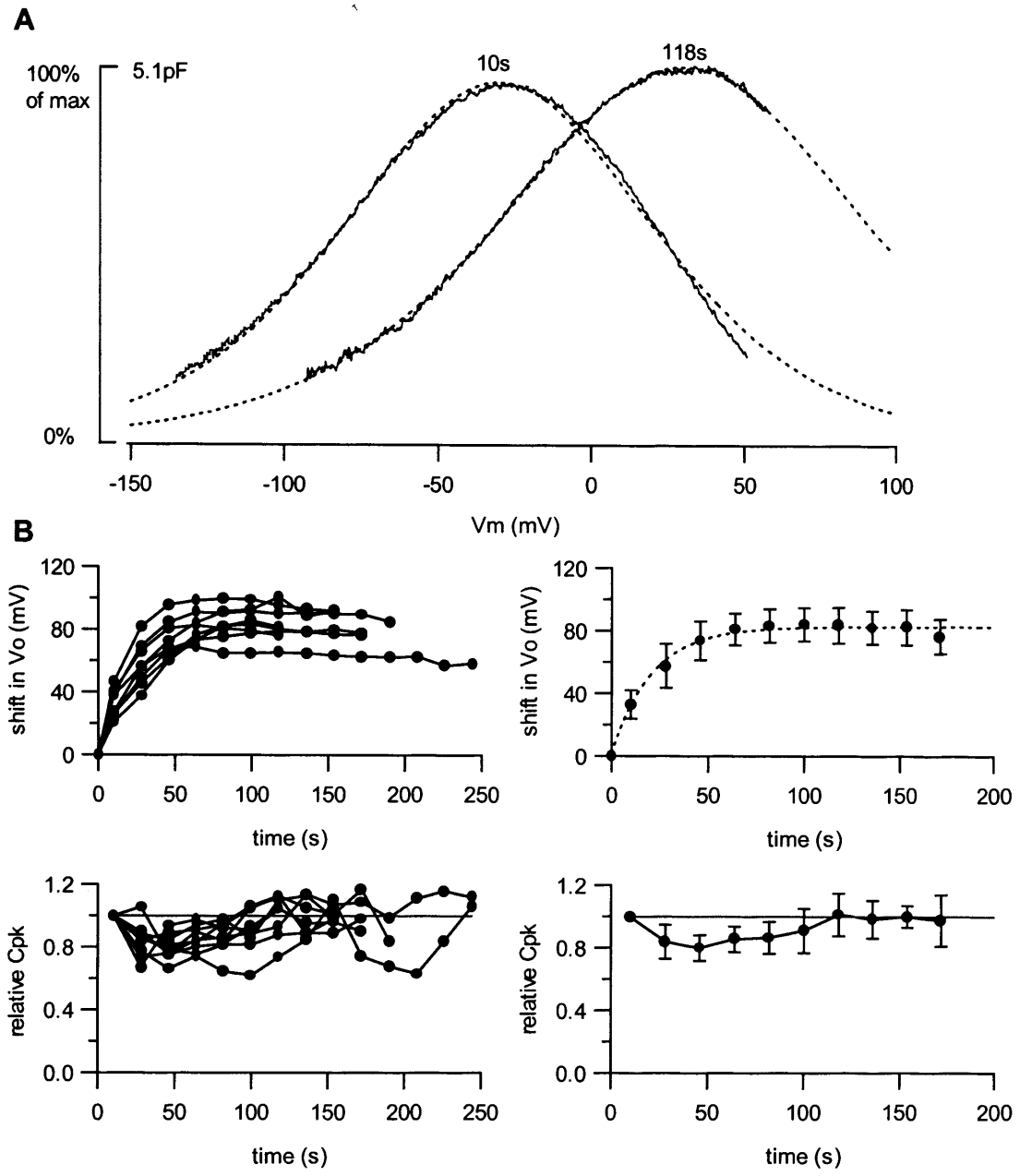

Figure 6.8 There was no decrease in the C_{pk} of the NLC when Cl_i was completely replaced with sulphate and $Tris^+$ was used as the major cation. A) An example cell showing NLCs recorded in the whole-cell configuration. Traces were recorded at 18s intervals from 10s after break-in. The traces recorded at 10s and 118s are shown. The dotted lines show the B′(V) fits used to obtain values for the Boltzmann parameters. Maximum C_{pk} corresponded to the NLC 10s after break-in. On average maximum C_{pk} was 4.08 ± 1.32pF (n=9). B) The time-course of the shift in V_o relative to the instant of break-in (V_o-V_o(t=0s)) and C_{pk} relative to 10s after break-in (C_{pk}/C_{pk}(t=10s)). The left panel shows the time-course for individual cells, and the right panel shows the time course of the average values ± SD.

6.4 Discussion

6.4.1 Is Chloride Required to Generate a NLC?

In Ch.6.3.1 and Ch.6.3.2 it was shown that a NLC was still measured when cells were bathed in chloride-free solution and patched with chloride-free solution. This observation can be interpreted in two-ways: either chloride is required to generate a NLC but is not completely removed from the cell or chloride is not required to generate a NLC. The likelihood of each scenario is discussed below.

Is intracellular chloride completely removed from the cell?

In Ch.6.3.1 and Ch.6.3.2 it was found that the initial NLC, measured 10s after break-in, had a more positive V_o and smaller C_{pk} than cells patched with the same solutions in a high-chloride bath solution. In fact on average the initial NLC in chloride-free bath solution was comparable with the steady-state NLC when cells were patched with 1mM or 0mM [Cl_{pip}] in a high-chloride bath solution. Although in these experiments it was not possible to distinguish between the effects of reduced [Cl_e] and an indirect effect on [Cl_i], one interpretation of this observation was that the initial [Cl_i] was lower ([Cl_i] <1mM) in chloride-free bath solution than in high-chloride bath solution ([Cl_i]~150mM), due to chloride efflux from the cell. This interpretation was supported by evidence that the initial V_o of the NLC was more positive for cells that had spent longer in the chloride-free bath solution, which suggested that [Cl_i] decreased with time spent in the bath.

Following break-in the V_o of the NLC shifted to more positive V_m and C_{pk} decreased further. The residual NLC once steady-state was reached, had a far more

positive V_o and a smaller C_{pk} than cells patched with the same solutions in a high-chloride bath solution or cells patched with 1mM [Cl_{pip}] with [Cl_e] reduced to 1mM. This suggested that the residual NLC was shifted to such positive V_m as a result of a greatly reduced [Cl_i] rather than due to the removal of Cl_e, and further supported the proposal that Cl_i was not properly removed when cells were patched with chloride-free solution in a high chloride bath.

In summary the experimental observations of Ch.6.3.1 and Ch.6.3.2 indicated that the initial [Cl_i] of cells prior to being patched depended on [Cl_e], such that [Cl_i] approached [Cl_e]. The initial NLC observed in chloride-free bath solution suggested that the initial [Cl_i] was <1mM and the behaviour of the NLC observed following break-in when cells were patched in chloride-free solution suggested that the final [Cl_i] <<1mM. Thus it seems likely that [Cl_i] was effectively removed from the cell. However trace levels of chloride of up to 10μM could still remain due to the contamination of salts used to make up the solutions. For example D-Glucose has ~0.025% chloride contamination, which would give ~4μM for a 150mM solution.

Can Trace Levels of [Cl_i] and [Cl_e] account for the residual NLC observed?

A residual NLC remained when cells were patched with chloride-free solution in a chloride-free bath. This NLC had a C_{pk} of ~1.35 ± 1.41pF when sulphate was used to replace chloride, and a C_{pk} of ~1.89 ± 0.31pF when gluconate was used to replace chloride. The maximum NLC corresponding to saturating [Cl_i] was not determined for these cells, thus the reduction in the C_{pk} from maximum was estimated by comparing the residual NLC, with the maximum NLC found for different cells patched with the same solution in high-chloride bath solution. This gave an estimate

for the C_{pk} of the residual NLC of ~10% of maximum for sulphate replacement and ~30% of maximum for gluconate replacement.

This can be compared with the predictions of the chloride/sulphate exchanger model with intrinsic charge movement for the condition that both $[Cl_i]$ and $[Cl_e]$ are ~10μM, and both internal and external solutions contain a high concentration of sulphate. The predicted NLC in these conditions has a very positive V_o (shifted by ~200mV compared to the NLC produced when $[Cl_i]$ is 150mM), and is reduced to ~15% of maximum. This is in fact similar to the NLC observed when cells were patched and bathed with chloride-free solutions where both Cl_i and Cl_e were replaced with sulphate. Thus it appears that trace levels of chloride might be able to account for the residual NLC observed when chloride was replaced with sulphate. The residual NLC observed when cells were patched and bathed with chloride-free solutions where both Cl_i and Cl_e were replaced with gluconate was larger than when they were replaced with sulphate. However since the NLC observed when $[Cl_i]$ was reduced to either 10mM or 1mM was also larger for gluconate replacement, it would be expected that the residual NLC due to trace levels of chloride would also be larger with gluconate replacement.

It is important to note that any residual NLC as a result of contaminant levels of chloride would also be present in excised-patch recordings. However no residual NLC was found when Cl_i was replaced with either sulphate (Oliver et al. 2001) or gluconate (Ch.5.3.1) in excised patches. With sulphate replacement this may simply reflect the fact that the V_o of the NLC lies too far beyond the range of V_m measured. With gluconate replacement this may reflect the poorer signal to noise ratio below -50mV, and above 50mV due to the seal instability.

Alternative proposals for the origin of the residual NLC

Although it is possible that trace levels of chloride can account for the residual NLC found when cells were patched and bathed in chloride-free solutions, there are several other possibilities to explain the residual NLC:

1) The NLC could be generated by intracellular bicarbonate anions, which are known to produce a NLC (Oliver et al. 2001) and may be present due to CO_2 produced by the cells.
2) In the absence of chloride the replacement anion may substitute for chloride as a voltage-sensor. However this is particularly unlikely where sulphate was used to replace chloride, since sulphate is divalent and would be expected to generate a NLC with twice the slope (β) as the NLC generated by chloride. This was not observed.
3) Finally it is possible that the residual NLC was generated by the movement of intrinsic charged residues on the protein. This hypothesis was favoured by Rybalchenko and Santos-Sacchi (2003), who suggested that chloride was not the voltage-sensor. However in this case, it would be difficult to explain how increasing $[Cl_i]$ could produce a 3-10 fold increase in the C_{pk} of the NLC without chloride also being translocated across the membrane.

In summary, at present it is not clear what produces the residual NLC, but it appears most likely that the residual NLC is produced by trace levels of chloride and therefore chloride is required to produce the NLC.

6.4.2 In the Absence of any Chloride the NLC Depends on the Anion used to Replace Chloride

Following the observations made in Ch.5, it would be expected that the properties of any residual NLC would depend on the anion used to replace Cl_i. However a comparison of the observations made in Ch.6.3.1 and Ch.6.3.2 shows that the properties of the initial NLC measured 10s after break-in also depended on the anion used to replace Cl_e, which indicated that the initial ionic composition in the cell depended on the external anion species used to replace chloride. Thus when Cl_e was replaced with sulphate the V_0 of the initial NLC was more positive than that found when Cl_e was replaced with gluconate. This can be interpreted in two ways:

1) Sulphate and/or gluconate act on prestin extracellularly to influence the rate of chlroride flux out of the cell or
2) there is an influx of sulphate and/or gluconate, which subsequently influences the NLC from inside the cell.

6.4.3 The Effect of $Tris^+$ on the NLC

In Ch.5.3.3 completely replacing Cl_i with sulphate in the whole-cell configuration was shown to lead to a positive shift in V_0 (by 90mV) and a decrease in C_{pk} (to ~30%) However Rybalchenko and Santos-Sacchi (2003), previously showed that completely replacing chloride with sulphate led to a positive shift in V_0 (by ~100mV) but no decrease in C_{pk}. In Ch.6.3.3 it was proposed that the origin of this discrepancy was the difference in the cationic composition of the solutions used in the two different experiments. To test this hypothesis, the experiment was repeated using the same solutions as described by Rybalchenko and Santos-Sacchi (2003). Unlike the

observations of Ch.5.3.3, this was found to produce a positive shift in V_o (by ~83mV) and no decrease in C_{pk},, which was consistent with the previous observations (Rybalchenko and Santos-Sacchi 2003). Thus it was concluded that the cationic composition of the solutions did affect the behaviour of the NLC.

The effects of $Tris^+$ on dissociated OHCs are unknown. However various studies have suggested that $Tris^+$ is not physiologically inert. $Tris^+$ has been shown to increase the membrane permeability of *E-coli* (Irvin et al. 1981), cause cell swelling and promote Na^+ and K^+ efflux from human erythrocytes (Luthra et al. 1975, Bodemann and Karsch 1984) and produce an increase in free cytosolic calcium in myocardial cells (Bjerneroth et al. 1996). Therefore the effect on the NLC due to $Tris^+$ is may be due an indirect effect of other changes in the cell.

Surprisingly despite the differences between the observations made with Na^+ as the major cation and those in which $Tris^+$ was used, the shift in V_o was comparable in the two conditions. This may indicate that the shift in V_o is not completely coupled to the decrease in C_{pk}. This possibility discussed in more detail in Ch.7.

Chapter 7

General Discussion

At present two alternative models of prestin have been proposed:

1) In 2001 experimental observations led to the proposal that prestin uses extrinsic intracellular chloride (Cl_i) ions as a voltage-sensor, such that charge movement arises from the translocation of a chloride ion from the intracellular side of the membrane towards the extracellular side of the membrane (Oliver et al. 2001). Since extracellular chloride (Cl_e) was not found to affect the non-linear capacitance (NLC) they concluded that prestin was an incomplete transporter shuttling chloride ions across the membrane without allowing them to dissociate at the extracellular surface.
2) In 2003 contrasting experimental observations led to the proposal that chloride was not required to generate a NLC and was therefore not the voltage-sensor (Rybalchenko and Santos-Sacchi 2003). They concluded that the NLC was generated by an intrinsic voltage-sensor, and the dependence of the NLC on $[Cl_i]$ was due to an allosteric action of chloride on prestin. They found that the dependence of the NLC on $[Cl_i]$ depended on the anion species used to replace Cl_i and proposed that prestin has multiple binding sites for chloride and other anions. Additionally they identified a tension dependent chloride conductance, which they attributed to a stretch-activated channel.

In this thesis a third model has been proposed in which prestin is described as a chloride/sulphate exchanger, where the charge movement arises as a result of both a

chloride ion and intrinsic charged residues moving across the membrane. This model was shown to be able to reproduce the key experimental observations of the dependence of the NLC on $[Cl_i]$ found in excised patches (Fakler and Oliver 2002, Figure 1.4A), and was supported by evidence presented in this thesis that sulphate interacts with prestin. Such a model of prestin could account for the dependence of the NLC on the anion species, and may also underly the presence of a chloride conductance, thus making a stretch-activated channel unnecessary.

7.1 Prestin is Unlikely to be an Incomplete Transporter

In Ch.3 and Ch.4 it was shown that 'incomplete transport' models of prestin, in which chloride was required to generate a NLC were never able to produce any decrease in C_{pk} as $[Cl_i]$ was reduced. Similarly it is unlikely that a model in which chloride only has an allosteric effect on prestin could produce a decrease in C_{pk} as $[Cl_i]$ is reduced. In such a model, the only charge movement is produced when prestin moves between states with different charge orientations. Whilst chloride binding might alter the energy required to move prestin between states producing a shift in V_o, it would not affect the ability for all prestin molecules to be forced into one state given sufficient energy, so the maximum charge transferred would be unaffected. Therefore it would seem that these types of models poorly describe the behaviour of prestin.

However one possible explanation for the difference between the predictions of these models and the experimental observations is that the shift in V_o and decrease in C_{pk} might not be directly coupled, but rather the decrease in C_{pk} is produced as an indirect consequence of reducing $[Cl_i]$. There is some evidence that this might be the

case. For example in Ch5.3.3 it was shown that for the reduction of $[Cl_i]$ to 1mM, the shift in V_o measured from whole cells was consistent with that measured from excised patches, whereas the measured decrease in C_{pk} differed in the two recording configurations. Furthermore in Ch.6.3.3 it was shown that when $Tris^+$ was used as the major cation the shift in V_o was comparable to that measured when Na^+ was the major cation but the measured decrease in the C_{pk} was very different.

It is not known what the indirect effects of reducing Cl_i might be, but they could include surface charge effects due to the increase in divalence when sulphate is used to substitute chloride or a change in the osmotic pressure due to anion fluxes. However in previous studies other factors such as tension, temperature and the degree of phosphorylation did not produce a decrease in C_{pk} of a comparable magnitude to that observed when $[Cl_i]$ was reduced. Thus although these effects may contribute they are unlikely to account for the very large changes in C_{pk} observed when $[Cl_i]$ was reduced, instead it is more likely that the decrease in C_{pk} and Q_{max} observed when $[Cl_i]$ is reduced is a result of a direct action of chloride on prestin. Therefore assuming V_o and C_{pk} are coupled both the previous models are inadequate.

7.2 Is Prestin Likely to be a Chloride/Sulphate Exchanger?

In Ch.3 and Ch.4 it was shown that complete transport models of prestin could produce a decrease in C_{pk} as $[Cl_i]$ was reduced. In particular a model, which described prestin as a chloride/sulphate exchanger (Model 7) gave a close reproduction of experimental observations. Since prestin (SLC26A5) belongs to the SLC26 family of anion exchangers, several of which transport sulphate and all of which contain the

sulphate transport motif, this does not seem unreasonable. Furthermore in Ch.5 evidence was presented that showed that sulphate is likely to interact with prestin.

In this model the charge movement was produced by the translocation of a chloride ion and intrinsic charged residues across the membrane. In Ch.6 evidence was presented, which suggested that the translocation of chloride is normally required for charge movement. Previous observations showed that site-directed mutagenisis of several positively charged residues in prestin altered the voltage-dependence of the NLC (Oliver et al. 2001), which suggested that intrinsic charged residues might also be involved in charge movement.

This model of prestin proposes that prestin mediates electrogenic exchange and therefore its transport properties should be possible to identify using electrophysiological techniques. However since the anionic conductances due to prestin are expected to be small compared with the large cation conductances present in OHCs they remained difficult to resolve. Nevertheless in Ch.5 and Ch.6 evidence was presented that a chloride conductance is present in dissociated OHCs, and in Ch.6 it was suggested that sulphate and/or gluconate were also able to permeate the OHC membrane. This was consistent with the observations of Rybalchenko and Santos-Sacchi (2003), who used $Tris^+$ as the major cation and thereby reduced the cationic conductance. However since $Tris^+$ may also affect the characteristics of the I(V), these observations are not a good test of the model. Furthermore there is no direct evidence that links these conductances with prestin. Rybalchenko and Santos-Sacchi (2003) found that the anion conductance was tension sensitive and attributed it to a stretch-activated channel. However since prestin has similar tension dependence the

possibility remains that prestin may mediate these conductances. This has yet to be resolved.

7.3 Physiological Significance

In vivo, it is unlikely that OHCs are ever presented with sulphate and intracellular chloride is unlikely to be reduced below 1mM. Typically the $[Cl_i]$ of animal cells is believed to lie close to equilibrium (Hille 1992), which for an OHC with a resting membrane potential of –70mV would be ~10mM. The $[Cl_i]$ of OHCs in vivo is unknown but estimates for the resting $[Cl_i]$ in isolated cells range from ~8-20mM (Ohnishi S et al. 1992, Song et al. 2005). Therefore it is not clear whether any transport function of prestin plays a fundamental role *in vivo*, or whether it is insignificant in physiological conditions.

Nevertheless since *in vivo*, receptor potential changes produced by mechano-transduction causes the membrane potential to vary continuously, and prestin is particularly sensitive to changes in $[Cl_i]$ the regulation of chloride transport across the lateral membrane is essential. In most animal cells the passive distribution of chloride is achieved via chloride channels such as the ClC-channels, and chloride channels activated by GABA. Additionally a variety of chloride transporters including members of the SLC4 family, the SLC26 family and members of the SLC12 family such as the Na^+-K^+-Cl^- co-transporters may mediate active movement of chloride up its concentration gradient.

Similarly, in isolated OHCs, the intracellular pH has been shown to depend on $[Cl_e]$, suggesting the presence of a Cl^-/HCO_3^- exchanger (Ikeda K et al. 1992). Furthermore, changes in cell volume and length, and a concurrent decrease in $[Cl_i]$, which were induced by tetanic electric field stimulation were all inhibited by common

chloride channel blockers including 4,4'-diisothiocyanatostilbene-2, 2'-disulfonic acid (DIDS) and furosemide. This suggested the presence of chloride channels (Ohnishi S et al. 1992). Whilst several ClC channels have been identified in OHCs by RT-PCR (Kawasaki et al. 1999, Kawasaki et al. 2000) and the Cl^-/HCO_3^- exchanger SLC4A2 (AE2) has been identified in OHCs via a combination of RT-PCR and immunohistochemistry (Zimmermann et al. 2000), there remains little evidence to show that any of these proteins are localised to the cell membrane and are functional. Therefore at present it is still unclear which channels, and transporters are responsible for regulating $[Cl_i]$ in OHCs. Thus prestin may be required to play a role in maintaining the concentration of chloride and set its own voltage-sensitivity. Additionally since at least two of the anion exchangers in the SLC26 family (SLC26A3 and SLC26A6), mediate both chloride/sulphate exchange and chloride/bicarbonate exchange (Mount and Romero 2003) it is possible that *in vivo* rather than mediating chloride/sulphate exchange prestin mediates chloride/bicarbonate exchange and therefore plays a role in controlling the pH of cells.

7.4 Future Work

Although the chloride/sulphate exchanger model with intrinsic charge movement gave a close reproduction of the experimental observations of the dependence of the NLC on $[Cl_i]$, prestin has not yet been shown to have transport properties. This could be investigated further using a combination of techniques. The anionic conductances that would be associated with chloride/sulphate exchange could be further investigated using electrophysiological techniques and replacing chloride

with sulphate in solutions. In OHCs $NMDG^+$ could be used as the major cation to reduce the cation leak (Housley and Ahmore 1992). In order to directly link any anionic conductance with prestin it would also be ideal to compare the effects of replacing chloride with sulphate on the I(V) of cells transfected with prestin with untransfected cells. To further link a sulphate permeability with prestin, radiolabelling techniques could also be used to compare the uptake of radiolabelled sulphate in cells transfected with prestin with untransfected cells. Additionally since it is proposed here that prestin has a similar function to other members of the SLC26 family, it would be of interest to see how mutations in residues that are conserved amongst members of the transporter family, in particular the sulphate transport motif might affect the voltage-dependence of the NLC. To date only mutations on unconserved residues have been performed (Oliver et al.2001). Finally it is also clear that the chloride/sulphate model is a highly simplified description of prestin since does not take into account any other factors, which may affect the NLC. In particular the NLC is sensitive to tension, thus it would be useful to include a tension sensitive component in the model.

Glossary of Essential Terms and Symbols

OHC	Outer hair cell
NLC	Non-linear capacitance
B′(V)	Derivative of the Boltzmann function, which describes the shape of the NLC
Q	The gating charge transferred across the membrane
V	The applied voltage
Q_{max}	The maximum charge transferred across the membrane
C_{pk}	The maximum of the NLC
V_o	The potential corresponding to half-maximal charge transfer, or the peak of the NLC
β	The 'slope' of the Q(V) curve
Cl_o	Intracellular chloride
Cl_e	Extracellular chloride
α	Dielectric coefficient

References

Abramson J, Smirnova I, Kasho V, Verner G, Kaback HR, Iwata S. (2003) Structure and mechanism of the lactose permease of Escherichia coli. *Science.* **301**:610-5.

Accardi A, Miller C. (2004) Secondary active transport mediated by a prokaryotic homologue of ClC Cl- channels. *Nature.* **427**:803-7.

Accardi A, Pusch M. (2000) Fast and slow gating relaxations in the muscle chloride channel CLC-1. *J Gen Physiol.* **116**:433-44.

Adachi M, Iwasa KH. (1999) Electrically driven motor in the outer hair cell: effect of a mechanical constraint. *Proc Natl Acad Sci U S A.* **96**:7244-9.

Adachi M, Sugawara M, Iwasa KH. (2000) Effect of turgor pressure on outer hair cell motility. *J Acoust Soc Am.* **108**:2299-306.

Adams SV, DeFelice LJ.(2002) Flux coupling in the human serotonin transporter. *Biophys J.* **83**:3268-82.

Adams SV, DeFelice LJ. (2003) Ionic currents in the human serotonin transporter reveal inconsistencies in the alternating access hypothesis. *Biophys J.* **85**:1548-59.

Albers RW, (1967) Biochemical aspects of active transport. *Ann. Rev. Biochem.* **36**:727-756

Apell HJ, Karlish SJ. (2001) Functional properties of Na,K-ATPase, and their structural implications, as detected with biophysical techniques. *J Membr Biol.* **180**:1-9.

Apell HJ. (2004) How do P-type ATPases transport ions? *Bioelectrochemistry.* **63**:149-56.

Aravind L, Koonin EV. (2000) The STAS domain - a link between anion transporters and antisigma-factor antagonists. *Curr Biol.* **10**:R53-5.

Ashmore JF. (1987) A fast motile response in guinea-pig outer hair cells: the cellular basis of the cochlear amplifier. *J Physiol.* **388**:323-47.

Atkins PW, (1986) Physical Chemistry. 3rd edition. Oxford University Press

Bell GI, Burant CF, Takeda J, Gould GW.(1993) Structure and function of mammalian facilitative sugar transporters. *J Biol Chem.* **268**:19161-4.

Belyantseva IA, Adler HJ, Curi R, Frolenkov GI, Kachar B. (2000) Expression and localization of prestin and the sugar transporter GLUT-5 during development of electromotility in cochlear outer hair cells. *J Neurosci.* **20**:RC116.

Bjerneroth G, Li YC, Wiklund L, Ridefelt P, (1996) Effect of tris buffer on free cytosolic calcium in myocardial cells. *Crit Care Med.* **24**:1713-8

Bodemann HH, Karsch B, (1984) Transfer of tris buffer and effects on K^+ loss in human red blood cells and reconstituted ghosts. *Biochim Biophys Acta.* **772**:77-83

Brownell WE, Bader CR, Bertrand D, de Ribaupierre Y. (1985) Evoked mechanical responses of isolated cochlear outer hair cells. *Science.* **227**:194-6.

Cammack JN, Schwartz EA. (1996) Channel behavior in a gamma-aminobutyrate transporter. *Proc Natl Acad Sci U S A.* **93**:723-7.

Chambard JM, Ashmore JF. (2003) Sugar transport by mammalian members of the SLC26 superfamily of anion-bicarbonate exchangers. *J Physiol.* **550**:667-77.

Chen TY, Miller C. (1996) Nonequilibrium gating and voltage dependence of the ClC-0 Cl- channel. *J Gen Physiol.* **108**:237-50.

Colquhoun D, Hawkes AG, (1995) A Q-Matrix Cookbook: How to write only one program to calculate the single-channel and macroscopic predictions for any kinetic mechanism. In: Single-Channel Recordings Eds. Sakmann B, Neher E. New York:Plenum. pp589-636

Dallos P, Evans BN. (1995) High-frequency motility of outer hair cells and the cochlear amplifier. *Science.* **267**:2006-9.

Dallos P, Harris D. (1978) Properties of auditory nerve responses in absence of outer hair cells. *J Neurophysiol.* **41**:365-83.

DeFelice LJ, Blakely RD. (1996) Pore models for transporters? *Biophys J.* **70**:579-80.

DeFelice LJ. (2004) Transporter structure and mechanism. *Trends Neurosci.* **27**:352-9

Ding JP, Salvi RJ, Sachs F, (1991) Stretch-activated ion channels in guinea-pig outer hair cells. *Hearing Res.* **56**:19-28.

Dulon D, Zajic G, Schacht J. (1990) Increasing intracellular free calcium induces circumferential contractions in isolated cochlear outer hair cells. *J Neurosci.* **10**:1388-97.

Dutzler R. (2004) The structural basis of ClC chloride channel function. *Trends Neurosci.* **27**:315-20.

Dutzler R, Campbell EB, Cadene M, Chait BT, MacKinnon R.(2002) X-ray structure of a ClC chloride channel at 3.0 A reveals the molecular basis of anion selectivity. *Nature.* **415**:287-94.

Dutzler R, Campbell EB, MacKinnon R. (2003) Gating the selectivity filter in ClC chloride channels. *Science.* **300**:108-12.

Eskandari S, Kreman M, Kavanaugh MP, Wright EM, Zampighi GA. (2000) Pentameric assembly of a neuronal glutamate transporter. *Proc Natl Acad Sci U S A* **97**:8641-6.

Estevez R, Jentsch TJ. (2002) CLC chloride channels: correlating structure with function. *Curr Opin Struct Biol.* **12**:531-9.

Evans BN, Dallos P, Hallworth R. (1989) Asymmetries in motile responses of outer hair cells in simulated *in vivo* conditions. In: Cochlear Mechanisms. Eds. Wilson JP, Kemp DT. New York: Plenum. pp 205-206.

Everett LA, Green ED. (1999) A family of mammalian anion transporters and their involvement in human genetic diseases. *Hum Mol Genet.* **8**:1883-91.

Everett LA, Morsli H, Wu DK, Green ED. (1999) Expression pattern of the mouse ortholog of the Pendred's syndrome gene (Pds) suggests a key role for pendrin in the inner ear. *Proc Natl Acad Sci U S A.* **96**:9727-32.

Fakler B, Oliver D. (2002) Functional properties of prestin-how the motormolecule works In: Biophysics of the cochlea from molecules to models Ed. Gummer AW. World Scientific. pp 110-115

Forge A. (1991) Structural features of the lateral walls in mammalian cochlear outer hair cells. *Cell Tissue Res.* **265**:473-83.

Feynman RP, Leighton RB, Sands M. (1965) The Feynman lectures on physics. Volume 1. Addison-Wesley; World Student Series Edition.

Frank G, Hemmert W, Gummer AW. (1999) Limiting dynamics of high-frequency electromechanical transduction of outer hair cells. *Proc Natl Acad Sci U S A.* **96**:4420-5.

Frolenkov GI, Mammano F, Belyantseva IA, Coling D, Kachar B. (2000) Two distinct Ca(2+)-dependent signaling pathways regulate the motor output of cochlear outer hair cells. *J Neurosci.* **20**:5940-8.

Gadsby DC, Nakao M. (1989) Steady-state current-voltage relationship of the Na/K pump in guinea pig ventricular myocytes. *J Gen Physiol.* **94**:511-37.

Gale JE, Ashmore JF. (1997a)The outer hair cell motor in membrane patches. *Pflugers Arch.* **434**:267-71.

Gale JE, Ashmore JF. (1997b) An intrinsic frequency limit to the cochlear amplifier. *Nature.* **389**:63-6.

Galli A, Blakely RD, DeFelice LJ. (1996) Norepinephrine transporters have channel modes of conduction. *Proc Natl Acad Sci U S A.* **93**:8671-6.

Gasbjerg PK, Brahm J. (1991) Kinetics of bicarbonate and chloride transport in human red cell membranes. *J Gen Physiol.* **97**:321-49.

Gadsby DC, Nakao M. (1989) Steady-state current-voltage relationship of the Na/K pump in guinea pig ventricular myocytes. *J Gen Phyysiol.* **94**:511-37

Gadsby DC, Rakowski RF, De Weer P. (1993) Extracellular access to the Na,K Pump: Pathway similar to ion channel *Science* **260**:100-103

Geisler CD (1998) From sound to synapse, physiology of the mammaliam ear. Oxford University Press.

Gillis KD. (1995) Techniques for membrane capacitance measurements. In: Single Channel Recordings. Eds. Sakmann B, Neher E. New York:Plenum. pp155-198.

Greco FA, Solomon AK. (1997) Kinetics of chloride-bicarbonate exchange across the human red blood cell membrane. *J Membr Biol.* **159**:197-208.

Gulley RL, Reese TS. (1977) Regional specialization of the hair cell plasmalemma in the organ of corti. *Anat Rec.* **189**:109-23.

Gummer AW Ed. (2003) Discussion session; prestin. In Biophysics of the cochlea from molecules to models. World Scientific. pp 570-572.

Gunn RB, Frohlich O. (1979) Asymmetry in the mechanism for anion exchange in human red blood cell membranes. Evidence for reciprocating sites that react with one transported anion at a time. *J Gen Physiol.* **74**:351-74.

Hamill OP, Marty A, Neher E, Sakmann B, Sigworth FJ. (1981) Improved patch-clamp techniques for high-resolution current recording from cells and cell-free membrane patches. *Pflugers Arch.* **391**:85-100.

He DZ, Evans BN, Dallos P. (1994) First appearance and development of electromotility in neonatal gerbil outer hair cells. *Hear Res.* **78**:77-90.

Hernandez JA, Valle Lisboa JC. (2004) Reduced kinetic models of facilitative transport. *Biochim Biophys Acta.* **1665**:65-74.

Hilgemann DW. (1994) Channel-like function of the Na,K pump probed at microsecond resolution in giant membrane patches. *Science.* **263**:1429-32.

Hilgemann DW, Lu CC. (1999) GAT1 (GABA:Na+:Cl-) cotransport function. Database reconstruction with an alternating access model. *J Gen Physiol.* **114**:459-75.

Hille B. (1992) Ionic channels of excitable membranes. 2nd edition. Sunderland, Mass. USA Sinauer Ass.

Hirai T, Heymann JA, Shi D, Sarker R, Maloney PC, Subramaniam S. (2002) Three-dimensional structure of a bacterial oxalate transporter. *Nat Struct Biol.* **9**:597-600.

Holley MC. (1996) Outer hair cell motility. In: The cochlea: Springer handbook of auditory research. Eds. Dallos P, Popper AN, Fay RR. New York. Springer. pp 386-434.

Holley MC, Ashmore JF. (1988) On the mechanism of a high-frequency force generator in outer hair cells isolated from the guinea pig cochlea. *Proc R Soc Lond B Biol Sci.* **232**:413-29.

Holley MC, Ashmore JF. (1990) Spectrin, actin and the structure of the cortical lattice in mammalian cochlear outer hair cells. *J Cell Sci.* **96**:283-91.

Housley GD, Ashmore JF (1992) Ionic currents of outer hair cells isolated from the guinea-pig cochlea. *J.Physiol.* **448**:73-98.

Huang G, Santos-Sacchi J. (1993) Mapping the distribution of the outer hair cell motility voltage sensor by electrical amputation. *Biophys J.* **65**:2228-36.

Ikeda K, Saito Y, Nishiyama A, Takasaka T. (1992) Intracellular pH regulation in isolated cochlear outer hair cells of the guinea-pig.*J Physiol.* **447**:627-48.

Irvin RT, MacAlister TJ, Costerton JW. (1981) Tris(hydroxymethyl)aminomethane buffer modification of *Escherichia coli* outer membrane permeability. *J Bacteriol.* **145**:1397-1403.

Iwasa KH. (1997) Current noise spectrum and capacitance due to the membrane motor of the outer hair cell: theory. *Biophys J.* **73**:2965-71.

Iwasa KH, Adachi M. (1997) Force generation in the outer hair cell of the cochlea. *Biophys J.* **73**:546-55.

Iwasa KH, Li MX, Jia M, Kachar B. (1991) Stretch sensitivity of the lateral wall of the auditory outer hair cell from the guinea-pig. *Neurosci Lett.* **133**:171-174.
Jardetzky O. (1966) Simple allosteric model for membrane pumps. *Nature.* **211**:969-70

Jennings ML (1982) Stoichiometry of a half-turnover of band 3, the chloride transporter protein of human erythrocytes. *J Gen Physiol.* **79**:169-85.

Jennings ML, Schulz RK, Allen M (1990) Effects of membrane potential on electrically silent transport; potential-independent translocation and asymmetric potential-dependent substrate binding to the red blood cell anion exchange protein. *J Gen Physiol.* **96**:991-1012.

Kakehata S, Santos-Sacchi J. (1995) Membrane tension directly shifts voltage dependence of outer hair cell motility and associated gating charge. *Biophys J.* **68**:2190-7.

Kakehata S, Santos-Sacchi J. (1996) Effects of salicylate and lanthanides on outer hair cell motility and associated gating charge. *J Neurosci.* **16**:4881-9.

Kalinec F, Holley MC, Iwasa KH, Lim DJ, Kachar B. (1992) A membrane-based force generation mechanism in auditory sensory cells. *Proc Natl Acad Sci U S A.* **89**:8671-5.

Kavanaugh MP. (1998) Neurotransmitter transport: models in flux. *Proc Natl Acad Sci U S A.* **95**:12737-8.

Kawasaki E, Hattori N, Miyamoto E, Yamashita T, Inagaki C. (1999) Single-cell RT-PCR demonstrates expression of voltage-dependent chloride channels (ClC-1, ClC-2 and ClC-3) in outer hair cells of rat cochlea. *Brain Res.* **838**(1-2):166-70.

Kawasaki E, Hattori N, Miyamoto E, Yamashita T, Inagaki C. (2000) mRNA expression of kidney-specific ClC-K1 chloride channel in single-cell reverse transcription-polymerase chain reaction analysis of outer hair cells of rat cochlea. *Neurosci Lett.* **290**:76-8.

Kilic F, Rudnick G (2000) Oligomerization of serotonin transporter and its functional consequences. *Proc Natl Acad Sci U S A.* **97**:3106-11.

Knauf PA, Brahm J.(1989) Functional asymmetry of the anion-exchange protein, capnophorin: effects on substrate and inhibitor binding. Methods Enzymol. **173**:432-53.

Knauf PA, Law FY, Leung TW, Gehret AU, Perez ML.(2002) Substrate-dependent reversal of anion transport site orientation in the human red blood cell anion-exchange protein, AE1. Proc Natl Acad Sci U S A. **99**:10861-4.

Knauf PA, Mann NA.(1984) Use of niflumic acid to determine the nature of the asymmetry of the human erythrocyte anion exchange system. J Gen Physiol. **83**:703-25.

Larsson HP, Picaud SA, Werblin FS, Lecar H. (1996) Noise analysis of the glutamate-activated current in photoreceptors. *Biophys J.* **70**:733-42.

Lauger P. (1979) A channel mechanism for electrogenic ion pumps. *Biochim Biophys Acta.* **552**:143-61.

Lauger P. (1991) Electrogenic ion pumps. Sunderland, Mass. USA Sinauer Ass.

Lauger P, Apell HJ (1988) Transient behaviour of the Na^+/K^+-pump: microscopic analysis of nonstationary ion translocation. *Biochim Biophys Acta.* **944**:451-64.

Lester HA, Cao Y, Mager S. (1996) Listening to neurotransmitter transporters. *Neuron.* **17**:807-10.

Liberman MC. (1987) Chronic ultrastructural changes in acoustic trauma: serial-section reconstruction of stereocilia and cuticular plates. *Hear Res.* **26**:65-88.

Liberman MC, Gao J, He DZ, Wu X, Jia S, Zuo J. (2002) Prestin is required for electromotility of the outer hair cell and for the cochlear amplifier. *Nature.* **419**:300-4.

Lin F, Lester HA, Mager S. (1996) Single-channel currents produced by the serotonin transporter and analysis of a mutation affecting ion permeation. *Biophys J.* **71**:3126-35.

Lohi H, Kujala M, Kerkela E, Saarialho-Kere U, Kestila M, Kere J. (2000) Mapping of five new putative anion transporter genes in human and characterization of SLC26A6, a candidate gene for pancreatic anion exchanger. *Genomics.* **70**:102-12.

Lohi H, Lamprecht G, Markovich D, Heil A, Kujala M, Seidler U, Kere J. (2003) Isoforms of SLC26A6 mediate anion transport and have functional PDZ interaction domains. *Am J Physiol Cell Physiol.* **284**:C769-79.

Lu CC, Kabakov A, Markin VS, Mager S, Frazier GA, Hilgemann DW. (1995) Membrane transport mechanisms probed by capacitance measurements with megahertz voltage clamp. *Proc Natl Acad Sci U S A.* **92**:11220-4.

Ludwig J, Oliver D, Frank G, Klocker N, Gummer AW, Fakler B. (2001) Reciprocal electromechanical properties of rat prestin: the motor molecule from rat outer hair cells. *Proc Natl Acad Sci U S A.* **98**:4178-83.

Lue AJ, Brownell WE. (1999) Salicylate induced changes in outer hair cell lateral wall stiffness. *Hear Res.* **135**:163-8.

Luthra MG, Ekholm JE, Kim HD, Hanahan DJ. (1975) Effects of $Tris^+$ and histidine on human erythrocytes and conditions influencing their mode of action. *Biochim Biophys Acta.* **382**:634-49.

Maduke M, Miller C, Mindell JA. (2000) A decade of CLC chloride channels: structure, mechanism, and many unsettled questions. *Annu Rev Biophys Biomol Struct.* **29**:411-38.

Mager S, Min C, Henry DJ, Chavkin C, Hoffman BJ, Davidson N, Lester HA. (1994) Conducting states of a mammalian serotonin transporter. *Neuron.* **12**:845-59.

Magleby KL. (2003) Gating mechanism of BK (Slo1) channels: so near, yet so far. *J Gen Physiol.* **121**:81-96.

Mammano F, Kros CJ, Ashmore JF. (1995) Patch clamped responses from outer hair cells in the intact adult organ of Corti. *Pflugers Arch.* **430**:745-50.

Marty A, Neher E. (1995) Tight seal whole-cell recordings. In: Single Channel Recordings. Eds. Sakmann B, Neher E. New York: Plenum. pp 31-52.

Matsuda K, Zheng J, Du G, Deak L, Navarette EG, Dallos P. (2003) Protein kinase C and voltage-dependent capacitance in prestin-transfected TSA cells. In: Abstracts of the Association for Research in Otolaryngology.

Matsuda K, Zheng J, Du GG, Klocker N, Madison LD, Dallos P. (2004) N-linked glycosylation sites of the motor protein prestin: effects on membrane targeting and electrophysiological function. *J Neurochem.* **89**:928-38.

Meltzer J, Santos-Sacchi J. (2001) Temperature dependence of non-linear capacitance in human embryonic kidney cells transfected with prestin, the outer hair cell motor protein. *Neurosci Lett.* **313**:141-4.

Mount DB, Romero MF. (2003) The SLC26 gene family of multifunctional anion exchangers. *Pflugers Arch.* **447**:710-21

Nakao M, Gadsby DC. (1986) Voltage dependence of Na translocation by the Na/K pump. *Nature.* **323**:628-30.

Nakao M, Gadsby DC. (1989) [Na] and [K] dependence of the Na/K pump current-voltage relationship in guinea pig ventricular myocytes. *J Gen Physiol.* **94**:539-65.

Neher E, Marty A. (1982) Discrete changes of cell membrane capacitance observed under conditions of enhanced secretion in bovine adrenal chromaffin cells. *Proc Natl Acad Sci U S A.* **79**:6712-6.

Nobili R, Mammano F, Ashmore J. (1998) How well do we understand the cochlea? *Trends Neurosci.* **21**:159-67.

Ohnishi S, Hara M, Inoue M, Yamashita T, Kumazawa T, Minato A, Inagaki C. (1992) Delayed shortening and shrinkage of cochlear outer hair cells. *Am J Physiol.* **263**:C1088-95.

Oliver D, Fakler B. (1999) Expression density and functional characteristics of the outer hair cell motor protein are regulated during postnatal development in rat. *J Physiol.* **519**:791-800.

Oliver D, He DZ, Klocker N, Ludwig J, Schulte U, Waldegger S, Ruppersberg JP, Dallos P, Fakler B.(2001) Intracellular anions as the voltage sensor of prestin, the outer hair cell motor protein. *Science.* ;**292**:2340-3.

Ospeck M, Dong X, Iwasa KH. (2003) Limiting frequency of the cochlear amplifier based on electrmotility of outer hair cells. *Biophys J.* **84**:739-749.

Patlak CS (1957) Contributions to the theory of active transport: II. The gate type non-carrier mechanism and generalizations concerning tracer flow, efficiency and measurement of energy expenditure. *Bull. Math. Biophys.* **19**:209-235.

Philipson KD, Nicoll DA. (2000) Sodium-calcium exchange: a molecular perspective. *Annu Rev Physiol.* **62**:111-33

Pickles JO (1988) An introduction to the physiology of hearing. 2nd edition. Academic Press.

Pollice PA, Brownell WE (1993) Characterisation of the outer hair cell's lateral wall membranes. *Hear Res.* **70**:187-196.

Post RL, Hegyvary C, Kume S. (1972) Activation by adenosine triphosphate in the phosphorylation kinetics of sodium and potassium ion transport adenosine triphosphate. *J Biol Chem.* **247**: 6530-6540.

Pusch M, Ludewig U, Rehfeldt A, Jentsch TJ. (1995) Gating of the voltage-dependent chloride channel CIC-0 by the permeant anion. *Nature.* **373**:527-31.

Pusch M, Neher E. (1988) Rates of diffusional exchange between small cells and a measuring patch pipette. Pflugers Arch. **411**:204-211.

Rakowski RF. (1993) Charge movement by the Na/K pump in Xenopus Oocytes. *J Gen Physiol.* **101**:117-144.

Romero MF, Fulton CM, Boron WF. (2004) The SLC4 family of HCO_3^- transporters. *Pflugers Arch.* **447**:495-509.

Russell JM. (2000) Sodium-potassium-chloride cotransport. *Physiol Rev.* **80**:211-76.

Rybalchenko V, Santos-Sacchi J. (2003) Cl- flux through a non-selective, stretch-sensitive conductance influences the outer hair cell motor of the guinea-pig. *J Physiol.* **547**:873-91.

Rychkov GY, Pusch M, Astill DS, Roberts ML, Jentsch TJ, Bretag AH. (1996) Concentration and pH dependence of skeletal muscle chloride channel ClC-1. *J Physiol.* **497**:423-35.

Rychkov GY, Pusch M, Roberts ML, Jentsch TJ, Bretag AH. (1998) Permeation and block of the skeletal muscle chloride channel, ClC-1, by foreign anions. *J Gen Physiol.* **111**:653-65.

Santos-Sacchi J. (1989) Asymmetry in voltage-dependent movements of isolated outer hair cells from the organ of Corti. *J Neurosci.* **9**:2954-62.

Santos-Sacchi J. (1991) Reversible inhibition of voltage-dependent outer hair cell motility and capacitance. *J Neurosci.* **11**:3096-110.

Santos-Sacchi J, Huang G. (1998) Temperature dependence of outer hair cell nonlinear capacitance. *Hear Res.* **116**:99-106.

Santos-Sacchi J, Shen W, Zheng J, Dallos P. (2001) Effects of membrane potential and tension on prestin, the outer hair cell lateral membrane motor protein. *J Physiol.* **531**:661-6.

Sagar A, Rakowski RF. (1994) Access channel model for the voltage dependence of the forward-running Na^+/K^+ pump. *J Gen Physiol.* **103**:869-93.

Scott DA, Karniski LP. (2000) Human pendrin expressed in Xenopus laevis oocytes mediates chloride/formate exchange. *Am J Physiol Cell Physiol.* **278**:C207-11.

Sellick PM, Patuzzi R, Johnstone BM. (1982) Measurement of basilar membrane motion in the guinea pig using the Mossbauer technique.*J Acoust Soc Am.* **72**:131-41.

Shehata WE, Brownell WE, Dieler R. (1991) Effects of salicylate on shape, electromotility and membrane characteristics of isolated outer hair cells from guinea pig cochlea. *Acta Otolaryngol.* **111**:707-18.

Sonders MS, Zhu SJ, Zahniser NR, Kavanaugh MP, Amara SG. (1997) Multiple ionic conductances of the human dopamine transporter: the actions of dopamine and psychostimulants. *J Neurosci.* **17**:960-74.

Song L, Seeger A, Santos-Sacchi J. (2004) On membrane motor activity and chloride flux in the outer hair cell: lessons learned from the environmental toxin tributyltin. *Biophys J.* Epub ahead of print.

Su A, Mager S, Mayo SL, Lester HA. (1996) A multi-substrate single-file model for ion-coupled transporters. *Biophys J.* Feb;**70**:762-77.

Tunstall MJ, Gale JE, Ashmore JF. (1995) Action of salicylate on membrane capacitance of outer hair cells from the guinea-pig cochlea. *J Physiol.* **485**:739-52.
Van der Does C, Tampe R. (2004) Changing orders--primary and secondary membrane transporters revised. Chembiochem. **5**:1171-5

Veenhoff LM, Heuberger EH, Poolman B. (2002) Quaternary structure and function of transport proteins. *Trends Biochem Sci.* **27**:242-9.

Vidaver GA. (1966) Inhibition of parallel flux and augmentation of counter flux shown by transport models not involving a mobile carrier. *J Theor Biol.* **10**:301-6.

Wadiche JI, Kavanaugh MP. (1998) Macroscopic and microscopic properties of a cloned glutamate transporter/chloride channel. *J Neurosci.* **18**:7650-61.

Waldegger S, Moschen I, Ramirez A, Smith RJ, Ayadi H, Lang F, Kubisch C. (2001) Cloning and characterization of SLC26A6, a novel member of the solute carrier 26 gene family. *Genomics*. **72**:43-50. Erratum in: Genomics 2001 77(1-2):115.

Wang DN, Sarabia VE, Reithmeier RA, Kuhlbrandt W. (1994) Three-dimensional map of the dimeric membrane domain of the human erythrocyte anion exchanger, Band 3. *EMBO J.* **13**:3230-5.

Wright EM, Turk E. (2004) The sodium/glucose cotransport family SLC5. *Pflugers Arch.* **447**:510-8. Erratum in: Pflugers Arch. 2004 447(5):813-5.

Wu M, Santos-Sacchi J. (1998) Effects of lipophilic ions on outer hair cell membrane capacitance and motility. *J Membr Biol.* **166**:111-8.

Xie Q, Welch R, Mercado A, Romero MF, Mount DB. (2002) Molecular characterization of the murine Slc26a6 anion exchanger: functional comparison with Slc26a1. *Am J Physiol Renal Physiol.* **283**:F826-38.

Yernool D, Boudker O, Jin Y, Gouaux E. (2004) Structure of a glutamate transporter homologue from Pyrococcus horikoshii. *Nature.* **431**:811-8.

Zheng J, Shen W, He DZ, Long KB, Madison LD, Dallos P. (2000) Prestin is the motor protein of cochlear outer hair cells. *Nature.* **405**:149-55.

Zheng J, Long KB, Shen W, Madison LD, Dallos P. (2001) Prestin topology: localization of protein epitopes in relation to the plasma membrane. *Neuroreport.* **12**:1929-35.

Zhu Q, Lee DW, Casey JR. (2003) Novel topology in C-terminal region of the human plasma membrane anion exchanger, AE1. *J Biol Chem.* **278**:3112-20.

Zimmermann U, Kopschall I, Rohbock K, Bosman GJ, Zenner HP, Knipper M. (2000) Molecular characterization of anion exchangers in the cochlea. *Mol Cell Biochem* **205**:25-37.